Jets in Soft-Collinear Effective Theory

by

Andrew Carl Hornig

A dissertation submitted in partial satisfaction of the

requirements for the degree of

Doctor of Philosophy

in

Physics

in the

Graduate Division

of the

University of California, Berkeley

Committee in charge:

Dr. Christian W. Bauer, Co-Chair

Professor Yasunori Nomura, Co-Chair

Professor Hitoshi Murayama

Professor Maciej Zworski

Spring 2010

Jets in Soft-Collinear Effective Theory

Abstract

Jets in Soft-Collinear Effective Theory

by

Andrew Carl Hornig

Doctor of Philosophy in Physics

University of California, Berkeley

Dr. Christian W. Bauer, Co-Chair

Professor Yasunori Nomura, Co-Chair

Factorization is the central ingredient in any theoretical prediction for collider experiments. I introduce a factorization formalism that can be applied to any desired observable, like event shapes or jet observables, for any number of jets and a wide range of jet algorithms in leptonic or hadronic collisions. This is achieved by using soft-collinear effective theory to prove the formal factorization of a generic fully-differential cross section in terms of a hard coefficient, and generic jet and soft functions. The factorization formula for any such observable immediately follows from our general result, including the precise definition of the functions appropriate for the observable in question.

As a first application, I present a new prediction of angularity distributions in e^+e^- annihilation. Angularities τ_a are an infinite class of event shapes which vary in their sensitivity to the substructure of jets in the final state, controlled by a continuous parameter $a < 2$. I calculate angularity distributions for all $a < 1$ to first order in the strong coupling α_s and resum large logarithms in these distributions to next-to-leading logarithmic (NLL) accuracy.

I then apply SCET to the more exclusive case of jet shapes. In particular, I make predictions for quark and gluon jet shape distributions in N-jet final states in e^+e^- collisions, defined with a cone or recombination algorithm, where I measure some jet shape observable on a subset of these jets. I demonstrate the consistent renormalization-group running of the functions in the factorization theorem for any number of measured and unmeasured jets, any number of quark and gluon jets, and any angular size R of the jets, as long as R is much smaller than the angular separation between jets. I calculate the jet and soft functions for angularity jet shapes τ_a to next-to-leading order (NLO) in α_s and resum large logarithms of τ_a to next-to-leading logarithmic (NLL) accuracy for both cone and k_T-type jets.

Finally, I apply SCET to the case of threshold resummmation at hadron colliders. Factorization theorems for processes at hadron colliders near the hadronic endpoint have largely focused on simple final states with either no jets (e.g., Drell-Yan) or one inclusive jet (e.g., deep inelastic scattering and prompt photon production). Factorization for the former type of process gives rise to a soft function that depends on timelike momenta whereas the soft function for the latter type depends on null momenta. I derive a factorization theorem that allows for an arbitrary number of jets, where the jets are defined with respect to a jet algorithm, together with any number of non-strongly interacting particles. I find the soft function in general depends on the null components of the soft momenta inside the jets and on the timelike component of the soft momentum outside of the jets. This generalizes and interpolates between the soft functions for the cases of no jets and one inclusive jet.

Contents

List of Figures

List of Tables

Chapter 1

Introduction

High Energy Physics is approaching one of the most important and exciting periods in many years with the coming online of the CERN Large Hadron Collider (LHC). In addition to the potential discovery of the last ingredient of the Standard Model (SM), the Higgs boson, the LHC will search for evidence of many models of physics beyond the Standard Model that propose solutions to the problems of the SM.

We may find various kinds of signals of new physics at the LHC. On one hand, in a best-case scenario, new physics will appear as a smoking gun, and it will be the task of the high energy community at large to try to explain what we see and why. On the other hand, it might be that new physics is hiding behind SM backgrounds that are not well understood, a primary example being SM multijet signals. It is therefore of utmost importance to increase our understanding of these backgrounds. The development and application of tools that help our understanding of this area is the goal of this thesis.

In particular, the main approach to understanding collider signatures of the SM that forms the basis of this thesis is an analytically based approach that makes use of effective field theories (in particular Soft Collinear Effective Theory [19, 21, 33, 29], or SCET). SCET can be used to separate (or *factorize*) different energy scales from one another. This serves two functions. First, factorization of perturbative from non-perturbative energy scales allows for a model independent understanding of hadronization effects. Second, further factorization of the perturbative contribution into pieces that are only sensitive to a single energy scale allows for renormalization group evolution of each piece from its respective scale to a common scale, which resums logarithms of ratios of the disparate scales to which the various contributions are sensitive.

In order to apply SCET to multijet environments at the LHC, the definition of a jet itself, which in practice is made via a jet algorithm, needs to be incorporated into factorization formula. Jet algorithms are used to define more exclusive objects that still aim to connect short distance descriptions of QCD (partons) with long distance descriptions (hadrons). In Chapter 2, I explore how in detail jet algorithms can be incorporated into factorization formulas. After this is achieved, a wide variety of applications of this formalism can be performed.

For example, one of the topics that SCET can be applied to is in the understanding of jet substructure, an area of collider physics that has generated considerable interest in the literature. Jet substructure can be used to distinguish background QCD jets from those arising from the decay of new physics particles. Since this field is relatively unexplored from the perspective of SCET,

there is room for considerable progress in this area in the upcoming years.

As a first study in jet substructure, in Chapter 3 I describe a study of idealized hemisphere jets in e+e- collisions. For these jets, I did a thorough analysis of a class of event shapes called angularities, characterized by a continuous parameter a. The different angularity distributions assign differing weights to jet constituents at smaller or larger angles from the jet axis, and are dominated by jets with different pT. Thus, knowing the angularity of a jet for all values of a gives the profile of the jet.

Event shapes at hadron colliders are less interesting since it is not feasible to measure particles of arbitrarily low pT. In Chapter 4, I combine the ideas of using jet algorithms developed in Chapter 2 with the idea of measuring shapes of jets developed in Chapter 3 to measure the shape of some number M of jets in an exclusive multijet event of jet multiplicity $N \geq M$.

Another complication of predictions at hadron colliders is that all theoretical predictions must be made at the level of partons whereas measurements are made at the hadron level. As mentioned above, these two descriptions are linked for final state particles through the use of jet definitions. For the initial state interactions, a link between these two descriptions is made with parton distribution functions (PDFs), which give the probability to find a parton of momentum fraction x in a given hadron. However, because of the steepness of the PDFs in x, final states with real emission that is either highly collinear or soft is strongly favored over large angle emission, which leads to the presence of large logarithms in fixed-order predictions of the partonic level process. In Chapter 5, I discuss how these can be resummed in an arbitrary N-jet process at a hadron collider, where the jets are defined with respect to a jet algorthm.

Chapter 2

Factorization for Generic Jet Production[1]

1 Introduction

Factorization is the main ingredient in any theoretical prediction for collider experiments. Most factorization theorems are easy to understand intuitively. For example, the most basic factorization theorem for the production of lepton pairs in proton-proton collisions has the form

$$\sigma = \sum_{i,j} \hat{\sigma}_{ij} \otimes f_{i/P} \otimes f_{j/P} \,. \tag{2.1}$$

Here, the partonic cross section $\hat{\sigma}_{ij}$ describes the production of the two leptons from the two initial state partons i and j, while the parton distribution functions $f_{i/P}$ and $f_{j/P}$ describe the probability of finding the partons i and j in the proton. The parton distribution functions and the partonic cross section both depend on the momentum fractions of the partons with respect to the hadrons, and the $\otimes$ denotes the convolution in these variables. For more complicated processes, such as jet production, factorization formulas still exist, but are more complicated than for the Drell-Yan process.

While there is usually a simple intuitive picture leading to factorization theorems like Eq. (2.1), many open questions cannot be answered without a much more detailed understanding of the factorization theorem. First, precise field theoretical definitions of the different elements in terms of matrix elements of operators are required to calculate them systematically. Second, each of these elements depends on a renormalization scale μ, and the precise μ dependence cannot be obtained from the naive arguments given above. The fact that the final hadronic cross section is independent of μ allows one to derive renormalization group equations, which can be used to sum large logarithmic terms present in the perturbative results. Finally, it is important to understand under which circumstances the factorization theorems hold and when they break down. Thus, a more detailed understanding of factorization theorems is mandatory for a theoretical understanding of collider signatures.

Understanding factorization has a long history, and started with the seminal work of Collins, Soper and Sterman (see Refs. [94, 90, 92, 93] and references therein). It is instructive to

[1] This chapter was originally cowritten with Christian W. Bauer and Frank J. Tackmann [23].

remind the reader about the philosophy of these traditional factorization proofs, and to compare it to factorization proofs using effective fields theories, as discussed in this chapter. While the Lagrangian of the strong interaction is given in terms of partonic degrees of freedom, any perturbative calculation of partonic scattering amplitudes gives rise to infrared divergent results. These infrared divergences are a manifestation of the well-known fact that at long distances the strongly interacting degrees of freedom are hadrons, not partons, and that the binding of partons into hadrons is a nonperturbative effect. The infrared divergences in the partonic results are regulated, however, if the dimension of spacetime is chosen to be $D = 4 - 2\epsilon$, and manifest themselves as $1/\epsilon$ poles with $\epsilon < 0$. Thus, for $D \neq 4$ one can calculate the scattering cross section of two partons m and n, and by the same intuitive picture as before, one expects that the partonic scattering cross section factorizes as

$$\sigma_{mn} = \sum_{i,j} \hat{\sigma}_{ij} \otimes f_{i/m} \otimes f_{j/n} \,. \tag{2.2}$$

In this case, $f_{i/m}$ $[f_{j/n}]$ denotes the probability to find the parton i $[j]$ in the parton m $[n]$. This probability has a well-defined expression order by order in perturbation theory, and is infrared divergent in the limit $D \to 4$. Under the *assumption* that any infrared-safe (finite as $D \to 4$) result is the same in the hadronic ($D = 4$) and partonic ($D \neq 4$) theories, the factorization of long distance and short distance physics in the hadronic theory can be proven by showing to all orders in perturbation theory that $\hat{\sigma}_{ij}$ in the partonic theory is indeed finite in the limit $D \to 4$. Traditional factorization proofs therefore use diagrammatic techniques to show that all infrared-divergent terms in σ_{mn} are contained in the partonic distributions $f_{i/m}$ and $f_{j/n}$.

Proofs of factorization theorems in soft-collinear effective theory (SCET) [19, 21, 33, 29], on the other hand, use a different approach. By construction, the correct effective field theory reproduces the long distance dynamics of the underlying theory in a particular kinematic limit. SCET is constructed to reproduce the long distance physics for processes involving highly energetic particles, and the *assumption* is now that SCET is indeed the correct effective field theory of QCD in this particular kinematic limit. What is important is that this assumption can be tested in perturbation theory.

The physics at short distances, in general, is not properly described by the dynamics of the effective field theory itself, but can be determined by demanding that the effective theory reproduces the underlying theory order by order in perturbation theory. This matching calculation can be performed using partonic degrees of freedom, because the effective theory reproduces the long distance physics of the full theory ensuring that all infrared divergences cancel in the matching calculation. Thus, the effective theory gives a result of the form

$$\sigma = \sum_{i,j} \mathrm{SD}_{ij} \otimes \mathrm{LD}_{ij} \,, \tag{2.3}$$

where SD_{ij} describes the short distance physics governing the scattering of two partons i and j into anything, while LD_{ij} describes the long distance probability of two protons to give two partons i and j. The final step in the proof of the factorization formula is to show that

$$\mathrm{LD}_{ij} = f_{i/P} \otimes f_{j/P} \tag{2.4}$$

where $f_{i/P}$ are now matrix elements of operators defined in SCET. This is accomplished in SCET by exploiting the dynamics of the effective theory, as will be discussed in much more detail later.

The first factorization proof in SCET was for $B \to D\pi$ decays [27], but it was soon realized that SCET can be used to reproduce factorization for simple QCD processes with back-to-back jets [20, 26, 24, 160]. Recently, there has been progress in studying factorization and the resummation of perturbative corrections for some weighted cross sections in $e^+e^- \to$ hadrons [157, 124, 125, 18, 172], Drell-Yan [137, 138, 40], deep inelastic scattering [160, 82, 161, 83, 39], and Higgs production [127, 138].

While such fully inclusive observables have proven to be very useful in capturing generic features of hadronic events, they are not well suited to identify specific short distance processes. For this reason, jet observables are usually considered, in which hadrons that are "close together" are collected into jets of particles. The idea is that QCD radiation will turn a single parton produced in a short distance process into a jet of hadrons, such that the total momentum of the jet can be used as a measure of the momentum of the original parton. Thus, jet observables can be used to directly test the underlying short distance process that produced the event, as long as the jets are well separated from the beam axis and their dependence on the underlying event is very small.

Of course, the definition of a jet depends on the precise meaning of "close together", and there are many algorithms available which group the final state particles into jets [182, 88, 80, 89, 66, 68, 67, 119, 136, 113, 171, 112]. To calculate jet cross sections perturbatively, we need a jet algorithm that is infrared safe, such that a partonic calculation does not lead to infrared divergences in $D = 4$ dimensions. Which algorithm is chosen by experimentalists is usually determined by practical considerations, such as speed and algorithmic robustness.

In this chapter, we develop a factorization formalism that can be applied to any desired observable, like event shapes or jet observables. In particular, for N-jet production in hadronic collisions, we show that the cross section factorizes into a hard function, $\hat{\sigma}_{ij,k_1\ldots k_N}$, describing the underlying partonic process to produce N partons, convoluted with N jet functions, J_{k_i}, a soft function, S, and parton distribution functions, $f_{i,j/P}$,

$$\sigma = \sum_{i,j,k_n} \hat{\sigma}_{ij,k_1\ldots k_N} \otimes J_{k_1} \otimes \cdots \otimes J_{k_N} \otimes S \otimes f_{i/P} \otimes f_{j/P}\,. \tag{2.5}$$

The jet functions J_{k_i} are the final-state analog of the parton distribution functions. They describe how the final partons from the hard interaction evolve into the observed jets, and contain all dependence on the actual jet algorithm. The soft function S is a nonperturbative object, which describes, for example, how color is rearranged to allow the colored partons to form color-singlet jets. The effective theory allows to give precise field-theoretic definitions of all objects in this factorization formula. Whether the differential cross section in some observable factorizes in the usual sense depends on whether the observable is dominated by factorizable kinematic configurations and whether it is inclusive enough to allow perturbative calculations of the jet functions.

In Sec. 2, we first define a generic differential cross section written in terms of functional derivatives, and then show in Sec. 3 how observables are constructed from this generic cross section. In Sec. 4, we derive a factorization formula for this differential cross section, which relates it to convolutions over generic building blocks. To focus on the overall structure of the result, this derivation will be schematic in the sense that we will ignore the explicit color and spin structure of the underlying interaction. As a first example, in Sec. 5, we apply our results to the production of two-jet events in e^+e^- collisions, including all color and spin information. We reproduce the known results for event shape and hemisphere mass distributions, and obtain results for observables based

on cone jet algorithms. In Sec. 6, we apply our formalism to hadronic collisions. We derive the factorization formula for two-jet production in pp collisions, focussing on the simplest subprocess $qq' \to qq'$. Our conclusions and outlook are presented in Sec. 7.

2 Energy and three-momentum configuration of an event

The differential cross section in any observable O is given by

$$\frac{\mathrm{d}\sigma}{\mathrm{d}O} = \frac{1}{2p_I^2} \sum_X |\langle X|\mathcal{Q}|I\rangle|^2 \, (2\pi)^4 \delta^4(p_I - p_X) \, \delta[O - f_O(X)] \,, \tag{2.6}$$

where $|I\rangle$ denotes the initial state containing two particles with total momentum $p_I = (E_{\mathrm{cm}}, \mathbf{0})$, $|X\rangle$ denotes an arbitrary final state with total momentum p_X, and the sum over X includes a sum over states, as well as all final-state phase-space integrations. Finally, $\mathcal{Q}$ stands for the relevant operator responsible for the underlying hard interaction.

The function $f_O(X)$ computes the value of the observable for a given final state X, and in general depends on the four-momenta of all particles in X. The four-momentum configuration of X can be described by its energy configuration $\omega_X(\Omega)$ and three-momentum configuration $\mathbf{k}_X(\Omega)$. If X has n particles with four-momenta $p_i = (E_i, \mathbf{p}_i)$, we have

$$\omega_X(\Omega) = \sum_{i=1}^n E_i \, \delta(\Omega - \Omega_i) \,, \qquad \mathbf{k}_X(\Omega) = \sum_{i=1}^n \mathbf{p}_i \, \delta(\Omega - \Omega_i) \,, \tag{2.7}$$

where $\Omega_i \equiv \Omega(\mathbf{p}_i)$ is the direction of the three-momentum $\mathbf{p}_i$. More generally, we can think of $\omega(\Omega)$ and $\mathbf{k}(\Omega)$ as the distribution of energy and three-momentum over the solid angle Ω, as measured experimentally.

To integrate over ω and $\mathbf{k}$, we define a functional integration measure as usual by discretization. We divide Ω into bins $\{\Omega_k\}$, and define the set of discrete variables $\{\omega_k\}$ and $\{\mathbf{k}_k\}$ as the integrals of $\omega(\Omega)$ and $\mathbf{k}(\Omega)$ over the bins $\{\Omega_k\}$,[2]

$$\omega_k = \int_{\Omega_k} \mathrm{d}\Omega \, \omega(\Omega) \,, \qquad \mathbf{k}_k = \int_{\Omega_k} \mathrm{d}\Omega \, \mathbf{k}(\Omega) \,. \tag{2.8}$$

Then

$$\begin{aligned} \mathcal{D}\omega(\Omega) &\equiv \mathcal{D}\omega(\Omega) \, \theta[\omega(\Omega)] = \prod_k \mathrm{d}\omega_k \, \theta(\omega_k) \,, \\ \mathcal{D}\mathbf{k}(\Omega) &\equiv \mathcal{D}\mathbf{k}(\Omega) \, \delta[\Omega(\mathbf{k}(\Omega)) - \Omega] = \prod_k \frac{\mathrm{d}^3\mathbf{k}_k}{(2\pi)^3} \, \delta(\Omega(\mathbf{k}_k) - \Omega_k) = \prod_k \frac{|\mathbf{k}_k|^2 \, \mathrm{d}\,|\mathbf{k}_k|}{(2\pi)^3} \,. \end{aligned} \tag{2.9}$$

The θ-functional in $\mathcal{D}\omega(\Omega)$ restricts $\omega(\Omega)$ to be positive, while the δ-functional in $\mathcal{D}\mathbf{k}(\Omega)$ restricts $\mathbf{k}(\Omega)$ to point into the direction Ω.

[2]This is slightly different from the usual definition of $\mathcal{D}\phi(x)$ for some field $\phi(x)$, where the discrete variables $\phi_k = \phi(x_k)$ are taken as the values of ϕ at the points x_k. The difference is an irrelevant overall constant. In our case, taking the integrals is the more natural choice and makes the connection to the usual phase-space integration simpler.

The integration measure in Eq. (2.9) still includes unphysical configurations. To only allow physical configurations, we have to include a mass-shell condition. Taking a fixed invariant-mass distribution $\mu(\Omega)$ as boundary condition, we get

$$\begin{aligned}\int_{\mu(\Omega)} \mathcal{D}\omega(\Omega)\,\mathcal{D}\mathbf{k}(\Omega) &\equiv \int \mathcal{D}\omega(\Omega)\,\mathcal{D}\mathbf{k}(\Omega)\,\delta\big[\omega(\Omega)^2 - \mathbf{k}(\Omega)^2 - \mu(\Omega)^2\big] \\ &= \int \prod_k \mathrm{d}\omega_k\,\frac{|\mathbf{k}_k|^2\,\mathrm{d}\,|\mathbf{k}_k|}{(2\pi)^3}\,\delta(\omega_k^2 - |\mathbf{k}_k|^2 - \mu_k^2)\,\theta(\omega_k)\,, \end{aligned} \tag{2.10}$$

where $\mu_k = \int_{\Omega_k} \mathrm{d}\Omega\,\mu(\Omega)$. This fixes the direction of all particles, but could include different final states X, as long as they have the same invariant-mass distribution $\mu(\Omega)$. If we instead restrict the integration to a state X, having n particles with masses m_i, we recover the standard n-body phase space for X,

$$\begin{aligned}\int_X \mathcal{D}\omega(\Omega)\,\mathcal{D}\mathbf{k}(\Omega) &\equiv \int \prod_{i=1}^n \mathrm{d}\Omega_i \int_{X(\Omega_1,\ldots,\Omega_n)} \mathcal{D}\omega(\Omega)\,\mathcal{D}\mathbf{k}(\Omega) \\ &= \int \prod_{i=1}^n \mathrm{d}\Omega_i \int \prod_{k=1}^n \mathrm{d}\omega_k\,\frac{|\mathbf{k}_k|^2\,\mathrm{d}\,|\mathbf{k}_k|}{(2\pi)^3}\,\delta(\omega_k^2 - |\mathbf{k}_k|^2 - m_k^2)\,\theta(\omega_k) \\ &= \int \prod_{i=1}^n \frac{\mathrm{d}^4 p_i}{(2\pi)^3}\,\delta(p_i^2 - m_i^2)\,\theta(p_i^0) \equiv \int \mathrm{d}\Phi_X\,. \end{aligned} \tag{2.11}$$

On the right-hand side of the first line, we first integrate $\omega(\Omega)$ and $\mathbf{k}(\Omega)$ with the boundary condition that there are exactly n particles with masses m_i moving in the directions Ω_i, denoted as $X(\Omega_1,\ldots,\Omega_n)$, which is then integrated over the particle's positions Ω_i. In the second line, in the discretization only the integrals over those n bins survive that happen to contain a particle. Together with the Ω_i integrations, this reduces to the standard n-body phase space for X. In the following, we will mostly drop the dependence of $\omega(\Omega)$ and $\mathbf{k}(\Omega)$ on Ω, but one should always keep in mind that ω and $\mathbf{k}$ are *functions* of Ω. We will still use square brackets to denote functionals $f[\omega]$ and $f[\mathbf{k}]$.

Returning to Eq. (2.6), we now assume that $f_O(X)$ does not depend on any internal quantum numbers of X, but only on the four-momenta of all particles in X.[3] In this case, f_O can be written as a functional of the energy and three-momentum configurations,

$$f_O \equiv f_O[\omega, \mathbf{k}] \qquad \text{with} \qquad f_O(X) \equiv f_O[\omega_X, \mathbf{k}_X]\,. \tag{2.12}$$

We now define an energy-momentum flow operator $\mathcal{E}^\mu \equiv \mathcal{E}^\mu(\Omega)$, whose eigenvalues are the energy and three-momentum configurations of the state $|X\rangle$ in Eq. (2.7),

$$\mathcal{E}^0(\Omega)\,|X\rangle = \omega_X(\Omega)\,|X\rangle\,, \qquad \boldsymbol{\mathcal{E}}(\Omega)\,|X\rangle = \mathbf{k}_X(\Omega)\,|X\rangle\,. \tag{2.13}$$

The energy flow operator $\mathcal{E}^0(\Omega)$ has been used previously, for example to study two-jet event shape distributions [150, 146, 152, 44, 157, 18] and jet energy-flow correlations [185, 184, 186, 133]. In

[3]Note that most information about internal quantum numbers, such as the number of b-jets, is obtained from four-momentum information alone.

terms of the energy-momentum tensor

$$T^{\mu\nu} = \sum_{\phi\in\mathcal{L}} \frac{\partial\mathcal{L}}{\partial(\partial_\mu\phi)}\,\partial^\nu\phi - g^{\mu\nu}\mathcal{L}\,, \tag{2.14}$$

we can write $\mathcal{E}^\mu(\Omega)$ as [150, 18]

$$\mathcal{E}^\mu(\Omega) = \lim_{R\to\infty} R^2 \int_0^\infty \mathrm{d}t\,\mathbf{n}^i\,T^{\mu i}(t, R\,\mathbf{n})\,. \tag{2.15}$$

Here, $\mathbf{n}\equiv\mathbf{n}(\Omega)$ is the unit three-vector pointing in the direction identified by Ω. Therefore, $\mathcal{E}^\mu(\Omega)$ measures the total four-momentum arriving over time at infinity in the direction Ω. An expression for $\mathcal{E}^0(\Omega)$ similar to Eq. (2.15) in terms of an integral over R for $t\to\infty$ was derived in Refs. [184, 84]. An explicit proof of Eq. (2.15) for $\mathcal{E}^0(\Omega)$ for scalars and Dirac fermions can be found in Ref. [18].

Using Eqs. (2.12) and (2.13), we can write Eq. (2.6) as

$$\begin{aligned}\frac{\mathrm{d}\sigma}{\mathrm{d}O} &= \frac{1}{2p_I^2}\sum_X \langle I|\mathcal{Q}^\dagger|X\rangle\langle X|\mathcal{Q}|I\rangle\,(2\pi)^4\delta^4(p_I-p_X)\,\delta(O-f_O[\omega_X,\mathbf{k}_X]) \\ &= \frac{1}{2p_I^2}\int\mathcal{D}\omega\,\mathcal{D}\mathbf{k}\int\mathrm{d}^4x\,\langle I|\mathcal{Q}^\dagger(x)\,\delta[\omega-\mathcal{E}^0]\,\delta[\mathbf{k}-\boldsymbol{\mathcal{E}}]\mathcal{Q}(0)|I\rangle\,\delta(O-f_O[\omega,\mathbf{k}]) \\ &\equiv \int\mathcal{D}\omega\,\mathcal{D}\mathbf{k}\,\frac{\delta\sigma}{\delta\omega\,\delta\mathbf{k}}\,\delta(O-f_O[\omega,\mathbf{k}])\,. \end{aligned}\tag{2.16}$$

In the second line, we shift $\mathcal{Q}^\dagger$ to position x, turning the momentum conservation into an integral over x, and rewrite ω_X and $\mathbf{k}_X$ in terms of $\mathcal{E}^\mu$. This removes any explicit dependence on the final state X, allowing us to perform the sum over all final states states $\sum_X |X\rangle\,\langle X| = 1$.

For the rest of this chapter, we will assume for simplicity that X only contains massless particles. The extension to the general case is straightforward. In this case, $f_O\equiv f_O[\omega]$ only depends on ω, and we can integrate over $\mathbf{k}$ to find

$$\frac{\mathrm{d}\sigma}{\mathrm{d}O} = \int\mathcal{D}\omega\,\frac{\delta\sigma}{\delta\omega}\,\delta(O-f_O[\omega])\,, \tag{2.17}$$

where the generic differential cross section $\delta\sigma/\delta\omega$ is defined as

$$\begin{aligned}\frac{\delta\sigma}{\delta\omega} &= \frac{1}{2p_I^2}\int\mathrm{d}^4x\,\langle I|\mathcal{Q}^\dagger(x)\,\delta[\omega-\mathcal{E}^0]\,\mathcal{Q}(0)|I\rangle \\ &= \frac{1}{2p_I^2}\int\frac{\mathrm{d}^4p}{(2\pi)^4}\,\langle I|\mathcal{Q}^\dagger(0)\,\delta[\omega-\mathcal{E}^0]\,\mathcal{Q}(p)|I\rangle\,. \end{aligned}\tag{2.18}$$

In the second line, we have written the result in terms of $\mathcal{Q}(p)$, the Fourier transform of $\mathcal{Q}(x)$. (To simplify the notation we use the same symbol for operators in position and momentum space and simply distinguish them by their arguments.)

Equation (2.17) can be regarded as the master formula of our formalism, and its ingredients are the subject of the following sections. We first discuss the functional $f_O[\omega]$ in the next section and then the factorization of $\delta\sigma/\delta\omega$ in Sec. 4. Then in Secs. 5 and 6 we show how to combine these two elements to obtain a factorized form of $\mathrm{d}\sigma/\mathrm{d}O$ for specific processes and observables.

3 Constructing Observables

The form of the functional $f_O[\omega]$ depends on the observable under consideration, and in this section we will give a few examples of how to construct $f_O[\omega]$ for specific observables. To get used to our notation, we start with the simple example of the total four-momentum of the final state. Next, we consider event shapes, which are fully inclusive observables. Finally, we discuss jet observables, which are less inclusive and defined with respect to a specific jet algorithm.

3.1 Total Four-Momentum

The total energy and three-momentum of the state X are

$$E_X = \sum_{i=1}^{n} E_i = \int \mathrm{d}\Omega\, \omega_X(\Omega)\,, \qquad \mathbf{p}_X = \sum_{i=1}^{n} \mathbf{p}_i = \int \mathrm{d}\Omega\, \mathbf{n}(\Omega)\, \omega_X(\Omega)\,, \tag{2.19}$$

where we used that for massless particles $\mathbf{k}(\Omega) = \mathbf{n}(\Omega)\,\omega(\Omega)$. Hence, we define

$$P^\mu[\omega] = \int \mathrm{d}\Omega\, n^\mu(\Omega)\, \omega(\Omega)\,, \tag{2.20}$$

where $n^\mu(\Omega) = (1, \mathbf{n}(\Omega))$. From Eqs. (2.17) and (2.18) we get

$$\frac{\mathrm{d}\sigma}{\mathrm{d}^4 P} = \int \mathcal{D}\omega\, \frac{\delta\sigma}{\delta\omega}\, \delta^4(P - P[\omega]) = \frac{1}{2p_I^2} \int \mathrm{d}^4 x\, \langle I|\mathcal{Q}^\dagger(x)\, \delta^4(P - \hat{P})\, \mathcal{Q}(0)|I\rangle\,. \tag{2.21}$$

In the second step we performed the integration over ω and used that (for massless fields) $P^\mu[\mathcal{E}^0]$ yields the momentum operator $\hat{P}^\mu = (\hat{P}^0, \hat{\mathbf{P}})$,[4]

$$P^\mu[\mathcal{E}^0] = \int \mathrm{d}\Omega\, \mathcal{E}^\mu(\Omega) = \lim_{t\to\infty} \int \mathrm{d}\mathbf{x}\, T^{\mu 0}(t, \mathbf{x}) = \hat{P}^\mu\,. \tag{2.23}$$

3.2 Event Shapes

Event shapes are defined with respect to the thrust axis of an event. Given a final state X, one first calculates the thrust axis $\mathbf{t} \equiv \mathbf{t}(X)$, which is defined as the unit three-vector $\mathbf{t}$ that maximizes the sum

$$\sum_{i=1}^{n} |\mathbf{t}\cdot\mathbf{p}_i|\,, \tag{2.24}$$

which runs over all particles in X. Given $\mathbf{t}$, one then calculates the observable of interest. A generic class of event shapes can be written as

$$f_e(X) = \frac{1}{E_{\mathrm{cm}}} \sum_{i=1}^{n} g_e(\eta_{\mathbf{t}}(p_i))\, \left|\mathbf{p}_{\mathbf{t}}^T(p_i)\right|\,, \tag{2.25}$$

[4]To see this explicitly, consider the current $j^\nu(x) \equiv T^{\mu\nu}(x)$ (for fixed μ),

$$\int \mathrm{d}\Omega\, \mathcal{E}^\mu(\Omega) = \lim_{R\to\infty} \int_0^\infty \mathrm{d}t \int_{\partial S(R)} \mathrm{d}S\, \mathbf{n}\cdot\mathbf{j}(t,\mathbf{x}) = \int_0^\infty \mathrm{d}t \int \mathrm{d}\mathbf{x}\, \boldsymbol{\nabla}\cdot\mathbf{j}(t,\mathbf{x}) = \lim_{t\to\infty} \int \mathrm{d}\mathbf{x}\, j^0(t,\mathbf{x})\,, \tag{2.22}$$

where in the last step we used current conservation $\partial_\mu j^\mu(x) = 0$.

where the rapidity $\eta_{\mathbf{t}}$ and transverse momentum $\mathbf{p}_{\mathbf{t}}^T$ are measured with respect to $\mathbf{t}$. For example, for thrust [55, 123], jet broadening [75], and the C-parameter [111], the function $g_e(\eta)$ has the form

$$g_T(\eta) = e^{-|\eta|}\,, \qquad g_B(\eta) = 1\,, \qquad g_C(\eta) = \frac{3}{\cosh\eta}\,. \tag{2.26}$$

The thrust axis can be obtained from the energy configuration of the final state, and can therefore be written as a functional $\mathbf{t}[\omega]$. It is defined (for massless particles) as maximizing the integral

$$\int \mathrm{d}\Omega\ |\mathbf{t}\cdot\mathbf{n}(\Omega)|\ \omega(\Omega)\,, \tag{2.27}$$

which for $\omega = \omega_X$ reduces to Eq. (2.24). Using $\left|\mathbf{p}_{\mathbf{t}}^T\right| = E/\cosh\eta_{\mathbf{t}}$, we can write Eq. (2.25) in terms of ω

$$f_e[\omega] = \int \mathrm{d}\mathbf{t}\,\delta(\mathbf{t}-\mathbf{t}[\omega])\,f_e[\omega;\mathbf{t}]\,, \tag{2.28}$$

with

$$f_e[\omega;\mathbf{t}] = \frac{1}{E_{\mathrm{cm}}}\int \mathrm{d}\Omega\, g_e(\eta_{\mathbf{t}})\,\frac{\omega(\Omega)}{\cosh\eta_{\mathbf{t}}}\,, \tag{2.29}$$

where the solid angle Ω is decomposed with respect to the thrust axis as $\Omega = (\eta_{\mathbf{t}}, \phi_{\mathbf{t}})$, and $\eta_{\mathbf{t}} = \tanh^{-1}(\cos\theta_{\mathbf{t}})$.

3.3 Jet Observables

3.3.1 General Features of Jet Algorithms

A jet algorithm $\mathcal{J}$ acting on a final state X returns the set of momenta of all particles in the event, grouped together into the different subsets belonging to each jet plus a set of particles not belonging to any jet, which we take to be soft:

$$\mathcal{J}(X) = \{\{p^\mu\}_1, \ldots, \{p^\mu\}_{\mathcal{N}}, \{p^\mu\}_s\}\,. \tag{2.30}$$

In terms of the energy configuration ω, we can write the action of the jet algorithm as

$$\mathcal{J}[\omega] = \{\omega_1^{\mathrm{jet}}, \ldots, \omega_{\mathcal{N}}^{\mathrm{jet}}, \omega^{\mathrm{soft}}\}\,, \tag{2.31}$$

where ω_i^{jet} is the part of ω corresponding to jet i, and ω^{soft} is the remaining soft part of ω not assigned to any jet, such that

$$\omega = \omega_1^{\mathrm{jet}} + \cdots + \omega_{\mathcal{N}}^{\mathrm{jet}} + \omega^{\mathrm{soft}}\,. \tag{2.32}$$

We formally split the action of the jet algorithm into two distinct steps. We first define a quantity $\mathbf{j}$ that contains all global information about ω required to construct the individual jet configurations ω_i from ω. For example, $\mathbf{j}$ contains the total number of jets and the direction of each jet. That is, $\mathbf{j}$ is analogous to the thrust axis in the case of event shapes. Hence, a jet algorithm $\mathcal{J}$ provides a functional $\mathbf{j}_{\mathcal{J}}[\omega]$, which returns the required information $\mathbf{j}$ for a given ω. Second, we define functionals $\mathcal{J}_i[\omega;\mathbf{j}]$ that project out the part of ω belonging to the i-th jet. That is, for $\mathbf{j} = \mathbf{j}_{\mathcal{J}}[\omega]$, by definition

$$\mathcal{J}_i[\omega;\mathbf{j}_{\mathcal{J}}[\omega]] = \omega_i^{\mathrm{jet}}\,, \qquad \mathcal{J}_s[\omega;\mathbf{j}_{\mathcal{J}}[\omega]] = \omega^{\mathrm{soft}}\,. \tag{2.33}$$

We stress that $\mathcal{J}_i[\omega;\mathbf{j}]$ only encodes the actual projection, which is completely specified by the specifics of the jet algorithm and the information provided by $\mathbf{j}$. Thus, for a given $\mathbf{j}$, $\mathcal{J}_i$ can be applied to any ω. For example, by definition, $\mathcal{J}_i$ satisfies the consistency conditions

$$\mathcal{J}_i\big[\omega_j^{\text{jet}};\mathbf{j}_{\mathcal{J}}[\omega]\big] = \begin{cases} \omega_i^{\text{jet}} & \text{for} \quad i = j \\ 0 & \text{for} \quad i \neq j\,. \end{cases} \tag{2.34}$$

For simplicity, we will keep the dependence on $\mathcal{J}$ implicit from now on and simply write $\mathbf{j}[\omega]$.

3.3.2 Construction of Jet Observables

We can now write a generic jet observable as

$$f_O[\omega] = \int \mathrm{d}\mathbf{j}\, \delta(\mathbf{j} - \mathbf{j}[\omega])\, f_O[\omega;\mathbf{j}]\,, \tag{2.35}$$

where, in general, $f_O[\omega;\mathbf{j}]$ has the form

$$f_O[\omega;\mathbf{j}] = f_O[\mathcal{J}_1[\omega;\mathbf{j}],\ldots,\mathcal{J}_{\mathcal{N}}[\omega;\mathbf{j}]]\,, \tag{2.36}$$

and $\mathcal{N}$ is the total number of jets given by $\mathbf{j}$. Most jet observables only depend on the total four-momentum of each jet. In this case, using Eq. (2.20)[5], we have

$$f_O[\omega;\mathbf{j}] = \left[\prod_{i=1}^{\mathcal{N}} \int \mathrm{d}^4P_i\, \delta^4(P_i - P[\mathcal{J}_i[\omega;\mathbf{j}]])\right] g_O(P_1,\ldots,P_{\mathcal{N}})\,. \tag{2.37}$$

The function $g_O(P_1,\ldots,P_{\mathcal{N}})$ computes the observable of interest from the given jet momenta P_i. It is analogous to the function $g_e(\eta)$ for event shapes. Some simple examples would be the total number of jets or the invariant mass of two jets,

$$g_{\mathcal{N}}(P_1,\ldots,P_{\mathcal{N}}) = \mathcal{N}\,, \qquad g_{m_{ij}}(P_1,\ldots,P_{\mathcal{N}}) = (P_i + P_j)^2\,. \tag{2.38}$$

Similar to Eq. (2.37), one can easily define observables depending on additional information about the individual jets, for example, one can imagine observables which depend on a weighted integral of the energies of all particles in a jet.

3.3.3 Examples of Jet Algorithms

Of course, in practice, how the action of the jet algorithm is separated into $\mathbf{j}[\omega]$ and $\mathcal{J}_i[\omega;\mathbf{j}]$ depends on the actual algorithm, and we will briefly discuss a few examples here. Since most jet algorithms do not have a simple analytic expression for generic final states, it will not be possible to obtain $\mathbf{j}[\omega]$ analytically, either. However, this is not a limitation, because we can always define $\mathbf{j}[\omega]$ by acting with the full jet algorithm on ω and only returning the necessary global information. The more relevant, and perhaps nontrivial, task is to figure out the information required in $\mathbf{j}$, and to define the projections $\mathcal{J}_i[\omega;\mathbf{j}]$ accordingly.

[5]For jet algorithms, Eq. (2.20) corresponds to the so-called E-scheme, which defines the total jet momentum as the sum of the particle momenta.

The simplest example is probably the hemisphere jet algorithm [88, 80, 89], for which the number of jets is always 2, and the only relevant global information is the axis perpendicular to the plane separating the two hemispheres, which is usually taken to be the thrust axis $\mathbf{t}$. Hence, we can write $\mathbf{j}$ as

$$\mathbf{j} = \{2; \mathbf{t}\}\,, \qquad \mathbf{j}[\omega] = \{2; \mathbf{t}[\omega]\}\,, \tag{2.39}$$

where by convention we included the number of jets in $\mathbf{j}$. The corresponding projections $\mathcal{J}_1$ and $\mathcal{J}_2$ return the two hemispheres defined by the thrust axis,

$$\mathcal{J}_1[\omega; \mathbf{j}] = \omega(\Omega)\,\theta\big(0 \le \theta_{\mathbf{t}} < \pi/2\big)\,, \qquad \mathcal{J}_2[\omega; \mathbf{j}] = \omega(\Omega)\,\theta\big(\pi/2 \le \theta_{\mathbf{t}} < \pi\big)\,, \tag{2.40}$$

where $\Omega \equiv (\theta_{\mathbf{t}}, \phi_{\mathbf{t}})$ is given with respect to $\mathbf{t}$. Note that here we have $\mathcal{J}_s[\omega, \mathbf{j}] = 0$. Typical observables constructed from these individual jets are their invariant masses, $g_{M^2_{1,2}}(P_1, P_2) = P^2_{1,2}$. Another class of observables is given by the event shapes in Eq. (2.29), for which $f_O[\omega, \mathbf{j}] \equiv f_e[\omega, \mathbf{t}]$.

A less trivial example is a cone jet algorithm [182, 136, 113, 171, 112]. In this case, the necessary global information returned by $\mathbf{j}[\omega]$ is the number of jets $\mathcal{N}$, and the direction $\mathbf{j}_i$ of each jet,

$$\mathbf{j} = \{\mathcal{N}; \mathbf{j}_1, \ldots, \mathbf{j}_{\mathcal{N}}\}\,. \tag{2.41}$$

For instance, in e^+e^- collisions one can define an $\mathcal{N}$-jet final state as one admitting a minimum number $\mathcal{N}$ directions $\mathbf{j}_i$ such that the total energy outside an opening half angle R about each direction is less than some fraction ϵ. For $\mathcal{N} = 2$, and with the additional constraint $\mathbf{j}_1 = -\mathbf{j}_2$, this is equivalent to the original Sterman-Weinberg jet definition [182]. For a given set $\mathbf{j}$, the projections are then simply

$$\mathcal{J}_i[\omega; \mathbf{j}] = \omega(\Omega)\,\theta(R - \theta_{\mathbf{j}_i})\,, \tag{2.42}$$

where R is the cone radius and $\Omega \equiv (\theta_{\mathbf{j}_i}, \phi_{\mathbf{j}_i})$ is given with respect to $\mathbf{j}_i$ for each i.

As with all observables, we require jet algorithms that are infrared safe, which is not the case for many cone jet algorithms. An example of an infrared-safe cone jet algorithm is the seedless infrared-safe (SIS) cone jet algorithm [171]. For illustration of our method, we will use the snowmass cone algorithm [136, 112] as an example, however our approach can easily be adapted to the SIS algorithm or any other infrared-safe jet algorithm.

For hadronic collisions, the variables (η, ϕ), defined with respect to the beam axis, have simple transformations under boosts along the beam direction, and so are favored over (θ, ϕ). In the Snowmass cone algorithm, jets are defined by cones of constant radius R in (η, ϕ) space. When applied to massless particles, the directions $\mathbf{j}_i$ are given by the solutions of [6]

$$0 = \int \mathrm{d}\Omega\, \frac{\omega(\Omega)}{\cosh\eta}\, [\Omega - \Omega(\mathbf{j}_i)]\, \theta\big(R - \sqrt{[\eta - \eta(\mathbf{j}_i)]^2 + [\phi - \phi(\mathbf{j}_i)]^2}\big)\,, \tag{2.43}$$

where $\Omega = (\eta, \phi)$ is now measured with respect to the beam axis, and $\Omega(\mathbf{j}_i) = (\eta(\mathbf{j}_i), \phi(\mathbf{j}_i))$ are the coordinates of the i-th jet direction. Equation (2.43) is the analog of Eq. (2.27) for the thrust axis. The corresponding projections are

$$\mathcal{J}_i[\omega; \mathbf{j}] = \omega(\Omega)\,\theta\big(R - \sqrt{[\eta - \eta(\mathbf{j}_i)]^2 + [\phi - \phi(\mathbf{j}_i)]^2}\big)\,. \tag{2.44}$$

[6] For some configurations ω, this equation can admit multiple sets of solutions $\mathbf{j}$, containing a different number of jets. This happens when there are overlapping cones, and one has to decide whether to split or merge these.

Finally, k_T jet algorithms [66, 68, 67, 119] also fit our general definition of algorithms. Although their definition contains a cut on some distance measure, the precise size and shape of a jet also depends on the details of the energy configuration ω. Hence, there is no simple expression for the projections $\mathcal{J}_i[\omega;\mathbf{j}]$ for arbitrary ω and $\mathbf{j}$. In principle, they are well defined (albeit complicated) for a fixed number of particles, in which case integrals over the energy configuration reduce to normal phase space integrals [see Eq. (2.11)]. In practical applications, it is easiest to apply the algorithm numerically.

4 Factorization of $\delta\sigma/\delta\omega$

In this section, we prove a factorization theorem for the generic differential distribution $\delta\sigma/\delta\omega$ defined in Eq. (2.18). This will allow us to separate the various scales in the problem and write our result in terms of convolutions over simpler functions, each of which captures only the physics at a certain energy scale. The factorization proof uses arguments similar to those used to prove factorization for event shape distributions in Ref. [18]. The central ingredient in addition to the usual factorization of soft and collinear degrees of freedom in SCET will be the use of the energy flow operator $\mathcal{E}^\mu(\Omega)$ defined in Eq. (2.15).

When deriving the factorization formula, we will ignore all color and spin structure of the SCET operators, and denote all collinear fields by ϕ, regardless of whether they correspond to quarks, anti-quarks or gluons. This schematic notation will allow us to focus on the issues directly related to the proof of factorization. Of course, to obtain the full result for the cross section, the color and spin information has to be included, and we illustrate how this is achieved when discussing explicit examples in Secs. 5 and 6.

4.1 Matching QCD onto SCET in Momentum Space

Usually, the matching of QCD onto SCET is performed in position space by expanding the relevant QCD operator $\mathcal{Q}(x)$ in terms of SCET operators $\mathcal{O}(x)$,

$$\mathcal{Q}(x) = \sum_{\{n_i,\tilde{p}_i\}} e^{-\mathrm{i}\sum \tilde{p}_i\cdot x}\, C_{\{n_i\}}(\{\tilde{p}_i\})\, \mathcal{O}_{\{n_i,\tilde{p}_i\}}(x)\,. \tag{2.45}$$

Here, $C_{\{n_i\}}\mathcal{O}_{\{n_i,\tilde{p}_i\}}$ stands for a sum over several SCET operators with the same number of collinear directions, each with its own Wilson coefficient. The Wilson coefficients are determined by taking matrix elements of both sides, and expanding the full-theory matrix elements $\langle\mathcal{Q}(x)\rangle$ in terms of the matrix elements $\langle\mathcal{O}(x)\rangle$ evaluated in SCET. Note also that at this point the operators include all incoming and outgoing fields, whether they are strongly interacting or not.

The operator $\mathcal{O}_{\{n_i,\tilde{p}_i\}}(x)$ is written in terms of (gauge-invariant) collinear SCET fields $\phi_{n,\tilde{p}}(x)$. Each field depends on a large label momentum $\tilde{p}^\mu = \tilde{p}^- n^\mu/2 + \tilde{p}_\perp^\mu$ with $n^2 = 0$ and $\tilde{p}_\perp \sim \mathcal{O}(\lambda\tilde{p}^-)$, and has a residual x dependence corresponding to a residual momentum $k \sim \mathcal{O}(\lambda^2\tilde{p}^-)$, so the total momentum of the field is $p = \tilde{p} + k$. Thus, one can think of the fields $\phi_{n,\tilde{p}}(x)$ as being written in label momentum space and residual position space. With this interpretation, the sum over all labels n_i and $\tilde{p}_i$ in Eq. (2.45) corresponds to taking the remaining label Fourier transform to convert the right-hand side to full position space.

This separation into discrete label and continuous residual components is conceptually convenient when formulating the effective theory, and means that phase space is divided up as

$$\int \mathrm{d}^4 p = \sum_{n,\tilde{p}} \int \mathrm{d}^4 k \,. \tag{2.46}$$

The concrete choice of the discrete labels n and $\tilde{p}$ is determined by the external momenta. As is well-known, this choice is arbitrary at subleading order in λ, which can be exploited to derive constraints from reparametrization invariance [81, 162].

However, in practical applications, especially with more than one collinear direction, the label choice can easily get obscured during the calculation. One example is four-momentum conservation for two back-to-back jets with collinear momenta $p_1 = \tilde{p}_1 + k_1$ and $p_2 = \tilde{p}_2 + k_2$,

$$\int \mathrm{d}^4 x \, e^{\mathrm{i}(\tilde{p}_1 - \tilde{p}_2 + k_1 - k_2)\cdot x} = \delta_{\tilde{p}_1,\tilde{p}_2} \int \mathrm{d}^4 x \, e^{\mathrm{i}(k_1 - k_2)x} = \delta_{\tilde{p}_1,\tilde{p}_2+\delta_k} \int \mathrm{d}^4 x \, e^{\mathrm{i}(k_1 - k_2 + \delta_k)x} \,, \tag{2.47}$$

where $\delta_k \sim \mathcal{O}(k_{1,2})$. Both equations are correct and correspond to different choices of the label momenta. Using the first equality, as is often done, may seem somewhat ad hoc, but one simply makes an implicit choice of, say, $\tilde{p}_2$ relative to $\tilde{p}_1$. Of course, this is only justified if $\tilde{p}_2$ was not already chosen somewhere else. Furthermore, at the end of the day, one often has to recombine some leftover label sums and residual integrations, e.g.,

$$\sum_n \int \mathrm{d}k_\perp \sim \int \mathrm{d}\Omega \,, \tag{2.48}$$

corresponding to unconstrained phase space integrations of external particles.

With several collinear directions, keeping track of all label choices and dealing with leftover label sums and residual integrations quickly becomes very cumbersome. To avoid all of these issues, it is convenient to perform the matching entirely in momentum space, so Eq. (2.45) becomes

$$\mathcal{Q}(p) = \sum_{\{n_i,\tilde{p}_i\}} \biggl(\prod_i \int \frac{\mathrm{d}^4 k_i}{(2\pi)^4} \biggr) (2\pi)^4 \delta^4\Bigl(p - \sum_i (\tilde{p}_i + k_i) \Bigr) \, C_{\{n_i\}}(\{\tilde{p}_i\}) \, \mathcal{O}_{\{n_i,\tilde{p}_i\}}(\{k_i\}) \,. \tag{2.49}$$

Here, $\mathcal{Q}(p)$ is the Fourier transform of $\mathcal{Q}(x)$, and $\mathcal{O}_{\{n_i,\tilde{p}_i\}}(\{k_i\})$ is written in terms of momentum-space SCET fields, $\phi_{n,\tilde{p}}(k)$, which are obtained by taking the remaining residual Fourier transform of $\phi_{n,\tilde{p}}(x)$,

$$\phi_{n,\tilde{p}}(k) = \int \mathrm{d}^4 x \, e^{\mathrm{i}k\cdot x} \, \phi_{n,\tilde{p}}(x) \,. \tag{2.50}$$

We can imagine that the matching is performed at fixed total momentum $p_i = \tilde{p}_i + k_i$ of each field in $\mathcal{O}_{\{n_i,\tilde{p}_i\}}$. We then choose the field labels directly during the matching such that $\mathbf{n} = \mathbf{p}/|\mathbf{p}|$ for each field. With this choice, $\tilde{p}^- \equiv p^- = p^0 + |\mathbf{p}|$, $p^+ \equiv k^+ = p^0 - |\mathbf{p}|$, and $p_\perp = 0$. This allows us to recombine the label sums and residual integrations in Eq. (2.49) into $\mathrm{d}^4 p_i$ integrals[7]

$$\sum_{n,\tilde{p}} \int \frac{\mathrm{d}^4 k}{(2\pi)^4} \equiv \int \frac{\mathrm{d}^4 p}{(2\pi)^4} = \int \frac{\mathrm{d}p^- \mathrm{d}p^+ \, \mathrm{d}\Omega}{(2\pi)^4} \, \frac{(p^- - p^+)^2}{8} \,, \tag{2.51}$$

[7] We suppress that, strictly speaking, the integral over p should be restricted to only include collinear momenta, which is equivalent to excluding the zero-bin region [163] from the integral.

where $\Omega \equiv \Omega(\mathbf{p})$ is the solid angle corresponding to the direction of $\mathbf{p}$. We also keep the dependence on the labels implicit and simply write the fields in the operator in terms of their total momentum p,

$$\phi(p) \equiv \phi_{n,\tilde{p}}(k)\,, \qquad \mathcal{O}(\{p_i\}) \equiv \mathcal{O}_{\{n_i,\tilde{p}_i\}}(\{k_i\})\,. \tag{2.52}$$

Hence, the final form of the matching becomes

$$\mathcal{Q}(p) = \left(\prod_i \int \frac{\mathrm{d}^4 p_i}{(2\pi)^4}\right) (2\pi)^4 \delta^4\Big(p - \sum_i p_i\Big)\, C(\{p_i\})\, \mathcal{O}(\{p_i\})\,, \tag{2.53}$$

where here and in the following it is understood that the Wilson coefficient C only depends on the directions $\mathbf{n}_i = \mathbf{p}_i/|\mathbf{p}_i|$ and large components $p_i^- = p_i^0 + \mathbf{p}_i$ of the momenta p_i.

4.2 Factorization Proof

Starting from the definition of $\delta\sigma/\delta\omega$ in Eq. (2.18), in the first step we match QCD onto SCET. According to Eq. (2.53), the matching condition takes the form

$$\begin{aligned}\mathcal{Q}(p) = &\left(\prod_{i=a,b,1}^{N} \int \frac{\mathrm{d}^4 p_i}{(2\pi)^4}\right) C_N(p_a, p_b; p_1, \ldots, p_N) \\ &\times \mathcal{O}_I(p_a, p_b)\, \mathcal{O}_F(p_1, \ldots, p_N)\, (2\pi)^4 \delta^4\left(p - p_a - p_b + \sum_{i=1}^{N} p_i\right).\end{aligned} \tag{2.54}$$

Here, p_a and p_b are initial state collinear momenta, and the operator $\mathcal{O}_I$ is responsible for annihilating the initial state. Similarly, $p_1, \ldots, p_N$ are N final state collinear momenta, and the operator $\mathcal{O}_F$, defined as

$$\mathcal{O}_F(p_1, \ldots, p_N) = \prod_{i=1}^{N} \phi^\dagger(p_i)\,, \tag{2.55}$$

is responsible for creating the final state. Equation (2.54) is valid in any region of multi-body phase space that is dominated by N jets of collinear particles, corresponding to N collinear directions, that are well separated from each other and the beam axis, i.e., the initial collinear directions $p_{a,b}$. The dominant power corrections to Eq. (2.54) scale like $p_i^2/p_i \cdot p_j$.

The different collinear fields in $\mathcal{O}_I$ and $\mathcal{O}_F$ interact with each other only through the exchange of soft gluons. These interactions are eliminated to all orders in α_s and leading order in the power counting by the usual field redefinition in SCET [29],

$$\phi_{n,\tilde{p}}(x) = Y_n(x)\, \phi^{(0)}_{n,\tilde{p}}(x)\,, \tag{2.56}$$

where $Y_n(x)$ denotes the appropriate soft Wilson line along the direction n in the color representation of $\phi_{n,\tilde{p}}(x)$. For color singlet fields, $Y(x) = 1$. As usual, we will drop the superscript on the redefined fields and operators henceforth. In terms of the redefined fields, the matching condition

in Eq. (2.54) takes the form

$$\mathcal{Q}(p) = \biggl(\prod_{i=a,b,1}^{N}\int\frac{\mathrm{d}^4p_i}{(2\pi)^4}\biggr)\,C_N(p_a,p_b;p_1,\ldots,p_N)\int\frac{\mathrm{d}^4k_s}{(2\pi)^4} \\ \times\,\mathcal{O}_I(p_a,p_b)\,\mathcal{O}_F(p_1,\ldots,p_N)\,\mathcal{O}_S(k_s)\,(2\pi)^4\delta^4\biggl(p-p_a-p_b+k_s+\sum_{i=1}^{N}p_i\biggr)\,, \tag{2.57}$$

where the soft operator $\mathcal{O}_S(k_s)$ contains the Fourier transform of the time-ordered product of all soft Wilson lines,

$$\mathcal{O}_S(k_s) = \int\mathrm{d}^4x\,e^{-\mathrm{i}k_s\cdot x}\,T\biggl[Y_{n_a}(x)\,Y_{n_b}(x)\biggl(\prod_{i=1}^{N}Y_{n_i}^\dagger(x)\biggr)\biggr]\,. \tag{2.58}$$

Having factored the operator $\mathcal{Q}(p)$, we next move our attention to the $\delta[\omega-\mathcal{E}^0]$ term in Eq. (2.18). After the field redefinition, the leading-order SCET Lagrangian with $N+2$ collinear directions can be written as

$$\mathcal{L}_{\mathrm{SCET}} = \sum_{i=a,b,1}^{N}\mathcal{L}_i + \mathcal{L}_s\,, \tag{2.59}$$

where $\mathcal{L}_i$ only contains collinear fields in the direction n_i, and $\mathcal{L}_s$ is the purely soft Lagrangian. Since the energy-momentum flow operator, defined in Eq. (2.15), is linear in the Lagrangian of the theory, we have

$$\mathcal{E}^\mu(\Omega) = \sum_{i=a,b,1}^{N}\mathcal{E}_i^\mu(\Omega) + \mathcal{E}_s^\mu(\Omega)\,, \tag{2.60}$$

where $\mathcal{E}_{i,s}^\mu(\Omega)$ is defined analogously to Eq. (2.15), but using the energy-momentum tensor obtained from the Lagrangian $\mathcal{L}_{i,s}$ only. Thus, $\mathcal{E}_i^\mu(\Omega)$ describes the energy-momentum flow in the i-th collinear sector, while $\mathcal{E}_s^\mu(\Omega)$ describes the remaining soft energy-momentum flow. This allows us to write

$$\delta[\omega-\mathcal{E}^0] = \biggl(\prod_{i=a,b,1}^{N}\int\mathcal{D}\omega_i\,\delta[\omega_i-\mathcal{E}_i^0]\biggr)\int\mathcal{D}\omega_s\,\delta[\omega_s-\mathcal{E}_s^0]\,\delta\biggl[\omega-\omega_s-\sum_{i=a,b,1}^{N}\omega_i\biggr]\,. \tag{2.61}$$

Combining Eqs. (2.61) and (2.57) with Eq. (2.18), and letting $\Phi_N=\{p_a,p_b;p_1,\ldots,p_N\}$ denote a point in $(2\to N)$-body phase space (with $\mathrm{d}\Phi_N$ the corresponding phase space measure), $\delta\sigma/\delta\omega$ can be written as

$$\frac{\delta\sigma}{\delta\omega} = \frac{1}{2p_I^2}\int\mathrm{d}\Phi_N'\,\mathrm{d}\Phi_N\,C_N^*(\Phi_N')\,C_N(\Phi_N)\int\frac{\mathrm{d}^4k_s'}{(2\pi)^4}\,\frac{\mathrm{d}^4k_s}{(2\pi)^4}\biggl(\prod_{i=a,b,1}^{N}\int\mathcal{D}\omega_i\biggr)\int\mathcal{D}\omega_s \\ \times\,\Bigl\langle I\Bigl|(\mathcal{O}_I\mathcal{O}_F\mathcal{O}_S)^\dagger(\Phi_N',k_s')\biggl(\prod_{i=a,b,1}^{N}\delta[\omega_i-\mathcal{E}_i^0]\biggr)\delta[\omega_s-\mathcal{E}_s^0]\,(\mathcal{O}_I\mathcal{O}_F\mathcal{O}_S)(\Phi_N,k_s)\Bigr|I\Bigr\rangle \\ \times\,(2\pi)^4\delta^4(\Phi_N'-k_s)\,\delta\biggl[\omega-\omega_s-\sum_{i=a,b,1}^{N}\omega_i\biggr]\,. \tag{2.62}$$

Since there are no interactions between the different collinear sectors or the soft sector in Eq. (2.59), we can factorize the forward matrix element into a product of several matrix elements.

First, for each final state collinear sector we get the vacuum expectation value of two collinear fields, with an insertion of $\delta[\omega_i - \mathcal{E}_i^0]$ between the fields, which restricts the collinear energy configuration to ω_i. Since the matrix element conserves four momentum, we can write it as

$$\langle 0|\phi(p_i')\,\delta[\omega_i - \mathcal{E}_i^0]\,\phi^\dagger(p_i)|0\rangle = (2\pi)^4\delta^4(p_i' - p_i)\,J(p_i;\omega_i)\,, \tag{2.63}$$

which defines the momentum-space jet function $J(p_i;\omega_i)$. Integrating both sides over p_i, we obtain the equivalent definition in position space in terms of the standard fields $\phi_{n,\tilde{p}}(x)$,

$$J(p_i;\omega_i) = \int \mathrm{d}^4x\, e^{\mathrm{i}k_i\cdot x}\,\langle 0|\phi_{n_i,\tilde{p}_i}(x)\,\delta[\omega_i - \mathcal{E}_i^0]\,\phi^\dagger_{n_i,\tilde{p}_i}(0)|0\rangle\,. \tag{2.64}$$

Momentum conservation implies that $J(p;\omega)$ only has support for configurations ω that satisfy $P[\omega] = p$, where $P[\omega]$ is defined in Eq. (2.20). One can also define a jet function $J(\omega) = \int \mathrm{d}^4p\, J(p;\omega)$, which has support for any (physically allowed) ω, but we find it conceptually and notationally easier to keep the total momentum of ω as an explicit separate argument.

At leading order in the power counting, any hadron in the initial state is bound by collinear interactions only, and thus does not interact with the soft sector. Hence, we can factor out the soft matrix element,

$$\langle 0|\mathcal{O}_S^\dagger(k_s')\,\delta[\omega_s - \mathcal{E}_s^0]\,\mathcal{O}_S(k_s)|0\rangle = (2\pi)^4\delta^4(k_s' - k_s)\,(2\pi)^4\delta(k_s - P[\omega_s])\,S(\omega_s)\,, \tag{2.65}$$

which defines the soft function $S(\omega_s)$, and we again used momentum conservation. Note that $\mathcal{O}_S$ and S depend on the $N+2$ collinear directions with respect to which the Wilson lines are defined, which is hidden in our notation. The soft function $S(\omega_s)$ is defined with support for any physical ω_s, and the total soft momentum is given by $k_s = P[\omega_s]$.

The remaining initial state matrix element can be written as

$$\begin{aligned}&\langle I|\mathcal{O}_I^\dagger(p_a', p_b')\,\delta[\omega_a - \mathcal{E}_a^0]\,\delta[\omega_b - \mathcal{E}_b^0]\,\mathcal{O}_I(p_a,p_b)|I\rangle \\ &\qquad = (2\pi)^4\delta^4(p_a' - p_a)\,(2\pi)^4\delta^4(p_b' - p_b)\,I(p_a,p_b;\omega_a,\omega_b)\,,\end{aligned} \tag{2.66}$$

and defines the initial-state function $I(p_a,p_b;\omega_a,\omega_b)$. In writing Eq. (2.66) we already used that the matrix element will factorize for the two collinear sectors, which allows us to write two separate momentum-conserving δ functions. As for the jet function, we choose to keep the momenta $p_{a,b}$ explicit in the definition of $I(p_a,p_b;\omega_a,\omega_b)$, so its support is restricted by momentum conservation to $P[\omega_a+\omega_b] = p_I - p_a - p_b$. For e^+e^- collisions, the initial-state function reduces to a calculable leptonic matrix element, as discussed in Sec. 5.1. For hadronic collisions, it can be reduced to parton distribution functions, but also allows one to treat the underlying event or beam remnants, as discussed in Sec. 6.2.

Combining Eqs. (2.63), (2.65), and (2.66) with Eq. (2.62), we can perform the integrals

over all primed momenta, and arrive at

$$\begin{aligned}\frac{\delta\sigma}{\delta\omega} &= \frac{1}{2p_I^2}\biggl(\prod_{i=1}^{N}\int\frac{\mathrm{d}^4p_i}{(2\pi)^4}\,\mathcal{D}\omega_i\,J(p_i;\omega_i)\biggr)\int\frac{\mathrm{d}^4p_a}{(2\pi)^4}\,\frac{\mathrm{d}^4p_b}{(2\pi)^4}\,\mathcal{D}\omega_a\,\mathcal{D}\omega_b\,I(p_a,p_b;\omega_a,\omega_b)\\ &\quad\times|C_N(p_a,p_b;p_1,\dots,p_N)|^2\int\mathcal{D}\omega_s\,S(\omega_s)\\ &\quad\times(2\pi)^4\delta^4\biggl(p_a+p_b-P[\omega_s]-\sum_{i=1}^{N}p_i\biggr)\,\delta\biggl[\omega-\omega_s-\sum_{i=a,b,1}^{N}\omega_i\biggr]\,. \end{aligned}\tag{2.67}$$

As anticipated, the fully differential cross section $\delta\sigma/\delta\omega$ is given by the product of a hard coefficient, $|C_N|^2$, N jet functions, $J(p_i;\omega_i)$, an initial-state function, $I(p_a,p_b;\omega_a,\omega_b)$, and a soft function, $S(\omega_s)$. Note that there are no power corrections to Eq. (2.67) other than from higher-order SCET operators in the matching of QCD onto SCET and higher-order contributions to the Lagrangian, which could in principle be included systematically. One should keep in mind that this factorization is purely academic at this point, because all ingredients depend on the precise energy configuration in each sector of the theory. The energy configurations are obviously very different for partonic and hadronic states, and therefore the functions J, I, and S cannot be calculated perturbatively. One should think of them as fully exclusive functions.

The importance of Eq. (2.67) lies in the fact that it establishes factorization for a generic N-jet like kinematic configuration. In our formalism, the question whether the cross section $\mathrm{d}\sigma/\mathrm{d}O$ for a particular observable factorizes is two-fold. First, a given value of the observable has to be dominated by factorizable kinematic configurations. If this is the case, one can immediately obtain a factorized form for $\mathrm{d}\sigma/\mathrm{d}O$ from Eq. (2.67) via Eq. (2.17). This means that *any* jet observable (meaning any observable whose definition restricts it to N-jet configurations) is formally factorizable. The second, and more important, question then is whether one is able to determine the relevant functions, J, I, and S, for a given observable.

For sufficiently inclusive observables, the jet functions, $J(p_i;\omega_i)$, will be smeared enough, i.e., integrated over ω_i with a sufficiently smooth weight function, such that we can trust their perturbative calculation. Similarly, the soft function, $S(\omega_s)$, and (for hadronic collisions) the initial-state function, $I(p_a,p_b;\omega_a,\omega_b)$, have to be smeared enough (integrated over ω_s and $\omega_{a,b}$) to reduce to nonperturbative functions that are universal between different processes. For such observables, one obtains a factorization formula in the more traditional sense, which allows for the perturbative calculation of all ingredients, with the exception of maybe a traditional soft function or initial state parton distribution functions.

To study the structure of the factorization for a specific observable, and obtain explicit definitions of the relevant jet, soft, and initial state functions, it is usually required to also expand the kinematics of the process, because Eq. (2.67) still mixes momentum components with different scaling in SCET. In this way, one obtains a result that formally is fully leading order in the power counting. As discussed above, with our choice of field labels the components $p_i^{\mp}=p_i^0\pm|\mathbf{p}_i|$ are defined with respect to the direction of the momentum p_i itself, so $p_{i\perp}=0$ and $\mathbf{n}_i=\mathbf{p}_i/|\mathbf{p}_i|$. Since $p_i^-\gg p_i^+$, to leading order the phase space in Eq. (2.51) is

$$\int\frac{\mathrm{d}^4p_i}{(2\pi)^4}=\int\frac{\mathrm{d}p_i^-\,\mathrm{d}p_i^+\,\mathrm{d}\Omega_i}{(2\pi)^4}\,\frac{(p_i^-)^2}{8}\,.\tag{2.68}$$

Furthermore, expanding the momentum conserving δ function, we find

$$\delta^4\biggl(p_a + p_b - P[\omega_s] - \sum_{i=1}^{N} p_i\biggr) = \delta^4\biggl(p_a^- \frac{n_a}{2} + p_b^- \frac{n_b}{2} - \sum_{i=1}^{N} p_i^- \frac{n_i}{2}\biggr)\,. \tag{2.69}$$

Equation (2.67) together with Eqs. (2.68) and (2.69) provides the final factorized form of the fully differential cross section $\delta\sigma/\delta\omega$ for N jets, and is the main result of this chapter. In the remaining part of the chapter we will show how to use this result to understand the factorization properties of several observables. We will focus mostly on simple two-jet final states, for which the kinematics is simple enough to explicitly perform all phase space integrations analytically. All our examples, however, follow directly from our general result, and the extensions to more complicated final states should be obvious.

5 $e^+e^- \to$ 2 Jets

In this section, we show how to apply the result in Eq. (2.67) to the simplest case of two-jet events in e^+e^- collisions. The analysis simplifies considerably because of the absence of strongly interacting particles in the initial state, and due to the back-to-back nature of the jets and the corresponding need for only a single collinear direction, e.g., the thrust axis. We first give explicit definitions of the operators $\mathcal{O}_I$, $\mathcal{O}_F$, and $\mathcal{O}_S$, including all relevant spin and color information, and then define all the ingredients in the factorized form of $\delta\sigma/\delta\omega$. We then apply this generic formula to the special cases of event shape observables in the limit $e \to 1$ and to hemisphere jet masses, whose factorization is well understood [146, 152, 149, 44, 47]. Factorization for the former was proven using SCET in Refs. [157, 18] and for the latter in Ref. [124], and we show how to reproduce these results. We then consider the factorization of generic observables defined for cone jet algorithms, and obtain the definition of the relevant cone jet functions and cone soft function. In SCET, cone jets were previously discussed in Refs. [26, 24, 187] using Sterman-Weinberg cones.

5.1 Generic Expression

For $e^+e^- \to 2$ jets, including the full spin and color information, the three SCET operators entering the matching in Eq. (2.57) are[8]

$$\begin{aligned}
\mathcal{O}_I^{\mu}(p_a, p_b) &= \bar{e}(-p_a)\gamma^{\mu}e(p_b)\,,\\
\mathcal{O}_{F\mu}^{cd}(p_1, p_2) &= \bar{\chi}^c(p_1)\gamma_{\mu}\chi^d(-p_2)\,,\\
\mathcal{O}_S^{cd}(k_s) &= \int \mathrm{d}^4x\, e^{-\mathrm{i}k_s\cdot x}\, T\bigl[Y_{n_1}^{\dagger\, ce}(x)\, Y_{n_2}^{ed}(x)\bigr]\,,
\end{aligned} \tag{2.70}$$

where $\chi^c(p) = [W\xi]^c(p)$ denotes a noninteracting collinear quark field of color c and charge $e\,Q_f$ (where f denotes the flavor), moving in the $\mathbf{p}/|\mathbf{p}|$ direction. Note that we are distinguishing particle and anti-particles by the sign of the momentum argument on the field. The soft Wilson lines along

[8] We only give the result for an intermediate photon here, and include the Z boson contribution later.

an outgoing collinear direction are[9]

$$Y_n^\dagger(x) = P\exp\left[\mathrm{i}g_s\int_0^\infty \mathrm{d}s\, n\cdot A_s(x+s\,n)\right], \tag{2.71}$$

where P denotes path ordering. The Wilson coefficient at tree level is given by

$$C_2(p_a,p_b;p_1,p_2) = \frac{\mathrm{i}e^2\,Q_f}{2\,p_a\cdot p_b}\left[1+\mathcal{O}(\alpha_s)\right]. \tag{2.72}$$

Since the initial state is not strongly interacting, the initial-state function in Eq. (2.66), including the average over initial spins, reduces to

$$\begin{aligned} &I^{\mu\nu}(p_a,p_b;\omega_a,\omega_b)\\ &\quad= \frac{1}{4}\sum_{\text{spins}}\int\frac{\mathrm{d}^4p_a'}{(2\pi)^4}\,\frac{\mathrm{d}^4p_b'}{(2\pi)^4}\,\big\langle e^+e^-\big|\bar e(p_b')\gamma^\mu e(-p_a')\,\delta[\omega_a-\mathcal{E}_a^0]\,\delta[\omega_b-\mathcal{E}_b^0]\,\bar e(-p_a)\gamma^\nu e(p_b)\big|e^+e^-\big\rangle\\ &\quad= (2\pi)^4\delta(p_a-p_{e^+})\,(2\pi)^4\delta(p_b-p_{e^-})\,\delta[\omega_a]\,\delta[\omega_b]\,L^{\mu\nu}, \end{aligned} \tag{2.73}$$

where $p_{e^\pm}$ are the momenta of the incoming leptons and

$$L^{\mu\nu} = p_{e^-}^\mu p_{e^+}^\nu + p_{e^+}^\mu p_{e^-}^\nu - g^{\mu\nu}\,(p_{e^-}\cdot p_{e^+}) \tag{2.74}$$

is the well-known leptonic tensor. Note that as we do not consider any initial state radiation from the incoming leptons, $\mathcal{E}_{a,b}^0=0$ in Eq. (2.73).

Using $\phi(p_1)=\chi_\alpha^c(p_1)$ and $\phi(p_2)=\bar\chi_\beta^d(-p_2)$ in Eq. (2.63) (where α, β are spinor indices), the quark and anti-quark jet functions become (with the sum over spins implicit)

$$\begin{aligned} J_{\alpha'\alpha}^{c'c}(p_1;\omega_1) &= \int\frac{\mathrm{d}^4p_1'}{(2\pi)^4}\,\big\langle 0\big|\chi_{\alpha'}^{c'}(p_1')\,\delta[\omega_1-\mathcal{E}_1^0]\,\bar\chi_\alpha^c(p_1)\big|0\big\rangle = \delta^{c'c}\Big(\frac{\not{n}_1}{2}\Big)_{\alpha'\alpha}J(p_1;\omega_1),\\ \bar J_{\beta'\beta}^{d'd}(p_2;\omega_2) &= \int\frac{\mathrm{d}^4p_1'}{(2\pi)^4}\,\big\langle 0\big|\bar\chi_{\beta'}^{d'}(-p_2')\,\delta[\omega_2-\mathcal{E}_2^0]\,\chi_\beta^d(-p_2)\big|0\big\rangle = \delta^{d'd}\Big(\frac{\not{n}_2}{2}\Big)_{\beta\beta'}\bar J(p_2;\omega_2), \end{aligned} \tag{2.75}$$

where the spin-singlet and color-singlet jet functions are defined as

$$\begin{aligned} J(p_1;\omega_1) &= \frac{1}{4N_c}\int\frac{\mathrm{d}^4p_1'}{(2\pi)^4}\,\mathrm{tr}\big\langle 0\big|\not{\bar n}_1\chi(p_1')\,\delta[\omega_1-\mathcal{E}_1^0]\,\bar\chi(p_1)\big|0\big\rangle,\\ \bar J(p_2;\omega_2) &= \frac{1}{4N_c}\int\frac{\mathrm{d}^4p_2'}{(2\pi)^4}\,\mathrm{tr}\big\langle 0\big|\bar\chi(-p_2')\,\delta[\omega_2-\mathcal{E}_2^0]\,\not{\bar n}_2\chi(-p_2)\big|0\big\rangle. \end{aligned} \tag{2.76}$$

Here, tr denotes the trace over spin and color indices and N_c is the number of colors. At lowest order in perturbation theory, we have $J(p;\omega)=\bar J(p;\omega)=2\pi\,\delta(p^+)\,\theta(p^-)\,\delta[\omega(\Omega)-p^0\,\delta(\Omega-\Omega(\mathbf{p}))]$.

From Eq. (2.65), the soft function is defined as

$$S_{n_1n_2}^{d'c'cd}(\omega_s) = \frac{1}{N_c}\int\frac{\mathrm{d}^4k_s'}{(2\pi)^4}\,\frac{\mathrm{d}^4k_s}{(2\pi)^4}\,\big\langle 0\big|\mathcal{O}_S^{\dagger\,d'c'}(k_s')\,\delta[\omega_s-\mathcal{E}_s^0]\,\mathcal{O}_S^{cd}(k_s)\big|0\big\rangle, \tag{2.77}$$

[9] For a discussion of the different choices of boundary conditions for in- and outgoing Wilson lines see for example Ref. [9].

where we made explicit the dependence of S on the directions $n_{1,2}$ of the Wilson lines in $\mathcal{O}_S$, and the factor $1/N_c$ is included by convention. Contracting with the trivial color structure of the jet functions in Eq. (2.75), we obtain the color-singlet soft function

$$S_{n_1 n_2}(\omega_s) = \delta^{c'c}\,\delta^{d'd}\,S^{d'c'cd}_{n_1 n_2}(\omega_s) = \frac{1}{N_c}\,\mathrm{tr}\big\langle 0\big|\overline{T}\big[(Y^\dagger_{n_2}Y_{n_1})(0)\big]\,\delta[\omega_s-\mathcal{E}^0_s]\,T\big[(Y^\dagger_{n_1}Y_{n_2})(0)\big]\big|0\big\rangle\,. \tag{2.78}$$

Since the spin structure of the jet functions in Eq. (2.75) factorizes, we can contract all vector and spinor indices,

$$L_{\mu\nu}\Big(\frac{\not{n}_1}{2}\Big)_{\alpha'\alpha}\gamma^\nu_{\alpha\beta}\Big(\frac{\not{n}_2}{2}\Big)_{\beta\beta'}\gamma^\mu_{\beta'\alpha'} = E^2_{\mathrm{cm}}(1-\cos\theta_1\,\cos\theta_2)\,, \tag{2.79}$$

where E_{cm} is the total energy and $\theta_{1,2}$ are the angles of $\mathbf{p}_{1,2}$ with respect to the e^+e^- beam axis in the center-of-mass frame. Thus, combining all pieces with Eq. (2.67), we find

$$\begin{aligned}\frac{\delta\sigma}{\delta\omega} &= \frac{8\pi^2\alpha^2\,Q_f^2\,N_c}{E^4_{\mathrm{cm}}}\int\frac{\mathrm{d}^4p_1}{(2\pi)^4}\,\mathcal{D}\omega_1\,J(p_1;\omega_1)\int\frac{\mathrm{d}^4p_2}{(2\pi)^4}\,\mathcal{D}\omega_2\,\bar{J}(p_2;\omega_2)H_2(p_1,p_2)\,(1-\cos\theta_1\cos\theta_2)\\ &\quad\times\int\mathcal{D}\omega_s\,S_{n_1n_2}(\omega_s)\,(2\pi)^4\delta^4(p_{e^+}+p_{e^-}-P[\omega_s]-p_1-p_2)\,\delta[\omega-\omega_1-\omega_2-\omega_s]\,,\end{aligned} \tag{2.80}$$

where the hard coefficient $H_2(p_1,p_2)=1+\mathcal{O}(\alpha_s)$ is defined by

$$|C_2(p_{e^+},p_{e^-};p_1,p_2)|^2 = \Big(\frac{4\pi\alpha\,Q_f}{E^2_{\mathrm{cm}}}\Big)^2 H_2(p_1,p_2)\,. \tag{2.81}$$

Equation (2.80) specializes Eq. (2.67) to generic 2-jet configurations ω in e^+e^- collisions.

Next, we expand the kinematics. Using Eq. (2.69), the momentum conserving δ function becomes

$$\begin{aligned}&\delta^4\Big(p^-_{e^+}\frac{n_{e^+}}{2}+p^-_{e^-}\frac{n_{e^-}}{2}-p^-_1\frac{n_1}{2}-p^-_2\frac{n_2}{2}\Big)\\ &\qquad=\frac{8}{E^2_{\mathrm{cm}}}\,\delta(p^-_1-E_{\mathrm{cm}})\,\delta(p^-_2-E_{\mathrm{cm}})\,\delta(\cos\theta_1+\cos\theta_2)\,\delta(\phi_1-\phi_2-\pi)\,,\end{aligned} \tag{2.82}$$

where as before in the center-of-mass frame $p_I = p_{e^+}+p_{e^-} = (E_{\mathrm{cm}},\mathbf{0})$. The δ functions allow us to perform the p^-_1, p^-_2, and Ω_2 integrations in Eq. (2.80), and imply that p_1 and p_2 are back-to-back, as expected for two-jet events. In particular, $\mathbf{n}_1=-\mathbf{n}_2$, so we can write $p_{1,2}$ in terms of the components $(p^+,p^-,\mathbf{n})$ as

$$p_1 = \big(p^+_1,E_{\mathrm{cm}},\mathbf{n}(\Omega)\big)\,,\qquad p_2=\big(p^+_2,E_{\mathrm{cm}},-\mathbf{n}(\Omega)\big)\,, \tag{2.83}$$

where $\Omega=(\theta,\phi)\equiv\Omega_1$ describes the orientation of the momenta relative to the beam axis. We also write $S_{n_1n_2}\equiv S_{\mathbf{n}(\Omega)}$. Similar to the Wilson coefficient C_2, the hard coefficient $H_2(p_1,p_2)$ does not depend on the small momentum components $p^+_{1,2}$. Since $p^-_i=E_{\mathrm{cm}}$, we define $H_2(E_{\mathrm{cm}})\equiv H_2(p_1,p_2)$. Combining everything with Eq. (2.80), using Eq. (2.68), and writing the momenta in terms of their components, we have

$$\begin{aligned}\frac{\delta\sigma}{\delta\omega} &= H_2(E_{\mathrm{cm}})\int\frac{\mathrm{d}\Omega}{2\pi}\int\frac{\mathrm{d}p^+_1}{2\pi}\,\mathcal{D}\omega_1\,J(p^+_1,E_{\mathrm{cm}},\mathbf{n}(\Omega);\omega_1)\int\frac{\mathrm{d}p^+_2}{2\pi}\,\mathcal{D}\omega_2\,\bar{J}(p^+_2,E_{\mathrm{cm}},-\mathbf{n}(\Omega);\omega_2)\\ &\quad\times\frac{\mathrm{d}\sigma_0}{\mathrm{d}\cos\theta}\int\mathcal{D}\omega_s\,S_{\mathbf{n}(\Omega)}(\omega_s)\,\delta[\omega-\omega_1-\omega_2-\omega_s]\,,\end{aligned} \tag{2.84}$$

where

$$\frac{\mathrm{d}\sigma_0}{\mathrm{d}\cos\theta} = \frac{\pi\alpha^2}{2E_{\mathrm{cm}}^2}\, N_c\, Q_f^2\,(1+\cos^2\theta) \tag{2.85}$$

is the Born differential cross section. The exchange of a Z boson can be included by using

$$\begin{aligned}\frac{\mathrm{d}\sigma_0}{\mathrm{d}\cos\theta} = \frac{\pi\alpha^2}{2E_{\mathrm{cm}}^2}\, N_c \Bigg\{ &\left[Q_f^2 - \frac{2\, v_e v_f Q_f}{1-m_Z^2/E_{\mathrm{cm}}^2} + \frac{(v_e^2+a_e^2)(v_f^2+a_f^2)}{(1-m_Z^2/E_{\mathrm{cm}}^2)^2}\right](1+\cos^2\theta) \\ &+ \left[\frac{4\, a_e a_f Q_f^2}{1-m_Z^2/E_{\mathrm{cm}}^2} - \frac{8\, v_e a_e v_f a_f}{(1-m_Z^2/E_{\mathrm{cm}}^2)^2}\right]\cos\theta\Bigg\}, \end{aligned} \tag{2.86}$$

where $v_{e,f}$ and $a_{e,f}$ are the standard vector and axial couplings to the Z.

Equation (2.84) is the penultimate formula for generic observables in $e^+e^- \to 2$ jet events. Each of the ingredients in Eq. (2.84) is a completely exclusive object that depends on the energy distribution of the individual partons. The details of how to integrate over the energy configurations to arrive at perturbative jet functions and a universal soft function depend on the observable in question, but since all observable independent simplifications have been done, a wide range of factorization theorems can now be obtained with relative ease. We illustrate this with a few examples in the following subsections.

5.2 Event Shapes in the Limit $e \to 1$

Combining Eqs. (2.17) and (2.28), the differential cross section in some event shape e is

$$\frac{\mathrm{d}\sigma}{\mathrm{d}e} = \int \mathrm{d}\mathbf{t} \int \mathcal{D}\omega\, \frac{\delta\sigma}{\delta\omega}\, \delta(\mathbf{t}-\mathbf{t}[\omega])\, \delta(e - f_e[\omega;\mathbf{t}])\,. \tag{2.87}$$

For $e \to 1$, the final state is dominated by two highly collimated jets, and hence, we can use the result for $\delta\sigma/\delta\omega$ in Eq. (2.84). The integration over ω is trivial and sets $\omega = \omega_1 + \omega_2 + \omega_s$. Since $\omega_{1,2}$ describe collinear energy configurations along $\pm\mathbf{n}(\Omega)$, we have $\mathbf{t}[\omega_1+\omega_2+\omega_s] = \mathbf{n} + \mathcal{O}(\lambda^2)$ [18]. This allows us to integrate over $\mathbf{t}$,

$$\begin{aligned}\frac{\mathrm{d}\sigma}{\mathrm{d}e} = H_2(E_{\mathrm{cm}}) &\int \frac{\mathrm{d}\Omega}{2\pi} \int \frac{\mathrm{d}p_1^+}{2\pi}\, \mathcal{D}\omega_1\, J(p_1^+, E_{\mathrm{cm}}, \mathbf{n}(\Omega);\omega_1) \int \frac{\mathrm{d}p_2^+}{2\pi}\, \mathcal{D}\omega_2\, \bar{J}(p_2^+, E_{\mathrm{cm}}, -\mathbf{n}(\Omega);\omega_2) \\ &\times \frac{\mathrm{d}\sigma_0}{\mathrm{d}\cos\theta} \int \mathcal{D}\omega_s\, S_{\mathbf{n}(\Omega)}(\omega_s)\, \delta(e - f_e[\omega_1+\omega_2+\omega_s;\mathbf{n}(\Omega)])\,. \end{aligned} \tag{2.88}$$

From Eq. (2.29), we see that $f_e[\omega;\mathbf{n}]$ is linear in ω, from which it follows that we can write $f_e[\omega_1+\omega_2+\omega_s;\mathbf{n}] = f_e[\omega_1;\mathbf{n}] + f_e[\omega_2;\mathbf{n}] + f_e[\omega_s;\mathbf{n}]$. This implies

$$\begin{aligned}\delta(e - f_e[\omega_1+\omega_2+\omega_s;\mathbf{n}]) = \int &\mathrm{d}e_1\, \mathrm{d}e_2\, \mathrm{d}e_s\, \delta(e-e_1-e_2-e_s) \\ &\times \delta(e_1 - f_e[\omega_1;\mathbf{n}])\, \delta(e_2 - f_e[\omega_2;\mathbf{n}])\, \delta(e_s - f_e[\omega_s;\mathbf{n}])\,, \end{aligned} \tag{2.89}$$

which separates the ω dependencies in Eq. (2.88). We stress that this is not a requirement for the factorization of $\mathrm{d}\sigma/\mathrm{d}e$, as demonstrated by Eq. (2.88). In fact, the full event-shape functional $f_e[\omega] = f_e[\omega, \mathbf{t}[\omega]]$ is not linear in ω and does not obey a similar separation, because $\mathbf{t}[\omega]$ is not linear in ω. The crucial ingredient for the factorization is the linearity of the energy-momentum

tensor and the resulting separation of the energy flow operator in Eqs. (2.60) and (2.61). However, without Eq. (2.89) the jet and soft functions depend on the full energy distributions ω_i, and are therefore neither perturbatively calculable, nor universal enough to be extracted from data. The important point about Eq. (2.89) is that it allows us to perform the ω integrations in Eq. (2.88), and to define inclusive event-shape jet and soft functions

$$\begin{aligned} J(e_1) &= \int \frac{\mathrm{d}p_1^+}{2\pi}\, \mathcal{D}\omega_1\, J(p_1^+, E_{\mathrm{cm}}, \mathbf{n}; \omega_1)\, \delta(e_1 - f_e[\omega_1; \mathbf{n}])\,, \\ \bar{J}(e_2) &= \int \frac{\mathrm{d}p_2^+}{2\pi}\, \mathcal{D}\omega_2\, \bar{J}(p_2^+, E_{\mathrm{cm}}, \mathbf{n}; \omega_2)\, \delta(e_2 - f_e[\omega_2; \mathbf{n}])\,, \\ S(e_s) &= \int \mathcal{D}\omega_s\, S_{\mathbf{n}}(\omega_s)\, \delta(e_s - f_e[\omega_s; \mathbf{n}])\,. \end{aligned} \tag{2.90}$$

With the definitions in Eqs. (2.76) and (2.78), these are identical to the definitions given in Ref. [18]. For $\bar{J}(e_2)$ we used that $f_e[\omega, \mathbf{n}] = f_e[\omega, -\mathbf{n}]$ because the sign of the thrust vector is irrelevant. By rotational invariance, after integrating over $\omega_{1,2}$, the jet functions $J(e_1)$, $\bar{J}(e_2)$, do not depend on the value of $\mathbf{n}$ on the right-hand side. This would not be true if the thrust axis $\mathbf{n}$ in $f_e[\omega; \mathbf{n}]$ would be different from the momentum direction $\mathbf{n}$ in $J(p^+, E_{\mathrm{cm}}, \mathbf{n}; \omega)$. Similarly, after integrating over ω_s, the soft function $S(e_s)$ is independent of $\mathbf{n}$, because the direction of the Wilson lines in $S_{\mathbf{n}}(\omega_s)$ coincides with the thrust axis. Thus, using Eq. (2.90) and integrating over Ω, we obtain the final result

$$\frac{\mathrm{d}\sigma}{\mathrm{d}e} = H_2(E_{\mathrm{cm}})\, \sigma_0 \int \mathrm{d}e_1\, \mathrm{d}e_2\, \mathrm{d}e_s\, J(e_1)\, \bar{J}(e_2)\, S(e_s)\, \delta(e - e_1 - e_2 - e_s)\,. \tag{2.91}$$

where $\sigma_0 = \int \mathrm{d}\cos\theta\, \mathrm{d}\sigma_0/\mathrm{d}\cos\theta$ is the total Born cross section. Equation (2.91) agrees with the result of Ref. [18].

5.3 Double Differential Hemisphere Mass Distribution

Combining Eqs. (2.17) and (2.37), the double differential hemisphere mass distribution is

$$\frac{\mathrm{d}^2\sigma}{\mathrm{d}M_1^2\, \mathrm{d}M_2^2} = \int \mathrm{d}^4P_1 \int \mathrm{d}^4P_2\, \frac{\mathrm{d}^2\sigma}{\mathrm{d}^4P_1\, \mathrm{d}^4P_2}\, \delta(M_1^2 - P_1^2)\, \delta(M_2^2 - P_2^2)\,, \tag{2.92}$$

where the cross section differential in the total momentum of each jet for the hemisphere jet algorithm is

$$\frac{\mathrm{d}^2\sigma}{\mathrm{d}^4P_1\, \mathrm{d}^4P_2} = \int \mathrm{d}\mathbf{t} \int \mathcal{D}\omega\, \frac{\delta\sigma}{\delta\omega}\, \delta(\mathbf{t} - \mathbf{t}[\omega])\, \delta^4(P_1 - P[\mathcal{J}_1[\omega; \mathbf{t}]])\, \delta^4(P_2 - P[\mathcal{J}_2[\omega; \mathbf{t}]])\,. \tag{2.93}$$

Here, $P[\omega]$ is given in Eq. (2.20) and $\mathcal{J}_i[\omega; \mathbf{t}]$ in Eq. (2.40). Combining these we have

$$\begin{aligned} P^\mu_{\mathrm{hemi}\,1}[\omega; \mathbf{t}] &\equiv P^\mu[\mathcal{J}_1[\omega; \mathbf{t}]] = \int \mathrm{d}\Omega\, n^\mu(\Omega)\, \omega(\Omega)\, \theta(0 \le \theta_{\mathbf{t}} < \pi/2)\,, \\ P^\mu_{\mathrm{hemi}\,2}[\omega; \mathbf{t}] &\equiv P^\mu[\mathcal{J}_2[\omega; \mathbf{t}]] = \int \mathrm{d}\Omega\, n^\mu(\Omega)\, \omega(\Omega)\, \theta(\pi/2 \le \theta_{\mathbf{t}} \le \pi)\,. \end{aligned} \tag{2.94}$$

In general, Eq. (2.93) will receive contributions from final states containing several distinct collinear momenta, corresponding to SCET operators with $N \geq 2$. However, if the final states are restricted to the kinematic region of small hemisphere invariant masses $M_i^2 = P_i^2 \sim \mathcal{O}(\lambda^2 E_{\rm cm}^2)$, corresponding to two collimated jets, the operator with $N = 2$ collinear directions gives the dominant contribution, with the corrections suppressed by powers of λ. Thus, we can apply the result for $\delta\sigma/\delta\omega$ in Eq. (2.84) in this region.

The integral over $\mathbf{t}$ can be performed as in the previous subsection, which sets $\mathbf{t} = \mathbf{n} + \mathcal{O}(\lambda^2)$. As Eq. (2.94) is linear in ω, we then have

$$P_{\text{hemi}\,i}[\omega; \mathbf{n}] = P_{\text{hemi}\,i}[\omega_1 + \omega_2 + \omega_s; \mathbf{n}] = P_{\text{hemi}\,i}[\omega_1; \mathbf{n}] + P_{\text{hemi}\,i}[\omega_2; \mathbf{n}] + P_{\text{hemi}\,i}[\omega_s; \mathbf{n}]\,. \tag{2.95}$$

To understand the size of $P_{\text{hemi}\,i}[\omega_j]$ for $i = j$ and $i \neq j$, we need to think about states in SCET in some more detail. Since the direction n labelling the collinear fields in SCET is a conserved quantum number, there exists a basis for the physical states which have a fixed value of n as well. This implies that for a given SCET state with momentum p, one has to identify the value of the direction n as well. Of course, to have the same final states as in full QCD, one needs $\sum_n |p, n\rangle^{\rm SCET} = |p\rangle^{\rm QCD}$, i.e. one has to be careful not to double count the physical states. Certainly, a convenient choice is to define the SCET states such that for every momentum p there is only a single value n. For our problem, the simplest choice is to assign the label $n_1 = (1, \mathbf{n})$ to all states with momentum in hemisphere 1, and $n_2 = (1, -\mathbf{n})$ to all states in hemisphere 2. This choice implies

$$P_{\text{hemi}\,i}[\omega_{j\neq i}; \mathbf{n}] = 0 \qquad \text{and} \qquad P_{\text{hemi}\,i}[\omega_i; \mathbf{n}] = p_i\,, \tag{2.96}$$

where $p_i = P[\omega_i]$ is the total momentum of ω_i, i.e., the momentum in $J(p_i; \omega_i)$. The power counting of SCET implies that $\ell_i = P_{\text{hemi}\,i}[\omega_s] \sim \lambda^2 E_{\rm cm}^2$, where ℓ_i can be interpreted as the total soft momentum in each hemisphere. Thus, using Eq. (2.83) we can expand

$$M_i^2 = P_i^2 = p_i^2 + 2p_i \cdot \ell_i + \ell_i^2 = E_{\rm cm}(p_i^+ + n_i \cdot \ell_i) + \mathcal{O}(\lambda^4 E_{\rm cm}^2)\,. \tag{2.97}$$

Since our observables M_i^2 only depend on p_i^+ and $n_i \cdot \ell_i$, we can do the remaining integrations in Eq. (2.84), and define the corresponding jet and soft functions

$$\begin{aligned}
J(E_{\rm cm} p_1^+) &= \frac{1}{2\pi E_{\rm cm}} \int \mathcal{D}\omega_1\, J(p_1^+, E_{\rm cm}, \mathbf{n}; \omega_1)\,, \\
\bar{J}(E_{\rm cm} p_2^+) &= \frac{1}{2\pi E_{\rm cm}} \int \mathcal{D}\omega_2\, \bar{J}(p_2^+, E_{\rm cm}, \mathbf{n}; \omega_2)\,, \\
S_{\rm hemi}(\ell_1^+, \ell_2^+) &= \int \mathcal{D}\omega_s\, S_{\mathbf{n}}(\omega_s)\, \delta(\ell_1^+ - n_1 \cdot P_{\text{hemi}\,1}[\omega_s; \mathbf{n}])\, \delta(\ell_2^+ - n_2 \cdot P_{\text{hemi}\,2}[\omega_s; \mathbf{n}])\,.
\end{aligned} \tag{2.98}$$

Again, after integrating over $\omega_{1,2,s}$, the jet functions, $J(p_1^2)$ and $\bar{J}(p_2^2)$, and the hemisphere soft function, $S_{\rm hemi}(\ell_1^+, \ell_2^+)$, do not depend on $\mathbf{n}$ due to rotational invariance. The SCET hemisphere soft function has been discussed previously in Refs. [124, 132, 125, 130]. The above definition provides an operator definition of $S_{\rm hemi}(\ell_1^+, \ell_2^+)$ in SCET, and is equivalent to the definition in Ref. [152]. Putting everything together, we obtain for the double differential hemisphere mass distribution

$$\frac{{\rm d}^2\sigma}{{\rm d}M_1^2\, {\rm d}M_2^2} = H_2(E_{\rm cm})\, \sigma_0 \int {\rm d}\ell_1^+\, {\rm d}\ell_2^+\, J(M_1^2 - E_{\rm cm}\ell_1^+)\, \bar{J}(M_2^2 - E_{\rm cm}\ell_2^+)\, S_{\rm hemi}(\ell_1^+, \ell_2^+)\,, \tag{2.99}$$

which agrees with the massless limit of the result in Ref. [124].

5.4 Two-Jet Cone Algorithms

As the last example in this section, we consider the cross section for two-jet final states obtained from an infrared-safe cone jet algorithm. Since the discussion follows closely that of the previous two subsection, we keep it short, mainly highlighting the differences. Combining Eqs. (2.17) and (2.37) with $\mathcal{N} = 2$ we have

$$\begin{aligned}\frac{\mathrm{d}\sigma}{\mathrm{d}O} &= \int \mathrm{d}\mathbf{j}_1\,\mathrm{d}\mathbf{j}_2 \int \mathcal{D}\omega\,\frac{\delta\sigma}{\delta\omega}\,\delta(\mathbf{j}_1 - \mathbf{j}_1[\omega])\,\delta(\mathbf{j}_2 - \mathbf{j}_2[\omega]) \\ &\quad\times \int \mathrm{d}^4P_1\,\delta^4(P_1 - P_{\mathrm{cone}}[\omega;\mathbf{j}_1]) \int \mathrm{d}^4P_2\,\delta^4(P_2 - P_{\mathrm{cone}}[\omega;\mathbf{j}_2])\,\delta(O - g_O(P_1,P_2))\,, \end{aligned} \tag{2.100}$$

where $\mathbf{j}_i[\omega]$ denotes the i-th jet direction returned by $\mathbf{j}[\omega]$, and the functionals for the total jet momenta are now defined for example using Eq. (2.42)

$$P^\mu_{\mathrm{cone}}[\omega;\mathbf{j}_i] \equiv P^\mu[\mathcal{J}_i[\omega;\mathbf{j}]] = \int \mathrm{d}\Omega\,n^\mu(\Omega)\,\omega(\Omega)\,\theta(R - \theta_{\mathbf{j}_i})\,. \tag{2.101}$$

As before, Eq. (2.100) receives in general contributions from operators with $N \geq 2$. However, if the final state is restricted to two jets with small invariant masses, $M_i^2 = P_i^2 \sim \mathcal{O}(\lambda^2 E_{\mathrm{cm}}^2)$, the result for $\delta\sigma/\delta\omega$ in Eq. (2.84) for $N = 2$ gives the dominant contribution, with corrections suppressed by powers of λ. The restriction on the kinematics of the final state is now provided by the jet algorithm, or by the combination of jet algorithm and observable.

For a good jet algorithm, the result of $\mathbf{j}[\omega]$ should not depend on ω_s up to power corrections. This is equivalent to the requirement that the jet algorithm should not be infrared sensitive. Furthermore, since ω_i describes a collinear energy configuration along $\mathbf{n}_i$, by a similar argument as in the case of thrust, up to power corrections, the direction of the jets is aligned with the direction of the collinear fields. Therefore,

$$\mathbf{j}_i[\omega_1 + \omega_2 + \omega_s] = \mathbf{n}_i + \mathcal{O}(\lambda^k)\,. \tag{2.102}$$

The power of k depends on the details of the algorithm, e.g., for the hemisphere jet algorithm, where $\mathbf{j}$ is the thrust axis, we had $k = 2$.

To define the states in SCET, we assign the label n_i to states with momentum lying in the i-th cone, so there is again no overlap between states with the same momentum but different n inside the cones. The precise definition of states with momentum outside any of the cones is not important at this point. With this definition, $P_{\mathrm{cone}}[\omega_{j\neq i};\mathbf{n}_i] = 0$, and since Eq. (2.101) is linear in ω, we have

$$P_{\mathrm{cone}}[\omega_1 + \omega_2 + \omega_s;\mathbf{n}_i] = P_{\mathrm{cone}}[\omega_i;\mathbf{n}_i] + P_{\mathrm{cone}}[\omega_s;\mathbf{n}_i] \equiv q_i + \ell_i\,, \tag{2.103}$$

where $q_i = P_{\mathrm{cone}}[\omega_i;\mathbf{n}_i]$ and $\ell_i = P_{\mathrm{cone}}[\omega_s;\mathbf{n}_i]$ are the total collinear and soft momentum in each cone. Equation (2.102) implies that $q_i + \ell_i$ are aligned along $\mathbf{n}_i$ up to power corrections. In addition, note that $q_i^\pm \equiv q_i^\pm(R)$ is a function of the cone size R (and the used jet algorithm). For $R = \pi$ the cones become hemispheres, and thus $q_i^\pm(\pi) = p_i^\pm$, while at lowest order in perturbation theory, $q_i^\pm(R) = p_i^\pm - \mathcal{O}(\alpha_s)$. Thus, for large enough R, $q_i^\pm/p_i^\pm \sim 1$ with the corrections calculable in perturbation theory. (Generically, we expect the perturbative corrections to contain logarithms of π/R. Similar phase space logarithms have been studied for the case of Sterman-Weinberg jets in

Ref. [187].) Hence, as $q_i^\pm$ obeys the same power counting as $p_i^\pm$ for reasonable R, any observable that does not vanish at leading order in the SCET power counting can be written as

$$g_O(P_1, P_2) \equiv g_O(q_1^+ + \ell_1^+, q_1^-, q_2^+ + \ell_2^+, q_2^-, \mathbf{n}) + \mathcal{O}(\lambda^m)\,, \tag{2.104}$$

where, m is not necessarily the same as k and also depends on the observable.

Since Eq. (2.104) only depends on $q_i^\pm$, the result for $\mathrm{d}\sigma/\mathrm{d}O$ can be expressed in terms of the cone jet and soft functions

$$\begin{aligned}
J_{\mathrm{cone}}(q_1^+, q_1^-) &= \int \frac{\mathrm{d}p_1^+}{2\pi}\, \mathcal{D}\omega_1\, J(p_1^+, E_{\mathrm{cm}}, \mathbf{n}; \omega_1)\, \delta(q_1^+ - n_1{\cdot}P_{\mathrm{cone}}[\omega_1; \mathbf{n}])\, \delta(q_1^- - n_2{\cdot}P_{\mathrm{cone}}[\omega_1; \mathbf{n}])\,, \\
\bar{J}_{\mathrm{cone}}(q_2^+, q_2^-) &= \int \frac{\mathrm{d}p_2^+}{2\pi}\, \mathcal{D}\omega_2\, \bar{J}(p_2^+, E_{\mathrm{cm}}, \mathbf{n}; \omega_2)\, \delta(q_2^+ - n_1{\cdot}P_{\mathrm{cone}}[\omega_2; \mathbf{n}])\, \delta(q_2^- - n_2{\cdot}P_{\mathrm{cone}}[\omega_2; \mathbf{n}])\,, \\
S_{\mathrm{cone}}(\ell_1^+, \ell_2^+) &= \int \mathcal{D}\omega_s\, S_{\mathbf{n}}(\omega_s)\, \delta(\ell_1^+ - n_1{\cdot}P_{\mathrm{cone}}[\omega_s; \mathbf{n}])\, \delta^4(\ell_2^+ - n_2{\cdot}P_{\mathrm{cone}}[\omega_s; -\mathbf{n}])\,,
\end{aligned} \tag{2.105}$$

where as before $n_{1,2} = (1, \pm\mathbf{n})$, and the functions on the left-hand side do not depend on $\mathbf{n}$. Combining Eq. (2.84) with Eq. (2.100) and using the above definitions, we obtain the final result for the factorized differential cross section

$$\begin{aligned}
\frac{\mathrm{d}\sigma}{\mathrm{d}O} = H_2(E_{\mathrm{cm}}) \int \frac{\mathrm{d}\Omega}{2\pi}\, \frac{\mathrm{d}\sigma_0}{\mathrm{d}\cos\theta} \int \mathrm{d}q_1^+\, \mathrm{d}q_1^-\, J_{\mathrm{cone}}(q_1^+, q_1^-) \int \mathrm{d}q_2^+\, \mathrm{d}q_2^-\, \bar{J}_{\mathrm{cone}}(q_2^+, q_2^-) \\
\times \int \mathrm{d}\ell_1^+\, \mathrm{d}\ell_2^+\, S_{\mathrm{cone}}(\ell_1^+, \ell_2^+)\, \delta\big(O - g_O(q_1^+ + \ell_1^+, q_1^-, q_2^+ + \ell_2^+, q_2^-, \mathbf{n}(\Omega))\big)\,.
\end{aligned} \tag{2.106}$$

To our knowledge, factorization for jet distributions has not received much attention in the literature (however, see Refs. [187, 144]), and this is the first time any factorization theorem for jet observables based on jet algorithms has been proven in the framework of SCET.

For many observables, such as the transverse momentum distribution, the dependence on the soft momenta and the small components q_i^+ is power suppressed, which allows us to integrate over these to obtain

$$\frac{\mathrm{d}\sigma}{\mathrm{d}O} = H_2(E_{\mathrm{cm}}) \int \frac{\mathrm{d}\Omega}{2\pi}\, \frac{\mathrm{d}\sigma_0}{\mathrm{d}\cos\theta} \int \mathrm{d}q_1^-\, J_{\mathrm{cone}}(q_1^-) \int \mathrm{d}q_2^-\, \bar{J}_{\mathrm{cone}}(q_2^-)\, S_{\mathrm{cone}}\, \delta\big(O - g_O(q_1^-, q_2^-, \mathbf{n}(\Omega))\big)\,, \tag{2.107}$$

where $\int \mathrm{d}l^+ \mathrm{d}l^-\, S_{\mathrm{cone}}(l^+, l^-) \equiv S_{\mathrm{cone}}$ is perturbatively calculable up to small power corrections and we defined

$$J_{\mathrm{cone}}(q_1^-) = \int \mathrm{d}q_1^+\, J_{\mathrm{cone}}(q_1^+, q_1^-)\,, \qquad \bar{J}_{\mathrm{cone}}(q_2^-) = \int \mathrm{d}q_2^+\, \bar{J}_{\mathrm{cone}}(q_2^+, q_2^-)\,. \tag{2.108}$$

6 Towards $pp \to 2$ Jets

In the previous section we have focused on two-jet production in e^+e^- collisions. In this section, we extend these results to include hadrons in the initial state. Jet production in hadronic collisions is in several ways more complicated than for e^+e^- collisions. First, there are several different partonic processes contributing to $pp \to 2$ jets. Second, the operators describing the short

distance process now contain strongly interacting particles for both initial and final states, giving rise to a more involved color and Dirac structure. Finally, there are several additional matrix elements required to describe the long distance physics. These are the parton distribution function describing how the initial state partons are distributed inside the incoming proton, as well as new soft functions.

In this chapter, we will only consider the simplest partonic process $qq' \to qq'$, and work only to tree level in the matching from QCD onto SCET. This simplifies the discussion dramatically, since only a single operator contributes at this order. Furthermore, due to the absence of gluons in the initial or final state, the only additional nonperturbative ingredients are the parton distributions of finding a quark inside the proton and the new soft function. The complete analysis of $pp \to 2$ jets is considerably more involved and will be discussed elsewhere [22].

6.1 Matching onto SCET at Tree Level

At tree level, only a single operator is required in SCET to describe the partonic process $qq' \to qq'$, schematically

$$\mathcal{O}(p_a, p_b; p_1, p_2) = C_4(p_a, p_b; p_1, p_2)\, \mathcal{O}_I(p_a, p_b)\, \mathcal{O}_F(p_1, p_2)\, \mathcal{O}_S(k_s)\,, \tag{2.109}$$

where we define the Wilson coefficient C_4 to contain all the kinematic and Dirac factors. The operators $\mathcal{O}_I$, $\mathcal{O}_F$, and $\mathcal{O}_S$ are defined as

$$\begin{aligned}
\mathcal{O}_{I\,\alpha\beta}^{cd}(p_a, p_b) &= \chi_\alpha^c(p_a)\, \chi_\beta^d(p_b)\,, \\
\mathcal{O}_{F\,\gamma\delta}^{ef}(p_1, p_2) &= \bar\chi_\gamma^e(p_1)\, \bar\chi_\delta^f(p_2)\,, \\
\mathcal{O}_S^{ec\,fd}(k_s) &= \int \mathrm{d}^4x\, e^{-\mathrm{i}k_s\cdot x}\, T\big[(Y_{n_1}^\dagger T^A \tilde Y_{n_a})^{ec}(x)\, (Y_{n_2}^\dagger T^A \tilde Y_{n_b})^{fd}(x)\big]\,,
\end{aligned} \tag{2.110}$$

where subscripts denote spinor and superscripts color indices. The Wilson lines for the outgoing fields are defined as in Eq. (2.71), while for the incoming fields they are

$$\tilde Y_n(x) = P\, \exp\left[\mathrm{i}g_s \int_{-\infty}^0 \mathrm{d}s\, n\cdot A_s(x + sn)\right]. \tag{2.111}$$

The Wilson coefficient is given by

$$C_4(p_a, p_b; p_1, p_2) = \frac{\mathrm{i}g_s^2}{\hat t}\, (\gamma^\mu)_{\gamma\alpha}\, (\gamma_\mu)_{\delta\beta}\,, \tag{2.112}$$

where we stress again that we are only working to tree level in the matching. The variable $\hat t$ is one of the usual Mandelstam variables defined in terms of the partonic momenta

$$\hat s = (p_a + p_b)^2\,, \qquad \hat t = (p_a - p_1)^2\,, \qquad \hat u = (p_a - p_2)^2\,. \tag{2.113}$$

6.2 New Nonperturbative Matrix Elements

There are two sources of additional matrix elements which cannot be calculated perturbatively. First, the operator $\mathcal{O}_I$ now includes strongly interacting degrees of freedom, and the matrix

elements involving the initial state protons are no longer calculable. Second, the soft operator contains four Wilson lines, rather than just two as for e^+e^- collisions. This implies that a new soft function is required. In this section we define all required nonperturbative matrix elements needed for the process $pp \to 2$ jets via the partonic process $qq' \to qq'$.

Since the initial state hadrons are moving along different light cones, they are described by two sets of SCET Lagrangians which do not interact with each another. Therefore, the physics of the two initial states completely factorizes, in the same way as the final state partons in different directions factorize from one another, and we can write $|I\rangle = |P_a\rangle\ |P_b\rangle$ and $\mathcal{O}_I(p_a, p_b) = \mathcal{O}_I^a(p_a)\mathcal{O}_I^b(p_b)$, such that we can factorize the initial state matrix element as

$$\begin{aligned}&\langle I|\mathcal{O}_I^\dagger(p_a', p_b')\,\delta[\omega_a - \mathcal{E}_a^0]\,\delta[\omega_b - \mathcal{E}_b^0]\,\mathcal{O}_I(p_a, p_b)|I\rangle \\ &\quad = \langle P_a|\mathcal{O}_I^{a\,\dagger}(p_a')\,\delta[\omega_a - \mathcal{E}_a^0]\,\mathcal{O}_I^a(p_a)|P_a\rangle\,\langle P_b|\mathcal{O}_I^{b\,\dagger}(p_b')\,\delta[\omega_b - \mathcal{E}_b^0]\,\mathcal{O}_I^b(p_b)|P_b\rangle\,. \end{aligned} \tag{2.114}$$

For the case considered here, the operators $\mathcal{O}_I^a$ and $\mathcal{O}_I^b$ contain just a single quark field, $(\mathcal{O}_I^a)_\alpha^c = \chi_\alpha^c(p_a)$ and $(\mathcal{O}_I^b)_\beta^d = \chi_\beta^d(p_b)$. The resulting matrix elements define the parton distribution functions to find the quarks q and q' in the initial protons $P_{a,b}$.

$$\int \frac{\mathrm{d}^4 p_a'}{(2\pi)^4} \big\langle P_a\big|\bar\chi_{\alpha'}^{c'}(p_a')\,\delta[\omega_a - \mathcal{E}_a^0]\,\chi_\alpha^c(p_a)\big|P_a\big\rangle = \frac{1}{2N_c}\,\delta^{c'c}\left(\frac{\bar{n}\!\!\!/_a}{2}\right)_{\alpha\alpha'} f_{q/P}(p_a;\omega_a)\,, \tag{2.115}$$

and similarly for $f_{q'/P}(p_b;\omega_b)$. (Note that since we are distinguishing particles and antiparticles by the sign of their momentum, there is no anti-quark distribution on the right-hand side.) Combining these results gives the initial state function

$$I_{\alpha'\alpha\,\beta'\beta}^{c'c\,d'd}(p_a, p_b; \omega_a, \omega_b) = \frac{1}{4N_c^2}\,\delta^{c'c}\,\delta^{d'd}\left(\frac{\bar{n}\!\!\!/_a}{2}\right)_{\alpha\alpha'}\left(\frac{\bar{n}\!\!\!/_b}{2}\right)_{\beta\beta'} f_{q/P}(p_a;\omega_a)\,f_{q'/P}(p_b;\omega_b)\,. \tag{2.116}$$

In most cases of experimental interest, the observable is independent of $\omega_{a,b}$ and the plus- and transverse components of the collinear momentum, which means we can integrate over these to obtain the standard parton distribution function [91, 20, 160]

$$f_{q/P}(x_a) = \int \frac{\mathrm{d}^4 p_a}{(2\pi)^4}\,\mathcal{D}\omega_a\,f_{q/P}(p_a;\omega_a)\,\delta(p_a^- - x_a E_{\mathrm{cm}})\,, \tag{2.117}$$

while everywhere else up to power corrections we can use

$$p_a = x_a E_{\mathrm{cm}}\,\frac{n_a}{2}\,, \qquad p_b = x_b E_{\mathrm{cm}}\,\frac{n_b}{2}\,, \tag{2.118}$$

with $n_a = (1, \mathbf{n}_{P_a})$ and $n_b = (1, \mathbf{n}_{P_b})$ now aligned along the direction of the incoming protons.

While the dependence on ω in our generalized distributions $f_{q/I}(p;\omega)$ is not of relevance for most processes of interest, it describes the energy configuration of the remnant of the proton after the hard scattering. Thus, this matrix element provides a field-theoretical definition of the beam remnant. In particular, this means that the effect of the beam remnant is properly taken into account in our factorization proof in Sec. 4. In principle, operators $\mathcal{O}_I$ with more than one collinear field in the directions n_a and n_b can be included as well, and would describe multiple scatterings of partons originating from the initial protons. These additional hard scatterings give rise to what is usually referred to as the underlying event [178, 176]. Thus, these effects are also

taken into account in our factorization proof. Moreover, our formalism provides a field-theoretic basis to study the underlying event. The details are left for future work.

Since we only work to tree level in the matching from QCD to SCET, there is only a single soft function required for the process $qq' \to qq'$. After contracting with the color structures of the initial state function and the q and q' quark jet functions $J^{e'e}_{\gamma'\gamma}(p_1;\omega_1)$ and $J^{f'f}_{\delta'\delta}(p_2;\omega_2)$ (defined in the first line of Eq. (2.75)), we obtain

$$\begin{aligned} S_{n_a n_b n_1 n_2}(\omega_s) &= \frac{2}{N_c C_F} \int \frac{\mathrm{d}^4 k_s'}{(2\pi)^4} \frac{\mathrm{d}^4 k_s}{(2\pi)^4} \left\langle 0\middle| \mathcal{O}_S^{\dagger ce\,df}(k_s')\, \delta[\omega_s - \mathcal{E}_s^0]\, \mathcal{O}_S^{ec\,fd}(k_s)\middle|0\right\rangle \\ &= \frac{2}{N_c C_F} \left\langle 0\middle| \overline{T}\big[(\tilde{Y}_{n_a}^\dagger T^B Y_{n_1})^{ce}(0)\,(\tilde{Y}_{n_b}^\dagger T^B Y_{n_2})^{df}(0)\big]\, \delta[\omega_s - \mathcal{E}_s^0] \right. \\ &\qquad \left. \times T\big[(Y_{n_1}^\dagger T^A \tilde{Y}_{n_a})^{ec}(0)\,(Y_{n_2}^\dagger T^A \tilde{Y}_{n_b})^{fd}(0)\big]\middle|0\right\rangle . \end{aligned} \tag{2.119}$$

6.3 Generic Expression

Combining Eqs. (2.67), (2.75), (2.112), (2.115) and (2.119), the $qq' \to qq'$ contribution to $\delta\sigma/\delta\omega$ for 2-jet production can be written as

$$\begin{aligned} \frac{\delta\sigma}{\delta\omega} &= \frac{1}{2E_{\mathrm{cm}}^2} \Bigg(\prod_{i=a,b,1,2} \int \frac{\mathrm{d}^4 p_i}{(2\pi)^4}\, \mathcal{D}\omega_i \Bigg) \frac{1}{4N_c^2}\, f_{q/P}(p_a;\omega_a)\, f_{q'/P}(p_b;\omega_b)\, J(p_1;\omega_1)\, J(p_2;\omega_2) \\ &\quad \times\, H_4(p_a,p_b;p_1,p_2)\, \frac{N_c C_F}{2} \int \mathcal{D}\omega_s\, S_{n_a n_b n_1 n_2}(\omega_s) \\ &\quad \times (2\pi)^4 \delta^4(p_a + p_b - P[\omega_s] - p_1 - p_2)\, \delta[\omega - \omega_a - \omega_b - \omega_1 - \omega_2 - \omega_s] , \end{aligned} \tag{2.120}$$

where (at tree level in the matching)

$$H_4(p_a,p_b;p_1,p_2) = \frac{g_s^4}{\hat{t}^2}\, \frac{1}{4}\, \mathrm{tr}[\not{p}_a \gamma_\mu \not{p}_1 \gamma_\nu]\, \frac{1}{4}\, \mathrm{tr}[\not{p}_b \gamma^\mu \not{p}_2 \gamma^\nu] = \frac{2g_s^4}{\hat{t}^2}\, (n_a{\cdot}n_b\; n_1{\cdot}n_2 + n_a{\cdot}n_2\; n_b{\cdot}n_1) . \tag{2.121}$$

As discussed before, most observables are independent of the energy configurations ω_a and ω_b, i.e., $f_O[\omega_a + \omega_b + \omega_1 + \omega_2 + \omega_s] = f_O[\omega_1 + \omega_2 + \omega_s]$. Therefore we can drop these beam remnant configuration in the δ functional for ω and integrate over them in the parton distribution functions. Furthermore, inserting

$$1 = E_{\mathrm{cm}}^2 \int_0^1 \mathrm{d}x_a \int_0^1 \mathrm{d}x_b\, \delta(p_a^- - x_a E_{\mathrm{cm}})\, \delta(p_b^- - x_b E_{\mathrm{cm}}) , \tag{2.122}$$

and using Eqs. (2.117) and (2.118), the expression for $\delta\sigma/\delta\omega$ becomes

$$\begin{aligned} \frac{\delta\sigma}{\delta\omega} &= \frac{C_F}{16 N_c} \int_0^1 \mathrm{d}x_a\, \mathrm{d}x_b\, f_{q/P}(x_a)\, f_{q'/P}(x_b) \int \frac{\mathrm{d}^4 p_1}{(2\pi)^4}\, \mathcal{D}\omega_1\, J(p_1;\omega_1) \int \frac{\mathrm{d}^4 p_2}{(2\pi)^4}\, \mathcal{D}\omega_2\, J(p_2;\omega_2) \\ &\quad \times\, H_4\Big(E_{\mathrm{cm}} x_a \frac{n_a}{2}, E_{\mathrm{cm}} x_b \frac{n_b}{2}; p_1, p_2\Big) \int \mathcal{D}\omega_s\, S_{n_a n_b n_1 n_2}(\omega_s) \\ &\quad \times (2\pi)^4 \delta^4\Big(E_{\mathrm{cm}} x_a \frac{n_a}{2} + E_{\mathrm{cm}} x_b \frac{n_b}{2} - P[\omega_s] - p_1 - p_2\Big)\, \delta[\omega - \omega_s - \omega_1 - \omega_2] , \end{aligned} \tag{2.123}$$

where $n_{a,b} = (1, \mathbf{n}_{P_{a,b}})$ are now aligned with the directions of the incoming protons. As in Sec. 5, this can be simplified further by expanding the kinematics. After some algebra, we obtain

$$\frac{\delta\sigma}{\delta\omega} = \int \frac{\mathrm{d}\Omega_p}{2\pi} \int_0^1 \mathrm{d}x_a\, \mathrm{d}x_b \int \frac{\mathrm{d}p_1^+}{2\pi}\, \mathcal{D}\omega_1\, J(p_1^+, p_1^-, \mathbf{n}_1; \omega_1) \int \frac{\mathrm{d}p_2^+}{2\pi}\, \mathcal{D}\omega_2\, J(p_2^+, p_2^-, \mathbf{n}_2; \omega_2)$$
$$\times f_{q/P}(x_a)\, f_{q'/P}(x_b)\, \frac{\mathrm{d}\sigma_0}{\mathrm{d}\cos\theta_p} \int \mathcal{D}\omega_s\, S_{n_a n_b n_1 n_2}(\omega_s)\, \delta[\omega - \omega_s - \omega_1 - \omega_2]\,, \tag{2.124}$$

where the angular integral is defined in the center-of-mass frame of the partonic collision. Both the large p_i^- components and the directions $\mathbf{n}_i$ are functions of the partonic center-of-mass angular variables, Ω_p, and the energy fractions of the incoming partons, $x_{a,b}$. They are defined by

$$\begin{aligned} p_1^-(\Omega_p, x_a, x_b) &= \frac{E_{\mathrm{cm}}}{2}\left[x_a(1+\cos\theta_p) + x_b(1-\cos\theta_p)\right], \\ p_2^-(\Omega_p, x_a, x_b) &= \frac{E_{\mathrm{cm}}}{2}\left[x_a(1-\cos\theta_p) + x_b(1+\cos\theta_p)\right], \\ \mathbf{n}_i(\Omega_p, x_a, x_b) &= \mathbf{n}(\Omega_i)\,, \end{aligned} \tag{2.125}$$

where $\Omega_i = (\theta_i, \phi_i)$ are given by

$$\begin{aligned} \cos\theta_1 &= \frac{x_a(1+\cos\theta_p) - x_b(1-\cos\theta_p)}{x_a(1+\cos\theta_p) + x_b(1-\cos\theta_p)}\,, & \phi_1 &= \phi_p \\ \cos\theta_2 &= \frac{x_a(1-\cos\theta_p) - x_b(1+\cos\theta_p)}{x_a(1-\cos\theta_p) + x_b(1+\cos\theta_p)}\,, & \phi_2 &= \phi_p + \pi\,. \end{aligned} \tag{2.126}$$

Finally, the differential cross section $\mathrm{d}\sigma_0/\mathrm{d}\cos\theta_p$ is given by

$$\frac{\mathrm{d}\sigma_0}{\mathrm{d}\cos\theta_p} = \frac{\pi\alpha_s^2 C_F}{2N_c}\, \frac{1}{x_a\, x_b\, E_{\mathrm{cm}}^2}\, \frac{4 + (1+\cos\theta_p)^2}{(1-\cos\theta_p)^2}\,, \tag{2.127}$$

which agrees with the well known expression in terms of the Mandelstam variables $\hat{s}, \hat{t}, \hat{u}$

$$\frac{\mathrm{d}\sigma_0}{\mathrm{d}\hat{t}} = \frac{\pi\alpha_s^2 C_F}{N_c}\, \frac{\hat{s}^2 + \hat{u}^2}{\hat{s}^2\, \hat{t}^2}\,. \tag{2.128}$$

6.4 Jet Observables

As an example how to use Eq. (2.124), we derive a factorized cross section for infrared-safe cone jet observables, which was also studied in Ref. [144]. The required steps are very similar to the derivation given in Sec. 5.4, and we only highlight the differences that arise from having protons in the initial state. First, $\delta\sigma/\delta\omega$ depends on the parton distribution functions $f_{q/P}(x_a)$ and $f_{q'/P}(x_b)$. Second, while for e^+e^- collisions one often uses the variables θ and ϕ to denote the direction of jets, in pp collisions it is more appropriate to use the rapidity instead of the angle θ, due to the easier transformation properties under boosts along the beam direction. This gives cone jet functions J_{cone} that have exactly the same form as in Eq. (2.124) but use the corresponding cone projections in place of Eq. (2.42) to define the functionals $P_{\mathrm{cone}}[\omega; \mathbf{j}_i]$ in Eq. (2.101). The final difference is that the cone soft function now explicitly depends on the orientation of the directions $\mathbf{n}_i$ relative to the

beam axis, since it contains Wilson lines in both the directions of the incoming protons and the outgoing jets. In particular, this implies that the nonperturbative physics described by this cone soft function depends on the rapidities of the outgoing jets. The experimental determination of the soft function is thus considerably more difficult for hadronic collisions than for e^+e^- collisions.

Keeping in mind these differences, we can follow the same steps as in Sec. 5.4 to obtain the factorization formula for generic two-jet observable using cone jets:

$$\begin{aligned}\frac{\mathrm{d}\sigma}{\mathrm{d}O} &= \int \frac{\mathrm{d}\Omega_p}{2\pi} \int_0^1 \mathrm{d}x_a\, \mathrm{d}x_b\, f_{q/P}(x_a)\, f_{q'/P}(x_b)\, \frac{\mathrm{d}\sigma_0}{\mathrm{d}\cos\theta_p} \\ &\quad \times \int \mathrm{d}q_1^+\, \mathrm{d}q_1^-\, J_{\mathrm{cone}}(q_1^+, q_1^-) \int \mathrm{d}q_2^+\, \mathrm{d}q_2^-\, J_{\mathrm{cone}}(q_2^+, q_2^-) \\ &\quad \times \int \mathrm{d}\ell_1^+\, \mathrm{d}\ell_2^+\, S^{\mathrm{cone}}_{\mathbf{n}_1\mathbf{n}_2}(\ell_1^+, \ell_2^+)\, \delta\big(O - g_O(q_1^+ + \ell_1^+, q_1^-, q_2^+ + \ell_2^+, q_2^-, \mathbf{n}_1, \mathbf{n}_2)\big)\,, \end{aligned} \tag{2.129}$$

where the cone soft function is now defined as

$$S^{\mathrm{cone}}_{\mathbf{n}_1\mathbf{n}_2}(\ell_1^+, \ell_2^+) = \int \mathcal{D}\omega_s\, S_{n_a n_b n_1 n_2}(\omega_s)\, \delta(\ell_1^+ - n_1\cdot P_{\mathrm{cone}}[\omega_s; \mathbf{n}_1])\, \delta(\ell_2^+ - n_2\cdot P_{\mathrm{cone}}[\omega_s; \mathbf{n}_2])\,. \tag{2.130}$$

As for e^+e^-, many jet observables only depend on the large momentum components and the direction of the jets. In this case, we can perform the integrals over p_i^+ and ℓ_i^+. Integrating over ℓ_i^+ we define

$$\int \mathrm{d}\ell_1^+\, \mathrm{d}\ell_2^+\, S^{\mathrm{cone}}_{\mathbf{n}_1,\mathbf{n}_2}(\ell_1^+, \ell_2^+) \equiv S^{\mathrm{cone}}_{\mathbf{n}_1,\mathbf{n}_2}\,, \tag{2.131}$$

which is now perturbatively calculable up to small power corrections. We obtain

$$\begin{aligned}\frac{\mathrm{d}\sigma}{\mathrm{d}O} &= \int \frac{\mathrm{d}\Omega_p}{2\pi} \int_0^1 \mathrm{d}x_a\, \mathrm{d}x_b\, f_{q/P}(x_a)\, f_{q'/P}(x_b)\, \frac{\mathrm{d}\sigma_0}{\mathrm{d}\cos\theta_p} \int \mathrm{d}q_1^-\, J(q_1^-) \int \mathrm{d}q_2^-\, J(q_2^-) \\ &\quad \times S^{\mathrm{cone}}_{\mathbf{n}_1,\mathbf{n}_2}\, \delta\big(O - g_O(q_1^-, q_2^-, \mathbf{n}_1, \mathbf{n}_2)\big)\,, \end{aligned} \tag{2.132}$$

where the jet functions integrated over p_i^+ are defined as in Eq. (2.108).

7 Conclusions and Outlook

We have developed a new formalism for obtaining factorization theorems for almost any observable of interest at high energy colliders. We argued that any observable differential cross section can be written in terms of two building blocks, a fully differential cross section describing the energy and momentum distribution of a given event, together with the restriction of how to obtain the desired observable from this distribution. For events containing only massless particles in the final state, the only information required to define observables O is the energy configuration ω of the event, and we therefore focused on the cross section fully differential in ω, which we denoted as $\delta\sigma/\delta\omega$. By integrating this energy distribution with an appropriate functional $f_O[\omega]$, the differential cross section $\mathrm{d}\sigma/\mathrm{d}O$ in any observable O can be obtained.

Our main result is the proof of factorization for the fully differential cross section, $\delta\sigma/\delta\omega$, using soft-collinear effective theory. It relies on the fact that $\delta\sigma/\delta\omega$ can be written directly in terms of a matrix element of well-defined operators in SCET using the energy flow operator. The

linearity of the energy flow operator allowed us to factorize $\delta\sigma/\delta\omega$ into simpler building blocks, each of which is defined by matrix elements of operators in the effective theory and contains a single scale allowing for a systematic program of logarithmic resummation. After the factorized form of $\delta\sigma/\delta\omega$ for a given process is determined once and for all, it can be used to study the factorization properties of specific observables. The question of whether a given differential cross section $\mathrm{d}\sigma/\mathrm{d}O$ factorizes in the traditional sense depends on whether the form of $f_O[\omega]$ is such that it smears the individual matrix elements in $\delta\sigma/\delta\omega$ into objects that can be either calculated perturbatively or determined experimentally from other processes.

Using our formalism, we were able to directly study the factorization properties of the fully differential cross section, independent from the observable-specific functional $f_O[\omega]$. While the question of whether the differential cross section in a given observable factorizes in the traditional sense still needs to be asked on an observable-by-observable basis, this disentanglement demonstrates to what length the steps taken in factorization proofs are observable independent. It turns out that it is the observable independent analysis that requires most of the calculational work. The fact that we can study factorization on an observable independent level could potentially be relevant for Monte Carlo event generation. It should be possible to make a connection between our factorized result for $\delta\sigma/\delta\omega$ for generic N-jet production and the N-body partonic calculations that were introduced in Refs. [34, 35] as input for an event generation framework. If so, our results could be used to provide improved theoretical inputs for event generation. However, more work in this direction is needed.

To demonstrate the simplicity with which factorization formulas for specific observables can be obtained from the factorized result for $\delta\sigma/\delta\omega$, we have applied our results to several simple observables in $e^+e^- \to 2$ jets. We first reproduced the known results for event shape and hemisphere mass distributions, and then obtained factorization formulas for generic observables defined in terms of the total jet momenta obtained from cone jet algorithms, which so far have not been studied in SCET. We have also explored some of the issues arising in jet production in hadronic collisions by studying the partonic subprocess $qq' \to qq'$ using tree level matching from QCD onto SCET. In particular, we showed that the more complicated structure requires a soft function that is more complicated from the case of e^+e^- scattering. We also showed how parton distribution functions arise in our formalism, and commented on how it could be used to study beam remnants and underlying events.

It should be clear from these examples how our generic N-jet formalism can be applied to the study of observables in more complicated processes, such as processes with heavy vector bosons and more than two jets in the final state, which are crucial for many measurements at the upcoming LHC. It is these more complicated processes where the power of our new formalism becomes increasingly pronounced. While the number and complexity of Dirac and color structures grows quickly for any exhaustive study of factorization with two or more final state jets, the application of our formalism is straightforward and in fact facilitates recycling the bulk of the work needed or already known in the literature for a particular observable, to be used for other observables of interest.

Chapter 3

Effective Predictions of Event Shapes: Factorized, Resummed, and Gapped Angularity Distributions[1]

1 Introduction

Event shapes probe the hadronic final states produced in hard scattering processes for jet-like structure [99]. Two-jet event shapes e in hadronic e^+e^- annihilations are constructed so that one of the kinematic endpoints corresponds to the limit of two back-to-back perfectly collimated jets. Different event shapes vary in their sensitivity to particles close to or far away from the jet axis and thus used in tandem probe the substructure of jets [4, 3]. Some examples of two-jet event shapes are the familiar thrust [55, 123], jet masses [88, 80, 89], and jet broadening [75], and the more recently introduced angularities [47]. The shape of the distributions in these variables depend on several energy scales, namely, the scale Q of the hard scattering, the scale of the invariant mass or typical transverse momentum of the jet μ_J, and the scale $\Lambda_{\rm QCD}$ of soft radiation from the jets involved in color recombination occurring during hadronization. Event shapes thus probe the behavior of QCD over a large range of energy scales, and indeed have been the source of some of the most precise extractions of the strong coupling constant α_s [41, 102, 51].

Dependence on strong interactions at soft scales near $\Lambda_{\rm QCD}$ where QCD is nonperturbative would render predictive calculations impossible, without the use of factorization. Factorization separates an observable into pieces depending on each individual relevant energy scale. Those pieces depending on large scales can be calculated perturbatively, while those depending on soft scales remain nonperturbative. If these soft functions are, however, universal among different observables or physical processes, then calculations of the factorized observables become predictive. A large number of two-jet event shape distributions in e^+e^- annihilation can be factorized into hard, jet, and soft functions:

$$\frac{1}{\sigma_{\rm tot}}\frac{{\rm d}\sigma}{{\rm d}e} = H(Q;\mu)\int {\rm d}e_1\,{\rm d}e_2\,{\rm d}e_s\,J_1(e_1;\mu)J_2(e_2;\mu)S(e_s;\mu)\delta(e-e_1-e_2-e_s)\,, \tag{3.1}$$

[1] This chapter was originally cowritten with Christopher Lee and Gregory Ovanesyan [134].

where $H(Q;\mu)$ is the hard coefficient dependent only on the hard scattering $e^+e^- \to q\bar{q}$ at center-of-mass energy Q, $J_{1,2}$ are jet functions describing the perturbative evolution of the initially produced partons $q, \bar{q}$ into collimated jets of lower-energy partons, and finally $S(e_s;\mu)$ is the soft function describing the color exchange between the two jets leading to the hadronization of their constituent partons. This description introduces dependence on a factorization scale μ, at which the cross-section is factorized, into each of the individual functions. This dependence must cancel in the whole combination in Eq. (3.1). The full distribution and the individual jet and soft functions contain terms of the form $(1/e)\alpha_s^n \ln^m e$ which become large in the two-jet limit $e \to 0$. The dependence of the hard, jet, and soft functions on the factorization scale μ can be determined from renormalization group equations, which can be used to resum the large logarithms [96].

The formidable achievements of proofs of factorization theorems for hard scattering cross-sections in QCD span a long and monumental history [93, 181]. More recently many of these theorems were reformulated in the language of soft-collinear effective theory (SCET) [19, 21, 33, 29]. This was done for two-jet event shapes for light quark jets in the series of papers [26, 24, 157, 18] and for top quark jets in [124, 125]. Some of the relations between the full and effective theory formulations of factorization were explored in [157, 18]. Equivalent results can be formulated in either language, although our discussion below will be in the context of SCET, which we find advantageous for its intuitive framework for separating physics at hard, collinear, and soft scales and its explicit Lagrangian for interactions between collinear and soft modes. These features facilitate the implementation of factorization and resummation of logarithms of ratios of all the relevant energy scales. At the same time that the effective theory provides us an intuitive framework in which to analyze the behavior of event shape distributions, the properties of the angularities themselves will in turn illuminate properties of the effective theory, and in particular, the conditions under which it is valid for the observables under consideration.

To describe the conditions under which the distribution in a particular event shape factorizes as in Eq. (3.1), it is useful to write event shapes in a generic form. Many event shapes can be written in the form,

$$e(X) = \frac{1}{Q} \sum_{i \in X} \left| \mathbf{p}_\perp^i \right| f_e(\eta_i) \,, \tag{3.2}$$

where the sum is over all particles i in the final state X, $\mathbf{p}_\perp^i$ is the transverse momentum of the ith particle and η_i its rapidity relative to the thrust axis. Each choice of the weight function f_e determines a different event shape. For example, for the thrust and jet broadening, $f_{1-T}(\eta) = \mathrm{e}^{-|\eta|}$ and $f_B(\eta) = 1$. A continuous set of event shapes which generalize the thrust and jet broadening are the *angularities* τ_a [47], corresponding to the choice

$$f_{\tau_a}(\eta) = \mathrm{e}^{-|\eta|(1-a)} \,, \tag{3.3}$$

where a is any real number $a < 2$. For $a \geq 2$, the function in Eq. (3.3) weights particles collinear to the thrust axis too strongly and makes the quantity Eq. (3.2) sensitive to collinear splitting, and thus not infrared-safe. The factorization theorem Eq. (3.1), however, is valid only for $a < 1$. At $a = 1$, the distribution of events in τ_1 is dominated by jets with invariant mass of order Λ_{QCD}. Thus, the jet and soft scales coincide, and the distribution cannot be divided into separately infrared-safe jet and soft functions, at least in the traditional form of the factorization theorem. This breakdown can be seen in the uncontrollable growth of a number of nonperturbative power corrections as $a \to 1$ [47, 157], or in the failure to cancel infrared divergences in the perturbative calculation of the jet

or soft functions in the same limit, as we have recently explored in Ref. [135]. We review this breakdown of factorization in the explicit perturbative calculations we perform below. Any choice of weight function f_e that sets a jet scale at or lower than the soft scale will ruin the factorization Eq. (3.1).

The distributions for which the factorization in Eq. (3.1) breaks down might still factorize in a different form, by distinguishing collinear and soft modes not by their invariant mass, but by their rapidity, as proposed in [163]. We do not, however, pursue such a strategy here, and focus only on angularities with strictly $a < 1$.[2]

The soft function evaluated at a scale $\mu_s \sim \Lambda_{\rm QCD}$ is nonperturbative. Evaluated at a higher scale, however, it can be calculated in perturbation theory. An appropriate model for the soft function should interpolate between these two regimes. In our analysis we adopt a model like that proposed for hemisphere jet masses in [132] and for b-quark distributions in [159], in which the soft function is a convolution,

$$S(e_s;\mu) = \int \mathrm{d}e_s'\, S^{\rm PT}(e_s - e_s';\mu) f^{\rm exp}(e_s' - \Delta_e)\,, \tag{3.4}$$

where $S^{\rm PT}$ is the partonic soft function calculated in perturbation theory, and $f^{\rm exp}$ is a nonperturbative model function. The gap parameter Δ_e, proposed in Ref. [132], enters $f^{\rm exp}$ through a theta function $\theta(e_s - \Delta_e)$ so that the minimum possible value of an event shape e of final states is Δ_e, which is zero in the partonic distribution, but is nonzero due to hadronization in the actual distribution. The full soft function $S(e_s;\mu)$ inherits its scale dependence from $S^{\rm PT}(e_s;\mu)$ and thus has a well-defined running with the scale μ.

The partonic soft function $S^{\rm PT}(e_s;\mu)$ contains a renormalon ambiguity due to the behavior of the perturbative series at high orders. This ambiguity should not be present in the full physical distribution or the soft function, so the ambiguity in $S^{\rm PT}$ is canceled by a corresponding ambiguity in Δ_e. Shifting from Δ_e to a renormalon-free gap parameter $\bar{\Delta}_e(\mu) = \Delta_e - \delta_e(\mu)$ removes the ambiguity from the entire soft function Eq. (3.4). This greatly reduces the uncertainty in the predicted distribution due to such renormalon ambiguities. These features were demonstrated in [132] for jet mass and thrust distributions. In this chapter, we extend the soft function model and demonstrate that a similar cancellation occurs for angularities τ_a.

Many studies of nonperturbative soft power corrections in event shape distributions have been based on the behavior of the perturbative expansions of the distributions, either the behavior of their renormalon ambiguities [164, 45] or their dependence on a postulated "infrared" effective coupling α_s at low scales [108, 109, 110]. In particular, they led to the proposal of a universal soft power correction to the mean values of event shape distributions in the form [109, 110]

$$\langle e\rangle = \langle e\rangle_{\rm PT} + \frac{c_e \mathcal{A}}{Q}\,, \tag{3.5}$$

where $\langle e\rangle_{\rm PT}$ is the mean value of the partonic distribution, and the coefficient of the $1/Q$ power correction is an exactly-calculable number c_e dependent on the choice of event shape multiplied by an unknown nonperturbative parameter $\mathcal{A}$ which is universal for numerous event shape distributions. In [157] the operator definition of the soft function in the factorization theorem Eq. (3.1)

[2] Even though traditional factorization breaks down for $a = 1$ (jet broadening), the resummation of jet broadening in QCD was performed in [75, 106] and nonperturbative effects were discussed in [107].

was used to prove the relation Eq. (3.5) to all orders in α_s. For angularities, $c_{\tau_a} = 2/(1-a)$. This scaling of the power correction with a was observed in [49] based on the behavior of the resummed perturbative series for angularity distributions after imposing an IR cutoff on the scale in $\alpha_s(\mu)$ and in [48] based on analysis of the distributions using dressed gluon exponentiation [128]. Below we will review the proof of the scaling in [157] based on the operator definition of the soft function independently of its perturbative expansion, and later use the scaling rule to constrain the nonperturbative model we adopt for the soft function in angularity distributions.

The history of calculating event shape distributions using perturbation theory in QCD goes all the way back to QCD's earliest years. The thrust distribution for light quark jets to $\mathcal{O}(\alpha_s)$ was calculated in [101], to which our fixed-order results for $\mathrm{d}\sigma/\mathrm{d}\tau_a$ reduce at $a = 0$. The resummation of the thrust distribution to NLL was performed in QCD in [73, 76] and to LL in SCET in [32, 172] (and later extended to N^{3}LL in [41]). Our results are consistent with these SCET results at the appropriate orders for $a = 0$. The jet mass distribution for top quark jets was calculated and resummed to the same order in [125], with which we agree on the SCET jet and soft functions for $a = 0$ in the limit $m_t = 0$. The jet and soft functions for thrust or jet mass distributions can be derived easily from the "ordinary" SCET jet function $J(k^+)$, and the hemisphere soft function $S(k^+, k^-)$, because the thrust and jet mass depend only on a single light-cone component of the total four-momentum in each hemisphere (cf. [73]). These standard jet and soft functions were calculated to two-loop order in [37, 38, 130]. Angularities for arbitrary a, however, depend on *both* light-cone components $k^\pm$ in *each* hemisphere, thus requiring the new calculations we perform below.

In the original introduction of the angularities τ_a [47] the resummation of logarithms was achieved to the same next-to-leading-logarithmic (NLL) order that we achieve below, but without full inclusion of next-to-leading-order (NLO) jet and soft functions for the τ_a-distribution, which we calculate explicitly here for the first time. This improves the accuracy of our result for small τ_a. Our result is also improved in this region by adopting the soft function model Eq. (3.4) which cures unphysical behavior of the point-by-point distribution $\mathrm{d}\sigma/\mathrm{d}\tau_a$ as $\tau_a \to 0$ due to renormalon ambiguities. The results of [47] converted to the traditional form of an NLL resummed event shape distribution [73] were subsequently matched to fixed-order QCD at $\mathcal{O}(\alpha_s^2)$ numerically in [49], improving the accuracy of the large-τ_a region. We perform this fixed-order matching only at $\mathcal{O}(\alpha_s^1)$.

Comparing our result to those of [47, 49] elucidates the relation between SCET and traditional QCD-based approaches to resumming logarithms more generally. While the advantages of SCET in achieving factorization or resummation of logarithms through renormalization group evolution can of course be formulated without the explicit language of the effective theory (see, e.g., [47, 96]), the effective theory nevertheless unifies these concepts and methods in an intuitive framework that, we have found, allows us greater facility in improving the precision and reliability of our predictions of event shape distributions. Even though we do not go beyond the existing NLL resummation of logarithms of τ_a [47, 49], the flexibility in the effective theory to vary the scales $\mu_{H,J,S}$, where logarithms in the hard, jet, and soft functions are small and from which we run each function to the factorization scale μ, allows additional improvements. For example, we are able to avoid any spurious Landau pole singularities which the traditional approaches usually encounter. (For previous discussions on how the effective theory avoids spurious Landau poles present in the traditional approach, see Refs. [160, 36, 39].)

The plan of the chapter is as follows. In Sec. 2, we review the demonstration of factorization of event shape distributions in the formalism of SCET that was presented in [18], recalling the introduction of the event shape operator $\hat{e}$ that returns the value of an event shape e of a final state X, constructed from the energy-momentum tensor. In Sec. 3, we calculate the jet and soft functions appearing in the factorization theorem for angularity distributions for $a < 1$ to one-loop order in α_s. We recall the observations of [135] about how the breakdown of factorization as $a \to 1$ is observed in the infrared behavior of these functions in perturbation theory. In Sec. 4 we solve the renormalization group equations obeyed by the hard, jet, and soft functions and resum leading and next-to-leading logarithms of τ_a in the perturbative expansions of these functions, and explain how we match the resummed distributions onto the fixed-order prediction of QCD at $\mathcal{O}(\alpha_s)$. In Sec. 5 we construct a model for the soft function in angularity distributions for all $a < 1$, based on existing models for hemisphere and thrust soft functions which contain a nonperturbative gap parameter introduced in [132], which cancels the renormalon ambiguity in the perturbative series for the soft function. In Sec. 6 we present plots of our final predictions of angularity distributions using all the results of Secs. 3–5. In Sec. 7 we compare and contrast the SCET approach to predicting resummed angularity distributions to those based on factorization and RG evolution in full QCD [47] and to the traditional approach to resummation [49, 73]. In Sec. 8 we present our conclusions, and in the Appendices, we verify a consistency relation among the hard, jet, and soft anomalous dimensions for arbitrary a, provide some technical details necessary for the solution of the RG equations for the jet and soft functions, and explain our procedure to calculate angularity distributions at fixed-order in QCD at $\mathcal{O}(\alpha_s)$, noting the hitherto unnoticed property of the angularities that they fail to separate two- and three-jet-like events for values of $a \lesssim -2$, and so cease to behave exactly as "two-jet" event shapes.

2 Review of Factorization of Event Shape Distributions

We begin by reviewing the factorization of event shape distributions in the formalism of SCET, presented in [18].

2.1 Event shape distributions in full QCD

The full QCD distribution of events in $e^+e^- \to$ hadrons in an event shape variable e is given, to leading-order in electroweak couplings, by

$$\frac{\mathrm{d}\sigma}{\mathrm{d}e} = \frac{1}{2Q^2} \sum_X \int \mathrm{d}^4x \, \mathrm{e}^{iq\cdot x} \sum_{i=V,A} L^i_{\mu\nu} \langle 0| \, j_i^{\mu\dagger}(x) \, |X\rangle \, \langle X| \, j_i^{\nu}(0) \, |0\rangle \, \delta(e - e(X)) \,, \tag{3.6}$$

where $q = (Q, \mathbf{0})$ is the total four-momentum in the center-of-mass frame, the sum is over final states X, and $e(X)$ is the value of the event shape e of the state X. The final state is produced by the vector and axial currents,

$$j_i^\mu = \sum_{f,a} \bar{q}_f^a \Gamma_i^\mu q_f^a \,, \tag{3.7}$$

where $\Gamma_V^\mu = \gamma^\mu$ and $\Gamma_A^\mu = \gamma^\mu\gamma^5$ and the sum is over quark flavors f and colors a. The leptonic tensor, which includes contributions from an intermediate photon and Z boson, is given by

$$L_{\mu\nu}^V = -\frac{e^4}{3Q^2}\left(g_{\mu\nu} - \frac{q_\mu q_\nu}{Q^2}\right)\left[Q_f^2 - \frac{2Q^2 v_e v_f Q_f}{Q^2 - M_Z^2} + \frac{Q^4(v_e^2+a_e^2)v_f^2}{(Q^2-M_Z^2)^2}\right] \tag{3.8a}$$

$$L_{\mu\nu}^A = -\frac{e^4}{3Q^2}\left(g_{\mu\nu} - \frac{q_\mu q_\nu}{Q^2}\right)\frac{Q^4(v_e^2+a_e^2)a_f^2}{(Q^2-M_Z^2)^2}\,, \tag{3.8b}$$

where Q_f is the electric charge of f in units of e, and v_f, a_f are the vector and axial charges of f,

$$v_f = \frac{1}{2\sin\theta_W\cos\theta_W}(T_f^3 - 2Q_f\sin^2\theta_W)\,, \quad a_f = \frac{1}{2\sin\theta_W\cos\theta_W}T_f^3. \tag{3.9}$$

As shown in [18], the sum over hadronic final states remaining in Eq. (3.6) can be performed by introducing an operator $\hat{e}$ that gives the event shape $e(X)$ of a final state X. This operator can be constructed from a momentum flow operator, which in turn is constructed from the energy-momentum tensor. That is,

$$\hat{e}\,|X\rangle \equiv e(X)\,|X\rangle = \frac{1}{Q}\int_{-\infty}^{\infty}\mathrm{d}\eta\, f_e(\eta)\mathcal{E}_T(\eta;\hat{t})\,|X\rangle\,, \tag{3.10}$$

where $\hat{t}$ is the operator yielding the thrust axis of final state X, and $\mathcal{E}_T(\eta;\hat{t})$ is the transverse momentum flow operator, yielding the total transverse momentum flow in the direction given by rapidity η, measured with respect to the thrust axis, in a final state X,

$$\mathcal{E}_T(\eta;\hat{t})\,|X\rangle \equiv \frac{1}{\cosh^3\eta}\int_0^{2\pi}\mathrm{d}\phi\lim_{R\to\infty}R^2\int_0^\infty \mathrm{d}t\,\hat{n}_i T_{0i}(t,R\hat{n})\,|X\rangle = \sum_{i\in X}\left|\mathbf{p}_\perp^i\right|\delta(\eta-\eta_i)\,|X\rangle\,, \tag{3.11}$$

which is closely related to the energy flow operator proposed in [150]. The thrust axis operator $\hat{t}$ can be constructed explicitly, as shown in [18]. After matching onto SCET, however, an explicit construction is not necessary, as the thrust axis is simply given by the jet axis $\mathbf{n}$ labeling the two-jet current. The difference between the two axes introduces power corrections in λ which are subleading, as long as $a < 1$ [47, 18]. Using the operator $\hat{e}$, we perform the sum over X in Eq. (3.6), leaving

$$\frac{\mathrm{d}\sigma}{\mathrm{d}e} = \frac{1}{2Q^2}\int \mathrm{d}^4x\,\mathrm{e}^{iq\cdot x}\sum_{i=V,A}L_{\mu\nu}^i\,\langle 0|\,j_i^{\mu\dagger}(x)\delta(e-\hat{e})j_i^\nu(0)\,|0\rangle\,. \tag{3.12}$$

2.2 Factorization of event shape distributions in SCET

To proceed to a factorized form of the distribution Eq. (3.12), we match the current j^μ and the operator $\hat{e}$ onto operators in SCET. To reproduce the endpoint region of the two-jet event shape distribution, we match the QCD currents j_i^μ onto SCET operators containing fields in just two back-to-back collinear directions,

$$j_i^\mu(x) \;=\; \sum_{\mathbf{n}}\sum_{\tilde{p}_n,\tilde{p}_{\bar{n}}} C_{n\bar{n}}(\tilde{p}_n,\tilde{p}_{\bar{n}};\mu)\mathcal{O}_{n\bar{n}}(x;\tilde{p}_n,\tilde{p}_{\bar{n}})\,, \tag{3.13}$$

summing over the direction $\mathbf{n}$ of the light-cone vectors $n, \bar{n} = (1, \pm\mathbf{n})$, and label momenta $\tilde{p}_n, \tilde{p}_{\bar{n}}$. The two-jet operators [24, 20], after the BPS field redefinition [29] with soft Wilson lines, are

$$\mathcal{O}_{n\bar{n}}(x; \tilde{p}_n, \tilde{p}_{\bar{n}}) = e^{i(\tilde{p}_n - \tilde{p}_{\bar{n}})\cdot x} \bar{\chi}_{n,p_n}(x) Y_n(x) \Gamma_i^\mu \overline{Y}_{\bar{n}}(x) \chi_{\bar{n},p_{\bar{n}}}(x)\,, \tag{3.14}$$

where $\Gamma_V^\mu = \gamma_\perp^\mu$ and $\Gamma_A^\mu = \gamma_\perp^\mu \gamma_5$. The soft Wilson lines are the path-ordered exponentials of soft gluons,

$$Y_n(x) = P \exp\left[ig \int_0^\infty n \cdot A_s(ns + x)\right], \qquad \overline{Y}_{\bar{n}}(x) = P \exp\left[ig \int_0^\infty \bar{n} \cdot \bar{A}_s(\bar{n}s + x)\right], \tag{3.15}$$

with $A_s, \bar{A}_s$ respectively in the fundamental or anti-fundamental representation. The jet fields $\chi_n = W_n^\dagger \xi_n$ and $\chi_{\bar{n}} = W_{\bar{n}}^\dagger \xi_{\bar{n}}$ are combinations of collinear quark fields made invariant under collinear gauge transformations by Wilson lines of collinear gluons [21, 33], where

$$W_n(x) = \sum_{\text{perms}} \exp\left[-g \frac{1}{\bar{\mathcal{P}}} \bar{n} \cdot A_{n,q}(x)\right], \tag{3.16}$$

where q is the label momentum of the collinear gluon field A_n, and $\bar{\mathcal{P}}$ is a label momentum operator which acts as $\bar{\mathcal{P}} A_{n,q} = (\bar{n} \cdot q) A_{n,q}$ [33]. Recall that, in SCET, collinear momenta $p_c^\mu = \tilde{p}^\mu + k^\mu$ are divided into a large label piece, $\tilde{p}^\mu = (\bar{n} \cdot \tilde{p}) n^\mu/2 + \tilde{p}_\perp^\mu$, and a residual piece, k^μ, where $\bar{n} \cdot \tilde{p}$ is $\mathcal{O}(Q)$, $\tilde{p}_\perp$ is $\mathcal{O}(Q\lambda)$, and k is $\mathcal{O}(Q\lambda^2)$. The residual momenta are the same size as soft momenta, k_s, of $\mathcal{O}(Q\lambda^2)$. Below, however, we will see how the natural scaling of the collinear modes varies with the choice of observable τ_a. The integral over x in Eq. (3.12) enforces that the label momenta of the jet fields in the two-jet operator satisfy $\bar{n} \cdot \tilde{p}_n = -n \cdot \tilde{p}_{\bar{n}} = Q$ and $\tilde{p}_n^\perp = \tilde{p}_{\bar{n}}^\perp = 0$.

We must also match the operator $\hat{e}$ in full QCD onto SCET. To do so we simply replace the QCD energy-momentum tensor $T^{\mu\nu}$ appearing in the definition Eq. (3.11) with the energy-momentum tensor in SCET, and, as noted above, set the thrust axis equal to the jet axis $\mathbf{n}$ in the two-jet operator $\mathcal{O}_{n\bar{n}}$. After the BPS field redefinition, to leading order in λ the SCET energy-momentum tensor is a direct sum over contributions from fields in the $n, \bar{n}$ collinear and soft sectors, since the Lagrangian splits into these separate sectors with no interactions between them. (Beyond leading order in λ, there are power-suppressed terms in the SCET Lagrangian in which interactions between collinear and soft fields do not decouple following the BPS field redefintion [28, 81, 168, 30].) Then the event shape operator $\hat{e}$ splits into separate collinear and soft operators,

$$\hat{e} = \hat{e}_n + \hat{e}_{\bar{n}} + \hat{e}_s\,, \tag{3.17}$$

where each $\hat{e}_i$ is constructed only from the energy-momentum tensor of sector i of the effective theory. So, finally, the event shape distribution in SCET factorizes into purely hard, collinear and soft functions,

$$\frac{1}{\sigma_0} \frac{\mathrm{d}\sigma}{\mathrm{d}e} = H(Q;\mu) \int \mathrm{d}e_n\, \mathrm{d}e_{\bar{n}}\, \mathrm{d}e_s\, \delta(e - e_n - e_{\bar{n}} - e_s) J_n(e_n;\mu) J_{\bar{n}}(e_{\bar{n}};\mu) S(e_s;\mu)\,, \tag{3.18}$$

where the hard coefficient is the squared amplitude of the two-jet matching coefficient,

$$H(Q;\mu) = \left|C_{n\bar{n}}(Qn/2, -Q\bar{n}/2;\mu)\right|^2\,, \tag{3.19}$$

and the jet and soft functions are given by the matrix elements of collinear and soft operators,

$$S(e_s;\mu) = \frac{1}{N_C}\,\mathrm{Tr}\,\langle 0|\,\overline{Y}^\dagger_{\bar n}(0) Y_n^\dagger(0)\delta(e_s-\hat e_s) Y_n(0)\overline{Y}_{\bar n}(0)\,|0\rangle\ , \tag{3.20}$$

and

$$J_n(e_n;\mu) = \int \frac{\mathrm{d}l^+}{2\pi}\mathcal{J}_n(e_n,l^+;\mu)\,, \quad J_{\bar n}(e_{\bar n};\mu) = \int \frac{\mathrm{d}k^-}{2\pi}\mathcal{J}_{\bar n}(e_{\bar n},k^-;\mu)\,, \tag{3.21}$$

where

$$\mathcal{J}_n(e_n,l^+;\mu)\left(\frac{\bar n\!\!\!/}{2}\right)_{\alpha\beta} = \frac{1}{N_C}\,\mathrm{Tr}\int \mathrm{d}^4x\,\mathrm{e}^{il\cdot x}\,\langle 0|\,\chi_{n,Q}(x)_\alpha \delta(e_n-\hat e_n)\bar\chi_{n,Q}(0)_\beta\,|0\rangle \tag{3.22a}$$

$$\mathcal{J}_{\bar n}(e_{\bar n},k^-;\mu)\left(\frac{n\!\!\!/}{2}\right)_{\alpha\beta} = \frac{1}{N_C}\,\mathrm{Tr}\int \mathrm{d}^4x\,\mathrm{e}^{ik\cdot x}\,\langle 0|\,\bar\chi_{\bar n,-Q}(x)_\beta \delta(e_{\bar n}-\hat e_{\bar n})\chi_{\bar n,-Q}(0)_\alpha\,|0\rangle\ . \tag{3.22b}$$

In Eqs. (3.20), (3.22a), and (3.22b), the traces are over colors. Also, in Eq. (3.18), we have divided the distribution by the total Born cross-section for $e^+e^-\to q\bar q$,

$$\sigma_0 = \frac{4\pi\alpha^2 N_C}{3Q^2}\sum_f\left[Q_f^2 - \frac{2Q^2 v_e v_f Q_f}{Q^2-M_Z^2} + \frac{Q^4(v_e^2+a_e^2)(v_f^2+a_f^2)}{(Q^2-M_Z^2)^2}\right]. \tag{3.23}$$

The n-collinear jet function J_n depends only on the $l^+\equiv n\cdot l$ component of the residual momentum, and $J_{\bar n}$ on $k^-\equiv \bar n\cdot k$, as only the $n\cdot\partial$ derivative appears in the n-collinear Lagrangian, and $\bar n\cdot\partial$ in the $\bar n$-collinear Lagrangian, at leading order in λ [21]. In angularity distributions, the jet functions are independent of the residual transverse momenta $k_\perp, l_\perp$ as long as $a<1$ [18].

In Secs. 3 and 4 we calculate the above hard, jet, and soft functions for angularity distributions to next-to-leading order in α_s, and solve for their dependence on μ through the renormalization group equations, which will allow us to sum large logarithms of τ_a.

2.3 Universal first moment of the soft function

As shown in [157], the behavior of the soft function Eq. (3.20) under Lorentz boosts in the **n** direction implies a universal form for its first moment. The vacuum $|0\rangle$ and the Wilson lines $Y_{n,\bar n}(0), \overline{Y}_{n,\bar n}(0)$ are all invariant under such boosts, while the transverse momentum flow operator $\mathcal{E}_T(\eta)$ appearing in the definition of $\hat e_s$ transforms as $\mathcal{E}_T(\eta)\to\mathcal{E}_T(\eta')$ under a boost by rapidity $\eta'-\eta$. These properties imply that the first moment of $S(e_s;\mu)$ is given by

$$\int \mathrm{d}e_s\, e_s\, S(e_s;\mu) = \frac{c_e\mathcal{A}(\mu)}{Q}\,, \tag{3.24}$$

where

$$c_e = \frac{1}{Q}\int_{-\infty}^{\infty}\mathrm{d}\eta\, f_e(\eta) \tag{3.25}$$

$$\mathcal{A}(\mu) = \frac{1}{N_C}\,\mathrm{Tr}\,\langle 0|\,\overline{Y}^\dagger_{\bar n}(0) Y_n^\dagger(0)\mathcal{E}_T(0) Y_n(0)\overline{Y}_{\bar n}(0)\,|0\rangle\ . \tag{3.26}$$

The coefficient c_e is exactly calculable from the definition of the event shape e Eq. (3.2) while $\mathcal{A}(\mu)$ is not fully calculable due to the contribution of nonperturbative effects, but is completely independent of the choice of variable e. The first moment Eq. (3.24) is universal for all event shapes of the form Eq. (3.2) in this sense. For angularities, using Eq. (3.3) and Eq. (3.25),

$$c_a = \int_{-\infty}^{\infty} \mathrm{d}\eta\, \mathrm{e}^{-|\eta|(1-a)} = \frac{2}{1-a}\,. \tag{3.27}$$

This scaling of the first moment of the soft function for angularities will constrain the parameterization of the nonperturbative model for the soft function that we introduce in Sec. 5.

3 Fixed-order Perturbative Calculations of Hard, Jet, and Soft Functions

In this section we calculate at next-to-leading order, that is, $\mathcal{O}(\alpha_s)$, in perturbation theory the hard, jet, and soft functions, $H(Q;\mu)$, $J_a^{n,\bar{n}}(\tau_a^{n,\bar{n}};\mu)$, and $S_a(\tau_a^s;\mu)$, in the factorization theorem for angularity distributions, which is given by Eq. (3.18) with $e = \tau_a$.[3]

3.1 Hard function at NLO

The hard function $H(Q;\mu)$, given by Eq. (3.19), is the squared amplitude of the two-jet matching coefficient $C_{n\bar{n}}(Q,-Q;\mu)$. This matching coefficient was calculated, for example, in [160] in the context of DIS and in [24] for e^+e^- annihilation, to NLO. It is found by calculating a matrix element of the QCD current Eq. (3.7) and SCET current Eq. (3.13) (for example, $\langle q(p_q)\bar{q}(p_{\bar{q}})|\, j_i^\mu\, |0\rangle$), and requiring that the two match. Since the matching of the currents is independent of the observable being calculated, we do not need to repeat the matching calculation here, and simply quote the result. The matching coefficient $C_{n\bar{n}}(\tilde{p}_n,\tilde{p}_{\bar{n}};\mu)$ in the SCET current Eq. (3.13) is given by

$$C_{n\bar{n}}(\tilde{p}_n,\tilde{p}_{\bar{n}};\mu) = 1 - \frac{\alpha_s C_F}{4\pi}\left[8 - \frac{\pi^2}{6} + \ln^2\left(\frac{\mu^2}{2\tilde{p}_n\cdot\tilde{p}_{\bar{n}}}\right) + 3\ln\left(\frac{\mu^2}{2\tilde{p}_n\cdot\tilde{p}_{\bar{n}}}\right)\right], \tag{3.28}$$

Here and in the remainder of this section, $\alpha_s \equiv \alpha_s(\mu)$. The hard function $H(Q;\mu)$ in Eq. (3.19) is thus

$$H(Q;\mu) = 1 - \frac{\alpha_s C_F}{2\pi}\left(8 - \frac{7\pi^2}{6} + \ln^2\frac{\mu^2}{Q^2} + 3\ln\frac{\mu^2}{Q^2}\right). \tag{3.29}$$

The additional contribution to the coefficient of π^2 in going from Eq. (3.28) to Eq. (3.29) is due to the sign of $2\tilde{p}_n\cdot\tilde{p}_{\bar{n}} = -Q^2$, following the conventions of [33].

The bare SCET two-jet operators in Eq. (3.14) are renormalized by the relation

$$\mathcal{O}^{(0)}_{n\bar{n}}(x;\tilde{p}_n,\tilde{p}_{\bar{n}}) = Z_{\mathcal{O}}(\tilde{p}_n,\tilde{p}_{\bar{n}};\mu)\mathcal{O}_{n\bar{n}}(x;\tilde{p}_n,\tilde{p}_{\bar{n}})\,, \tag{3.30}$$

where the renormalization constant, calculated using dimensional regularization to regulate the UV divergences in $d = 4-2\epsilon$ dimensions, is given by

$$Z_{\mathcal{O}}(\tilde{p}_n,\tilde{p}_{\bar{n}};\mu) = 1 + \frac{\alpha_s C_F}{4\pi}\left[\frac{2}{\epsilon^2} + \frac{2}{\epsilon}\ln\left(\frac{\mu^2}{2\tilde{p}_n\cdot\tilde{p}_{\bar{n}}}\right) + \frac{3}{\epsilon}\right]. \tag{3.31}$$

[3] Note that here and below a superscript n on a quantity is not a power but denotes "n-collinear" just as $\bar{n}$ denotes "$\bar{n}$-collinear" and s denotes "soft".

Matching the QCD current Eq. (3.7) onto only two-jet operators in SCET is sufficient to describe accurately the two-jet region near $\tau_a = 0$ of angularity distributions. To calculate accurately also the tail region to $\mathcal{O}(\alpha_s)$, where the jets broaden and an additional jet begins to form, we would need to include a basis of three-jet operators in Eq. (3.13) as well [32, 165]. But since we are mainly interested in obtaining the correct shape of the two-jet region, we do not pursue this approach here. We will simply calculate the whole distribution in SCET with only two-jet operators, and the match the tail region numerically onto the fixed-order prediction of full QCD. This will be described more precisely in Sec. 4.4.

3.2 Cutting rules for weighted matrix elements

The jet and soft functions that typically appear in factorizations of hard cross-sections in SCET are defined in terms of matrix elements of the products of collinear and soft fields, which are related to the imaginary part of the matrix element of a time-ordered product of the fields according to the optical theorem,

$$\int \mathrm{d}^4x\, \mathrm{e}^{iq\cdot x} \big\langle 0\big|\phi(x)\phi^\dagger(0)\big|0\big\rangle = \mathrm{Disc}\left[\int \mathrm{d}^4x\, \mathrm{e}^{iq\cdot x} \big\langle 0\big|\mathrm{T}\,\phi(x)\phi^\dagger(0)\big|0\big\rangle\right]. \tag{3.32}$$

The right-hand side is then related to the sum of all cuts of the relevant Feynman diagrams using the standard Cutkosky cutting rules.

However, for more generic jet observables such as angularities for $a \neq 0$, the jet and soft functions that appear in factorization proofs contain matrix elements in which additional operators are inserted between the collinear and soft fields in the definition of the traditional jet and soft functions [23]. For the matrix elements involving the extra insertion of such operators, we need to generalize the cutting rules for calculating these matrix elements from Feynman diagrams.

For the case of angularities, the jet and soft functions given in Eqs. (3.20), (3.22a), and (3.22b) differ from the traditional jet and soft functions by the insertion of the delta function operator $\delta(\tau_a - \hat{\tau}_a)$. We denote the appropriate generalized prescription for calculating the new matrix element from the Feynman diagrams of time-ordered perturbation theory as the "τ_a-discontinuity,"

$$\int \mathrm{d}^4x\, \mathrm{e}^{iq\cdot x} \big\langle 0\big|\phi(x)\,\delta(\tau_a - \hat{\tau}_a)\,\phi^\dagger(0)\big|0\big\rangle \equiv \mathrm{Disc}_{\tau_a}\left[\int \mathrm{d}^4x\, \mathrm{e}^{iq\cdot x} \big\langle 0\big|\mathrm{T}\phi(x)\phi^\dagger(0)\big|0\big\rangle\right]. \tag{3.33}$$

The Disc_{τ_a} prescription is to cut the diagrams contributing to the matrix element of time-ordered operators just as for the usual matrix elements in Eq. (3.32) but to insert an additional factor of $\delta(\tau_a - \tau_a(X))$ for each cut, where X is the final state created by the cut.[4] This prescription corresponds to reinserting a sum over a complete set of final states between the delta function operator and $\phi^\dagger(0)$ in Eq. (3.33), and is precisely how we would calculate the full differential cross-section as written in Eq. (3.6). In the next two subsections we illustrate extensively the use of the Disc_{τ_a} prescription.

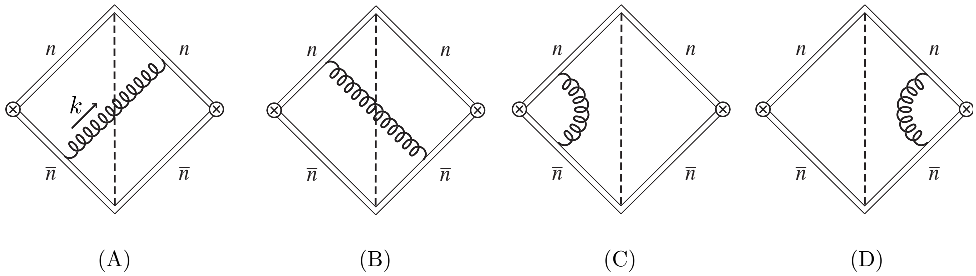

Figure 3.1: The (A), (B) real and (C), (D) virtual contributions to the soft function. The gluons all have momentum k.

3.3 Calculation of the soft function to NLO

The diagrams that contribute to the soft function are shown in Fig. 3.1. From Eqs. (3.3), (3.10), and (3.11), the contribution to the angularity from an on-shell soft gluon with momentum k is

$$\tau_a^s = \frac{|\mathbf{k}_\perp|}{Q} e^{-\frac{1-a}{2}\left|\ln\frac{k^+}{k^-}\right|} = \begin{cases} \frac{1}{Q}\,|k^+|^{1-\frac{a}{2}}\,|k^-|^{\frac{a}{2}} & \text{for} \quad k^- \geq k^+ \\ \frac{1}{Q}\,|k^-|^{1-\frac{a}{2}}\,|k^+|^{\frac{a}{2}} & \text{for} \quad k^+ \geq k^- \end{cases} . \tag{3.34}$$

Since cutting a gluon puts it on shell, the operator $\hat{\tau}_a^s$ returns these values when acting on a cut soft gluon. When no gluon is in the final state cut, the operator $\hat{\tau}_a^s$ simply returns zero. The real and virtual diagrams then contain delta functions, which we denote δ_R and δ_V, respectively,

$$\begin{aligned} \delta_R \equiv \delta_R(\tau_a^s, k) &= \theta(k^- - k^+)\,\delta\Big(\tau_a^s - \frac{1}{Q}\,\big|k^+\big|^{1-\frac{a}{2}}\,\big|k^-\big|^{\frac{a}{2}}\Big) & \text{(3.35a)} \\ &\quad + \theta(k^+ - k^-)\,\delta\Big(\tau_a^s - \frac{1}{Q}\,\big|k^-\big|^{1-\frac{a}{2}}\,\big|k^+\big|^{\frac{a}{2}}\Big)\,, \\ \delta_V \equiv \delta_V(\tau_a^s) &= \delta(\tau_a^s)\,. & \text{(3.35b)} \end{aligned}$$

In terms of these delta functions, the (bare) perturbative soft function can be written

$$S_a^{\mathrm{PT}(0)}(\tau_a^s;\mu) = \delta(\tau_a^s) + 2$$ 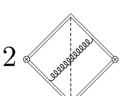 $$\delta_R + 2$$ 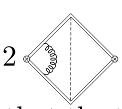 $$\delta_V\,, \tag{3.36}$$

where we used that the tree level contribution is just $\delta(\tau_a^s)$ and that the two real and the two virtual diagrams in Fig. 3.1 give identical contributions.

In pure dimensional regularization, the virtual contributions are scaleless and hence vanish so we only need to evaluate the real diagrams. They add to

$$2$$ 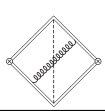 $$\delta_R = 2g^2\mu^{2\epsilon}C_F\, n\!\cdot\!\bar{n}\int\frac{\mathrm{d}^d k}{(2\pi)^d}\frac{1}{k^-}\frac{1}{k^+}2\pi\delta(k^-k^+ - |\mathbf{k}_\perp|^2)\,\theta(k^-)\delta_R(\tau_a^s, k)\,. \tag{3.37}$$

[4] The operator-based method that was developed in [167] for calculating weighted cross-sections can be used to relate matrix elements such as in the left-hand side of Eq. (3.33) directly to the ordinary discontinuity of matrix elements of time-ordered products of fields. However, for the scope of this chapter, we choose simply to apply the prescription Eq. (3.33).

Performing the k integrals gives

$$S_a^{\mathrm{PT}(0)}(\tau_a^s;\mu) = \delta(\tau_a^s) + \theta(\tau_a^s)\frac{\alpha_s C_F\, n\cdot\bar{n}}{\pi(1-a)}\left(\frac{4\pi\mu^2}{Q^2}\right)^{\epsilon}\frac{1}{\Gamma(1-\epsilon)}\frac{1}{\epsilon}\left(\frac{1}{\tau_a^s}\right)^{1+2\epsilon}. \tag{3.38}$$

Nonzero values of τ_a^s regulate the IR divergences and so here the $1/\epsilon$ pole is of UV origin, $\epsilon = \epsilon_{\mathrm{UV}}$.

Applying the distribution relation (valid for $\epsilon < 0$)

$$\frac{\theta(x)}{x^{1+2\epsilon}} = -\frac{\delta(x)}{2\epsilon} + \left[\frac{\theta(x)}{x}\right]_+ - 2\epsilon\left[\frac{\theta(x)\ln x}{x}\right]_+ + \mathcal{O}(\epsilon^2)\,, \tag{3.39}$$

where

$$\left[\frac{\theta(x)\ln^n(x)}{x}\right]_+ \equiv \lim_{\beta\to 0}\left[\frac{\theta(x-\beta)\ln^n(x)}{x} + \frac{\ln^{n+1}\beta}{n+1}\delta(x-\beta)\right], \tag{3.40}$$

to Eq. (3.38) we obtain the final result for the (bare) angularity soft function,

$$S_a^{\mathrm{PT}(0)}(\tau_a^s;\mu) = \int \mathrm{d}\tau_a^{s'}\, Z_S(\tau_a^s - \tau_a^{s'};\mu) S_a(\tau_a^{s'};\mu)\,, \tag{3.41}$$

where to NLO the renormalized soft function, S_a^{PT}, is given by

$$S_a^{\mathrm{PT}}(\tau_a^s;\mu) = \delta(\tau_a^s)\left[1 - \frac{\alpha_s C_F}{\pi(1-a)}\left(\frac{1}{2}\ln^2\frac{\mu^2}{Q^2} - \frac{\pi^2}{12}\right)\right] + \frac{2\alpha_s C_F}{\pi(1-a)}\left[\frac{\theta(\tau_a^s)}{\tau_a^s}\ln\frac{\mu^2}{(Q\tau_a^s)^2}\right]_+, \tag{3.42}$$

and the renormalization factor, Z_S, is given by

$$Z_S(\tau_a^s;\mu) = \delta(\tau_a^s)\left[1 - \frac{\alpha_s C_F}{\pi(1-a)}\left(\frac{1}{\epsilon^2} + \frac{1}{\epsilon}\ln\frac{\mu^2}{Q^2}\right)\right] + \frac{1}{\epsilon}\frac{2\alpha_s C_F}{\pi(1-a)}\left[\frac{\theta(\tau_a^s)}{\tau_a^s}\right]_+. \tag{3.43}$$

3.4 IR structure of the soft function

While the mathematical identity in Eq. (3.39) allowed us to arrive at our final result, Eq. (3.42), the origin of the $1/\epsilon$ poles became obscured through its use. In fact, the use of Eq. (3.39) is only valid for $\epsilon < 0$ which suggests that the $1/\epsilon$ pole on the right-hand side of Eq. (3.39) is of IR origin. The virtual diagrams, while formally zero in pure dimensional regularization, play the role of converting this IR divergence into a UV divergence by adding a quantity proportional to $(1/\epsilon_{\mathrm{UV}} - 1/\epsilon_{\mathrm{IR}})$ to the coefficient of $\delta(\tau_a^s)$, if the final result is in fact free of IR divergences. Naïvely it seems that this conversion cannot possibly occur for arbitrary a, because the $1/\epsilon$ poles in the real diagrams have a-dependent coefficients (see Eq. (3.43)), while the virtual diagrams contain no apparent a dependence. Nevertheless, by carefully examining the contribution of both the real and virtual diagrams, we will show that, for $a < 1$, the virtual diagrams play precisely this role and convert each IR divergence in the real graphs into UV, but that for $a \geq 1$, this cancellation is incomplete. This is accomplished through an analysis of integration regions in the loop momentum integrals that avoids the use of explicit IR regulators. Our presentation here complements our discussion of these issues in [135].

Using that $\int_0^1 \mathrm{d}x \left[\ln^n(x)/x\right]_+ = 0$, the contribution to the coefficient of $\delta(\tau_a^s)$ can be isolated by integrating the diagrams over τ_a^s from 0 to 1. We find that the contribution from the real diagrams can be written as

$$\int_0^1 \mathrm{d}\tau_a^s \left[2 \; \delta_R \right] = \frac{\alpha_s C_F \, n\cdot\bar{n}}{2\pi} \frac{\left(4\pi\mu^2\right)^\epsilon}{\Gamma(1-\epsilon)} \int_{\mathcal{R}} \mathrm{d}k^+ \mathrm{d}k^- (k^+k^-)^{-1-\epsilon} \,, \tag{3.44}$$

where $\mathcal{R}$ is given by the region of positive k^+ and k^- such that

$$\begin{aligned} (k^-)^{\frac{a}{2}} (k^+)^{1-\frac{a}{2}} &< Q \quad \text{for} \quad k^- \geq k^+ \\ (k^+)^{\frac{a}{2}} (k^-)^{1-\frac{a}{2}} &< Q \quad \text{for} \quad k^- \leq k^+ \,. \end{aligned} \tag{3.45}$$

This region is plotted in Fig. 3.2A for various values of a.

The contribution of the virtual diagrams to the coefficient of $\delta(\tau_a^s)$ sums to

$$\begin{aligned} \int_0^1 \mathrm{d}\tau_a^s \left[2 \; \delta_V \right] &= 2g^2\mu^{2\epsilon} C_F \, n\cdot\bar{n} \int \frac{\mathrm{d}^d k}{(2\pi)^d} \frac{1}{k^- - i0^+} \frac{1}{k^+ + i0^+} \frac{i}{k^+k^- - |\mathbf{k}_\perp|^2 - i0^+} \\ &= -\frac{\alpha_s C_F \, n\cdot\bar{n}}{2\pi} \frac{\left(4\pi\mu^2\right)^\epsilon}{\Gamma(1-\epsilon)} \int_{\mathcal{V}} \mathrm{d}k^+ \mathrm{d}k^- (k^+k^-)^{-1-\epsilon} \,, \end{aligned} \tag{3.46}$$

where $\mathcal{V}$ is the entire positive k^+, k^- quadrant, plotted in Fig. 3.2B.

The two contributions to $\delta(\tau_a^s)$, Eqs. (3.44) and (3.46), are each both UV and IR divergent, but as we will show, their sum is convergent for $\epsilon > 0$ and so is only UV divergent. Since the form of the integrand is the same and the virtual contribution differs only by an overall minus sign, it converts the region of integration of the real contribution, $\mathcal{R}$, into the complementary part of the positive k^+, k^- quadrant (see Fig. 3.2) which does not include the IR divergent regions $k^\pm \to 0$. Note that as $a \to 1$, the boundary of the region of integration $\mathcal{R}$ approaches the curve of constant $k^+k^- = Q^2$. With this boundary, the integral over the region $\mathcal{S}$ does not converge for either positive or negative ϵ, implying that both IR and UV divergences are present.

That the region $\mathcal{S}$ has only UV divergence for $a < 1$ and has both UV and IR divergence for $a = 1$ is perhaps more clearly seen in the $k^-, \mathbf{k}_\perp^2$ plane. The integral of the soft diagrams over τ_a^s in terms of these variables is given by

$$\int_0^1 \mathrm{d}\tau_a^s \left[2 \; \delta_R + 2 \; \delta_V \right] = -\frac{\alpha_s C_F \, n\cdot\bar{n}}{2\pi} \frac{\left(4\pi\mu^2\right)^\epsilon}{\Gamma(1-\epsilon)} \int_{\mathcal{S}} \frac{\mathrm{d}k^- \mathrm{d}\mathbf{k}_\perp^2}{k^- (\mathbf{k}_\perp^2)^{1+\epsilon}} \,,$$

and the resulting region $\mathcal{S}$ in terms of k^- and $\mathbf{k}_\perp^2$ for $a \leq 1$ is

$$\left(\frac{\mathbf{k}_\perp^2}{Q^2}\right)^{-\frac{a}{2(1-a)}} < \left(\frac{k^-}{Q}\right) < \left(\frac{\mathbf{k}_\perp^2}{Q^2}\right)^{\frac{2-a}{2(1-a)}} \quad \text{with} \quad \mathbf{k}_\perp^2 > Q^2 \,. \tag{3.47}$$

The region $\mathcal{S}$ is plotted for several values of a in Fig. 3.2D. The limiting case $a = 1$ clearly includes the IR divergent region $k^- \to 0$ for all $\mathbf{k}_\perp^2 > Q^2$.

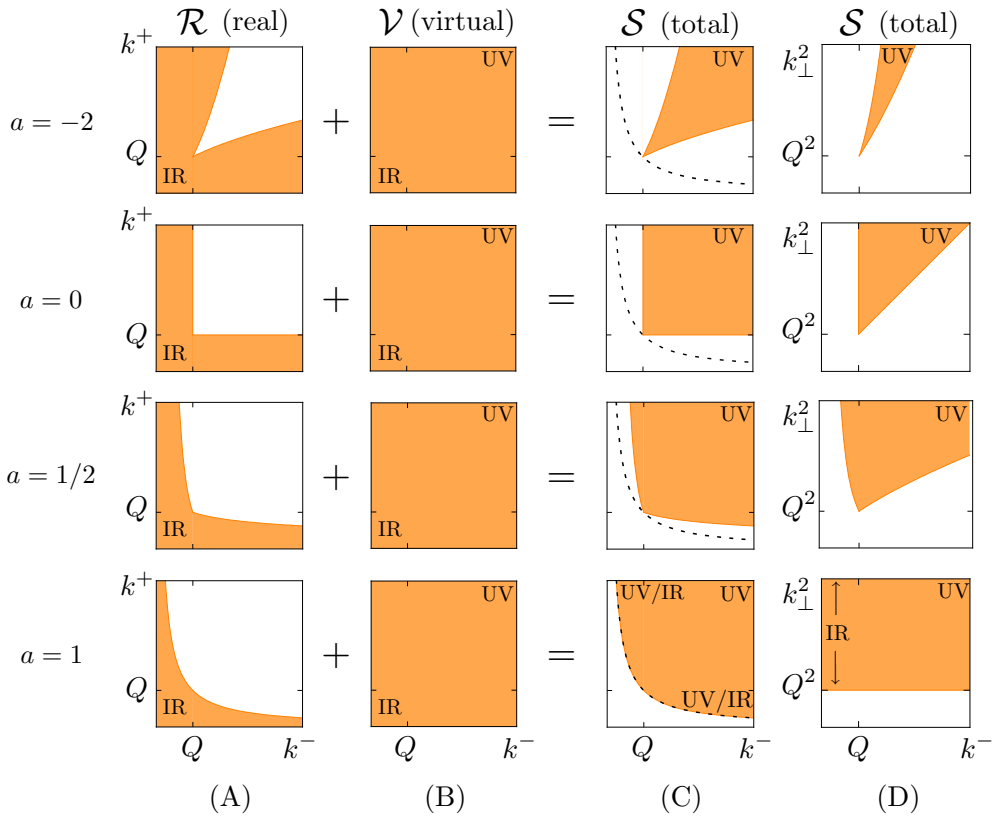

Figure 3.2: The regions of integration for the coefficent of $\delta(\tau_a^s)$ in $S_a^{(0)}(\tau_a^s)$ in the (A), (B), (C) k^-, k^+ and (D) $k^-, \mathbf{k}_\perp^2$ planes. The regions of integration for both (A) the real contribution $\mathcal{R}$ and (B) the virtual contribution $\mathcal{V}$ contain both UV and IR divergences. Since the integrands for the two contributions differ only by an overall minus sign, (C) the region resulting in their sum $\mathcal{S}$, is the complement of $\mathcal{R}$ and contains only UV divergences for $a < 1$. The dashed line in (C) represents the line of constant $k^+k^- = Q^2$.

Performing the integral over $\mathcal{S}$ we obtain

$$\int_0^1 \mathrm{d}\tau_a^s \, S_a^{(0)}(\tau_a^s; \mu) = 1 - \frac{\alpha_s C_F \, n\cdot\bar{n}}{2\pi(1-a)} \left(\frac{4\pi\mu^2}{Q^2}\right)^\epsilon \frac{1}{\epsilon^2 \, \Gamma(1-\epsilon)} \,. \tag{3.48}$$

After expanding Eq. (3.48) in ϵ, we find that the coefficient of $\delta(\tau_a^s)$ in Eq. (3.42) is unchanged, except that for $a < 1$ all the $1/\epsilon$ poles are unambiguously of UV origin.

A lesson from this analysis is that in pure dimensional regularization, the coefficient of $(1/\epsilon_{\mathrm{UV}} - 1/\epsilon_{\mathrm{IR}})$ in a virtual diagram cannot be determined from the virtual diagram alone, but only together with the real diagram whose IR divergence it is supposed to cancel. The reason that the virtual subtraction can depend on a even though by itself it is independent of a is that the area of overlap between the integration regions of real and virtual diagrams depends on a.

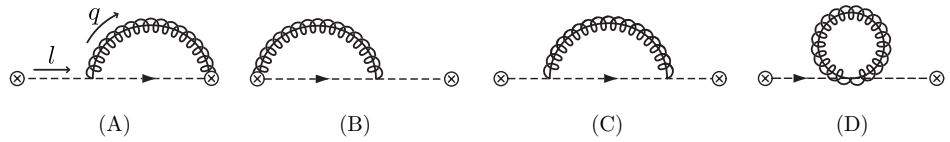

Figure 3.3: Diagrams contributing to the angularity jet function $\mathcal{J}_a^n(\tau_a^n, l^+)$ with incoming momentum $l = \frac{n}{2}Q + \frac{\bar{n}}{2}l^+$ and gluon momentum q: (A) Wilson line emission diagram and (B) its mirror; (C) sunset and (D) tadpole QCD-like diagrams. The contributions to the jet function $J_a^n(\tau_a^n)$ are given by the integrals of these diagrams over the + component of the incoming momentum, $\int \mathrm{d}l^+ \mathcal{J}_a^n(\tau_a^n, l^+) = 2\pi J_a^n(\tau_a^n)$.

3.5 Calculation of the jet functions to NLO

Now we proceed to calculate the jet functions given by Eqs. (3.21) and (3.22). The diagrams that contribute to J_a^n are shown in Fig. 3.3, and the Feynman rules necessary to calculate these diagrams are found in [21]. The total momentum flowing through each diagram is $Qn/2 + l$, with the label component $Qn/2$ specified by the labels on the jet fields in the matrix elements in Eq. (3.22a), and l the residual momentum. The total momentum of the gluon in each loop is q, which has both label and residual components. All results for the anti-quark jet function $J_a^{\bar{n}}$ can be found from those for the quark jet function J_a^n with the replacement $n \leftrightarrow \bar{n}$ and so we calculate explicitly only J_a^n.

Cutting the diagrams in Fig. 3.3 in all possible places, we can cut through the gluon loops or through one of the individual quark propagators connected to a current. We naturally call these classes of cut diagrams "real" and "virtual" respectively. The real and virtual diagrams contain the delta functions,

$$\begin{aligned}
\delta_R &\equiv \delta_R(\tau_a^n, q, l^+) \equiv \delta\Big(\tau_a^n - \frac{1}{Q}\Big[(q^-)^{\frac{a}{2}}(q^+)^{1-\frac{a}{2}} + (Q-q^-)^{\frac{a}{2}}(l^+-q^+)^{1-\frac{a}{2}}\Big]\Big)\,, \\
\delta_V &\equiv \delta_V(\tau_a^n, l^+) \equiv \delta\Big(\tau_a^n - \big(l^+/Q\big)^{1-\frac{a}{2}}\Big)\,,
\end{aligned} \tag{3.49}$$

which are obtained using Eq. (3.34). In this case we simply consider the contribution to τ_a from a final state with a single on-shell collinear quark of momentum l for δ_V and from a final state consisting of an on-shell collinear gluon of momentum q together with an on-shell collinear quark of momentum $l-q$ for δ_R, and use that the '$-$' component of momentum is always larger than the '+' component for on-shell collinear particles. The momentum l flowing through the diagrams in Fig. 3.3 has a label component which is fixed to be $Qn/2$ by the labels on the collinear fields in the matrix element in Eq. (3.22a).

Before turning to evaluate the diagrams in Fig. 3.3, we first perform a few simplifications to facilitate the computation. First, we note that the Wilson line emission diagram, Fig. 3.3A, and its mirror, Fig. 3.3B, give identical contributions. Second, we employ the fact that the number and complexity of jet function diagrams needed in loop calculations is reduced by noticing that the QCD-like diagrams can be computed using ordinary QCD Feynman rules with appropriate insertions of the projection operators P_n and $P_{\bar{n}}$ [38, 14]. In particular, for our one-loop example

we use that the sum of Fig. 3.3C and Fig. 3.3D reduces to

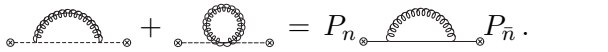

(3.50)

Next, we relate the τ_a^n-discontinuity to the ordinary discontinuity,

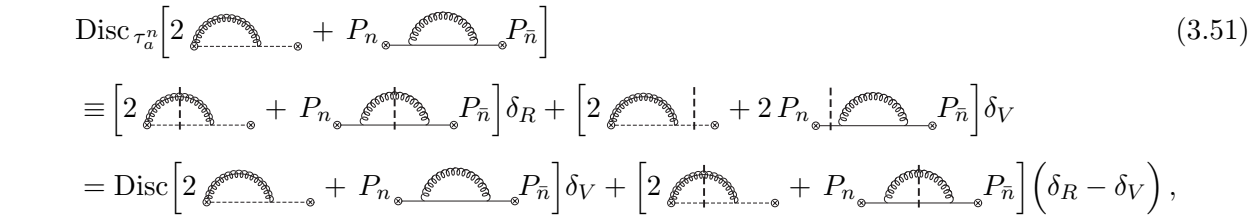

(3.51)

where in the third line the we used that the real diagrams induced by taking the discontinuity in the first term cancel the coefficient of δ_V in the second term.

Now, since $\delta_V(\tau_a^n, l^+)$ has no dependence on the loop momentum q, it factors out of the $\mathrm{d}^d q$ integrand. This implies that, after adding the tree level contribution to the one-loop τ_a^n-discontinuity in Eq. (3.51), we can write the NLO jet function as

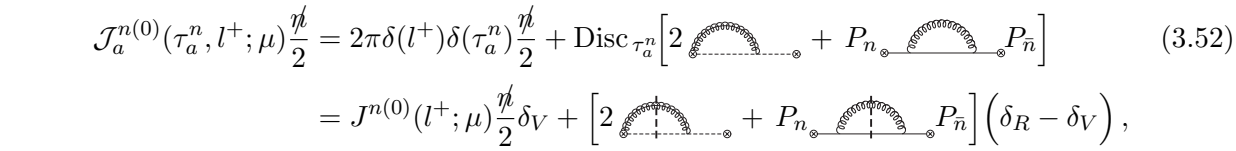

(3.52)

where $J_n^{(0)}(l^+;\mu)$ is the standard jet function [29],

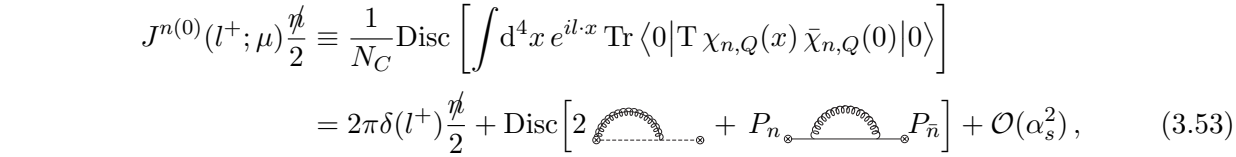

(3.53)

containing no additional operator insertions. Each term on the second line of Eq. (3.52) is then well-defined[5] and straightforwardly calculable. In fact, $J^n(l^+;\mu)$ has been calculated to two loops [38], and we expect that the techniques we employed above are the most practical way to extend our results to two loops. The additional term on the second line of Eq. (3.52) is a sum of real emission diagrams containing a difference of the delta functions δ_R and δ_V. Note that for the special case $a = 0$, $\delta_V(\tau_a^n, l^+) = \delta_R(\tau_a^n, q, l^+)$ and this additional term vanishes, so $J^n = J^n_{a=0}$. This is why only the standard jet function is needed when $a = 0$.

To find the angularity jet function $J_a^n(\tau_a^n;\mu)$, we must integrate Eq. (3.52) over l^+ as in Eq. (3.21),

$$J_a^{n(0)}(\tau_a^n;\mu) = \int \frac{\mathrm{d}l^+}{2\pi} \mathcal{J}_a^{n(0)}(\tau_a^n, l^+;\mu)\,. \tag{3.54}$$

[5] By this we mean that had we evaluated the individual cut virtual QCD-like diagrams contained in the first line of Eq. (3.52) directly, we would have encountered the complication of cutting one lone quark propagator and thus putting the second lone, uncut quark propagator on shell also.

By integrating the known one-loop expression for $J_n^{(0)}(l^+;\mu)$ (see, e.g., [25, 53]), we find that the contribution of the first term in Eq. (3.52) is

$$\int\frac{\mathrm{d}l^+}{2\pi}J^{n(0)}(l^+;\mu)\,\delta_V=\delta(\tau_a^n)\biggl\{1+\frac{\alpha_sC_F}{4\pi}\biggl[\frac{4}{\epsilon^2}+\frac{3}{\epsilon}+\frac{4}{\epsilon}\ln\frac{\mu^2}{Q^2}+2\ln^2\frac{\mu^2}{Q^2}+3\ln\frac{\mu^2}{Q^2}+7-\pi^2\biggr]\biggr\}-\frac{1}{1-a/2}\frac{\alpha_sC_F}{4\pi}\biggl[\biggl(\frac{4}{\epsilon}+3+8\ln\frac{\mu}{Q(\tau_a^n)^{1/(2-a)}}\biggr)\biggl(\frac{\theta(\tau_a^n)}{\tau_a^n}\biggr)\biggr]_+. \tag{3.55}$$

It is well known that all $1/\epsilon$ poles in this expression are of UV origin.

We find that the term involving the real QCD-like diagram in Eq. (3.52) is

$$\begin{aligned}&\int\frac{\mathrm{d}l^+}{2\pi}\Bigl[\,P_n\otimes\!\!\smile\!\!\otimes P_{\bar n}\Bigr]\Bigl(\delta_R-\delta_V\Bigr) \qquad (3.56)\\ &=-g^2\mu^{2\epsilon}C_F(d-2)\frac{\not n}{2}\int\frac{\mathrm{d}l^+}{2\pi}\biggl(\frac{1}{l^+}\biggr)^2\int\frac{\mathrm{d}^dq}{(2\pi)^d}(l^+-q^+)\\ &\quad\times\Bigl((-2\pi i)\delta(q^+q^--|\mathbf{q}_\perp|^2)\theta(q^-)\Bigr)\frac{1}{q^-}\Bigl(\delta_R(\tau_a^n,q,l^+)-\delta_V(\tau_a^n,l^+)\Bigr)\\ &\quad\times\Bigl((-2\pi i)\delta\bigl((Q-q^-)(l^+-q^+)-|\mathbf{q}_\perp|^2\bigr)\theta(Q-q^-)\Bigr)\\ &=\frac{\alpha_sC_F}{2\pi(2-a)}\frac{\not n}{2}\biggl(\frac{4\pi\mu^2}{Q^2}\biggr)^\epsilon\frac{2(1-\epsilon)}{\Gamma(1-\epsilon)}\biggl(\frac{1}{\tau_a^n}\biggr)^{1+\frac{\epsilon}{1-a/2}}\\ &\quad\times\int_0^1\mathrm{d}x\,x\left[\bigl(x^{a-1}+(1-x)^{a-1}\bigr)^{\frac{\epsilon}{1-a/2}}-\bigl(x(1-x)\bigr)^{-\epsilon}\right],\end{aligned}$$

where we defined $x\equiv q^-/Q$. This expression is finite as $\epsilon\to0$.

For the term involving the real Wilson line diagram, we find

$$\begin{aligned}&\int\frac{\mathrm{d}l^+}{2\pi}\Bigl[\,\smile\!\!\otimes\Bigr]\Bigl(\delta_R-\delta_V\Bigr) \qquad (3.57)\\ &=-g^2\mu^{2\epsilon}C_F\,n\cdot\bar n\frac{\not n}{2}\int\frac{\mathrm{d}l^+}{2\pi}\frac{1}{l^+}\int\frac{\mathrm{d}^dq}{(2\pi)^d}\frac{1}{q^-}\Bigl((-2\pi i)\delta(q^+q^--|\mathbf{q}_\perp|^2)\theta(q^-)\Bigr)\\ &\quad\times\biggl[(Q-q^-)\Bigl((-2\pi i)\delta\bigl((Q-q^-)(l^+-q^+)-|\mathbf{q}_\perp|^2\bigr)\theta(Q-q^-)\Bigr)\\ &\qquad-Q\Bigl((-2\pi i)\delta\bigl(Q(l^+-q^+)\bigr)\Bigr)\biggr]\Bigl(\delta_R(\tau_a^n,q,l^+)-\delta_V(\tau_a^n,l^+)\Bigr).\end{aligned}$$

The piece with δ_R can be written as

$$\begin{aligned}\int\frac{\mathrm{d}l^+}{2\pi}\Bigl[\,\smile\!\!\otimes\Bigr]\delta_R&=\theta(\tau_a^s)\frac{\alpha_sC_Fn\cdot\bar n}{2\pi(2-a)}\frac{\not n}{2}\biggl(\frac{4\pi\mu^2}{Q^2}\biggr)^\epsilon\frac{1}{\Gamma(1-\epsilon)}\biggl(\frac{1}{\tau_a^n}\biggr)^{1+\frac{\epsilon}{1-a/2}} \qquad (3.58)\\ &\quad\times\left[\int_0^1\frac{\mathrm{d}x}{x}\,(1-x)\left(x^{a-1}+(1-x)^{a-1}\right)^{\frac{\epsilon}{1-a/2}}-\int_0^\infty\frac{\mathrm{d}x}{x}x^{-\epsilon\frac{1-a}{1-a/2}}\right],\end{aligned}$$

and the piece with δ_V is

$$\int \frac{\mathrm{d}l^+}{2\pi}\Big[\ \Big]\delta_V = \theta(\tau_a^s)\frac{\alpha_s C_F n\cdot\bar{n}}{2\pi(2-a)}\frac{\not{n}}{2}\left(\frac{4\pi\mu^2}{Q^2}\right)^{\epsilon}\frac{1}{\Gamma(1-\epsilon)}\left(\frac{1}{\tau_a^n}\right)^{1+\frac{\epsilon}{1-a/2}} \times\left[\int_0^1\frac{\mathrm{d}x}{x}\,(1-x)\,(x(1-x))^{-\epsilon}-\int_0^\infty\frac{\mathrm{d}x}{x}x^{-\epsilon}\right]. \tag{3.59}$$

The second term in brackets in each of Eqs. (3.57), (3.58), and (3.59) corresponds to the zero-bin subraction [163] needed to avoid the double counting of soft modes [157, 140, 139]. Note that from the expressions in both Eqs. (3.58) and (3.59), the zero-bin contributions are scaleless and hence formally zero. Their role is to convert the IR divergence ($q^-\to 0$) in each integrand into a UV divergence ($q^-\to\infty$) for $a<1$. After this subtraction, both of the integrals over x in brackets are convergent for $\epsilon>0$.

Subtracting Eq. (3.59) from Eq. (3.58) and performing the integral over x we find that

$$\int\frac{\mathrm{d}l^+}{2\pi}\mathrm{Disc}\Big[2\ +\ P_n\ P_{\bar{n}}\Big]\Big(\delta_R-\delta_V\Big) \tag{3.60}$$
$$=-\frac{\alpha_s C_F}{2\pi(2-a)}\frac{\not{n}}{2}\left(\frac{4\pi\mu^2}{Q^2}\right)^{\epsilon}\frac{1}{\Gamma(1-\epsilon)}\frac{1}{\epsilon}\left(\frac{1}{\tau_a^n}\right)^{1+\frac{\epsilon}{1-a/2}}\left[\frac{2a}{1-a}+\epsilon^2\frac{2a(\pi^2-9)}{3(2-a)}\right.$$
$$\left.-\epsilon^2\frac{4}{1-a/2}\int_0^1\mathrm{d}x\frac{1-x+x^2/2}{x}\ln\left[(1-x)^{1-a}+x^{1-a}\right]+\mathcal{O}(\epsilon^3)\right],$$

where the overall $1/\epsilon$ pole is of UV origin from the discussion above.

Applying the relation Eq. (3.39) to Eq. (3.60) and adding the result to Eq. (3.55), we arrive at our final expression for the (bare) NLO angularity jet function,

$$J_a^{n(0)}(\tau_a^n;\mu)=\int\mathrm{d}\tau_a^{n\prime}\,Z_J(\tau_a^n-\tau_a^{n\prime};\mu)J_a^n(\tau_a^{n\prime};\mu)\,, \tag{3.61}$$

where the renormalized jet function, J_a^n, is

$$J_a^n(\tau_a^n;\mu)=\delta(\tau_a^n)\left\{1+\frac{\alpha_s C_F}{\pi}\left[\frac{1-a/2}{2(1-a)}\ln^2\frac{\mu^2}{Q^2}+\frac{3}{4}\ln\frac{\mu^2}{Q^2}+f(a)\right]\right\}$$
$$-\frac{\alpha_s C_F}{\pi}\left[\left(\frac{3}{4}\frac{1}{1-a/2}+\frac{2}{1-a}\ln\frac{\mu}{Q(\tau_a^n)^{1/(2-a)}}\right)\left(\frac{\theta(\tau_a^n)}{\tau_a^n}\right)\right]_+, \tag{3.62}$$

where we defined

$$f(a)\equiv\frac{1}{1-a/2}\left(\frac{7-13a/2}{4}-\frac{\pi^2}{12}\frac{3-5a+9a^2/4}{1-a}\right.$$
$$\left.-\int_0^1\mathrm{d}x\frac{1-x+x^2/2}{x}\ln\left[(1-x)^{1-a}+x^{1-a}\right]\right), \tag{3.63}$$

and the Z-factor is given by

$$Z_J(\tau_a^n;\mu)=\delta(\tau_a^n)\left[1+\frac{\alpha_s C_F}{\pi}\left(\frac{1-a/2}{1-a}\left(\frac{1}{\epsilon^2}+\frac{1}{\epsilon}\ln\frac{\mu^2}{Q^2}\right)+\frac{3}{4\epsilon}\right)\right]-\frac{1}{\epsilon}\frac{\alpha_s C_F}{\pi(1-a)}\left[\frac{\theta(\tau_a^n)}{\tau_a^n}\right]_+. \tag{3.64}$$

3.6 IR structure of the jet functions

As we showed in Sec. 3.5, the $1/\epsilon$ pole in front of the plus-distribution corresponds to a UV divergence. However, as we discussed for the case of the soft function in Sec. 3.4, the use of Eq. (3.39) means that we can not immediately make the same claim for the poles in the coefficient of $\delta(\tau_a^n)$. We now perform an analysis similar to that in Sec. 3.4 by integrating over $0 < \tau_a^n < 1$ to isolate this coefficient and study its divergent structure in the resulting q^-, $\mathbf{q}_\perp^2$ integration regions, complementing our discussion in [135].

The diagrams (C) and (D) in Fig. 3.3, being equivalent to diagrams in full QCD as noted above, are manifestly infrared-finite and do not need to be analyzed in further detail. The Wilson line graphs (A) and (B) potentially contain infrared divergences that we must identify more carefully.

If the jet function is infrared-safe, infrared divergences in virtual and real diagrams, with proper zero-bin subtractions taken, should cancel and leave purely UV divergent integrals. The contribution of the sum of the real and virtual Wilson line diagrams to the coefficient of $\delta(\tau_a^n)$ in the jet function $J_a^{n(0)}(\tau_a^n)$ is

$$2\int_0^1 \mathrm{d}\tau_a \int \frac{\mathrm{d}l^+}{2\pi}\Big[\quad \delta_V + \quad \delta_R\Big] \tag{3.65}$$

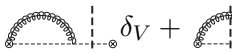

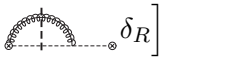

$$= -\frac{\alpha_s C_F}{\pi}\frac{(4\pi\mu^2)^\epsilon}{\Gamma(1-\epsilon)}\left[\int_{\tilde{\mathcal{J}}} \mathrm{d}q^-\mathrm{d}\mathbf{q}_\perp^2 \frac{1}{(\mathbf{q}_\perp^2)^{1+\epsilon}}\left(\frac{1}{q^-}-\frac{1}{Q}\right) - \int_{\mathcal{J}_0}\mathrm{d}q^-\mathrm{d}\mathbf{q}_\perp^2\frac{1}{(\mathbf{q}_\perp^2)^{1+\epsilon}}\frac{1}{q^-}\right],$$

where the last integral is the zero-bin subtraction of the naïve collinear integral in the first term. The naïve integration region $\tilde{\mathcal{J}}$ is shown in Fig. 3.4 and is given by $0 < q^- < Q$ and

$$\mathbf{q}_\perp^2 > \left\{ Q\left[\frac{1}{(Q-q^-)^{1-a}} + \frac{1}{(q^-)^{1-a}}\right]^{-1}\right\}^{\frac{1}{1-a/2}} . \tag{3.66}$$

The zero-bin region $\mathcal{J}_0$ is given by $q^- > 0$ and

$$\mathbf{q}_\perp^2 > \left[Q(q^-)^{1-a}\right]^{\frac{1}{1-a/2}} . \tag{3.67}$$

The resulting integral for the total contribution of the zero-bin-subtracted Wilson line diagrams to the coefficient of $\delta(\tau_a^n)$ in the jet function is

$$2\int_0^1 \mathrm{d}\tau_a \int \frac{\mathrm{d}l^+}{2\pi}\Big[\quad \delta_V + \quad \delta_R\Big] \tag{3.68}$$

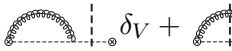

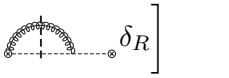

$$= -\frac{\alpha_s C_F}{\pi}\frac{(4\pi\mu^2)^\epsilon}{\Gamma(1-\epsilon)}\left[\int_{\mathcal{J}} \mathrm{d}q^-\mathrm{d}\mathbf{q}_\perp^2 \frac{1}{(\mathbf{q}_\perp^2)^{1+\epsilon}}\frac{\mathrm{sgn}(q^--Q)}{q^-} - \int_{\tilde{\mathcal{J}}}\mathrm{d}q^-\mathrm{d}\mathbf{q}_\perp^2\frac{1}{(\mathbf{q}_\perp^2)^{1+\epsilon}}\frac{1}{Q}\right],$$

where the region $\mathcal{J}$ resulting from combining $\tilde{\mathcal{J}}$ and $\mathcal{J}_0$, with a relative minus sign in the integrands, is also shown in Fig. 3.4.

The shape of the final integration region $\mathcal{J}$ in Fig. 3.4 demonstrates that the scaleless virtual and zero-bin integrals succeed in converting IR divergences in the real diagram contributions

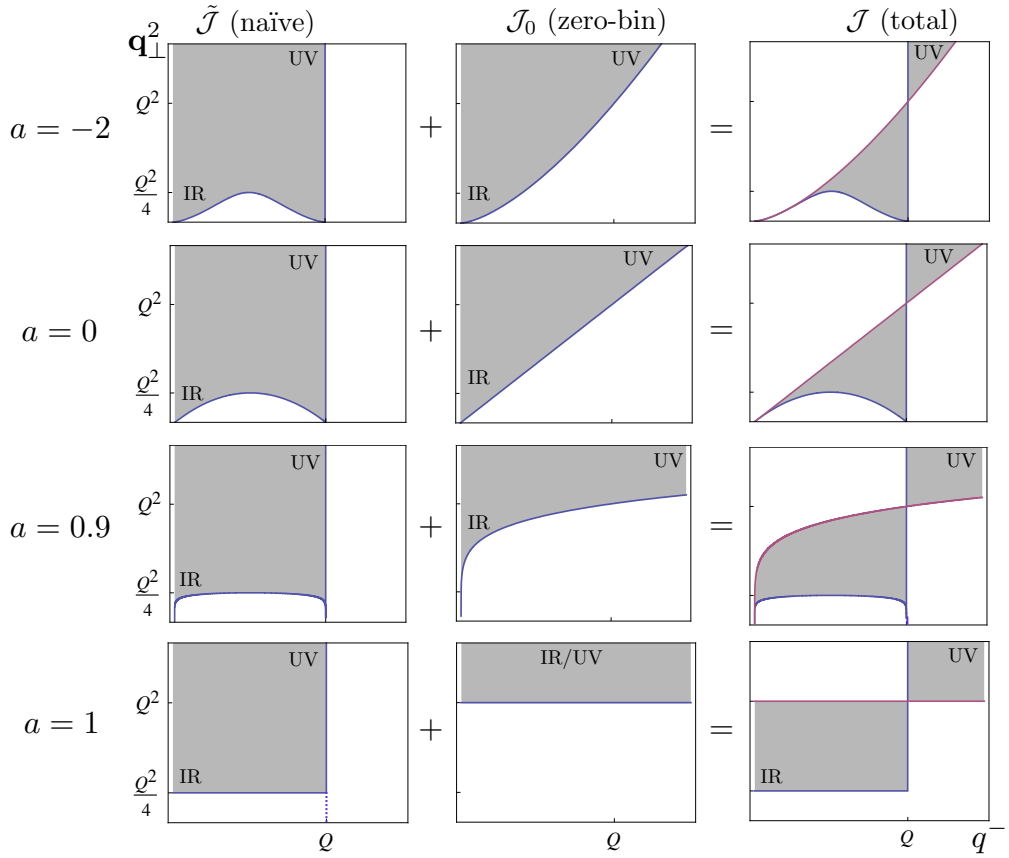

Figure 3.4: Regions of integration for the coefficient of $\delta(\tau_a^n)$ in the jet function $J_a^{n(0)}(\tau_a^n)$. The sum of naïve real and virtual Wilson line diagrams are integrated over the region $\tilde{\mathcal{J}}$ in the $q^-, \mathbf{q}_\perp^2$ plane. The sum of real and virtual zero-bin subtractions are integrated over $\mathcal{J}_0$, and the resulting sum of naïve diagrams and zero-bin subtractions over the region $\mathcal{J}$. Integrals over $\mathcal{J}$ have only UV divergences as long as $a < 1$. For $a = 1$, an IR divergent region remains.

into UV divergences for all $a < 1$. Eq. (3.68) converges for $\epsilon > 0$ if and only if $a < 1$. The result of performing this integration, after including the contributions of the QCD-like diagrams in Fig. 3.3C and D, agrees with the coefficient of $\delta(\tau_a^n)$ that is obtained by (naïvely) using the relation Eq. (3.39) in Eq. (3.60).

3.7 Infrared safety, factorizability, and the effective theory

In the one-loop calculations of soft and jet functions above, we observed that infrared safety of these functions, and, thus, factorizability of the angularity distributions, required $a < 1$. By analyzing explicitly the regions of integration over loop momenta in real and virtual graphs, we were able to identify when the loop integrals contained infrared or ultraviolet divergences. Cancellations of regions in real gluon diagrams sensitive to IR divergences relied crucially not only on the addition of virtual diagrams but also on zero-bin subtractions from collinear diagrams (see

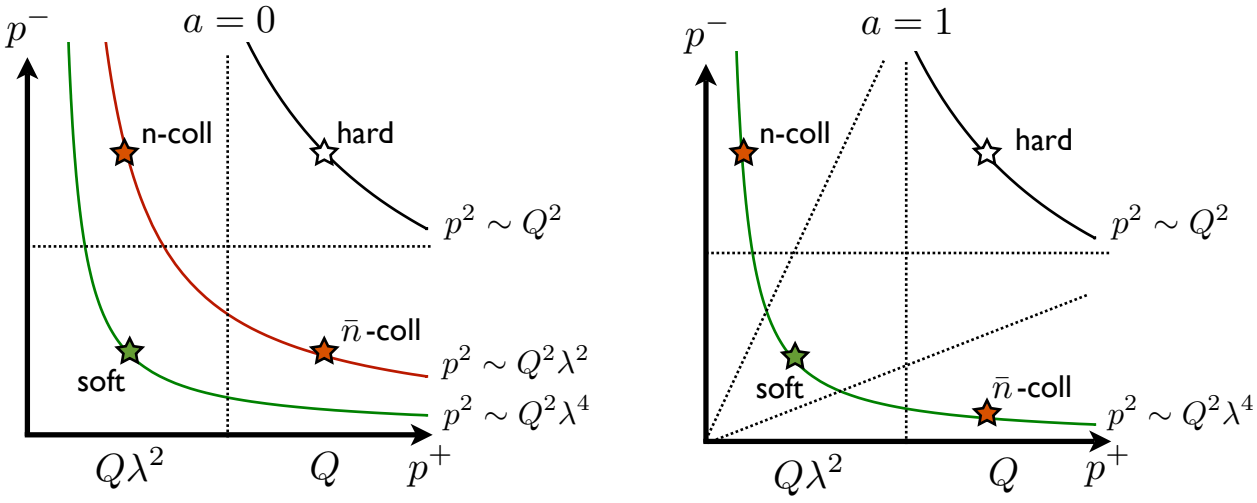

Figure 3.5: Scaling of SCET modes appropriate for angularities τ_a, $a = 0, 1$. For $a = 0$, the collinear modes dominating the τ_a distribution have virtualities $p^2 \sim (Q\lambda)^2$, parametrically separated from the soft scale $p^2 \sim (Q\lambda^2)^2$. These scalings correspond to the effective theory known as SCET$_{\rm I}$. For $a = 1$, the collinear modes in the distribution have typical $p^2 \sim (Q\lambda^2)^2$, coinciding with the soft scale. The collinear and soft modes are no longer separated by virtuality but instead by rapidity. These scalings correspond to SCET$_{\rm II}$. Collinear modes dominating angularity distributions for other values of a between 0 and 1 live at scales intermediate between these limits.

also examples in [163, 140, 139, 86]).

The shape of the momentum regions contributing to the one-loop soft function in Fig. 3.2 suggest a simple physical interpretation of the breakdown of factorization as $a \to 1$. In the $k^\pm$ plane, the region of integration in the sum of real and virtual graphs for $a = 1$ is the region above the line $k^+k^- = Q^2$. For angularity soft functions with $a < 1$, as $k^\pm \to \infty$, the loop integral goes over a region with k^+k^- strictly greater than Q^2, and in fact, $k^+k^- \to \infty$, while for $a > 1$, the loop integral enters the region with $k^+k^- < Q^2$, and in fact, $k^+k^- \to 0$. But this latter region, $k^+ \to \infty$ while $k^- \to 0$ or vice versa, is the region where collinear modes live, illustrated in Fig. 3.5. This means that collinear modes still contribute to the soft function even after the attempted factorization.

This suggests that for $a \geq 1$, the contributions of SCET$_{\rm I}$ soft and collinear modes to the angularity distribution have not actually been separated. In SCET$_{\rm I}$, soft, collinear, and hard modes can be distingushed by their well-separated virtualities, namely, $p_S^2 \sim (Q\lambda^2)^2$, $p_J^2 \sim (Q\lambda^{1/(1-a/2)})^2$, and $p_H^2 \sim Q^2$. At $a = 1$, the virtualities of soft and collinear modes contributing to the τ_a distribution coincide, and SCET$_{\rm I}$ must be matched onto SCET$_{\rm II}$ where collinear and soft modes both have virtualities $p^2 \sim (Q\lambda^2)^2$. In this case, the modes are no longer distinguished by their virtuality, but instead by their rapidity, as illustrated in Fig. 3.5. Ref. [163] suggested a modified version of the factorization theorem Eq. (3.1) in which soft and jet functions are defined either with cutoffs on rapidity or in dimensional regularization with the scale μ separated into two light-cone scales $\mu^\pm$, which must satisfy $\mu^+\mu^- = \mu^2$, with each of the two jet functions depending on one

of these scales, and the soft function on both. However, in the present chapter we do not pursue such a strategy and limit our analysis to angularities with strictly $a < 1$. For arbitrary values of a, the virtuality of collinear modes $p_J^2 \sim (Q\lambda^{1/(1-a/2)})^2$ suggests an interpretation as the modes of an effective theory "SCET$_{1+a}$."[6] Since our analysis and calculations utilize the framework of SCET$_{\rm I}$, we may expect non-negligible corrections to our results to arise for values of a less than but approaching 1, and for reasonable criteria for when corrections are negligible, our analysis is reliable for values of $a \lesssim 1/2$ [157].

4 NLL Resummation of Logarithms and Fixed-order Matching to QCD

The fixed-order NLO cross-section, obtained by using the fixed-order expressions for the hard, jet, and soft functions in Eqs. (3.29), (3.42), and (3.62) in the factorization formula Eq. (3.18), contain logarithms of μ divided by the scales Q, $Q\tau_a$, and the intermediate scale $Q\tau_a^{1/(2-a)}$. This means that there is no single choice for the scale μ that will simultaneously set all of the logarithms in the NLO cross-section to zero. For small τ_a, these scales become widely separated and the logarithms of ratios of these scales become large, which causes the perturbative series to break down. In Sec. 4.1 and Sec. 4.2, we take advantage of the effective theory framework separating the hard, jet, and soft contributions by evolving each of them separately through renormalization-group (RG) evolution which resums these logarithms. We then combine these RG-evolved functions into the full cross-section accurate to NLO at fixed order in α_s and resummed to NLL accuracy in Sec. 4.3.

Since our final result for the NLL/NLO resummed distribution is derived using an effective theory which is valid only in the small-τ_a limit, it does not get the larger-τ_a region as accurately as QCD at $\mathcal{O}(\alpha_s)$. To arrive at a result that retains NLL/NLO accuracy in the small-τ_a region while retaining the accuracy of QCD at $\mathcal{O}(\alpha_s)$ in the larger-τ_a region, we need to match our distribution onto QCD. This matching is constructed such that if we turn off the resummation, the distributions should agree with full QCD to $\mathcal{O}(\alpha_s)$. We perform this matching in Sec. 4.4.

4.1 Hard function at NLL

The anomalous dimension of the hard function in Eq. (3.29) can be found by requiring that matrix elements of the bare two-jet operator in Eq. (3.30) are independent of the scale μ, and is given by

$$\gamma_H(\mu) = -\gamma_{\mathcal{O}}(Qn/2, -Q\bar{n}/2; \mu) - \gamma_{\mathcal{O}}^*(Qn/2, -Q\bar{n}/2; \mu)\,, \tag{3.69}$$

where

$$\gamma_{\mathcal{O}}(\tilde{p}_n, \tilde{p}_{\bar{n}}; \mu) = -Z_{\mathcal{O}}^{-1}(\tilde{p}_n, \tilde{p}_{\bar{n}}; \mu)\mu\frac{\mathrm{d}}{\mathrm{d}\mu}Z_{\mathcal{O}}(\tilde{p}_n, \tilde{p}_{\bar{n}}; \mu) = \frac{\alpha_s C_F}{2\pi}\left(2\ln\frac{\mu^2}{2\tilde{p}_n\cdot\tilde{p}_{\bar{n}}} + 3\right)\,, \tag{3.70}$$

so that

$$\gamma_H(\mu) = -\frac{\alpha_s C_F}{\pi}\left(2\ln\frac{\mu^2}{Q^2} + 3\right)\,, \tag{3.71}$$

[6] We would like to thank M. Strassler for suggesting this terminology to CL.

which is the first term in the expansion of the anomalous dimension to all orders in α_s,

$$\gamma_H(\mu) = \Gamma_H[\alpha_s]\ln\frac{\mu^2}{Q^2} + \gamma_H[\alpha_s]\,. \tag{3.72}$$

Solving the RG equation,

$$\mu\frac{\mathrm{d}}{\mathrm{d}\mu}H(Q;\mu) = \gamma_H(\mu)H(Q;\mu)\,, \tag{3.73}$$

for $H(Q;\mu)$ gives

$$H(Q;\mu) = H(Q;\mu_0)e^{K_H}\left(\frac{\mu_0}{Q}\right)^{\omega_H}\,, \tag{3.74}$$

where ω_H and K_H are defined as

$$\omega_H \equiv \omega_H(\mu,\mu_0) \equiv \frac{8C_F}{\beta_0}\left[\ln r + \left(\frac{\Gamma^1_{\rm cusp}}{\Gamma^0_{\rm cusp}} - \frac{\beta_1}{\beta_0}\right)\frac{\alpha_s(\mu_0)}{4\pi}(r-1)\right] \tag{3.75a}$$

$$\begin{aligned} K_H \equiv K_H(\mu,\mu_0) \equiv{}& \frac{6C_F}{\beta_0}\ln r + \frac{16\pi C_F}{(\beta_0)^2}\left[\frac{r-1-r\ln r}{\alpha_s(\mu)}\right. \\ &\left. + \left(\frac{\Gamma^1_{\rm cusp}}{\Gamma^0_{\rm cusp}} - \frac{\beta_1}{\beta_0}\right)\frac{1-r+\ln r}{4\pi} + \frac{\beta_1}{8\pi\beta_0}\ln^2 r\right]. \end{aligned} \tag{3.75b}$$

Here $r = \frac{\alpha_s(\mu)}{\alpha_s(\mu_0)}$, and β_0, β_1 are the one-loop and two-loop coefficients of the beta function,

$$\beta[\alpha_s] = \mu\frac{\mathrm{d}\alpha_s}{\mathrm{d}\mu} = -2\alpha_s\left[\beta_0\left(\frac{\alpha_s}{4\pi}\right) + \beta_1\left(\frac{\alpha_s}{4\pi}\right)^2 + \cdots\right], \tag{3.76}$$

where

$$\beta_0 = \frac{11C_A}{3} - \frac{2n_f}{3} \qquad \text{and} \qquad \beta_1 = \frac{34C_A^2}{3} - \frac{10C_An_f}{3} - 2C_Fn_f\,. \tag{3.77}$$

The two-loop running coupling $\alpha_s(\mu)$ at any scale is given by

$$\frac{1}{\alpha_s(\mu)} = \frac{1}{\alpha_s(M_Z)} + \frac{\beta_0}{2\pi}\ln\left(\frac{\mu}{M_Z}\right) + \frac{\beta_1}{4\pi\beta_0}\ln\left[1 + \frac{\beta_0}{2\pi}\alpha_s(M_Z)\ln\left(\frac{\mu}{M_Z}\right)\right]. \tag{3.78}$$

In Eq. (3.74), we have used the fact that to all orders in perturbation theory, $\Gamma_H[\alpha_s]$ is proportional to $\Gamma_{\rm cusp}[\alpha_s]$, where

$$\Gamma_{\rm cusp}[\alpha_s] = \left(\frac{\alpha_s}{4\pi}\right)\Gamma^0_{\rm cusp} + \left(\frac{\alpha_s}{4\pi}\right)^2\Gamma^1_{\rm cusp} + \cdots\,. \tag{3.79}$$

The ratio of the one-loop and two-loop coefficients of $\Gamma_{\rm cusp}$ is [148]

$$\frac{\Gamma^1_{\rm cusp}}{\Gamma^0_{\rm cusp}} = \left(\frac{67}{9} - \frac{\pi^2}{3}\right)C_A - \frac{10n_f}{9}\,. \tag{3.80}$$

$\Gamma^1_{\rm cusp}$ and β_1 are needed in the expressions of ω_H and K_H for complete NLL resummation since we formally take $\alpha_s^2\ln\tau_a \sim \mathcal{O}(\alpha_s)$.

	$F=S$	$F=J$
j_F	1	$2-a$
Γ_F^0	$-8C_F\frac{1}{1-a}$	$8C_F\frac{1-a/2}{1-a}$
γ_F^0	0	$6C_F$

Table 3.1: Γ_F^0, γ_F and j_F for the jet and soft functions.

4.2 Jet and soft functions at NLL

The jet and soft functions obey the RG equation

$$\mu\frac{d}{d\mu}F(\tau;\mu)=\int_{-\infty}^{+\infty}\mathrm{d}\tau'\,\gamma_F(\tau-\tau';\mu)F(\tau';\mu)\,, \tag{3.81}$$

where $F=J,S$. The anomalous dimensions γ_F can be found from the Z-factors (given in Eqs. (3.43) and (3.64)) via the relation

$$\gamma_F(\tau-\tau';\mu)=-\int\mathrm{d}\tau''\,Z_F^{-1}(\tau-\tau'';\mu)\,\mu\frac{\mathrm{d}}{\mathrm{d}\mu}Z_F(\tau''-\tau';\mu)\,. \tag{3.82}$$

We find that

$$\gamma_J(\tau-\tau';\mu)=\frac{2\alpha_sC_F}{\pi}\left\{\delta(\tau-\tau')\left(\frac{1-a/2}{1-a}\ln\frac{\mu^2}{Q^2}+\frac{3}{4}\right)-\frac{1}{1-a}\left[\frac{\theta(\tau-\tau')}{\tau-\tau'}\right]_+\right\}, \tag{3.83}$$

and

$$\gamma_S(\tau-\tau';\mu)=\frac{2\alpha_sC_F}{\pi(1-a)}\left\{-\delta(\tau-\tau')\ln\frac{\mu^2}{Q^2}+2\left[\frac{\theta(\tau-\tau')}{\tau-\tau'}\right]_+\right\}. \tag{3.84}$$

Both anomalous dimensions are the first terms in the perturbative expansion of the general form to all orders in α_s [125, 129],

$$\gamma_F(\tau-\tau';\mu)=-\Gamma_F[\alpha_s]\left(\frac{2}{j_F}\left[\frac{\theta(\tau-\tau')}{(\tau-\tau')}\right]_+-\ln\frac{\mu^2}{Q^2}\,\delta(\tau-\tau')\right)+\gamma_F[\alpha_s]\delta(\tau-\tau')\,, \tag{3.85}$$

where the coefficients $\Gamma_F[\alpha_s],\gamma_F[\alpha_s]$ have the expansions

$$\Gamma_F[\alpha_s]=\left(\frac{\alpha_s}{4\pi}\right)\Gamma_F^0+\left(\frac{\alpha_s}{4\pi}\right)^2\Gamma_F^1+\cdots \tag{3.86}$$

and

$$\gamma_F[\alpha_s]=\left(\frac{\alpha_s}{4\pi}\right)\gamma_F^0+\left(\frac{\alpha_s}{4\pi}\right)^2\gamma_F^1+\cdots\,. \tag{3.87}$$

We summarize the coefficients Γ_F^0 and γ_F^0 and the j_F-values for the jet and soft functions in Table 3.1.

The solution of the RG equation Eq. (3.81) with the anomalous dimension γ_F of the form given in Eq. (3.85) with particular values of j_F was developed in the series of papers [39, 147, 10,

166]. Later, it was solved for arbitrary j_F in [125] using a convolution variable $t = Q^j\tau$ with mass dimension $j = j_F$. The resulting evolution equation for F is

$$F(\tau;\mu) = \int \mathrm{d}\tau'\, U_F(\tau-\tau';\mu,\mu_0) F(\tau';\mu_0)\,, \tag{3.88}$$

where the evolution kernel U_F is given to all orders in α_s by the expression

$$U_F(\tau-\tau';\mu,\mu_0) = \frac{e^{\tilde{K}_F+\gamma_E\tilde{\omega}_F}}{\Gamma(-\tilde{\omega}_F)} \left(\frac{\mu_0}{Q}\right)^{j_F\tilde{\omega}_F} \left[\frac{\theta(\tau-\tau')}{(\tau-\tau')^{1+\tilde{\omega}_F}}\right]_+\,, \tag{3.89}$$

where γ_E is the Euler constant and where $\tilde{\omega}_F$ and $\tilde{K}_F$ are defined as

$$\tilde{\omega}_F(\mu,\mu_0) \equiv \frac{2}{j_F}\int_{\alpha_s(\mu_0)}^{\alpha_s(\mu)} \frac{d\alpha}{\beta[\alpha]}\Gamma_F[\alpha]\,, \tag{3.90a}$$

$$\tilde{K}_F(\mu,\mu_0) \equiv \int_{\alpha_s(\mu_0)}^{\alpha_s(\mu)} \frac{d\alpha}{\beta[\alpha]}\gamma_F[\alpha] + 2\int_{\alpha_s(\mu_0)}^{\alpha_s(\mu)} \frac{d\alpha}{\beta[\alpha]}\Gamma_F[\alpha]\int_{\alpha_s(\mu_0)}^{\alpha} \frac{d\alpha'}{\beta[\alpha']}\,. \tag{3.90b}$$

The plus function in Eq. (3.89) for all $\omega < 1$ and $\omega \neq 0$ is defined as[7]

$$\begin{aligned}\left[\frac{\theta(x)}{x^{1+\omega}}\right]_+ &\equiv \lim_{\beta\to 0}\left[\frac{\theta(x-\beta)}{x^{1+\omega}} - \frac{\beta^{-\omega}}{\omega}\delta(x-\beta)\right] \\ &= -\frac{\delta(x)}{\omega} + \sum_{n=0}^{\infty}(-\omega)^n\left[\frac{\theta(x)\ln^n x}{x}\right]_+\,,\end{aligned} \tag{3.91}$$

with the latter plus functions defined in Eq. (3.40).

For the NLL parameters of the evolution kernel U_F, Eq. (3.90) gives

$$\omega_F(\mu,\mu_0) = -\frac{\Gamma_F^0}{j_F\,\beta_0}\left[\ln r + \left(\frac{\Gamma^1_{\rm cusp}}{\Gamma^0_{\rm cusp}} - \frac{\beta_1}{\beta_0}\right)\frac{\alpha_s(\mu_0)}{4\pi}(r-1)\right]\,, \tag{3.92a}$$

$$\begin{aligned}K_F(\mu,\mu_0) = &-\frac{\gamma_F^0}{2\beta_0}\ln r + \frac{-2\pi\Gamma_F^0}{(\beta_0)^2}\left[\frac{r-1-r\ln r}{\alpha_s(\mu)}\right. \\ &\left. + \left(\frac{\Gamma^1_{\rm cusp}}{\Gamma^0_{\rm cusp}} - \frac{\beta_1}{\beta_0}\right)\frac{1-r+\ln r}{4\pi} + \frac{\beta_1}{8\pi\beta_0}\ln^2 r\right]\,,\end{aligned} \tag{3.92b}$$

where we have used the fact that $\Gamma_F \propto \Gamma_{\rm cusp}$. This proportionality is well known for the $a = 0$ jet and soft functions. In Appendix 3.A we verify that it remains true for all $a < 1$.

From Eq. (3.88) we can write explicit formulas for the resummed jet and soft functions at any scale μ. Details of evaluating the integral over the convolution variable τ' are given in Appendix 3.B. For the soft function, we plug the fixed-order NLO result Eq. (3.42) at the scale μ_0

[7] Note that from the definition in Eq. (3.91), for $\omega < 0$ the '+' label can be dropped and so Eq. (3.91) is consistent with the distribution relation Eq. (3.39).

into Eq. (3.88), and obtain at the scale μ,

$$\begin{aligned} S_a(\tau_a;\mu) = {}& \frac{\mathrm{e}^{K_S+\gamma_E\omega_S}}{\Gamma(-\omega_S)}\left(\frac{\mu_0}{Q}\right)^{j_S\omega_S} \\ & \times\Bigg[\Bigg\{1-\frac{\alpha_s(\mu_0)C_F}{2\pi}\frac{1}{1-a}\Bigg(\ln^2\frac{\mu_0^2}{(Q\tau_a)^2}+4H(-1-\omega_S)\ln\frac{\mu_0^2}{(Q\tau_a)^2} \\ & \qquad +\frac{\pi^2}{2}+4\Big[[H(-1-\omega_S)]^2-\psi^{(1)}(-\omega_S)\Big]\Bigg)\Bigg\}\left(\frac{\theta(\tau_a)}{\tau_a^{1+\omega_S}}\right)\Bigg]_+, \end{aligned} \tag{3.93}$$

and for the jet function, plug in the fixed-order NLO result Eq. (3.62) at μ_0 into Eq. (3.88), and obtain at μ,

$$\begin{aligned} J_a^n(\tau_a;\mu) = {}& \frac{\mathrm{e}^{K_J+\gamma_E\omega_J}}{\Gamma(-\omega_J)}\left(\frac{\mu_0}{Q}\right)^{j_J\omega_J} \\ & \times\Bigg[\Bigg\{1+\frac{\alpha_s(\mu_0)C_F}{4\pi}\Bigg(\frac{2-a}{1-a}\ln^2\frac{\mu_0^2}{Q^2\tau_a^{\frac{2}{2-a}}}+\Big(3+\frac{4H(-1-\omega_J)}{1-a}\Big)\ln\frac{\mu_0^2}{Q^2\tau_a^{\frac{2}{2-a}}} \\ & +4f(a)+\frac{4}{(1-a)(2-a)}\Big[\frac{\pi^2}{6}+[H(-1-\omega_J)]^2-\psi^{(1)}(-\omega_J)\Big]\Bigg)\Bigg\}\left(\frac{\theta(\tau_a)}{\tau_a^{1+\omega_J}}\right)\Bigg]_+, \end{aligned} \tag{3.94}$$

where in the above two equations $K_F \equiv K_F(\mu,\mu_0)$, $\omega_F \equiv \omega_F(\mu,\mu_0)$, $H(z)$ is the harmonic number function, and $\psi^{(\nu)}(z)$ is the polygamma function.

4.3 Full distribution at NLL

By running the hard, jet, and soft functions from the scales $\mu_0 = \mu_H$, μ_J, and μ_S, respectively, to the common factorization scale μ and performing the convolution in Eq. (3.18) (see Appendix 3.B for details), we find for the final resummed expression for the two-jet angularity distribution with NLL/NLO perturbative accuracy

$$\frac{1}{\sigma_0}\frac{\mathrm{d}\sigma_2}{\mathrm{d}\tau_a}^{\mathrm{PT}}\Bigg|_{\mathrm{NLL/NLO}} = \Bigg[\Big(1+f_H+2f_J+f_S\Big)U_a^\sigma(\tau_a;\mu,\mu_H,\mu_J,\mu_S)\Bigg]_+, \tag{3.95}$$

where we defined

$$U_a^\sigma(\tau_a;\mu,\mu_H,\mu_J,\mu_S) \equiv \frac{e^{K+\gamma_E\Omega}}{\Gamma(-\Omega)}\left(\frac{\mu_H}{Q}\right)^{\omega_H}\left(\frac{\mu_J}{Q}\right)^{2j_J\omega_J}\left(\frac{\mu_S}{Q}\right)^{j_S\omega_S}\left(\frac{\theta(\tau_a)}{{\tau_a}^{1+\Omega}}\right), \tag{3.96}$$

where

$$\Omega \equiv 2\,\omega_J(\mu,\mu_J)+\omega_S(\mu,\mu_S) \tag{3.97}$$

$$K \equiv K_H(\mu,\mu_H)+2K_J(\mu,\mu_J)+K_S(\mu,\mu_S)\,, \tag{3.98}$$

with ω_H, K_H given by Eq. (3.75) and $\omega_{J,S}$ and $K_{J,S}$ given by Eq. (3.92) and

$$f_H = \frac{\alpha_s(\mu_H) C_F}{\pi} \left(-4 + \frac{7\pi^2}{12} - 2\ln^2 \frac{\mu_H}{Q} - 3\ln \frac{\mu_H}{Q} \right) \tag{3.99a}$$

$$f_J = \frac{\alpha_s(\mu_J) C_F}{\pi} \left[f(a) + \frac{3/4}{1-a/2} H(-1-\Omega) + \frac{\frac{\pi^2}{6} + H(-1-\Omega)^2 - \psi^{(1)}(-\Omega)}{2(1-a)(1-a/2)} \right. \tag{3.99b}$$
$$\left. + \frac{2-a}{1-a} \ln^2 \frac{\mu_J}{Q {\tau_a}^{1/(2-a)}} + \left(\frac{3}{2} + \frac{2}{1-a} H(-1-\Omega) \right) \ln \frac{\mu_J}{Q {\tau_a}^{1/(2-a)}} \right]$$

$$f_S = \frac{\alpha_s(\mu_S) C_F}{\pi} \left[\frac{1}{1-a} \left(-\frac{\pi^2}{4} - 2H(-1-\Omega)^2 + 2\psi^{(1)}(-\Omega) \right) \right. \tag{3.99c}$$
$$\left. - 2\ln^2 \frac{\mu_S}{Q\tau_a} - 4H(-1-\Omega) \ln \frac{\mu_S}{Q\tau_a} \right],$$

and $f(a)$ was defined in Eq. (3.63).

From these expressions, it is clear that the logarithms are minimized by choosing μ_H, μ_J, and μ_S of order Q, $Q{\tau_a}^{1/(2-a)}$, and $Q\tau_a$, respectively. We will describe in more detail precisely which values we choose for these scales when we plot the full distributions in Sec. 6.

4.4 Matching to QCD

One way to achieve matching onto QCD is to include three-jet operators in the matching of the QCD current onto the SCET operators in Eq. (3.13) [32, 165]. For the scope of this paper, however, we simply adopt the matching procedure described by [73], as implemented in [41].

To $\mathcal{O}(\alpha_s)$ the full QCD distribution will take the form

$$\frac{1}{\sigma_0} \frac{\mathrm{d}\sigma}{\mathrm{d}\tau_a} = \delta(\tau_a) + \left(\frac{\alpha_s}{2\pi} \right) A_a(\tau_a) + \mathcal{O}(\alpha_s^2) \,. \tag{3.100}$$

In Appendix 3.C we describe how to calculate $A_a(\tau_a)$ numerically. Meanwhile, the fixed-order two-jet angularity distribution in SCET at $\mathcal{O}(\alpha_s)$ is given by the convolution Eq. (3.18) of the fixed-order hard, jet, and soft functions Eqs. (3.29), (3.42), and (3.62). The result is independent of μ (except through $\alpha_s \equiv \alpha_s(\mu)$), and is given by

$$\frac{1}{\sigma_0} \frac{\mathrm{d}\sigma_2}{\mathrm{d}\tau_a} = \delta(\tau_a) D_a^\delta + \frac{\alpha_s}{2\pi} [D_a(\tau_a)]_+ \,, \tag{3.101}$$

where

$$D_a^\delta = 1 - \frac{\alpha_s C_F}{2\pi} \frac{1}{2-a} \left\{ 2 + 5a - \frac{\pi^2}{3}(2+a) \right.$$
$$\left. + 4 \int_0^1 \mathrm{d}x \frac{x^2 - 2x + 2}{x} \ln \left[x^{1-a} + (1-x)^{1-a} \right] \right\} \tag{3.102}$$

$$D_a(\tau_a) = -\frac{2C_F}{2-a} \frac{\theta(\tau_a)(3 + 4\ln \tau_a)}{\tau_a} \,. \tag{3.103}$$

The two-jet fixed-order SCET distribution Eq. (3.101) reproduces the most singular parts of the full QCD distribution[8] Eq. (3.100), that is, the coefficient of the $\delta(\tau_a)$, $1/\tau_a$ and $(1/\tau_a)\ln\tau_a$ pieces. The expression for $D_a(\tau_a)$ in Eq. (3.103) makes explicit that the angularities are not infrared-safe for $a = 2$.

The difference of the two fixed-order distributions Eq. (3.100) and Eq. (3.101) away from $\tau_a = 0$ is a purely integrable function,

$$r_a(\tau_a) \equiv \frac{1}{\sigma_0}\left(\frac{\mathrm{d}\sigma}{\mathrm{d}\tau_a} - \frac{\mathrm{d}\sigma_2}{\mathrm{d}\tau_a}\right) = \left(\frac{\alpha_s}{2\pi}\right)\left[A_a(\tau_a) - D_a(\tau_a)\right]. \tag{3.104}$$

By adding this remainder function to the NLL resummed SCET distribution, we obtain a result which both agrees with QCD to $\mathcal{O}(\alpha_s)$ and resums large logarithmic terms in the entire perturbative series with NLL/NLO accuracy. The matched distributions are thus defined as

$$\frac{1}{\sigma_0}\frac{\mathrm{d}\sigma^{\mathrm{PT}}}{\mathrm{d}\tau_a}\bigg|_{\mathrm{NLL/NLO}} = \frac{1}{\sigma_0}\frac{\mathrm{d}\sigma_2^{\mathrm{PT}}}{\mathrm{d}\tau_a}\bigg|_{\mathrm{NLL/NLO}} + r_a(\tau_a). \tag{3.105}$$

To find $r_a(\tau_a)$, we numerically obtain $A_a(\tau_a)$ from an analysis of the full QCD distributions away from $\tau_a = 0$ using the procedure described in Appendix 3.C, and then subtract out the expression for $D_a(\tau_a)$ given in Eq. (3.103).

For the case $a = 0$ (thrust), the analytic form of $\mathrm{d}\sigma^{\mathrm{PT}}/\mathrm{d}\tau_0$ is known [101], with which our formula Eq. (3.157) for $A_0(\tau_0)$ agrees. Using Eqs. (3.157) and (3.103), we obtain the remainder function

$$r_0(\tau_0) = \frac{\alpha_s C_F}{2\pi}\left[\frac{2(2-3\tau_0+3\tau_0^2)}{1-\tau_0}\frac{\ln(1-2\tau_0)}{\tau_0} - \frac{2(1-3\tau_0)}{1-\tau_0}\ln\tau_0 + 6 + 9\tau_0\right], \tag{3.106}$$

which we see is integrable down to $\tau_0 = 0$.

As a consistency check of this matching technique, we calculated the total integral[9] of our fixed-order result,

$$\sigma_{\mathrm{total}} = \int_0^{\tau_a^{\max}} \mathrm{d}\tau_a \left(\frac{1}{\sigma_0}\frac{\mathrm{d}\sigma_2^{\mathrm{PT}}}{\mathrm{d}\tau_a} + r_a(\tau_a)\right), \tag{3.107}$$

and compared with the total inclusive cross-section, $\sigma(e^+e^- \to X) = \sigma_0(1 + \alpha_s/\pi)$. We found that our results agreed to any arbitrary precision which could be achieved by our numerical computation.

5 Nonperturbative Model for the Soft Function

In this section we adapt the model for the soft function used in jet mass and thrust distributions as constructed in [132] to work for all angularities with $a < 1$. This model is designed to describe the small-τ_a region where perturbation theory breaks down, while leaving the perturbatively reliable large- and intermediate-τ_a regions unaffected. The gap parameter in this model is

[8] Technically, we mean that the difference of the two distributions integrated from 0 to ϵ vanishes as $\epsilon \to 0$.

[9] The upper limit on τ_a in Eq. (3.107), $\tau_a^{\max}$, is that of the maximally symmetric three-jet configuration, $\tau_{\mathrm{sym}}(a) = 1/3^{1-a/2}$ [49], but only for $a \gtrsim -2.6$ (see Appendix 3.C).

designed to turn off the soft function at energies below a minimum hadronic threshold. Such a parameter is known to have renormalon ambiguities [132], which must cancel those in the perturbative soft function (which we denote in this section as $S^{\rm PT}$) to yield a renormalon-free total soft function S. To ensure perturbative stability, a scheme is needed to explicitly enforce this cancellation order-by-order in perturbation theory. Recently, the position-mass scheme developed in Ref. [141] was used to define a renormalon-free gap parameter for hemisphere jet masses in Ref. [130]. This gap parameter obeys transitive RG evolution and has a well-behaved perturbative expansion. We implement this scheme generalized to arbitrary angularity.

5.1 Review of hemisphere and thrust soft function models

To motivate the functional form of the model function that we will use for all angularity distributions, we begin with the model hemisphere soft function constructed in [149]. This model is a function of two variables which can be chosen to be l^+ and l^-, defined as the $+$ and $-$ components of the momentum in the n and $\bar{n}$ hemispheres, respectively. It takes the form

$$f^{\rm exp}(l^+,l^-) = \theta(l^+)\theta(l^-)\frac{\mathcal{N}(A,B)}{\Lambda^2}\left(\frac{l^+l^-}{\Lambda^2}\right)^{A-1}\exp\left(\frac{-(l^+)^2-(l^-)^2-2Bl^+l^-}{\Lambda^2}\right). \tag{3.108}$$

The parameter A controls how steeply the soft function falls as $l^\pm \to 0$, and B contains information about the cross correlation of the soft particles in the two hemispheres. $f^{\rm exp}$ is normalizable for $A > 0$ and $B > -1$. Λ is an $\mathcal{O}(\Lambda_{\rm QCD})$ parameter that describes the range that hadronic effects can smear the soft function around a given l^+, l^-. Finally, $\mathcal{N}(A,B)$ is chosen such that $f^{\rm exp}$ is normalized to unity, $\int_{-\infty}^{+\infty} {\rm d}l^+ {\rm d}l^- f^{\rm exp}(l^+,l^-) = 1$.

In Ref. [125], this model was used to relate the total hemisphere soft function $S_{\rm hemi}(l^+,l^-)$ to the perturbative hemisphere soft function $S^{\rm PT}_{\rm hemi}(l^+,l^-)$ via the convolution

$$S_{\rm hemi}(l^+,l^-;\mu) = \int_{-\infty}^{+\infty} {\rm d}\tilde{l}^+ {\rm d}\tilde{l}^- S^{\rm PT}_{\rm hemi}(l^+-\tilde{l}^+, l^- - \tilde{l}^-;\mu) f^{\rm exp}(\tilde{l}^+ - \Delta, \tilde{l}^- - \Delta)\,. \tag{3.109}$$

where Δ is the gap parameter. This method of implementing the model function ensures a smooth continuation between the nonperturbative, model-dominated and the perturbative regions of the cross-section.

To use this expression in our formalism, we first relate the $a = 0$ soft function, $S_0(\tau_0,\mu)$, and the hemisphere soft function, $S_{\rm hemi}(l^+,l^-,\mu)$. Using that $\tau_0 = (l^+ + l^-)/Q$, we find

$$\begin{aligned} S_0(\tau_0;\mu) &= \int {\rm d}l^+ {\rm d}l^- S_{\rm hemi}(l^+,l^-;\mu)\,\delta\left(\tau_0 - \frac{l^+ + l^-}{Q}\right) \\ &= Q\int {\rm d}l\, S_{\rm hemi}(l, Q\tau_0 - l;\mu)\,. \end{aligned} \tag{3.110}$$

This gives the model function convolution for $S_0(\tau_0;\mu)$ as

$$\begin{aligned} S_0(\tau_0;\mu) &= Q\int {\rm d}l \int {\rm d}l^+ {\rm d}l^-\, S^{\rm PT}_{\rm hemi}(l-l^+, Q\tau_0 - l - l^-;\mu) f^{\rm exp}(l^+ - \Delta, l^- - \Delta) \\ &= \int {\rm d}\tau_0'\, S_0^{\rm PT}(\tau_0 - \tau_0';\mu) f^{\rm exp}\left(\tau_0' - \frac{2\Delta}{Q}\right), \end{aligned} \tag{3.111}$$

where (absorbing A and B dependent constants into the normalization $\mathcal{N}$)

$$f^{\exp}(\tau) \equiv Q^2 \int \mathrm{d}\tau'\, f^{\exp}(Q\tau - Q\tau', Q\tau')$$
$$= \theta(\tau)\,\mathcal{N}(A,B)\frac{Q}{\Lambda}\left(\frac{Q\tau}{\Lambda}\right)^{2A-1} {}_1F_1\left(\frac{1}{2}, \frac{1}{2}+A, (B-1)\frac{(Q\tau)^2}{2\Lambda^2}\right) e^{-(B+1)\frac{(Q\tau)^2}{2\Lambda^2}}\,. \qquad (3.112)$$

$f^{\exp}(\tau)$ inherits its normalization from $f^{\exp}(l^+, l^-)$, $\int_{-\infty}^{\infty}\mathrm{d}\tau f^{\exp}(\tau) = 1$.

5.2 Adaptation to all angularities

For nonzero a, we still want to use a convolution of the form

$$S_a(\tau_a;\mu) = \int \mathrm{d}\tau_a'\, S_a^{\mathrm{PT}}(\tau_a - \tau_a';\mu)\, f_a^{\exp}\left(\tau_a' - \frac{2\Delta_a}{Q}\right). \qquad (3.113)$$

Moreover, we would like to retain the functional form of $f^{\exp}$ since it has had relatively good success in describing different event shapes with the same values of A and B [149]. However, we must at a minimum modify $f^{\exp}$ so that the first moment of $S_a(\tau_a;\mu)$ satisfies the scaling relation given in Eqs. (3.24) and (3.27). In terms of the first moment of $S_a^{\mathrm{PT}}(\tau_a;\mu)$ and $f_a^{\exp}$, the first moment of $S_a(\tau_a;\mu)$ is

$$\int \mathrm{d}\tau_a\, \tau_a\, S_a(\tau_a;\mu) = \int \mathrm{d}\tau_a\, \tau_a \int \mathrm{d}\tau_a'\, S_a^{\mathrm{PT}}(\tau_a - \tau_a';\mu)\, f_a^{\exp}\left(\tau_a' - \frac{2\Delta_a}{Q}\right)$$
$$= S_a^{\mathrm{PT}[1]}(\mu) + \left[\int \mathrm{d}\tau_a\, S_a^{\mathrm{PT}}(\tau_a;\mu)\right]\left(\frac{2\Delta_a}{Q} + f_a^{\exp[1]}\right)$$
$$= S_a^{\mathrm{PT}[1]}(\mu) + \frac{2\Delta_a}{Q} + f_a^{\exp[1]}\,, \qquad (3.114)$$

where here $S_a^{\mathrm{PT}[1]}(\mu)$ and $f_a^{\exp[1]}$ are the first moments of $S_a^{\mathrm{PT}}(\tau_a;\mu)$ and $f_a^{\exp}(\tau_a)$, respectively, and in the third line we dropped α_s corrections to the $\mathcal{O}(\Lambda_{\mathrm{QCD}}/Q)$ power corrections Δ_a/Q and $f_a^{\exp[1]}$.

Since the first moment of the perturbative soft function, $S_a^{\mathrm{PT}[1]}$, already obeys the proper scaling (cf. Eq. (3.42)) we simply rescale the gap parameter,

$$\Delta_a = \frac{\Delta}{1-a}\,, \qquad (3.115)$$

and require that the parameters of $f_a^{\exp}$ vary from those in $f^{\exp}$ such that

$$f_a^{\exp[1]} \equiv \int \mathrm{d}\tau_a\, \tau_a\, f_a^{\exp}(\tau_a) = \frac{1}{1-a}\int \mathrm{d}\tau\, \tau\, f^{\exp}(\tau) = \frac{1}{1-a} f^{\exp[1]}\,. \qquad (3.116)$$

This latter condition is most easily satisfied by fixing A and B to their value at $a = 0$ and allowing $\Lambda \to \Lambda_a$ to vary accordingly. Note from the definition of $f^{\exp}$, Eq. (3.112), $\Lambda f^{\exp}(\Lambda\tau/Q)$ is independent of Λ and hence $\Lambda_a f_a^{\exp}(\Lambda_a\tau/Q) = \Lambda f^{\exp}(\Lambda\tau/Q)$ when A and B are fixed. This implies that

$$f_a^{\exp[1]} = \left(\frac{\Lambda_a}{Q}\right)^2 \int \mathrm{d}\tau_a\, \tau_a\, f_a^{\exp}\left(\frac{\Lambda_a}{Q}\tau_a\right) = \left(\frac{\Lambda_a\Lambda}{Q^2}\right)\int \mathrm{d}\tau\, \tau\, f^{\exp}\left(\frac{\Lambda}{Q}\tau\right) = \left(\frac{\Lambda_a}{\Lambda}\right) f^{\exp[1]}\,, \qquad (3.117)$$

and so to satisfy Eq. (3.116) we take $f_a^{\rm exp}$ to be defined as in Eq. (3.112) but with Λ replaced with Λ_a where

$$\Lambda_a = \frac{\Lambda}{1-a}\,. \tag{3.118}$$

5.3 Renormalon cancellation

We want to ensure that the $1/Q$ renormalon ambiguity in $S^{\rm PT}(\tau_a;\mu)$ is cancelled order-by-order in perturbation theory. To implement the position-mass renormalon cancellation scheme defined in Ref. [141] for jet-masses and applied to the $a=0$ gap parameter in Ref. [130], we first take the Fourier transform of $S_a(\tau_a;\mu)$ with respect to $Q\tau_a$,

$$\begin{aligned} S_a(x_a;\mu) &\equiv \int \mathrm{d}\tau_a\, e^{-iQ\tau_a x_a} S_a(\tau_a;\mu) \\ &= \int \mathrm{d}\tau_a\, e^{-iQ\tau_a x_a} \int \mathrm{d}\tau_a'\, S_a^{\rm PT}(\tau_a-\tau_a';\mu)\, f_a^{\rm exp}\Big(\tau_a' - \frac{2\Delta_a}{Q}\Big) \\ &= S_a^{\rm PT}(x_a;\mu)\, f^{\rm exp}(x_a) e^{-2i\Delta_a x_a} \\ &= \Big[S_a^{\rm PT}(x_a;\mu) e^{-2i\delta_a(\mu)x_a}\Big]\Big[f_a^{\rm exp}(x_a) e^{-2i\bar\Delta_a(\mu)x_a}\Big]\,, \end{aligned} \tag{3.119}$$

where in the second line we used Eq. (3.113) and in fourth line we split Δ_a into two μ dependent pieces, $\Delta_a = \bar\Delta_a(\mu) + \delta_a(\mu)$. Note that since Δ_a is μ-independent, $S_a^{\rm PT}$ and S_a obey the same RG equation.

Next, we demand that for some value R, the term in the first pair of brackets in the last line of Eq. (3.119) satisfies

$$\frac{\mathrm{d}}{\mathrm{d}(ix_a)} \ln\left[S_a^{\rm PT}(x_a;\mu) e^{-2i\delta_a(\mu)x_a}\right]_{ix_a=(Re^{\gamma_E})^{-1}} = 0\,, \tag{3.120}$$

a condition which guarantees no ambiguity in $S_a^{\rm PT}$ at order $1/Q$. This gives $\delta_a(\mu)$ to all orders in terms of $S_a^{\rm PT}(\tau_a;\mu)$ as

$$\delta_a(\mu) = -\frac{Q}{2}\frac{\int \mathrm{d}\tau_a\, \tau_a\, e^{-Q\tau_a/(Re^{\gamma_E})} S_a^{\rm PT}(\tau_a;\mu)}{\int \mathrm{d}\tau_a\, e^{-Q\tau_a/(Re^{\gamma_E})} S_a^{\rm PT}(\tau_a;\mu)}\,, \tag{3.121}$$

which to leading order is given by the expression

$$\delta_a^1(\mu) = -Re^{\gamma_E}\frac{8C_F}{1-a}\left(\frac{\alpha_s(\mu)}{4\pi}\right)\ln\frac{\mu}{R}\,. \tag{3.122}$$

Since $\Delta_a = \bar\Delta_a(\mu) + \delta_a(\mu)$ is μ-independent we find that to $\mathcal{O}(\alpha_s)$,

$$\mu\frac{\mathrm{d}}{\mathrm{d}\mu}\bar\Delta_a(\mu) = -\mu\frac{\mathrm{d}}{\mathrm{d}\mu}\delta_a(\mu) = Re^{\gamma_E}\left[\frac{8C_F}{1-a}\left(\frac{\alpha_s(\mu)}{4\pi}\right)\right] \equiv -Re^{\gamma_E}\left[\Gamma_S^0\left(\frac{\alpha_s(\mu)}{4\pi}\right)\right]. \tag{3.123}$$

Using that $\Gamma_{\bar\Delta}[\alpha_s] \propto \Gamma_S[\alpha_s]$ (cf. Refs. [130, 141]) to all orders and that, for arbitrary a, $\Gamma_S[\alpha_s] \propto \Gamma_{\rm cusp}[\alpha_s]$ (cf. App. 3.A), we find that the NLL expression for $\mu\,\mathrm{d}\bar\Delta_a/\mathrm{d}\mu$ is

$$\mu\frac{\mathrm{d}}{\mathrm{d}\mu}\bar\Delta_a(\mu) = -Re^{\gamma_E}\left[\Gamma_S^0\left(\frac{\alpha_s(\mu)}{4\pi}\right)\left(1+\frac{\Gamma_{\rm cusp}^1}{\Gamma_{\rm cusp}^0}\frac{\alpha_s(\mu)}{4\pi}\right)\right], \tag{3.124}$$

which has the solution

$$\bar{\Delta}_a(\mu) = \bar{\Delta}_a(\mu_0) - \frac{Re^{\gamma_E}}{2}\omega_S(\mu,\mu_0)\,, \tag{3.125}$$

where $\omega_S(\mu,\mu_0)$ is given in Eq. (3.92). Note that since $\delta_a^1(\mu)$ and $\bar{\Delta}_a(\mu) - \bar{\Delta}_a(\mu_0)$ are proportional to $1/(1-a)$, Eq. (3.115) suggests that we should choose $\bar{\Delta}_a(\mu_0)$ to be $\bar{\Delta}(\mu_0)/(1-a)$, where $\bar{\Delta}(\mu_0)$ is the best choice for $a=0$.

Expanding Eq. (3.113) in powers of α_s to $\mathcal{O}(\alpha_s)$ gives

$$S_a(\tau_a;\mu) = \int \mathrm{d}\tau_a' \left[S_a^{\mathrm{PT}}(\tau_a-\tau_a';\mu) + \frac{2\delta_a^1(\mu)}{Q}\frac{\mathrm{d}}{\mathrm{d}\tau_a'} S_a^{\mathrm{PT}}(\tau_a-\tau_a';\mu)\right] f^{\exp}\left(\tau_a' - \frac{2\bar{\Delta}_a(\mu)}{Q}\right), \tag{3.126}$$

where S_a^{PT} at NLO in the first term in brackets and at LO in the second term should be used since δ_a^1 is $\mathcal{O}(\alpha_s)$. Using the fixed-order expression $S_a^{\mathrm{PT}}(\tau_a;\mu) = \delta(\tau_a) + \mathcal{O}(\alpha_s)$ in the second term and integrating this term by parts gives

$$S_a(\tau_a;\mu) = \int \mathrm{d}\tau_a' \left[S_a^{\mathrm{PT}}(\tau_a-\tau_a';\mu)\, f_a^{\exp}\left(\tau_a' - \frac{2\bar{\Delta}_a(\mu)}{Q}\right)\right] - \frac{2\delta_a^1(\mu)}{Q}\frac{\mathrm{d}}{\mathrm{d}\tau_a} f_a^{\exp}\left(\tau_a - \frac{2\bar{\Delta}_a(\mu)}{Q}\right). \tag{3.127}$$

Evolving $S_a(\tau_a;\mu_S)$ to the scale μ with $U_S(\tau_a-\tau_a';\mu,\mu_S)$ as in Eq. (3.88) gives

$$\begin{aligned} S_a(\tau_a;\mu) = \int \mathrm{d}\tau_a' \Bigg[& S_a^{\mathrm{PT}}(\tau_a-\tau_a';\mu)\, f_a^{\exp}\left(\tau_a' - \frac{2\bar{\Delta}_a(\mu_S)}{Q}\right) \\ & - \frac{2\delta_a^1(\mu_S)}{Q}\, U_S(\tau_a-\tau_a';\mu,\mu_S)\frac{\mathrm{d}}{\mathrm{d}\tau_a'} f_a^{\exp}\left(\tau_a' - \frac{2\bar{\Delta}_a(\mu_S)}{Q}\right)\Bigg]. \end{aligned} \tag{3.128}$$

Here we keep $\bar{\Delta}_a$ and δ_a at the scale μ_S which is needed to achieve the $1/Q$ renormalon cancellation [131].

Finally, Eq. (3.128) implies that the total resummed distribution at NLL convoluted with the model function $f_a^{\exp}$ is

$$\begin{aligned} \frac{1}{\sigma_0}\frac{\mathrm{d}\sigma}{\mathrm{d}\tau_a}\bigg|_{\mathrm{NLL/NLO}} = \int \mathrm{d}\tau_a' \Bigg\{ & \frac{1}{\sigma_0}\frac{\mathrm{d}\sigma^{\mathrm{PT}}}{\mathrm{d}\tau_a}(\tau_a-\tau_a';\mu)\bigg|_{\mathrm{NLL/NLO}} f_a^{\exp}\left(\tau_a' - \frac{2\bar{\Delta}_a(\mu_S)}{Q}\right) \\ & - \frac{2\delta_a^1(\mu_S)}{Q}\Big[U_a^{\sigma}(\tau_a-\tau_a';\mu,\mu_H,\mu_J,\mu_S)\Big]_+ \frac{\mathrm{d}}{\mathrm{d}\tau_a'} f_a^{\exp}\left(\tau_a' - \frac{2\bar{\Delta}_a(\mu_S)}{Q}\right)\Bigg\}, \end{aligned} \tag{3.129}$$

where the resummed two-jet distribution matched to QCD, $\mathrm{d}\sigma^{\mathrm{PT}}/\mathrm{d}\tau_a|_{\mathrm{NLL/NLO}}$, is given in Eq. (3.105) and U_a^{σ} is given in Eq. (3.96).

5.4 Numerical results for the soft function

By plugging the partonic soft function Eq. (3.42) into the model Eq. (3.127), we obtain for the full convoluted model soft function to $\mathcal{O}(\alpha_s)$,

$$\begin{aligned} S_a(\tau_a;\mu) = & \left\{1 - \frac{\alpha_s C_F}{2\pi}\frac{1}{1-a}\left[\ln^2\left(\frac{\mu^2}{Q^2(\tau_a^{\Delta})^2}\right) - \frac{\pi^2}{6}\right]\right\} f_a^{\exp}\left(\tau_a^{\Delta}\right) - \frac{2\delta_1^a(\mu)}{Q}\frac{\mathrm{d}}{\mathrm{d}\tau_a} f^{\exp}(\tau_a^{\Delta}) \\ & + \frac{2\alpha_s C_F}{\pi}\frac{1}{1-a}\int_0^{\tau_a^{\Delta}} \mathrm{d}\tau' \frac{1}{\tau'}\ln\left(\frac{\mu^2}{Q^2\tau'^2}\right)\left[f_a^{\exp}\left(\tau_a^{\Delta}-\tau'\right) - f_a^{\exp}\left(\tau_a^{\Delta}\right)\right], \end{aligned} \tag{3.130}$$

where $\tau_a^\Delta \equiv \tau_a - 2\bar{\Delta}_a(\mu)/Q$. To integrate against the plus distributions in Eq. (3.42), we used the prescription

$$\int_0^a \mathrm{d}x \left[\frac{\theta(x)}{x}\right]_+ f(x) = \int_0^a \mathrm{d}x \frac{\theta(x)}{x}[f(x) - f(0)] + f(0)\ln a \tag{3.131a}$$

$$\int_0^a \mathrm{d}x \left[\frac{\theta(x)\ln x}{x}\right]_+ f(x) = \int_0^a \mathrm{d}x \frac{\theta(x)\ln x}{x}[f(x) - f(0)] + \frac{1}{2}f(0)\ln^2 a\,, \tag{3.131b}$$

which correspond to the definition of plus-functions given in Eq. (3.40). To minimize the logarithms in the peak region of the soft function while also avoiding the Landau pole in α_s, it is natural to choose the scale to be of order $\mu \gtrsim \Lambda_{\mathrm{QCD}}$. To minimize the logarithms for larger values of τ_a, it is natural to choose $\mu \sim Q\tau_a$. A scale choice that interpolates between these two regions is

$$\mu = \sqrt{\theta(Q\tau_a - \mu_S^{\min})(Q\tau_a - \mu_S^{\min})^2 + (\mu_S^{\min})^2}\,, \tag{3.132}$$

where the minimum scale is $\mu_S^{\min} \gtrsim \Lambda_{\mathrm{QCD}}$.

In Fig. 3.6, we plot $S_a(\tau_a;\mu)$ for six values of a between -2 and $1/2$. In each plot, we show the tree-level (LO) soft function with a gap parameter (solid gray), the one-loop (NLO) soft function with a gap parameter but without renormalon subtraction (dashed green), and the one-loop soft function with a gap and renormalon subtraction (solid blue). For the parameters in the model function Eq. (3.112) we take $A = 2.5, B = -0.4, \Lambda = 0.55$ GeV, as extracted from a fit to the jet mass distribution [149]. For the scale dependence of the gap parameter, we choose $\bar{\Delta}_0(1\text{ GeV}) = 100$ MeV and use Eq. (3.125) to evolve to other scales. We choose $R = 200$ MeV in the renormalon subtraction Eq. (3.122) and the minimum value of the scale in Eq. (3.132) to be $\mu_S^{\min} = 1$ GeV. We illustrate the variation of $S_a(\tau_a;\mu)$ with the scale μ by varying it between 0.8 and 1.2 times the formula in Eq. (3.132). The tree-level soft functions depend on μ only through the gap parameter $\bar{\Delta}_a(\mu)$ and thus artificially have smaller scale variation than the one-loop soft functions, at which order the nontrivial μ dependence is first probed.

The one-loop soft functions in Fig. 3.6 display unphysical behavior near $\tau_a = 0$ by taking negative values, due to the renormalon ambiguity in the perturbative series for the partonic soft function. By cancelling the renormalon ambiguity between the partonic soft function and the nonperturbative gap parameter Δ_a through Eq. (3.127), we obtain the renormalon-free one-loop soft functions. One of the plots of the soft function for $a = 1/2$ still exhibits a small negative dip after renormalon subtraction, but it is nevertheless much smaller than the original negative dip, and from its size may be expected to an effect of higher-order power corrections. The dip does not appear in the total cross-section calculated below in Sec. 6.

6 Numerical Results for the Full Distribution

In this section we plot the angularity distributions $\mathrm{d}\sigma/\mathrm{d}\tau_a$ which include LO and NLO perturbative hard, jet, and soft function contributions, resummation of large logarithmic terms to NLL accuracy, matching to QCD at $\mathcal{O}(\alpha_s)$, and the effects of the nonperturbative gapped soft functions.

In Fig. 3.7 we plot the angularity distributions given by Eq. (3.129), plugging in the NLL resummed partonic distribution given by Eq. (3.95) and matched according to Eq. (3.105). We

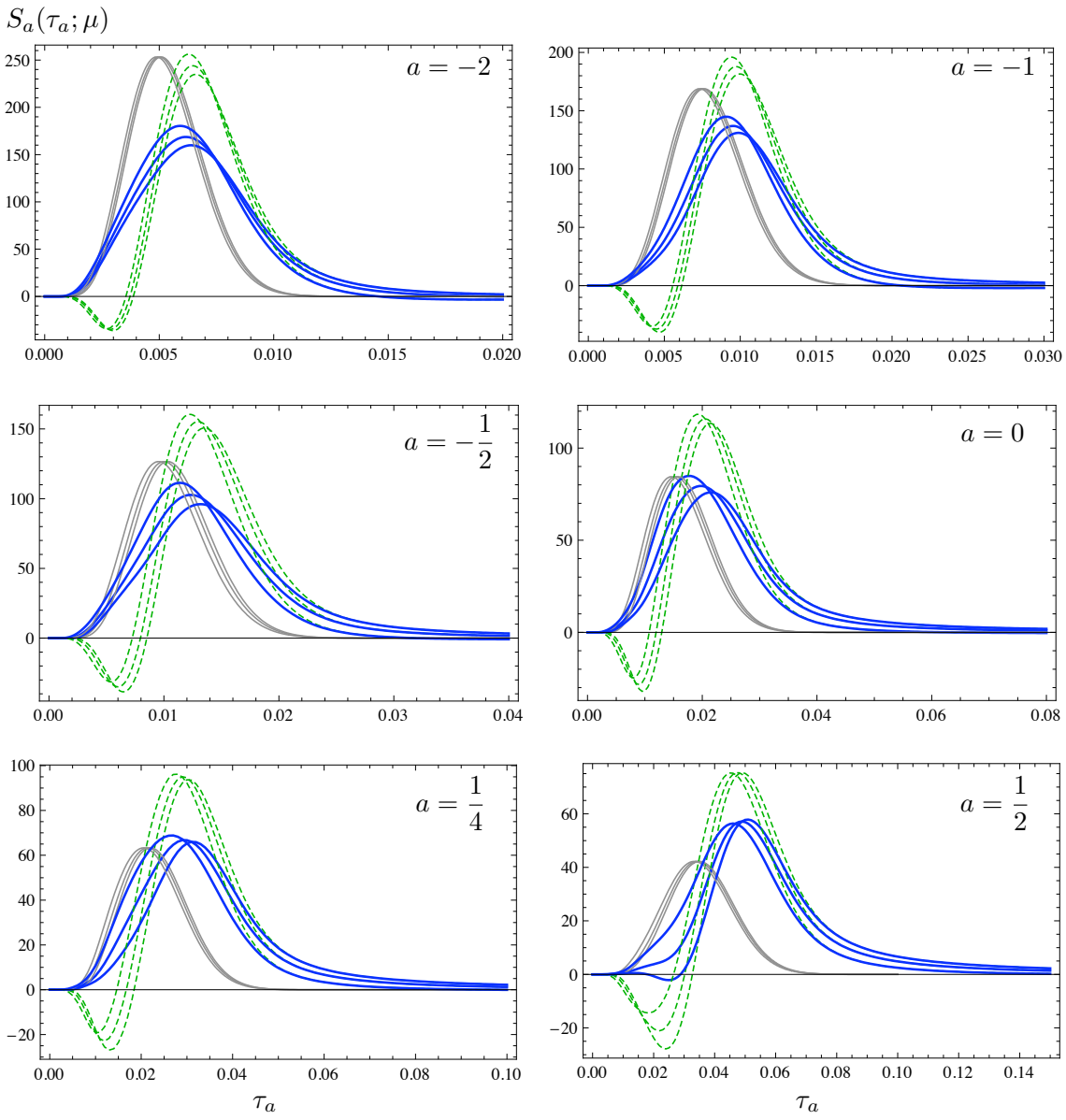

Figure 3.6: Angularity soft functions with a gap parameter, at tree-level (solid gray) and at one-loop with (solid blue) and without (dashed green) renormalon subtraction, for $Q = 100$ GeV, for several values of a as labeled on each plot. The variation of the soft functions with the scale μ is illustrated by first setting $\mu_S^{\min} = 1.0$ GeV in Eq. (3.132) and choosing μ to be $(0.8, 1, 1.2)$ times the formula in Eq. (3.132), with the plots for smaller values of μ_S peaking earlier in τ_a. For the model parameters we take $A = 2.5, B = -0.4, \Lambda = 0.55$ GeV. In the renormalon subtraction Eq. (3.122), we have chosen $R = 200$ MeV.

keep the same soft model function parameters as in the previous section. As noted earlier, the logarithms in the hard, jet, and soft functions are minimized by choosing $\mu_H = Q$, $\mu_J \sim Q\tau_a^{1/(2-a)}$, and $\mu_S \sim Q\tau_a$. In order to avoid the Landau pole in α_s as $\tau_a \to 0$, we choose the scales as in Eq. (3.132) ,

$$\mu_S = \sqrt{\theta(Q\tau_a - \mu_S^{\min})(Q\tau_a - \mu_S^{\min})^2 + (\mu_S^{\min})^2} \tag{3.133a}$$

$$\mu_J = \sqrt{\theta(Q\tau_a^{1/(2-a)} - \mu_J^{\min})(Q\tau_a^{1/(2-a)} - \mu_J^{\min})^2 + (\mu_J^{\min})^2}\,. \tag{3.133b}$$

We may vary $\mu_{S,J}^{\min}$ independently, or choose them in a correlated fashion suggested by their natural scaling $\mu_S \sim Q\lambda, \mu_J \sim Q\lambda^{1/(2-a)}$, that is,

$$\mu_J^{\min} = Q^{(1-a)/(2-a)}(\mu_S^{\min})^{1/(2-a)}\,. \tag{3.134}$$

In Fig. 3.7 we have done the latter. The NLL/NLO distributions exhibit negative values for small τ_a as a result of the renormalon ambiguity. Performing the renormalon subtraction in the soft function removes this pathology.

In Fig. 3.8 we plot angularity distributions for the values of a used in Fig. 3.7 on the same figure to illustrate clearly how they change with a. The range of τ_a populated by two-jet-like events grows with increasing a, so that the peak regions are populated by jets of increasing narrowness with increasing a. This is reflected in the scales $\mu_{J,S}$ in Eq. (3.133) drawing closer as a grows to 1.

In Fig. 3.9 we vary the hard, jet, and soft scales and plot the resulting variation of our final predictions for the distributions. First we vary the hard scale μ_H between $Q/2$ and $2Q$, plotting the result in the dark green band. Then we vary the collinear and soft scales $\mu_{J,S}$ between half and twice the values we chose in Eq. (3.133) and plot the result in the light blue band.

Although published data on e^+e^- angularity distributions for $a \neq 0$ are not yet available, data for the $a = 0$ (thrust) distribution are of course plentiful. The remaining difference between our prediction in Fig. 3.7 and existing measurements of the $a = 0$ distribution can be accounted for by higher-order perturbative corrections (see, for example, Fig. 6 in Ref. [41]), which are known but have not been included here, since we calculated the other angularity distributions only to NLL/NLO. For a sufficiently smaller than 1, we expect our predictions of all angularity distributions to agree with data to the same accuracy that the NLL/NLO $a = 0$ prediction agrees with the thrust data.

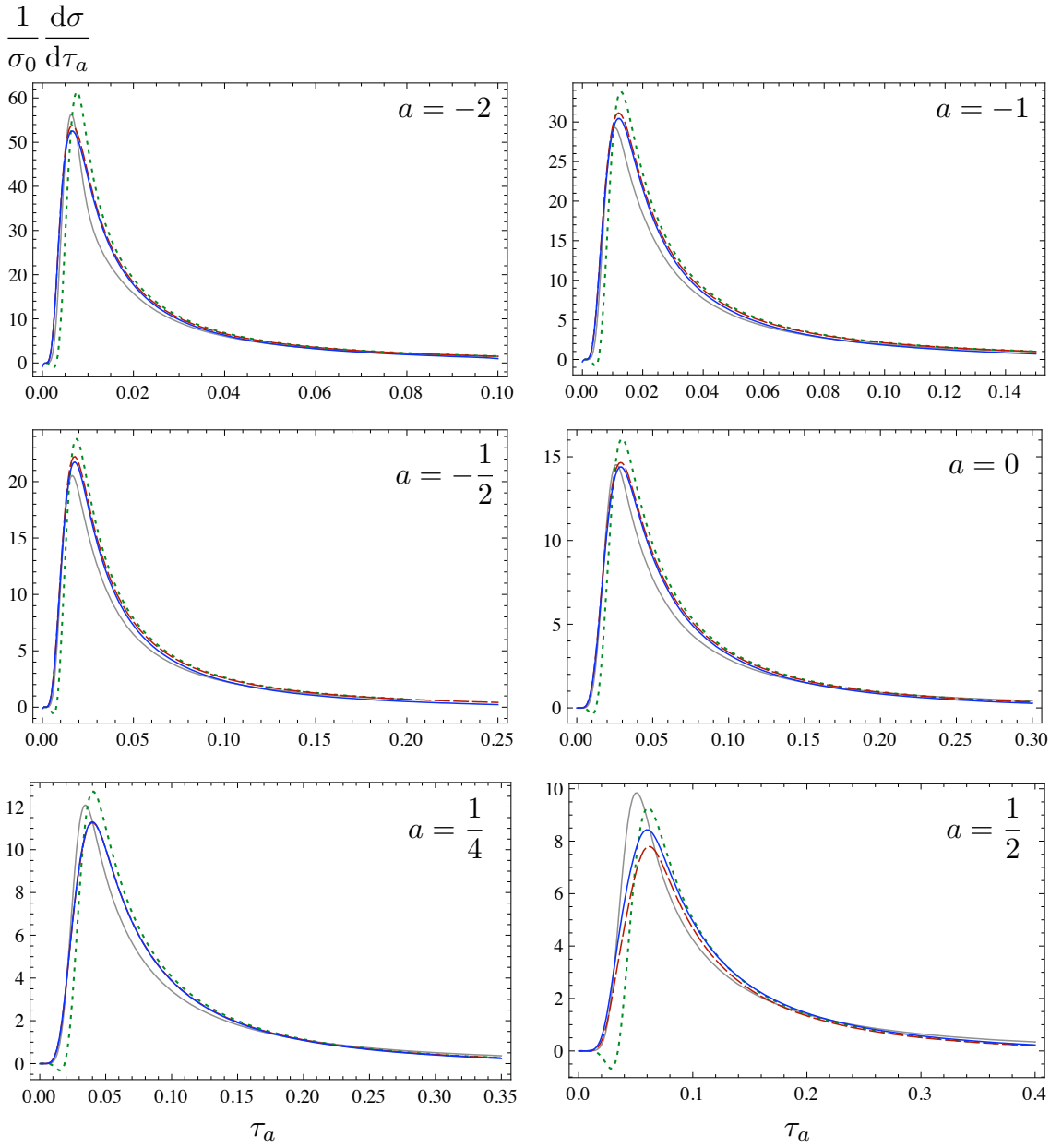

Figure 3.7: Angularity distributions at $Q = 100$ GeV for six values of a between -2 and $1/2$. The solid gray curves are the LO partonic distributions resummed to NLL and convoluted with the gapped soft model function. The dotted green curves are NLL/NLO convoluted with the gapped soft function but without renormalon subtraction. The dashed red curves are the same as the green but with renormalon subtraction, and the solid blue curves are the same as the red but matched to fixed-order QCD at $\mathcal{O}(\alpha_s)$. We choose the scales $\mu = Q, \mu_S^{\min} = 1$ GeV, and $\mu_J^{\min}$ given by Eq. (3.134). For the gap parameter we take $\bar{\Delta}_0(1\text{ GeV}) = 100$ MeV and in the renormalon subtraction $R = 200$ MeV.

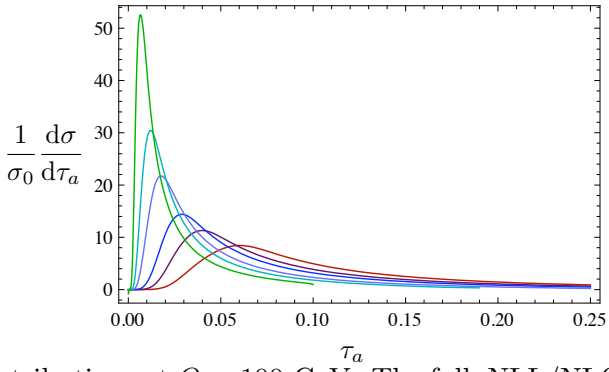

Figure 3.8: Angularity distributions at $Q = 100$ GeV. The full, NLL/NLO resummed, renormalon-subtracted distributions in Fig. 3.7 are here shown all on the same scale. The parameters are chosen the same as in Fig. 3.7. From highest to lowest peak value, the curves are for $a = -2, -1, -\frac{1}{2}, 0, \frac{1}{4}, \frac{1}{2}$.

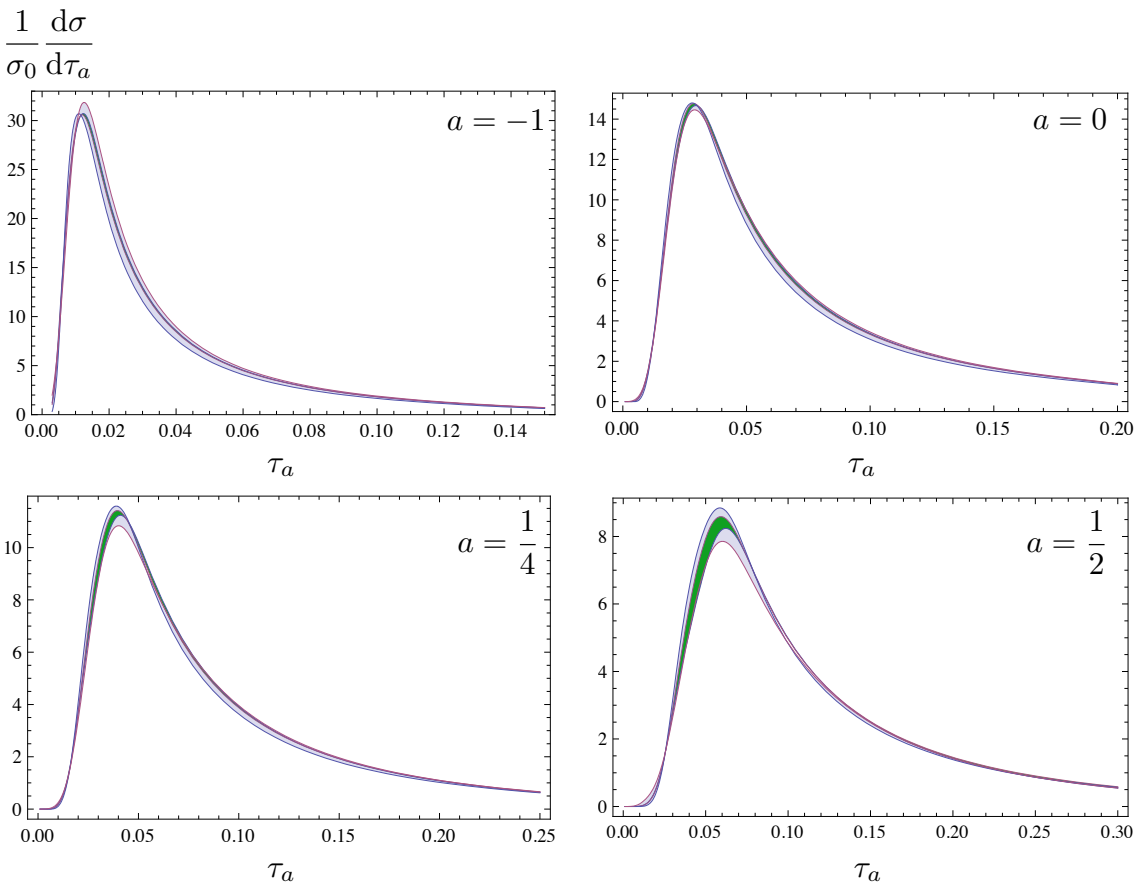

Figure 3.9: Hard scale variation (dark green band) and correlated jet and soft scale variation (light blue band) of the NLL/NLO resummed, renormalon-subtracted angularity distributions at $Q = 100$ GeV for $a = -1$, $a = 0$, $a = 1/4$, and $a = 1/2$. For the hard scale variation, μ_H varied between $Q/2$ and $2Q$ and for the correlated scale variation, μ_J and μ_S are varied between half the values given in Eq. (3.133) and twice these values.

7 Comparison to Previous Results and Classic Resummation

To compare to previous predictions of angularity distributions [47, 49] and focus more generally on the differences between SCET and alternative approaches to factorization and resummation, in this section we restrict our attention to the perturbative distribution both before matching, Eq. (3.95), and after matching, Eq. (3.105), leaving out the nonperturbative model of Sec. 5.

Our result for the unmatched NLL resummed distribution Eq. (3.95) involves an evolution factor U_a^σ, which resums all leading and next-to-leading logarithms (for example the $(1/\tau_a)\ln\tau_a$ and $1/\tau_a$ terms in the fixed-order $D_a(\tau)$ of Eq. (3.103)), and a multiplicative NLO prefactor $1 + f_H + 2f_J + f_S = 1 + \mathcal{O}(\alpha_s)$. Both the evolution factor and the NLO prefactor are sensitive to physics at the three distinct scales μ_H, μ_J, and μ_S. Keeping these scales arbitrary until after solving the RG equations in Sec. 4 and retaining the freedom to choose them only at the end provides a flexibility which is indispensable in achieving reliable predictions in the SCET approach. This approach has significant advantages over what we refer to as the classic approach to resummation in QCD [73].

To illustrate these advantages, we compare our results for angularity distributions to those obtained in full QCD [47, 49]. The analysis in Ref. [47] used a formalism of factorization and resummation of logarithms through renormalization-group evolution paralleling that of SCET, in principle containing all the advantages that we emphasize here, but which were not fully realized. Before arriving at the explicit prediction for the NLL resummed distribution $\mathrm{d}\sigma/\mathrm{d}\tau_a$ given in Ref. [49], the factorized result of Ref. [47] was first converted into the form of a resummed event shape distribution that would be obtained using the classic approach (and has been for $a = 0$).

One major advantage of the SCET approach over the classic approach is the presence of Landau pole singularities in the results of the classic approach that are not in the results from SCET, as also found in the cases of DIS and Drell-Yan [160, 36, 39]. We can illustrate why SCET avoids this for the case of angularities by returning to our results for the resummed jet and soft functions and for the final resummed distribution. From the expressions for the resummed soft function $S_a(\tau_a^s)$, Eq. (3.93), and for the resummed jet function $J_a^n(\tau_a^n)$, Eq. (3.94), one might be tempted to set $\mu_S = Q\tau_a^s$ and $\mu_J = Q(\tau_a^n)^{1/(2-a)}$, since the logarithms in Eqs. (3.93) and (3.94) are minimized for these choices. The problem with this choice is that the soft and jet functions still enter the convolution in the factorization theorem Eq. (3.1) and thus the scales in $\alpha_s(\mu_{J/S})$ run below $\tau_a^{n,s} = \Lambda_{\mathrm{QCD}}/Q$ even for $\tau_a > \Lambda_{\mathrm{QCD}}/Q$ (where $\tau_a = \tau_a^n + \tau_a^{\bar{n}} + \tau_a^s$) if these $\tau_a^{n,s}$ dependent scales are chosen. However, for a τ_a^s-independent choice of μ_S in the case of the soft function, for instance, the full functional dependence of the resummed $S(\tau_a^s;\mu)$ on τ_a^s and μ_S is such that after the integrals over τ_a^s, τ_a^n, and $\tau_a^{\bar{n}}$ needed to get to the final resummed distribution, Eq. (3.95), are performed, the resulting dependence on μ_S only comes in the combination $\mu_S/Q\tau_a$ in logarithms (and similarly for the jet functions). The proper choice is thus $\mu_S \sim Q\tau_a$ (and $\mu_J \sim Q\tau_a^{1/(2-a)}$) and not $\mu_S \sim Q\tau_a^s$. With this choice, Landau pole singularites never affect our result for $\tau_a > \Lambda_{\mathrm{QCD}}/Q$. Setting $\mu_S = Q\tau_a^s$ before doing the convolution Eq. (3.1) is equivalent to setting $\mu_S = Q/\nu$ in the Laplace transform with respect to ν of the distribution, which is the scale choice made in Ref. [47] needed to reproduce the classic result for $a = 0$. Thus, when transforming back to get $\mathrm{d}\sigma/\mathrm{d}\tau_a$, one inevitably runs into spurious Landau pole singularities with this scale choice[10], confirming the

[10] There are also inherent Landau pole singularities in the classic approach before transforming back to τ_a-space and thus not associated with making ν-dependent scale choices for $\mu_{J,S}$. In the classic approach, a prescription to avoid

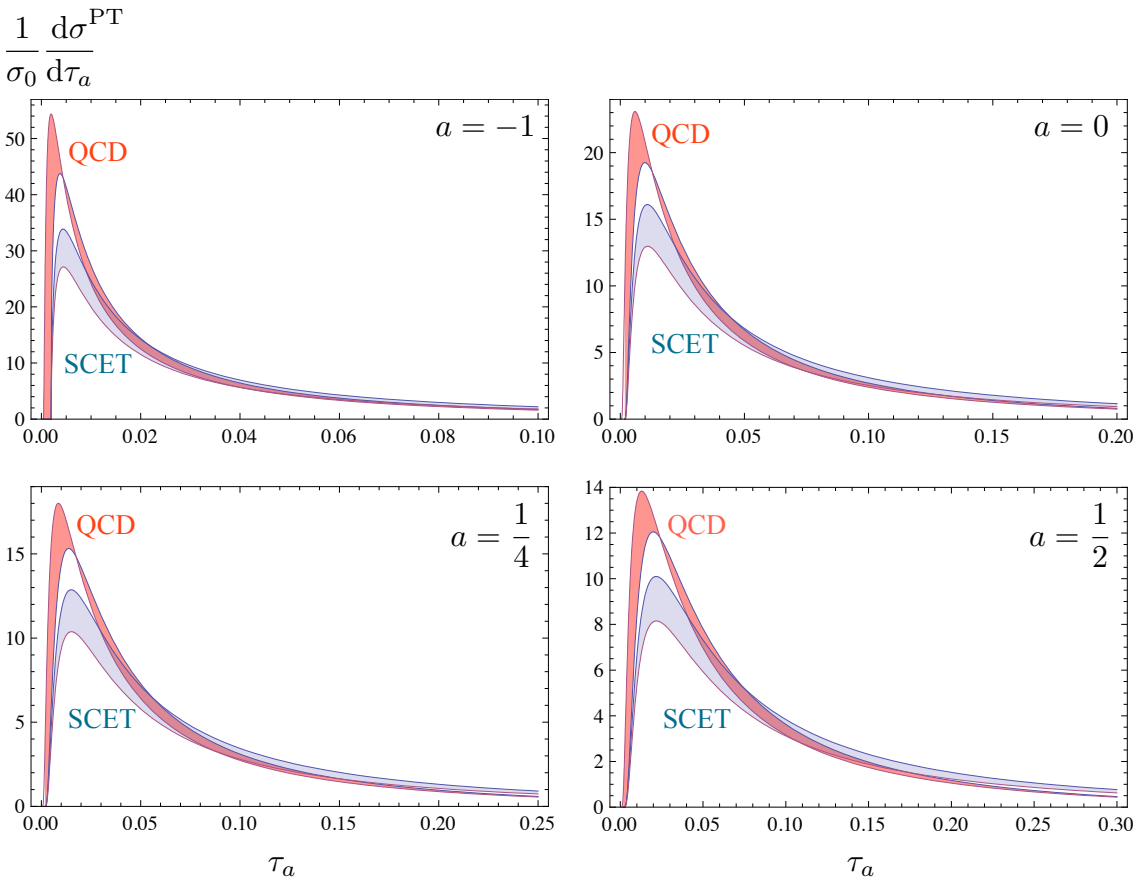

Figure 3.10: Factorization scale μ variation of the (unmatched, partonic) SCET NLL/LO (light blue band) and the classic QCD NLL/LO (red band) resummed results for angularity distributions. μ is varied over the range $\frac{Q}{2} \leq \mu \leq 2Q$ with $Q = 100$ GeV for the cases $a = -1$, $a = 0$, $a = 1/4$, and $a = 1/2$. To make a direct comparison to the QCD results, the scales in the SCET results have been chosen as $\mu = \mu_H = Q$, $\mu_J = Q\tau_a^{1/(2-a)}$, and $\mu_S = Q\tau_a$.

similar observation of [39].

Another difference between the explicit results we give and those given in [47] is that while both achieved resummation of logarithms to NLL accuracy, the latter does not include a full NLO calculation of the jet and soft functions in the distribution $\mathrm{d}\sigma/\mathrm{d}\tau_a$, that is, effectively does not have the prefactors $f_{H,J,S}$. As with our SCET results, the results of [47] are not as accurate as fixed-order QCD in the large-τ_a region and need to be matched. This matching was subsequently performed numerically to at $\mathcal{O}(\alpha_s^2)$ in Ref. [49]. We summarize this by saying that we have resummed logarithms of τ_a to NLL/NLO with $\mathcal{O}(\alpha_s)$ matching and Ref. [49] has resummed to NLL/LO with $\mathcal{O}(\alpha_s^2)$ matching.

The explicit dependence of the NLO prefactor on the separate scales $\mu_{H,J,S}$ makes it distinct from what is obtained by NLO matching to QCD in the large-τ_a region where the three

both types of Landau pole singularities is employed, but at the expense of introducing unphysical power corrections [73, 79]. The results of [49] plotted in Fig. 3.10 used the prescription of [73].

scales are comparable. Specifically, it improves the accuracy in the smaller-τ_a region where the distribution depends on physics at the three widely disparate scales separately, as revealed by the factorization theorem. We emphasize that even though the effects of including this NLO piece are formally of next-to-next-to-leading logarithmic (NNLL) accuracy (using the counting $\alpha_s \ln \tau_a \sim \mathcal{O}(1)$), it *is* natural to include it in our NLL resummed result since the dependence on the arbitrary scales $\mu_{H,J,S}$ is cancelled to order α_s in our NLL/NLO calculation.[11]

Finally, we point out that while SCET can incorporate $\mathcal{O}(\alpha_s^2)$ matching with, for example, a $\mathcal{O}(\alpha_s^2)$ QCD calculation or an event generator, the classic approach by itself is less easily generalized to achieve full NLL/NLO accuracy. The reason for this difference is that SCET predicts the evolution boundary conditions for the hard, jet, and soft functions, $H(Q;\mu_H)$ and $F(\tau_a;\mu_F)$ ($F = J, S$) in Eq. (3.88), for arbitrary scales $\mu_{H,J,S}$ order by order in perturbation theory. On the other hand, as discussed in Ref. [172], the classic approach in contrast must effectively use the evolution boundary conditions $F(\tau_a;\mu_0) = \delta(\tau_a)$, which are LO in the SCET point of view. An implication of this difference is that, since our NLO prefactor is formally part of the NNLL series, full NNLL resummation is a nontrivial task in the classic approach (e.g. [54, 100]) whereas it is straightforward in SCET, using no new techniques additional to the ones described above.

In Fig. 3.10, we compare our result with the classic result obtained in [47]. To make this comparison, we truncate our result to NLL/LO accuracy and make the scale choices that are equivalent to those that were made in Ref. [47] for the purpose of arriving at the classic resummed form. Namely, we run the jet and soft functions from their respective natural scales, $\mu_J = Q\tau_a^{1/(2-a)}$ and $\mu_S = Q\tau_a$, to the hard scale set to $\mu_H = Q$. In addition, in Ref. [47] the factorization scale μ was also chosen to be $\mu = \mu_H$, effectively turning off running between μ_H and μ. Thus, to make a genuine comparison, we vary μ both in the classic result given in [49] and in our result Eq. (3.95) over the range $Q/2$ to $2Q$, fixing $\mu_H = \mu$ in our result. Notice from the plots that the peak position appears to be more stable in the SCET results relative to the classic results and that there is a discrepancy in the overall normalization in the peak region, both of which may be attributed to power corrections arising from the spurious Landau poles present in the classic result.

8 Conclusions

We have calculated angularity distributions in e^+e^- collisions for $a < 1$ to $\mathcal{O}(\alpha_s)$ in fixed-order accuracy, resummed leading and next-to-leading large logarithms in the perturbative series, incorporated the effects of a nonperturbative model for the soft function with a gap parameter, and cancelled the leading renormalon ambiguities in the perturbative expansion of the distribution and the gap parameter. Our new results for the one-loop jet and soft functions for all $a < 1$ and the NLL resummation of logarithms of τ_a with explicit analytical dependence on the scales $\mu_{H,J,S}$ made possible what we believe are the most precise predictions of angularity distributions to date.

These predictions, especially after extension to higher orders in perturbation theory and resummation of logarithms, can prove useful in improving extraction of the strong coupling α_s or the parameters of nonperturbative models for the soft function. At the present time, in the absence

[11] More generally, in an $\mathrm{N}^n\mathrm{LL}/\mathrm{N}^m\mathrm{LO}$ calculation, the dependence on $\mu_{H,J,S}$ cancels up to order $\alpha_s^{\min\{n,m\}}$, as the $\mu_{H,J,S}$ derivative of the logarithm of the distribution receives contributions from the prefactor at order α_s^m and from the anomalous dimension at order α_s^n.

of a new linear collider, such extractions would require the re-analysis of LEP data to extract the angularity distributions.

We also gain insight into the steps that will be required to predict jet observables in hadronic collisions, a broad range of which have been studied in [13, 12] using the classic approach. An SCET-based framework to factorize jet observables in this environment was developed in [23]. Our analysis of angularities suggests that the study of any set of jet observables which vary in their sensitivity to narrower or wider jets or which depend on a jet algorithm picking out narrower or wider jets should be scrutinized in the same way as we did for angularities to determine whether the contributions of collinear and soft modes to each observable can be clearly separated. Also, our calculations of light quark angularity distributions in e^+e^- collisions can be extended to calculating individual jet shapes for jets of various origins to higher accuracy, contributing to strategies to use such jet shapes to distinguish experimentally different types of jets [4, 3].

While we have used SCET to calculate and explore the behavior of angularity distributions, the variation in behavior of the angularities has in turn shed light on the behavior and applicability of the effective theory. Varying a essentially varies the collinear scale of SCET, in effect interpolating between (and extrapolating beyond) SCET_I and SCET_II , and so angularities provide an ideal testing ground for the behavior of these effective theories.

It is natural and straightforward to consider further improvement of our predictions to higher perturbative accuracy and reduced nonperturbative uncertainty. We believe by using the cut diagram methods described above to obtain the angularity distributions to $\mathcal{O}(\alpha_s)$ we can extend our results to $\mathcal{O}(\alpha_s^2)$ in a straightforward manner. Also, all of the ingredients necessary for NNLL resummation at $a = 0$ are already known [41], and we would only need to calculate those pieces which change with a. The three-loop $\Gamma_{J,S}$ part of the jet and soft anomalous dimensions for arbitrary a can be obtained from known three-loop Γ_cusp [39] and the all-orders proportionality $\Gamma_{J,S} \propto \Gamma_\text{cusp}$ which we verified in Appendix 3.A. The only unknown ingredients are the two-loop non-cusp part of the jet and soft anomalous dimensions. These can be obtained solely from the UV divergences of the two-loop graphs, and would immediately extend our results to NNLL accuracy. As for nonperturbative effects in the angularity distributions, we have treated these effects in the soft function in the simplest manner possible, adapting the $a = 0$ soft model function to all a by rescaling its first moment. Comparison of these predictions to e^+e^- data can shed light on the reliability of this choice.

Angularities and other event shapes have proven to be powerful probes of QCD and its effective theories, and promise to play a key role in the new era of collider physics searching for signals of new physics amid a sea of jets and strong interactions.

3.A Relation Among Hard, Jet, Soft, and Cusp Anomalous Dimensions

In Eq. (3.92) we used that the $\Gamma_F[\alpha_s]$ part of the jet or soft function anomalous dimension, defined in Eq. (3.85), is proportional to the cusp anomalous dimension Γ_cusp to all orders in α_s. This fact is well known for the standard $a = 0$ jet function and soft functions. In this section we verify that this relation remains true for all a. Our strategy will be to show that $\Gamma_{J,S}[\alpha_s]$ must always remain proportional to $\Gamma_H[\alpha_s]$, which is independent of a and is already known to be proportional to Γ_cusp.

The consistency of the factorization theorem Eq. (3.18) requires a relation among the hard, jet, and soft function renormalization counterterms, and, thus, among the anomalous dimensions (see, e.g., [47, 125]). This relation can be derived by requiring that Eq. (3.18) remain true when written in terms of either the bare or renormalized hard, jet, and soft functions on the right-hand side. This requires that

$$Z_H^{-1}(\mu)\delta(\tau_J - \tau_S) = \int \mathrm{d}\tau' \int \mathrm{d}\tau'' Z_J(\tau_J - \tau'; \mu) Z_J(\tau' - \tau''; \mu) Z_S(\tau'' - \tau_S; \mu)\,, \tag{3.135}$$

to all orders in α_s. To $\mathcal{O}(\alpha_s)$, we can easily verify this relation using Eqs. (3.31), (3.43), and (3.64) with $Z_H(\mu) = |Z_{\mathcal{O}}(\mu)|^{-2}$. This relation amongst the counterterms requires in turn that the anomalous dimensions satisfy

$$-\gamma_H(\mu)\delta(\tau) = 2\gamma_J(\tau;\mu) + \gamma_S(\tau;\mu)\,. \tag{3.136}$$

To all orders in α_s the hard anomalous dimension takes the form of Eq. (3.72) and the jet and soft anomalous dimensions take the general form of Eq. (3.85) [129] , where the constant j_F is $j_J = 1/(2-a)$ for the jet function and $j_S = 1$ for the soft function. The constraint Eq. (3.136) then requires the three independent relations

$$0 = \frac{4}{j_J}\Gamma_J[\alpha_s] + \frac{2}{j_S}\Gamma_S[\alpha_s]\,, \tag{3.137}$$

$$-\Gamma_H[\alpha_s] = 2\Gamma_J[\alpha_s] + \Gamma_S[\alpha_s]\,, \tag{3.138}$$

$$-\gamma_H[\alpha_s] = 2\gamma_J[\alpha_s] + \gamma_S[\alpha_s]\,, \tag{3.139}$$

to all orders in α_s. These relations can be verified to $\mathcal{O}(\alpha_s)$ from Eq. (3.71) and Table 3.1. The first two relations Eqs. (3.137) and (3.138) taken together imply that

$$\Gamma_S[\alpha_s] = \frac{1}{1-a}\Gamma_H[\alpha_s]\,, \qquad \Gamma_J[\alpha_s] = -\frac{1-a/2}{1-a}\Gamma_H[\alpha_s]\,, \tag{3.140}$$

to all orders in α_s and for all $a < 1$. Since $\Gamma_H[\alpha_s] \propto \Gamma_{\mathrm{cusp}}$ and is independent of a, both $\Gamma_{S,J}[\alpha_s] \propto \Gamma_{\mathrm{cusp}}$ as well.

3.B Evaluation of Resummed Jet and Soft Functions and Full Distribution

To evaluate the resummed jet and soft functions, we used the following method. First, note that from the expressions for the evolution equation, Eq. (3.88), the form of the evolution kernel, Eq. (3.89), and the generic form of the NLO jet and soft functions,

$$F(\tau;\mu_0) = c_1\delta(\tau) + c_2\left(\frac{1}{\tau}\right)_+ + c_3\left(\frac{\ln\tau}{\tau}\right)_+\,, \tag{3.141}$$

the resummed jet and soft functions are proportional to

$$F(\tau;\mu) \propto \int \mathrm{d}\tau' \left[\frac{\theta(\tau-\tau')}{(\tau-\tau')^{1+\omega}}\right]_+ F(\tau';\mu_0) = c_1 W_1 + c_2 W_2 + c_3 W_3\,, \tag{3.142}$$

where

$$W_1 = \int \mathrm{d}\tau' \left[\frac{\theta(\tau-\tau')}{(\tau-\tau')^{1+\omega}}\right]_+ \delta(\tau')\,,$$
$$W_2 = \int \mathrm{d}\tau' \left[\frac{\theta(\tau-\tau')}{(\tau-\tau')^{1+\omega}}\right]_+ \left[\frac{\theta(\tau')}{\tau'}\right]_+\,,$$
$$W_3 = \int \mathrm{d}\tau' \left[\frac{\theta(\tau-\tau')}{(\tau-\tau')^{1+\omega}}\right]_+ \left[\frac{\theta(\tau')\ln(\tau')}{\tau'}\right]_+\,. \tag{3.143}$$

Next, note that from the definitions of the plus functions, Eqs. (3.40) and (3.91), we can find W_i as the coefficient of δ^i in the Taylor series of $W(\delta)$, where $W(\delta)$ is defined as

$$W(\delta) \equiv \int \mathrm{d}\tau' \left[\frac{\theta(\tau-\tau')}{(\tau-\tau')^{1+\omega}}\right]_+ \left[\frac{\theta(\tau')}{\tau'^{1+\delta}}\right]_+ = \frac{\Gamma(-\omega)\Gamma(-\delta)}{\Gamma(-\omega-\delta)} \left[\frac{\theta(\tau)}{\tau^{1+\omega+\delta}}\right]_+\,. \tag{3.144}$$

Eq. (3.144) follows from the fact that

$$\int \mathrm{d}\tau'' \left[\frac{\theta(\tau-\tau'')}{(\tau-\tau'')^{1+\omega_1}}\right]_+ \left[\frac{\theta(\tau''-\tau')}{(\tau''-\tau')^{1+\omega_2}}\right]_+ = \frac{\Gamma(-\omega_1)\Gamma(-\omega_2)}{\Gamma(-\omega_1-\omega_2)} \left[\frac{\theta(\tau-\tau')}{(\tau-\tau')^{1+\omega_1+\omega_2}}\right]_+\,. \tag{3.145}$$

By expanding both sides of Eq. (3.144) in δ and comparing like powers of δ, we find that

$$W_1 = \left[\frac{\theta(\tau)}{\tau^{1+\omega}}\right]_+\,, \qquad W_2 = \left[\Big(\ln(\tau) - H(-1-\omega)\Big)\left(\frac{\theta(\tau)}{\tau^{1+\omega}}\right)\right]_+\,,$$
$$W_3 = \left[\left(\frac{1}{2}\ln^2(\tau) - \ln(\tau)H(-1-\omega) + \frac{\pi^2}{12} + \frac{1}{2}H(-1-\omega)^2 - \frac{1}{2}\psi^{(1)}(-\omega)\right)\left(\frac{\theta(\tau)}{\tau^{1+\omega}}\right)\right]_+\,. \tag{3.146}$$

Here, $H(z)$ is the harmonic number function and $\psi^{(\nu)}(z)$ is the polygamma function.

The same technique can be used to analytically calculate the fully resummed cross-section, Eq. (3.18), directly from the unresummed jet and soft functions. The resummed cross-section is of the form

$$\frac{1}{\sigma_0}\frac{\mathrm{d}\sigma}{\mathrm{d}\tau}^{\mathrm{PT}} \propto \prod_{i=1}^{3}\left(\int \mathrm{d}\tau_i\, \mathrm{d}\tau_i'\, F_i(\tau_i';\mu_i) \left[\frac{\theta(\tau_i-\tau_i')}{(\tau_i-\tau_i')^{1+\omega_i}}\right]_+\right) \delta(\tau-\tau_1-\tau_2-\tau_3)\,. \tag{3.147}$$

where the jet and soft functions $F_i(\tau_i,\mu_i)$ are all of the form given in Eq. (3.141). These integrals can be done most easily by replacing the $F_i(\tau_i;\mu_i)$ on the right hand side of Eq. (3.147) with $\left[\theta(\tau)/\tau^{1+\delta_i}\right]_+$, expanding in δ_i before and after combining all the plus distributions using Eq. (3.145), and comparing like powers of the δ_i. The result for the resummed cross-section Eq. (3.95) then follows.

3.C Angularity Distribution in QCD to $\mathcal{O}(\alpha_s)$

In Sec. 6 we matched the NLL resummed two-jet angularity distributions in SCET onto the $\mathcal{O}(\alpha_s)$ fixed-order distributions in full QCD using the remainder function $r_a(\tau_a)$, defined in Eq. (3.104). In this section we provide some details of how we calculate the QCD contribution to $r_a(\tau_a)$ away from $\tau_a = 0$, $A_a(\tau_a)$. In the process, we show that for $a \lesssim -1.9$ the angularities of events with more two-jet like kinematics become degenerate with those of more three-jet like events and contribute to the same τ_a, and that for $a \lesssim -2.6$ the maximally symmetric three-jet event contributes to a smaller τ_a then some more two-jet like events. Thus, for small enough a, angularities fail to separate two-jet and three-jet like events.

Both the one loop $q\bar{q}$ and tree-level $q\bar{q}g$ final states contribute to $\mathrm{d}\sigma/\mathrm{d}\tau_a$ at $\mathcal{O}(\alpha_s)$. However, the $q\bar{q}$ final states' contribution is proportional to $\delta(\tau_a)$ and hence only contributes to A_a^δ. Thus to find $A_a(\tau_a)$ we only need to consider the tree-level $q\bar{q}g$ final states. Their contribution can be writtten as

$$\frac{1}{\sigma_0}\frac{\mathrm{d}\sigma}{\mathrm{d}\tau_a}^{q\bar{q}g} = \left(\frac{\alpha_s}{2\pi}\right) A_a(\tau_a)\,, \tag{3.148}$$

where

$$A_a(\tau_a) = C_F \int \mathrm{d}x_1\,\mathrm{d}x_2\,\frac{x_1^2+x_2^2}{(1-x_1)(1-x_2)}\delta\big(\tau_a - \tau_a(x_1,x_2)\big)\,, \tag{3.149}$$

and where $x_{1,2} \equiv 2E_{1,2}/Q$ are the energy fractions of any two of the three final-state partons. By momentum conservation, $x_1 + x_2 + x_3 = 2$. For a three-particle final state, the thrust axis is given by the direction of the particle with the largest energy. The $x_{1,2}$ phase space can be divided into three regions, as illustrated in Fig. 3.11A, according to which parton has the largest energy. In the region in which x_i is larger than $x_{j,k}$, the angularity $\tau_a(x_1,x_2)$ is given by

$$\tau_a(x_1,x_2)\Big|_{x_i>x_{j,k}} = \frac{1}{x_i}(1-x_i)^{1-a/2}\left[(1-x_j)^{1-a/2}(1-x_k)^{a/2} + (1-x_j)^{a/2}(1-x_k)^{1-a/2}\right]. \tag{3.150}$$

At each fixed value of $\tau_a = c$ in the distribution Eq. (3.148), the delta function restricts the integral over $x_{1,2}$ to a linear contour determined by the equation $\tau_a(x_1,x_2) = c$, where $\tau_a(x_1,x_2)$ is given by Eq. (3.150). Examples of these integration contours are shown in Fig. 3.11B.

It is sufficient to consider the part of the phase space corresponding to region III shown in Fig. 3.11, where $x_3 > x_{1,2}$. Integration over the remaining two regions can be related to the integration over region III by a trivial shift of variables of integration. Thus we need to solve

$$c = \frac{1}{2-x_1-x_2}(x_1+x_2-1)^{1-a/2}\left[(1-x_1)^{1-a/2}(1-x_2)^{a/2} + (1-x_1)^{a/2}(1-x_2)^{1-a/2}\right], \tag{3.151}$$

where $x_{1,2}$ lie in region III. To find an explicit one-variable parameterization for $x_{1,2}(w)$ which satisfies Eq. (3.151), we first absorb the factor $1/(2-x_1-x_2)$ inside the brackets and define

$$w \equiv \frac{1-x_1}{2-x_1-x_2}\,. \tag{3.152}$$

In terms of w, Eq. (3.151) can be written as

$$c = (x_1+x_2-1)^{1-a/2}\left[w^{1-a/2}(1-w)^{a/2} + w^{a/2}(1-w)^{1-a/2}\right]. \tag{3.153}$$

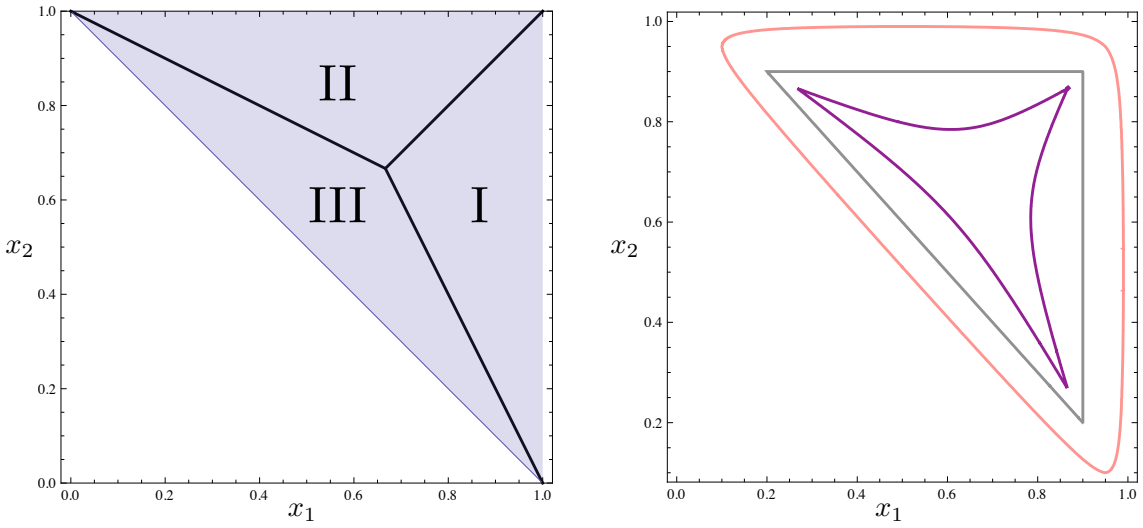

(A) (B)

Figure 3.11: (A) Phase space for three-particle $q\bar{q}g$ final state. The energy fractions $x_i = 2E_i/Q$ of the three particles satisfy $x_1 + x_2 + x_3 = 2$. In region I, $x_1 > x_{2,3}$, in region II, $x_2 > x_{1,3}$, and in region III, $x_3 > x_{1,2}$. The thrust axis is in the direction of the particle with the largest energy. (B) Contours of constant $\tau_a = 1/10$ for $a = -1$ (purple), $a = 0$ (gray), and $a = 1$ (pink). The differential cross-section $\mathrm{d}\sigma/\mathrm{d}\tau_a$ is given by integrals over these contours in the $x_{1,2}$ phase space.

Solving Eqs. (3.152, 3.153) for x_1, x_2 gives:

$$\begin{aligned} x_1(w) &= 1 - w + w\left(\frac{c}{w^{1-a/2}(1-w)^{a/2} + w^{a/2}(1-w)^{1-a/2}}\right)^{\frac{1}{1-a/2}}, \\ x_2(w) &= x_1(1-w). \end{aligned} \tag{3.154}$$

Clearly from Eq. (3.152), w lies in the interval $0 \le w \le 1$. The precise range of values for w is determined from the conditions $x_1(w) \le 2 - x_1(w) - x_2(w)$ and $x_2(w) \le 2 - x_1(w) - x_2(w)$. These inequalities can be simplified to

$$c \le \min\{F_a(w), F_a(1-w)\} = \begin{cases} F_a(w) & \text{for} \quad 0 \le w \le 1/2 \\ F_a(1-w) & \text{for} \quad 1/2 \le w \le 1 \end{cases}, \tag{3.155}$$

where

$$F_a(w) \equiv \frac{w(1-w)^{a/2}}{(1+w)^{1-a/2}}(w^{1-a} + (1-w)^{1-a}). \tag{3.156}$$

The function $F_a(w)$ is monotonically increasing over the range $0 < w < 1/2$ only for $2 > a \ge a_1 \approx -1.978$, but for $a < a_1$ turns out to have exactly one local maximum, $\tau_{\max}(a)$, and one local minimum, $\tau_{\min}(a)$. At $a = a_2 \approx -2.618$, $\tau_{\max}(a)$ is equal to the angularity of the

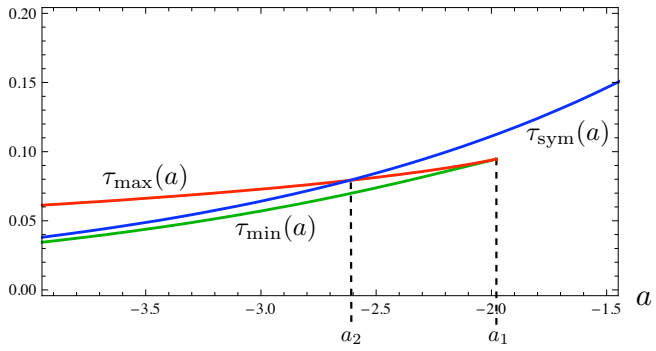

Figure 3.12: The local minimum (green line) and maximum (red line) of the function $F_a(w)$ over the range $0 < w < 1/2$ coincide at the point $a \equiv a_1 \approx -1.978$. At $a \equiv a_2 \approx -2.618$, the value of angularity for the maximally symmetric three-jet case, $\tau_{\rm sym}(a) = 1/3^{1-a/2}$ (blue line), intersects the local maximum and so for $a < a_2$, the value of maximum angularity for such a corresponds not to the maximally symmetric case but to a more two-jet like event.

symmetric three-jet configuration $x_1 = x_2 = x_3$ (where $w = 1/2$), $\tau_{\rm sym}(a) = 1/3^{1-a/2}$. Thus, the global maximum of τ_a over the whole range $0 \le w \le 1$, defined as $\tau_a^{\rm max}$, is $\tau_{\rm max}(a)$ for $a \le a_2$ and is $\tau_{\rm sym}(a)$ for $a \ge a_2$.

In Fig. 3.12, we show how the maximum and minimum of the function $F_a(w)$ depend on a, along with the a dependence of the symmetric three-jet configuration, and plot the special points a_1 and a_2.

In Fig. 3.13 we plot the boundary of τ_a ($F_a(w)$ for $0 \le w \le 1/2$ and $F_a(1-w)$ for $1/2 \le w \le 1$) together with the contours of constant $\tau_a(x_1, x_2) = c$ for different values of c in the full x_1-x_2 plane for the cases $a = -1$, $a = -2.3$, and $a = -4$, which qualitatively represent the three cases $a > a_1$, $a_1 > a > a_2$, and $a_2 > a$, respectively. From this analysis we conclude that for $a < a_1$ and especially $a < a_2$ angularities fail to separate two-jet like and three-jet like events.

To obtain $A_a(\tau_a)$, we evaluate the integral in Eq. (3.148) over the appropriate contours in the $x_{1,2}$ phase space numerically, except for $a = 0$, for which the integral can be evaluated analytically, giving (cf. [101])

$$A_0(\tau_0) = C_F \left[\frac{2(2 - 3\tau_0 + 3\tau_0^2)}{\tau_0(1-\tau_0)} \ln\left(\frac{1-2\tau_0}{\tau_0}\right) - \frac{3(1-3\tau_0)(1+\tau_0)}{\tau_0} \right] . \tag{3.157}$$

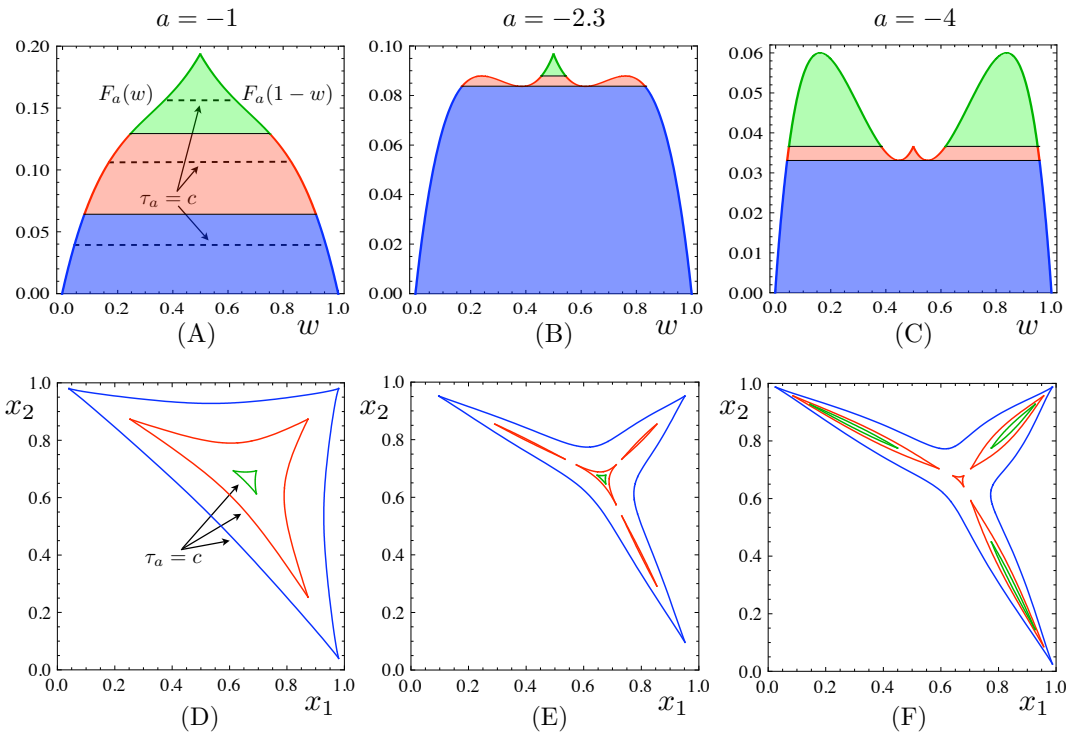

Figure 3.13: (A), (B), (C) Allowed regions for the parameter w as a function of fixed $\tau_a = c$ are bounded by the curves $F_a(w)$ and $F_a(1-w)$. For (A), (D) $a = -1$, the integration is over a single, continuous domain for all fixed $\tau_a = c$ but for (B), (E) $a = -2.3$ and (C), (F) $a = -4$, there are multiple disjoint regions of integration for large enough values of c. In (D), (E), and (F), the blue, red, and green curves represent contours of integration for fixed $\tau_a = c$, in order of increasing c, and correspond to integration over a range of w given by the lines of constant $\tau_a = c$ in the regions of the same color in (A), (B) and (C), respectively.

Chapter 4

Jet Shapes and Jet Algorithms in SCET[1]

1 Introduction

Jets provide troves of information about physics within and beyond the Standard Model of particle physics. On the one hand, jets display the behavior of Quantum Chromodynamics (QCD) over a wide range of energy scales, from the energy of the hard scattering, through intermediate scales of branching and showering, to the lowest scale of hadronization. On the other hand, jets contain signatures of exotic physics when produced by the decays of heavy, strongly-interacting particles such as top quarks or particles beyond the Standard Model.

Recently, several groups have explored strategies to probe jet substructure to distinguish jets produced by light partons in QCD from those produced by heavier particles [173, 60, 61, 56, 62, 63, 169, 153], and methods to "clean" jets of soft radiation to more easily identify their origin, such as "filtering" or "pruning" for jets from heavy particles [62, 120, 121] or "trimming" for jets from light partons [154]. Another type of strategy, explored in [3], to probe jet substructure is the use of *jet shapes*, which are modifications of event shapes [99] such as thrust. Jet shapes are continuous variables constructed by taking a weighted sum over the four-momenta of all particles constituting a jet. Different choices of weighting functions produce different jet shapes, and can be designed to probe regions closer to or further from the jet axis with greater sensitivity.[2]

Reliable theoretical prediction of jet observables in the presence of jet algorithms is made challenging by the presence of many scales, the logarithms of which can become large and spoil the behavior of perturbative expansions predicting these quantities. These scales include the jet energy, the cut on the angular size of a jet R, the measured value of the jet shape, and any other cut or selection parameters introduced by the jet algorithm.

Precisely this separation of scales, however, allows us to take advantage of the powerful theoretical tools of factorization and effective field theory. Factorization separates the calculation

[1] This chapter was originally cowritten with Stephen D. Ellis, Christopher Lee, Christopher K. Vermilion, Jonathan R. Walsh [116].

[2] The original "jet shape," to which the name properly belongs, is the variable $\Psi(r/R)$, the fraction of the total energy of a jet of radius R that is contained in a subjet of radius r [117, 118, 1] . This variable falls into the larger class of jet shapes we have described here and for which we have hijacked the name.

of a hard scattering cross section into hard, jet and soft functions each depending only on physics at a single scale [93, 181]. Renormalization group (RG) evolution of these functions between scales resums logarithms of these scales to all orders in α_s, with the logarithmic accuracy determined by the order to which the anomalous dimensions in the running are calculated [96]. Effective field theory organizes these concepts and tools into a conceptually simple framework unifying many ingredients going into traditional methods, such as power counting, gauge invariance, and resummation through RG evolution. The rules of effective theory facilitate proofs of factorization and achievement of logarithmic resummation at leading order in the power counting and make straightforward the improvement of results order-by-order in power counting and logarithmic accuracy of resummation.

Soft-collinear effective theory (SCET) [19, 21, 33, 29] has been successfully applied to the analysis of many hard scattering cross sections [20] including the production of jets. SCET is constructed by integrating out of QCD all degrees of freedom except those collinear to a lightlike direction n and those which are soft, that is, have much lower energy than the energy of the hard scattering or of the jets. Using this formalism, factorization and calculation of two-jet cross sections and event shape distributions in SCET were developed in [26, 24, 124, 18]. Later, these techniques were extended to the factorization of jet cross sections and observables using jet algorithms in [23]. Calculations in SCET of two-jet rates using jet algorithms have been performed in [24, 187], and more recently in [85]. Calculations of cross sections with more than two jet directions have been given in [32, 31, 42].

Resummation of large logarithms $(\ln e)/e$ of an event shape e near the kinematic endpoint of extremely collimated jets has now been performed in several cases both in traditional methods in QCD and in SCET. In QCD, these cases include next-to-leading-logarithmic (NLL) resummation of the thrust distribution in [76, 73], jet mass distributions in [73, 74, 97, 59], the jet broadening distribution in [75, 106], and the C-parameter in [77]. Resummation of an event shape distribution using the modern SCET method was first illustrated with the thrust distribution to LL accuracy in [172]. A method to extract precisely the top quark mass using resummed jet mass distributions in SCET to NLL accuracy was demonstrated in [125]. The $\mathrm{N^3LL}$ resummed thrust distribution in SCET was compared to LEP data to extract a value for the strong coupling α_s to high precision in [41]. Angularity distributions were resummed to NLL using SCET in [134] directly in the distribution instead of in moment space as in the QCD-based method used in [47].

Factorization and resummation of jet rates and jet observables while using a jet algorithm requires more care than with event shapes due to logarithms of phase space cuts that may not be resummable to all orders. Some exploration of these issues in SCET have been given in [187, 85]. Consistent all-orders resummation of logs of phase space cuts such as the angular size R of a jet or the energy cutoff Λ for emission outside of jets has not yet been completely demonstrated. There are logarithms of these parameters that may appear in fixed-order expansions, beginning at $\mathcal{O}(\alpha_s^2)$, that are not correctly reproduced by exponentiating lower order logs. This is the issue of "non-global" logarithms [97, 11, 8, 104].

In this work, we confine our focus to the particular but interesting problem of measuring a jet shape of one or more jets in an N-jet final state in e^+e^- annihilation, where the jets are defined using a cone algorithm or an inclusive recombination algorithm, and resumming logs of the jet shape in the narrow jet limit. We formulate a factorization theorem for such jet shape distributions, and aim to resum logs of the jet shape which become large for collimated jets to

NLL accuracy. Ref. [104] demonstrated the factorization of such a distribution into a "global" and "non-global" part, and our methods resum the logs in the global part, and at least a subset of those in the non-global part. We do not tackle the problem of ensuring full resummation of all non-global logs generated by phase space cuts, which would require an $\mathcal{O}(\alpha_s^2)$ analysis of jet and soft functions, beyond the scope of this work.

Nevertheless, we demonstrate, at $\mathcal{O}(\alpha_s)$, the nontrivial consistency of the factorization theorem for jet shape distributions even in the presence of these phase space cuts, as we reported in [114]. In order for a factorization theorem to be consistent, the anomalous dimensions of hard, jet, and soft functions must satisfy a very nontrivial constraint so that the physical cross section is independent of the factorization scale μ. We will find that these anomalous dimensions depend on algorithm phase space cut parameters and that the consistency condition is indeed satisfied, but only in the kinematic limit where jets are well-separated compared to their angular size R. Namely, we will find the consistency relation, and therefore the factorization theorem, is valid only for large $t = \tan(\psi/2)/\tan(R/2)$, where ψ is the minimum angle between any two jet axes. This condition manifests the range of validity of the effective theory constructed by adding together N copies of the collinear Lagrangian in SCET to a single soft sector Lagrangian to represent the dynamics of N identifiable jets in a final state.

For concreteness, for the jet shape, we choose to calculate the angularity τ_a of a jet, defined by (cf. [3, 47]),

$$\tau_a \equiv \frac{1}{2E_J} \sum_{i \in J} \left|\mathbf{p}_T^i\right| e^{-\eta_i (1-a)} , \tag{4.1}$$

where a is a parameter taking values $-\infty < a < 2$ (for IR safety), the sum is over all particles in the jet, E_J is the jet energy, $\mathbf{p}_T$ is the transverse momentum relative to the jet direction, and $\eta = -\ln \tan(\theta/2)$ is the (pseudo-)rapidity measured from the jet direction. However, our logic and methods are applicable to any suitable jet shape. We have organized our results in such a way that the pieces independent of the choice of jet shape and dependent only on the jet algorithm are easily identifiable, requiring recalculation only of the observable-dependent pieces to extend our results to other choices of jet shapes.

In this chapter, we will calculate to next-to-leading order (NLO) in α_s the jet and soft functions corresponding to N jets, where we measure the jet shape Eq. (4.1) of $M \leq N$ jets. We will demonstrate the consistency of the anomalous dimensions of hard, jet and soft functions to NLO for any number of total jets, any numbers of quark and gluon jets, any number of these jets whose shapes are measured, and any value of the distance measure R in cone or k_T-type algorithms (as long as $t \gg 1$). We calculate the finite parts of the SCET jet and soft functions to NLO, and resum logarithms of the jet shape τ_a to NLL accuracy.[3]

We will demonstrate the crucial role of zero-bin subtractions [163] from collinear jet functions in obtaining the consistent anomalous dimensions and the correct finite parts. In this case zero-bin subtractions are not merely scaleless integrals converting IR to UV divergences, but in fact contribute part (sometimes the most important part) of the correct nonzero result, as was already pointed out by [85, 86]. The relation of zero-bin subtractions in SCET to eikonal jet subtractions

[3] Jet shapes were also studied in the QCD factorization approach in [4]. In this work QCD jet functions for quark and gluon jets defined with an algorithm and whose jet masses m_J^2 are measured were calculated to $\mathcal{O}(\alpha_s)$. The jet mass corresponds to τ_a for $a = 0$. A fixed-order QCD jet function as defined in [4] is given by the convolution of our fixed-order SCET jet function and soft function for a measured jet away from $\tau_a = 0$.

from soft functions in traditional methods of QCD factorization was explored in [157, 140, 139].

We will find that the scale governing each measured jet function is set only by the measured value of the jet shape τ_a, and that the scale governing each unmeasured jet function is set by the scale of the angular cut R. The hard function depends on a large scale determined by the jet energies. The soft function, as we initially define it, will appear to depend on many scales, set by the value of τ_a for every individual measured jet (which may all be different), the angular cut R, and the threshold Λ for the minimum jet energy. When these scales are disparate, large logarithms remain in the soft function even after naive resummation. We will therefore introduce a framework to "refactorize" the naive soft function into individual pieces, each of which depends only on one soft scale. Each piece is the matching coefficient from a theory with a soft mode with virtuality given by one of these scales onto a theory with a soft mode with virtuality at the next lowest scale, with the original higher-scale soft mode integrated out. Running between these scales then resums logarithms of ratios thereof. We find that this procedure tames large logarithmic dependence on ratios of these various soft scales, including non-global logs of the form $\ln(\Lambda/\omega\tau_a)$. It was demonstrated in [47] that choosing $\omega\tau_a \sim \Lambda$ removed such non-global logs entirely. We allow for disparate Λ and $\omega\tau_a$, resumming logs arising at the NLL level, although there may be non-global logs starting at $\mathcal{O}(\alpha_s^2)$ which we still miss. Whether this procedure achieves NLL resummation including all the non-global logs is still an open question, outside the scope of the present work.

We will give an estimate of power corrections to the factorization theorem due to approximations we must make in its proof to the jet momenta and the action of the jet algorithm on collinear and soft particles. We will find for $R \sim \mathcal{O}(1)$ and $a < 1$, these remain small enough not to spoil the factorization. Algorithm-related power corrections to jet momenta were studied more quantitatively in [98], and their estimated R dependence is consistent with our observations. We do not address in this work the issue of power corrections to jet shapes due to hadronization. Event shape distributions are known to receive power corrections of the order $1/(\tau_a Q)$, enhanced in the endpoint region but suppressed by large energy. The endpoints of our jet shape distribution near $\tau_a \to 0$, therefore, will have to be corrected by a nonperturbative shape function. Such functions have been constructed for event shapes in [149, 132]. The shift in the first moment of event shape distributions induced by these shape functions was postulated to take a universal form in [109, 110] based on the behavior of single soft gluon emission, and the universality was proven to all orders in soft gluon emission at leading order in the SCET power counting in [157, 156]. This universality relied on the boost invariance of the soft function describing soft gluon radiation from two back-to-back collinear jets. The extent to which such universality may survive for jet shapes with multiple jets in arbitrary directions is an open question that must be addressed in order to construct appropriate soft shape function models to deal adequately with the power corrections to jet shapes from hadronization. Nonperturbative power corrections to jet observables from hadronization and the underlying event in hadron collisions were also studied in [98], and hadronization corrections were found to scale like $1/R$. In this work, we focus only on the perturbative calculation and resummation of large logarithms of jet shapes, and leave inclusion of nonperturbative power corrections for future work.

By comparing to the output of a Monte Carlo event generator, we can test both the accuracy of our perturbative resummed predictions and assess the extent to which hadronization corrections affect jet shapes. We will illustrate our results in the case of $e^+e^- \to 3$ jets, with the jets constrained to be in a configuration where each has equal energy and are maximally separated.

In both the effective theory and Monte Carlo, we can take the jets to have been produced by an underlying hard process $e^+e^- \to q\bar{q}g$. After placing cuts on jets to ensure each parton corresponds to a nearby jet, we measure the angularity jet shape of one of the jets. We compare our NLL resummed theoretical predictions with the Monte Carlo output for quark and gluon jet shapes with various values of a and R. We find that the dependencies on a and R of the shapes of the distribution and the peak value of τ_a agree well between the theory and Monte Carlo, with small but noticeable corrections due to hadronization. We can extract the hadronization dependence by comparing Monte Carlo output with hadronization turned on or off.

Our work is, to our knowledge, the first achieving factorization and resummation of a jet observable distribution in an exclusive N-jet final state defined by a non-hemisphere jet algorithm.[4] Having demonstrated the consistency of this factorization for any number of quark and gluon jets, measured and unmeasured jets, and phase space cuts in cone and k_T-type algorithms, and having constructed a framework to resum logarithms of jet shapes in the presence of these phase space cuts, we hope to have provided a starting point for future precision calculations of many jet observables both in e^+e^- and hadron-hadron collisions. The case of pp collisions will require a number of modifications, including turning two of our outgoing jet functions into incoming "beam functions" introduced in [183]. We leave this generalization for future work.

An outline of this chapter is as follows. In Sec. 2, we describe the jet shapes and jet algorithms we will use to calculate jet shape distributions in exclusive N-jet final states. In Sec. 3, we give a summary of the logic and method of the calculations we perform in subsequent sections. We tabulate the main results of the chapter in Table 4.1 appearing in this section. In Sec. 4 we give a brief overview of SCET and derive in detail the factorized cross section for a jet shape distribution in $e^+e^- \to 3$ jets and state the generalization to the distribution in M measured jet shapes in an N-jet cross section. In Sec. 5 we calculate jet functions for both measured and unmeasured jets defined with a jet algorithm to NLO. In Sec. 6 we calculate the NLO soft function for M measured jets in an N-jet cross section. In Sec. 7 we verify that the hard, jet, and soft anomalous dimensions satisfy the consistency relation to NLO if and only if $t \gg 1$ and perform resummation of logarithms of jet shapes to NLL accuracy. In Sec. 8 we use these results to give theoretical predictions for quark and gluon angularity jet shape distributions in Mercedes-Benz-like 3-jet events in e^+e^- annihilation, and compare to the output of a Monte Carlo event generator. Finally, in Sec. 9, we give our conclusions and outlook. We also collect a number of technical details and results for NLO finite pieces of jet and soft functions in the Appendices.

The reader wishing to follow the general structure of our ideas and logic and understand the basis of the final results of the chapter without working through all the technical details may read Secs. 2 and 3, and then skip to Sec. 8. Some short non-technical discussion also appears in Sec. 4.4.

2 Jet Shapes and Jet Algorithms

Event shapes, such as thrust, characterize events based on the distribution of energy in the final state by assigning differing weights to events with differing energy distributions. Events that are two-jet like, with two very collimated back-to-back jets, produce values of the observable at one end of the distribution, while spherical events with a broad energy distribution produce

[4] Dijet cross sections for cone jets were factorized and resummed in [143].

values of the observable at the other end of the distribution. While event shapes can quantify the global geometry of events, they are not sensitive to the detailed structure of jets in the event. Two classes of events may have similar values of an event shape but characteristically different structure in terms of number of jets and the energy distribution within those jets.

Jet shapes, which are event shape-like observables applied to single jets, are an effective tool to measure the structure of individual jets. These observables can be used to not only quantify QCD-like events, but study more complex, non-QCD topologies, as illustrated for light quark vs. top quark and Z jets in [3, 4]. Broad jets, with wide-angle energy depositions, and very collimated jets, with a narrow energy profile, take on distinct values for jet shape observables. In this work, we consider the example of the class of jet shapes called angularities, defined in Eq. (4.1) and denoted τ_a. Every value of a corresponds to a different jet shape. As a decreases, the angularity weights particles at the periphery of the jet more, and is therefore more sensitive to wide-angle radiation. Simultaneous measurements of the angularity of a jet for different values of a can be an additional probe of the structure of the jet.

A key component of the distribution of jet shapes is the jet algorithm, which builds jets from the final state particles in an event. (We are using the term "particle" generically here to refer to actual individual tracks, to cells/towers in a calorimeter, and to combinations of these objects within a jet.) Since the underlying jet is not intrinsically well defined, there is no unique jet algorithm and a wide variety of jet algorithms have been proposed and implemented in experiments. The details of each algorithm are motivated by particular properties desired of jets, and different algorithms have different strengths and weaknesses. In this work we will calculate angularity distributions for jets coming from a wide variety of algorithms. Because we calculate (only) at next-to-leading order, jet algorithms that implement the same phase space cuts at NLO simplify to the same algorithm. Two classes of algorithms, cone algorithms and recombination algorithms, each simplify to a generic jet algorithm at NLO.

Cone algorithms build jets by grouping particles within a fixed geometric shape, the cone, and finding "stable" cones. A cone contains all of the particles within an angle R of the cone axis, and the angular parameter R sets the size of the jet. In found jets (stable cones), the direction of the total three-momentum of particles in the cone equals the cone (jet) axis. Different cone algorithms employ different methods to find stable cones and deal with the "split/merge" problem of overlapping stable cones. The SISCone algorithm [171] is a modern implementation of the cone algorithm that finds all stable cones and is free of infrared unsafety issues. In the next-to-leading order calculation we perform, there are at most two particles in a jet, and all jets are well-separated and defined by a label direction associated with a collinear sector in SCET. Therefore, it is straightforward to find all stable cones, there are no issues with overlapping stable cones, and the phase space cuts of all cone algorithms are equivalent. This simplifies all standard cone algorithms to a generic cone-type algorithm, in which each particle is constrained to be within an angle R of the jet axis. For a two-particle jet, if we label the particles 1 and 2 and the jet axis $\mathbf{n}$, then the cone-like constraints for the two particles to be in a jet are

$$\text{cone jet: } \theta_{1\mathbf{n}} < R \text{ and } \theta_{2\mathbf{n}} < R\,. \tag{4.2}$$

This defines our cone-type algorithm.

Recombination algorithms build jets by recursively merging pairs of particles. Two distance metrics, defined by the algorithm, determine when particles are merged and when jets are

formed. A pairwise metric ρ_{pair} (the recombination metric) defines a distance between pairs of particles, and a single particle metric ρ_{jet} (the beam, or promotion, metric) defines a distance for each single particle. Using these metrics, a recombination algorithm builds jets with the following procedure:[5]

0. Begin with a list L of particles.

1. Find the smallest distance for all pairs of particles (using ρ_{pair}) and all single particles (using ρ_{jet}).

2a. If the smallest distance is from a pair, merge those particles together by adding their four momenta. Replace the pair in L with the new particle.

2b. If the smallest distance is from a single particle, promote that particle to a jet and remove it from L.

3. Loop back to step 1 until all particles have been merged into jets.

The k_T, Cambridge-Aachen, and anti-k_T algorithms are common recombination algorithms, and their distance metrics are part of a general class of recombination algorithms. For e^+e^- colliders, a class of recombination algorithms can be defined by the parameter α:

$$\begin{aligned} \rho_{\text{pair}}(i,j) &= \min\left(E_i^\alpha, E_j^\alpha\right)\frac{\theta_{ij}}{R} \\ \rho_{\text{jet}}(i) &= E_i^\alpha\,, \end{aligned} \tag{4.3}$$

where $\alpha = 1$ for k_T, 0 for Cambridge-Aachen, and -1 for the anti-k_T algorithm. The parameter R sets the maximum angle between two particles for a single recombination.[6] For a two-particle jet, the only phase space constraint imposed by this class of recombination algorithms is that the two particles be separated by an angle less than R:

$$\text{k}_\text{T} \text{ jet: } \theta_{12} < R\,. \tag{4.4}$$

This defines a generic recombination algorithm suitable for our calculation. We will denote this as the k_T-type algorithm.

Because jets are reliable degrees of freedom and provide a useful description of an event when they have large energy, in the description of an event we impose a cut Λ on the minimum energy of jets. An N-jet event, therefore, is one where N jets have energy larger than the cutoff Λ, with any number of jets having energy less than the cutoff. In our calculation, we impose the same constraint: any jet with energy less than Λ is not considered when we count the number of jets in the final state. This imposes phase space cuts: for a gluon radiated outside of all jets in the event, that gluon is required to have energy $E_g < \Lambda$ to maintain the same number of jets in the event. The proper division of phase space in calculating the jet and soft functions is a key part of the discussion below, and careful treatment of the phase space cuts is needed.

[5] This defines an *inclusive* recombination algorithm. Exclusive recombination algorithms are described along with other jet algorithms in [170].

[6] We use R for both cone and k_T algorithms for ease of notation. For k_T, this parameter is sometimes referred to as D. We emphasize that having the same size R for different algorithms does not in general guarantee the same sized jets.

3 Overview of Calculations and Main Results

In this section we give an overview of the calculations that we will present in the remainder of the chapter, explaining the logic and strategy in broad strokes.

We will first formulate and prove a factorization theorem for distributions in the jet shape variables we introduced in the previous sections. These jet shapes are measured in N-jet events defined with a cone or $\mathrm{k_T}$-type algorithm. Using the tools of SCET, we will derive in detail a factorization theorem for exclusive 3-jet production where we measure the angularity jet shape of one of the jets, and then perform the straightforward extension to N-jet production with $M \leq N$ measured jets.

We will give a review of the necessary technical details of SCET in Sec. 4.1. The important features of SCET are that it is an effective theory of QCD in which all but collinear and soft degrees of freedom have been integrated out, and a Lagrangian in terms of these remaining modes can be derived order-by-order in an expansion in λ, a small parameter formed by the ratio of soft to collinear or collinear to hard scales, determined by the kinematics of the process under study. In our case, λ is roughly the typical transverse momentum p_T of the constituent of a jet (relative to the jet direction) divided by the jet energy E_J, or the measured value of a jet shape τ_a. The size of λ may thus be different for different jets. The momentum p_n of collinear modes in the light-cone direction n in SCET are separated into a large "label" momentum $\tilde{p}_n$ containing $\mathcal{O}(E_J)$ and $\mathcal{O}(\lambda E_J)$ components and a "residual" component of $\mathcal{O}(\lambda^2 E_J)$, the same size as soft momenta. Effective theory fields have dynamical momenta only of this soft or residual scale. This fact, along with the fact that soft quarks and soft gluons can be shown to decouple from collinear modes at the level of the Lagrangian, makes possible the factorization of a jet shape distribution into hard, jet, and soft functions depending only on the dynamics at those respective scales.

We will formulate an effective theory with SCET collinear fields in N separate directions, and use it to factorize the distribution in M jet shapes in an N-jet final state. In addition to steps common to all factorization proofs in SCET (such as soft-collinear decoupling and collinear jet functions' dependence on residual momentum only in the $n \cdot k$ component) we will identify a number of additional criteria required for the factorization of jet shape cross sections with jets defined by a jet algorithm.

Two of these conditions enforce that there are exactly N jets in the final state. First, to ensure that the algorithm does not group final-state particles into fewer than N jets, the jets must be "well separated." This allows us to use as the effective theory Lagrangian a sum of N copies of the collinear part of the SCET Lagrangian for a single direction n and a soft part, and to construct a basis of N-jet operators built from fields from each of these sectors to produce the final state. The validity of using this Lagrangian and basis of N-jet operators requires that a parameter t measuring the separation between jets is large. Later calculations and the requirement of consistency among hard, jet, and soft anomalous dimensions will suggest a natural definition of $t = \tan(\psi/2)/\tan(R/2)$, where ψ is the minimum angle between two jets.

Second, to ensure that the jet algorithm does not find more than N jets, we place an energy cut Λ on the particles outside of the jets. We will take this energy Λ to scale as a soft momentum so that we will be able to identify the total energy of each jet with the "label" momentum on the SCET collinear jet field producing the jet, which introduces corrections that are subleading in the SCET power counting. These approximations have the effect that all particles with large energy grouped into a jet by the jet algorithm will remain in the same jet even after the approximations

we make to the action of the algorithm in order to prove our factorization theorem.

Third (and related to the first two), we will assume that the N-jet restriction on the final state can itself be factorized into a product of N 1-jet restrictions, one in each collinear sector, and a 0-jet restriction in the soft sector. We represent the energetic particles in the ith jet by collinear fields in the SCET Lagrangian in the n_i collinear sector and soft particles everywhere with fields in the soft part of the Lagrangian. We then stipulate that the jet algorithm acting on states in the n_i collinear sector find exactly one jet in that sector, and when acting on the soft final state find no additional jet in that sector.

In addition, as always, there are power corrections to the factorization theorem which we must ensure are small. One class of these corrections arises from approximating the jet axis of the measured jet with the collinear direction n_i, which labels that jet in the SCET Lagrangian. This direction n_i is the direction of the parent parton initiating the jet. The jet observable must be such that the difference between the parent parton direction and the jet axis identified by the algorithm makes a subleading correction to the calculated value of the jet observable. In the context of angularity event shapes, such corrections were estimated in [18, 47] and found to be negligible for $a < 1$, and we find the same condition for jet shapes.

In the presence of algorithms, however, there are additional power corrections due to the difference in the soft particles that are included or excluded in a jet by the actual algorithm and in its approximated form in the factorization theorem. We comment on the extent to which existing algorithms satisfy the criteria we need in deriving our all-orders factorization formula in Sec. 4.4, and find that with all the modern algorithms we examine the jet size R is required to be $R \sim \mathcal{O}(1)$.

When all power corrections are under control and the algorithm itself does not lead to a breakdown of factorization, our factorization theorem states that the cross section can be written as a certain convolution of hard, jet, and soft functions. The hard function is calculated by demanding that virtual corrections to operators in full QCD with N partons "match" those in SCET. Since this is given by virtual corrections alone, the hard function has no dependence on the jet algorithm or jet shape observable and is thus universal. The jet and soft functions, which respectively contain collinear and soft real emission information, do depend on the algorithm and observable. The running of the hard function, which can be obtained from the ultraviolet divergent part, is universal and can be found in the literature (e.g. in [87]). The finite terms in the hard function can be taken as the process-dependent virtual diagrams from the corresponding full QCD calculation. These finite terms, however, are not strictly needed at NLL accuracy, to which we work in this chapter. Thus the only new calculations we need to perform are for the divergent and finite parts of the jet and soft functions. For NLL accuracy, we do not need these finite pieces either, but they will suggest to us the natural scales $\mu_{J,S}$ at which to evaluate the jet and soft functions to minimize potentially large logarithms in the finite parts. We thus report the infinite parts of the bare jet and soft functions in the main text, and leave the finite parts in the Appendices.

We calculate the jet functions in Sec. 5 for measured quark jets, $J^q_\omega(\tau_a)$, unmeasured quark jets, J^q_ω, measured gluon jets, $J^g_\omega(\tau_a)$, and unmeasured gluon jets, J^g_ω, where $\omega = 2E_J$ is the label energy of the collinear jet field in each jet function. Unmeasured jets are sensitive to a scale related to the characteristic size of the jet R as defined by the algorithm. However, since we show that we need $R \sim \mathcal{O}(1)$ to minimize power corrections for commonly used algorithms (as we discussed above), and since small R is not practical in modern detectors, resummation of R is not the immediate goal of this chapter. Measured jets on the other hand are sensitive to the scale

$\omega_i \tau_a^i$, in addition to R. We find that collinear emissions that escape a jet are suppressed by Λ/ω_i once the zero-bin subtraction [163] to eliminate double-counting between soft and collinear modes is taken into account.

We calculate the soft function in Sec. 6. To do this, we split the soft function into several contributions from different parts of phase space in order to facilitate the calculation and elucidate its intuitive structure. We find it most convenient to split the soft function into an observable-independent part that arises from soft emission out of the jets, $S^{\rm unmeas}$, and a part that depends on our choice of angularities as the observable that arises from soft emission into measured jet i, $S^{\rm meas}(\tau_a^i)$. $S^{\rm unmeas}$ is hence sensitive to the scale Λ while $S^{\rm meas}(\tau_a^i)$ is sensitive the the scale $\omega_i \tau_a^i$.

Then, having calculated all the jet and soft function contributions at NLO, we extract the anomalous dimensions and perform renormalization-group (RG) evolution in Sec. 7. We find the hard anomalous dimension from existing results in the literature. The equivalence of the"top-down" and "bottom-up" approaches in effective theories (see, e.g., [58]) implies that we can either RG-evolve the jet and soft functions from their respective scales up to the hard scale or evolve the hard function down to the jet scale and the soft function from the jet scale to the soft scale [125]. This boils down to the simple fact that the physical cross section must be independent of the arbitrary factorization scale μ at which the hard, jet, and soft functions in the factorization theorem are evaluated. These observations imply that the sum of the jet and soft anomalous dimensions must be (minus) the universal N-jet hard function, giving a non-trivial consistency check on our factorization theorem.

For N jets whose angular separations from one another are given by angles ψ_{ij}, and a jet algorithm requiring that individual jets have angular extent R, we show in Sec. 7.3 that consistency is valid when, for every pair of jets i, j, we have that $t_{ij} \gg 1$, where

$$t_{ij} \equiv \frac{\tan\frac{\psi_{ij}}{2}}{\tan\frac{R}{2}}\,. \tag{4.5}$$

That is, our calculation of the anomalous dimensions indicates precisely what we should use for the jet separation parameter t, which we need to be large in order for our factorization proof to be valid. Notice that for back-to-back jets ($\psi_{ij} = \pi$), we have that $1/t_{ij} = 0$ exactly. Thus, for all cases previously considered in the literature, the jets are infinitely separated according to this measure, and no additional criterion regarding jet separation is required for consistency of the factorization and running.

It may seem mysterious that the calculations of the hard, jet, and soft functions themselves indicate the necessity for a large separation parameter t in order for the anomalous dimensions to satisfy consistency. Although we already specified this criterion qualitatively for the validity of introducing N separate collinear sectors in our SCET Lagrangian and N-jet operator, it may not be immediately apparent where this criterion is implemented in the actual calculations. It enters in the definition of the collinear jet functions. In the large-t limit, the N jets are infinitely separated from one another according to the measure given by Eq. (4.5). Therefore, in each collinear sector of SCET in direction n_i, we assume that the other $N-1$ jets are all maximally far away.

And indeed, when N-jet operators are constructed in SCET, each collinear jet field contains a Wilson line W_n, defined below in Eq. (4.14), of collinear gluons in the direction n that were emitted from the back-to-back direction $\bar{n}$. That is, the n_i-collinear sector assumes that all other hard directions are in the maximally-separated opposite direction $\bar{n}_i$. (This is similar to QCD

Category	Contribution	Symbol	Location
NLO contributions before resummation:	measured quark jet function	$J_\omega^q(\tau_a)$	Eq. (4.50)
	unmeas. quark jet function	J_ω^q	Eq. (4.56)
	measured quark jet function	$J_\omega^g(\tau_a)$	Eq. (4.64)
	unmeas. gluon jet function	J_ω^g	Eq. (4.65)
	summary of divergent parts of soft func. (any t)	—	Table 4.2
	total universal soft func. (large t)	S^{unmeas}	Eq. (4.85)
	total measured soft func. (large t)	$S^{\text{meas}}(\tau_a^i)$	Eq. (4.87)
anomalous dimensions:	—	—	Table 4.3
NLO contributions after resummation:	measured jet function	$f_J^i(\tau_a^i;\mu_J^i)$	Eq. (4.131a)
	measured soft function	$f_S(\tau_a^i;\mu_J^i)$	Eq. (4.131b)
	unmeas. jet function	$J_\omega^i(\mu_J)$	Eq. (4.132a)
	universal soft function	$S^{\text{unmeas}}(\mu_\Lambda)$	Eq. (4.132b)
Total NLL Distribution:	—	—	Eq. (4.128)

Table 4.1: Directory of main results. We tabulate the location of the key results of this chapter: the fixed-order NLO quark and gluon jet functions for jets whose shapes τ_a are measured or not; the fixed-order NLO contributions to the soft functions from parts of phase space where a soft gluon enters a measured jet, $S^{\text{meas}}(\tau_a)$, or not, S^{unmeas}; their anomalous dimensions; the contributions the jet and soft functions make to the finite part of the NLL resummed distributions; and the full NLL resummed jet shape distribution itself.

factorization proofs of hard scattering cross sections, e.g. in [47], in which this direction $\bar{n}$ is chosen to be along some arbitrary path ξ that is separated by an $\mathcal{O}(1)$ amount from the jet direction n.) Furthermore, the n_i-collinear jet function knows only its own color representation, and not those of the other jets. Meanwhile, the hard and soft functions we calculate "know" about all N jets and their precise directions and color representations. Therefore it is no surprise that, when we actually calculate the anomalous dimensions of these functions, we find that they are consistent with one another only in the limit that the separation parameter $t \to \infty$.

Even after requiring $t \gg 1$, the satisfaction of the consistency conditions is non-trivial. The hard function knows only about the direction of each jet and the jet function knows only the jet size R; the soft function knows about both. Furthermore, it is not sufficient only to include regions of phase space where radiation enters the measured jets. It is crucial to include radiation entering unmeasured jets, and also soft radiation outside of all jets with an upper energy cutoff of Λ. Only after including all of these contributions from the various parts of phase space do the jet, hard, and soft anomalous dimensions cancel and we arrive at a consistent factorization theorem.

The RG solutions for the soft function and our proof of factorization make it clear at this point that the assumption that the soft function is sensitive to a single scale is limited to the case that $\Lambda \sim \omega_i \tau_a^i$ for all jets i. However, we argue in Sec. 7.4 that in the case of a hierarchy of scales in the soft function, we can "refactorize" the soft function into multiple pieces to all orders, each

sensitive to a single scale. The result for the soft function, Eq. (4.127), resums logarithms of ratios of these various scales, although we leave as an open question whether non-global logs remain at $\mathcal{O}(\alpha_s^2)$ and higher.

We summarize where to find the results of the calculations outlined above in Table 4.1.

4 Factorization of Jet Shape Distributions in e^+e^- to N Jets

In this Section we formulate a factorization theorem for jet shape distributions in e^+e^- annihilation to N jets. All the formal aspects we need to describe an N-jet cross section appear already in the 3-jet cross section, so we will give explicit details only for that case. We will use the framework of Soft-Collinear Effective Theory (SCET), developed in [19, 21, 33, 29], to formulate the factorization theorem. We begin with a basic review of the relevant aspects of the effective theory.

4.1 Overview of SCET

SCET is the effective field theory for QCD with all degrees of freedom integrated out, other than those traveling with large energy but small virtuality along a light-like trajectory n, and those with small, or soft, momenta in all components. A particularly useful set of coordinates is light-cone coordinates, which uses light-like directions n and $\bar{n}$, with $n^2 = \bar{n}^2 = 0$ and $n \cdot \bar{n} = 2$. In Minkowski coordinates, we take $n = (1, 0, 0, 1)$ and $\bar{n} = (1, 0, 0, -1)$, corresponding to collinear particles moving in the $+z$ direction. A generic four-vector p^μ can be decomposed into components

$$p^\mu = \bar{n} \cdot p \frac{n^\mu}{2} + n \cdot p \frac{\bar{n}^\mu}{2} + p_\perp^\mu \,. \tag{4.6}$$

In terms of these components, $p = (\bar{n} \cdot p, n \cdot p, p_\perp)$, collinear and soft momenta scale with some small parameter λ as

$$p_n = E(1, \lambda^2, \lambda) \,, \quad p_s \sim E(\lambda^2, \lambda^2, \lambda^2) \,, \tag{4.7}$$

where E is a large energy scale, for example, the center-of-mass energy in an e^+e^- collision. λ is then the ratio of the typical transverse momentum of the constituents of the jet to the total jet energy. Quark and gluon fields in QCD are divided into collinear and soft effective theory fields with these respective momentum scalings:

$$q(x) = q_n(x) + q_s(x) \,, \quad A^\mu(x) = A_n^\mu(x) + A_s(x) \,. \tag{4.8}$$

We factor out a phase containing the largest components of the collinear momentum from the fields q_n, A_n. Defining the "label" momentum $\tilde{p}_n^\mu = \bar{n} \cdot \tilde{p}_n \frac{n^\mu}{2} + \tilde{p}_\perp^\mu$, where $\bar{n} \cdot \tilde{p}_n$ contains the $\mathcal{O}(1)$ part of the large light-cone component of the collinear momentum p_n, and $\tilde{p}_\perp$ the $\mathcal{O}(\lambda)$ transverse component, we can partition the collinear fields q_n, A_n into their labeled components,

$$q_n(x) = \sum_{\tilde{p} \neq 0} e^{-i\tilde{p}\cdot x} q_{n,p}(x) \,, \quad A_{n,p}^\mu(x) = \sum_{\tilde{p} \neq 0} e^{-i\tilde{p}\cdot x} A_{n,p}^\mu(x) \,. \tag{4.9}$$

The sums are over a discrete set of $\mathcal{O}(1, \lambda)$ label momenta into which momentum space is partitioned. The bin $\tilde{p} = 0$ is omitted to avoid double-counting the soft mode in Eq. (4.8) [163]. The

labeled fields $q_{n,p}, A_{n,p}$ now have spacetime fluctuations in x which are conjugate to "residual" momenta k of the order $E\lambda^2$, describing remaining fluctuations within each labeled momentum partition [33, 163]. It will be convenient to define label operators $\mathcal{P}^\mu = \bar{n}\cdot\mathcal{P}n^\mu/2 + \mathcal{P}_\perp^\mu$ which pick out just the label components of momentum of a collinear field:

$$\mathcal{P}^\mu \phi_{n,p}(x) = \tilde{p}^\mu \phi_{n,p}(x)\,. \tag{4.10}$$

Ordinary derivatives ∂^μ acting on effective theory fields $\phi_{n,p}(x)$ are of order $E\lambda^2$.

The final step to construct the effective theory fields is to isolate the two large components of the Dirac spinor $q_{n,p}$ for a fermion with lightlike momentum along n. The large components $\xi_{n,p}$ and the small $\Xi_{n,p}$ can be separated by the projections

$$\xi_{n,p} = \frac{\not{n}\bar{\not{n}}}{4} q_{n,p}\,, \quad \Xi_{n,p} = \frac{\bar{\not{n}}\not{n}}{4} q_{n,p}\,, \tag{4.11}$$

and we have $q_{n,p} = \xi_{n,p} + \Xi_{n,p}$. One can show, substituting these definitions into the QCD Lagrangian, that the fields $\Xi_{n,p}$ have an effective mass of order E and can be integrated out of the theory. The effective theory Lagrangian at leading order in λ is [21, 33, 29]

$$\mathcal{L}_{\rm SCET} = \mathcal{L}_\xi + \mathcal{L}_{A_n} + \mathcal{L}_s\,, \tag{4.12}$$

where the collinear quark Lagrangian $\mathcal{L}_\xi$ is

$$\mathcal{L}_\xi = \bar{\xi}_n(x)\left[in\cdot D + i\not{D}_\perp^c W_n(x)\frac{1}{i\bar{n}\cdot\mathcal{P}}W_n^\dagger(x) i\not{D}_\perp^c\right]\frac{\bar{\not{n}}}{2}\xi_n(x)\,, \tag{4.13}$$

where W_n is the Wilson line of collinear gluons,

$$W_n(x) = \sum_{\rm perms}\exp\left[-g\frac{1}{\bar{n}\cdot\mathcal{P}}\bar{n}\cdot A_n(x)\right]\,; \tag{4.14}$$

the collinear gluon Lagrangian $\mathcal{L}_{A_n}$ is

$$\begin{aligned}\mathcal{L}_{A_n} = {}& \frac{1}{2g^2}\,\mathrm{Tr}\left\{\left[i\mathcal{D}^\mu + gA_n^\mu, i\mathcal{D}^\nu + gA_n\right]\right\}^2 \\ & + 2\,\mathrm{Tr}\left\{\bar{c}_n\left[i\mathcal{D}_\mu, \left[i\mathcal{D}^\mu + gA_n^\mu, c_n\right]\right]\right\} + \frac{1}{\alpha}\,\mathrm{Tr}\left\{\left[i\mathcal{D}_\mu, A_n^\mu\right]\right\}\,,\end{aligned} \tag{4.15}$$

where c_n is the collinear ghost field and α the gauge-fixing parameter; and the soft Lagrangian $\mathcal{L}_s$ is

$$\mathcal{L}_s = \bar{q}_s i\not{D}_s q_s(x) - \frac{1}{2}\,\mathrm{Tr}\,G_s^{\mu\nu}G_{s\mu\nu}(x)\,, \tag{4.16}$$

which is identical to the form of the full QCD Lagrangian (the usual gauge-fixing terms are implicit). In the collinear Lagrangians, we have defined several covariant derivative operators,

$$D^\mu = \partial^\mu - igA_n^\mu - igA_s^\mu\,, \quad iD_c^\mu = \mathcal{P}^\mu + gA_n^\mu\,, \quad i\mathcal{D}^\mu = \mathcal{P}^\mu + in\cdot D\frac{\bar{n}^\mu}{2}\,. \tag{4.17}$$

In addition, there is an implicit sum over the label momenta of each collinear field and the requirement that the total label momentum of each term in the Lagrangian be zero.

Note the soft quarks do not couple to collinear particles at leading order in λ. Meanwhile, the coupling of the soft gluon field to a collinear field is in the component $n \cdot A_s$ only, according to Eqs. (4.13) and (4.15), which makes possible the decoupling of such interactions through a field redefinition of the soft gluon field given in [29]. We will utilize this soft-collinear decoupling to simplify the proof of factorization below.

The SCET Lagrangian Eq. (4.12) may be extended to include collinear particles in more than one direction [20]. One adds multiple copies of the collinear quark and gluon Lagrangians Eqs. (4.13) and (4.15) together. The collinear fields in each direction n_i constitute their own independent set of quark and gluon fields, and are governed in principle by different expansion parameters λ associated with the transverse momentum of each jet, set either by the angular cut R in the jet algorithm or by the measured value of the jet shape τ_a. Each collinear sector may be paired with its own associated soft field A_s with momentum of order $E\lambda^2$ with the appropriate λ. For the purposes of keeping the notation tractable while proving the factorization theorem in this section, we will for simplicity take all λ's to be the same, with a single soft gluon field A_s coupling to collinear modes in all sectors. In Sec. 7.4, we will discuss how to "refactorize" the soft function further into separate soft functions each depending only on one of the various possible soft scales.

The effective theory containing N collinear sectors and the soft sector is appropriate to describe QCD processes with strongly-interacting particles collimated in N well-separated directions. Thus, in addition to the power counting in the small parameter λ within each sector, guaranteeing that the particles in each direction are well collimated, we will find in calculating an N-jet cross section the need for another parameter that guarantees that the different directions n_i are well separated. This latter condition requires $t_{ij} \gg 1$, where t_{ij} is defined in Eq. (4.5).[7]

4.2 Jet Shape Distribution in $e^+e^- \to$ 3 Jets

Consider a 3-jet cross section differential in the jet 3-momenta $\mathbf{P}_{1,2,3}$, where we measure the shape τ_a^1 of jet number 1. The full theory cross section for $e^+e^- \to \gamma^* \to 3$ jets at center-of-mass energy Q is

$$\begin{aligned}\frac{d\sigma}{d\tau_a^1 d^3\mathbf{P}_{1,2,3}} = \frac{1}{2Q^2}\sum_X \left|\langle X|\, j^\mu(0)\,|0\rangle\, L_\mu\right|^2 (2\pi)^4\delta^4(Q-p_X)\delta_{N(\mathcal{J}(X)),3} \\ \times\,\delta\big(\tau_a^1 - \tau_a(\text{jet }1)\big)\prod_{j=1}^{3}\delta^3\big(\mathbf{P}_j - \mathbf{P}(\text{jet }j)\big)\,,\end{aligned} \tag{4.18}$$

where the $\mathcal{J}(X)$ is the jet algorithm acting on final state X, and $N(\mathcal{J}(X))$ is the number of jets identified by the algorithm [23]. $\mathbf{P}(\text{jet } j)$ is the 3-momentum of jet j, and is also a function of the output of the jet algorithm $\mathcal{J}(X)$. L_μ is the leptonic part of the amplitude for $e^+e^- \to \gamma^* \to q\bar{q}g$. The current j^μ is

$$j^\mu = \sum_a \bar{q}^a\gamma^\mu q^a, \tag{4.19}$$

[7] This condition is a consequence of our insistence on using operators with exactly N directions to create the final state. We could move away from the large-t limit and account for corrections to it by using a basis of operators with arbitrary numbers of jets and properly accounting for the regions of overlap between an N jet operator and $(N \pm 1)$-jet operators. This is outside the scope of the present work, where we limit ourselves to kinematics well described by an N-jet operator, and thus, limit ourselves to the large-t limit.

summing over colors a. For simplicity we work with a single quark flavor.

When the three jet directions are well separated, we can match the QCD current $j^\mu(x)$ onto a basis of three-jet operators in SCET [31, 165]. We build these operators from quark jet fields χ_n, related to collinear quark fields ξ_n by $\chi_n = W_n^\dagger \xi_n$, where W_n is given by Eq. (4.14), and a gluon jet field $B_n^\perp$ related to gluons A_n by

$$B_n^\perp = \frac{1}{g} W_n^\dagger (\mathcal{P}_\perp + A_n^\perp) W_n \,. \tag{4.20}$$

The matching relation is

$$j^\mu(x) = \sum_{n_1 n_2 n_3} \sum_{\tilde{p}_1 \tilde{p}_2 \tilde{p}_3} e^{i(\tilde{p}_1 - \tilde{p}_2 + \tilde{p}_3)\cdot x} C^\mu_{\alpha\beta\nu}(n_1, \tilde{p}_1; n_2, \tilde{p}_2; n_3, \tilde{p}_3) \bar{\chi}^\alpha_{n_1, p_1} (g B^{\perp\nu}_{n_3, p_3}) \chi^\beta_{n_2, p_2}(x) \,, \tag{4.21}$$

with sums over Dirac spinor indices α, β and Lorentz index ν, and over label directions $n_{1,2,3}$ and label momenta $\tilde{p}_{1,2,3}$. We have chosen to produce a quark in direction n_1, antiquark in n_2, and gluon in n_3. The matching coefficients $C^\mu_{\alpha\beta\nu}$ are found by equating QCD matrix elements of j^μ to SCET matrix elements of the right-hand side of Eq. (4.21). These coefficients have been found at tree level in [165]. The number of independent Dirac and Lorentz structures that can actually appear with nonzero coefficients is considerably smaller than suggested by Eq. (4.21) due to symmetries. We will keep the form of these coefficients general to make extension to N jets transparent, which would require the introduction of a basis of N jet fields in Eq. (4.21), with specified numbers of quark, antiquark, and gluon fields. We will not write the details for an N-jet cross section here, but the procedures are obvious extensions of all the steps in factorizing the 3-jet cross section below.

As a final step before factorization, we redefine the collinear fields to decouple collinear-soft interactions in the Lagrangian [29]:

$$\chi_n(x) = Y_n^\dagger(x) \chi_n^{(0)}(x) \tag{4.22a}$$

$$\bar{\chi}_n(x) = \bar{\chi}_n^{(0)}(x) Y_n(x) \tag{4.22b}$$

$$A_n(x) = \mathcal{Y}_n(x) A_n^{(0)}(x) \,, \tag{4.22c}$$

where Y_n is a Wilson line of soft gluons along the light-cone direction n,

$$Y_n(x) = P \exp\left[ig \int_0^\infty ds\, n \cdot A_s(ns + x) \right] , \tag{4.23}$$

with A_s in the fundamental representation.[8] $\mathcal{Y}_n$ is similar but in the adjoint representation. The new fields $\chi_n^{(0)}, A_n^{(0)}$ do not have interactions with soft fields in the SCET Lagrangian at leading order in λ. Henceforth, we use only these redefined fields, but for simplicity drop the (0) superscripts.

[8] The path choice (0 to ∞) in Eq. (4.23) is convenient for outgoing particles. The physical cross section is independent of whether the path goes to $\pm\infty$ if the transformation of the external states X is also taken into account [9].

The cross section in SCET can now be written,

$$\begin{aligned}\frac{d\sigma}{d\tau_a^1 d^3\mathbf{P}_{1,2,3}} = \frac{L^2}{6Q^2}\sum_X \delta_{N(\mathcal{J}(X)),3}\delta(\tau_a^1 - \tau_a(\text{jet } 1))\prod_{j=1}^{3}\delta^3(\mathbf{P}_j - \mathbf{P}(\text{jet } j)) \\ \times \sum_{n_{1,2,3}}\sum_{\tilde{p}_{1,2,3}}\int d^4x\, e^{i(Q-\tilde{p}_1+\tilde{p}_2-\tilde{p}_3)\cdot x} C^{\mu}_{\alpha\beta\nu}(n_{1,2,3};\tilde{p}_{1,2,3}) C^{*}_{\mu\gamma\delta\rho}(n_{1,2,3};\tilde{p}_{1,2,3}) \\ \times \langle 0|\,\bar{T}\Big\{\bar{\chi}^{a\delta}_{n_2,p_2} Y^{ab}_{n_2}\mathcal{Y}^{AB}_{n_3}(gB^{\perp\rho B}_{n_3,p_3})T^A_{bc}Y^{\dagger cd}_{n_1}\chi^{d\gamma}_{n_1,p_1}(x)\Big\}\,|X\rangle \\ \times \langle X|\,T\Big\{\bar{\chi}^{e\alpha}_{n_1,p_1} Y^{ef}_{n_1}\mathcal{Y}^{CD}_{n_3}(gB^{\perp\nu D}_{n_3,p_3})T^C_{fg}Y^{\dagger gh}_{n_2}\chi^{h\beta}_{n_2,p_2}(0)\Big\}\,|0\rangle\ .\end{aligned} \tag{4.24}$$

To proceed to factorize this cross section, it is convenient to rewrite the remaining delta functions that depend on the final state X in terms of operators acting on X. Those quantities depending on the jet algorithm $\mathcal{J}$ can be rewritten in terms of an operator containing the momentum flow operator,

$$\mathcal{E}_\mu(\mathbf{n}) = \lim_{R\to\infty}\int_0^\infty dt\, n_i T_{\mu i}(t, R\mathbf{n})\,, \tag{4.25}$$

where $T_{\mu\nu}$ is the energy-momentum tensor. The operator $\mathcal{E}_\mu(\mathbf{n})$ measures the flow of four-momentum P_μ in the direction $\mathbf{n}$ (cf. [18, 150, 44]), and the jet algorithm $\mathcal{J}$ can be written as an operator $\hat{\mathcal{J}}$ acting on the momentum flow in all directions [23]. Correspondingly we can define an operator for the 3-momentum of the jet, $\hat{\mathbf{P}}(J_j(\hat{\mathcal{J}}))$. In addition, the event shape $\tau_a(\text{jet } 1)$ can also be expressed as an operator $\hat{\tau}_a(J_1(\hat{\mathcal{J}}))$, built from the momentum flow operator, acting on the state $|X\rangle$ (cf. [18]):

$$\hat{\tau}_a(J_1(\hat{\mathcal{J}})) = \int d\eta\, e^{-\eta(1-a)}\mathcal{E}_T(\eta)\Theta(\eta - \eta_{\min}(J_1(\hat{\mathcal{J}})))\,. \tag{4.26}$$

The operator is constructed to count only particles actually entering the jet in direction n_1 determined by the action of the jet algorithm (for simplicity we will suppress the argument $J_1(\hat{\mathcal{J}})$ of $\hat{\tau}_a$ in the following, but add a superscript for the jet number). Using these operators, we can eliminate the X dependence in the delta functions in Eq. (4.24) and perform the sum over states X, obtaining

$$\begin{aligned}\frac{d\sigma}{d\tau_a^1 d^3\mathbf{P}_{1,2,3}} = \frac{L^2}{6Q^2}\sum_{n_{1,2,3}}\sum_{\tilde{p}_{1,2,3}}\int d^4x\, e^{i(Q-\tilde{p}_1+\tilde{p}_2-\tilde{p}_3)\cdot x} C^{\mu}_{\alpha\beta\nu}(n_{1,2,3};\tilde{p}_{1,2,3}) C^{*}_{\mu\gamma\delta\rho}(n_{1,2,3};\tilde{p}_{1,2,3}) \\ \times \langle 0|\,\bar{T}\Big\{\bar{\chi}^{a\delta}_{n_2,p_2} Y^{ab}_{n_2}\mathcal{Y}^{AB}_{n_3}(gB^{\perp\rho B}_{n_3,p_3})T^A_{bc}Y^{\dagger cd}_{n_1}\chi^{d\gamma}_{n_1,p_1}(x)\Big\} \\ \times \delta_{N(\hat{\mathcal{J}}),3}\delta(\tau_a^1 - \hat{\tau}_a^1)\prod_{j=1}^{3}\delta^3(\mathbf{P}_j - \hat{\mathbf{P}}(J_j(\hat{\mathcal{J}}))) \\ \times T\Big\{\bar{\chi}^{e\alpha}_{n_1,p_1} Y^{ef}_{n_1}\mathcal{Y}^{CD}_{n_3}(gB^{\perp\nu D}_{n_3,p_3})T^C_{fg}Y^{\dagger gh}_{n_2}\chi^{h\beta}_{n_2,p_2}(0)\Big\}\,|0\rangle\ .\end{aligned} \tag{4.27}$$

The matrix element can be calculated as the sum over cuts of time-ordered Feynman graphs, with the delta function operators inside the matrix element enforcing phase space restrictions from the jet algorithm and jet shape measurement on the final state created by the cut.

The operators $\hat{\tau}_a$ and $\hat{\mathcal{J}}$ depend linearly on the energy-momentum tensor, which itself splits linearly in SCET into separate collinear and soft pieces,

$$T_{\mu\nu} = \sum_i T^{n_i}_{\mu\nu} + T^s_{\mu\nu}\,, \tag{4.28}$$

which will aid us to factorize the full matrix element in Eq. (4.27) into separate collinear and soft matrix elements. To achieve this factorization, however, we must make some more approximations:

1. The contribution of soft particles and residual collinear momenta to the momentum $\mathbf{P}(\text{jet } j)$ of each jet can be neglected, and the jet momentum is just given by the label momentum $\tilde{p}_j$ of the collinear state $|X_j\rangle$. Thus the energy and jet axis of each jet is approximated to be that of the parent collinear parton initiating the jet. In particular, the mass of the jet is order λ^2 compared to its energy. So in this approximation we take the jet energy to be equal to the magnitude of its 3-momentum. On the other hand, we keep the leading non-zero contribution to the angularity even though it is also of order λ^2. These approximations also require that we treat the energy of any particles outside all of the jets, and thus the cutoff Λ, as a soft or residual energy.

2. The Kronecker delta restricting the total number of jets to 3 can be factored into three separate Kronecker deltas restricting the number of jets in each collinear direction n_i to 1, and one Kronecker delta restricting the soft particles not to create an additional jet. This approximation requires the separation between jets to be much larger than the size of any individual jet so that different jets do not overlap. Factoring the restriction on the number of jets in this way is one reason that the parameter t_{ij} in Eq. (4.5) is required to be large.

We describe to what extent the algorithms we consider actually satisfy these two approximations in Sec. 4.4. For now we assume these approximations and facts hold, which allows us to factor the cross section Eq. (4.24),

$$\begin{aligned}
\frac{d\sigma}{d\tau_a^1 dE_{1,2,3} d^2\Omega_{1,2,3}} &= \frac{L^2}{6Q^2} \sum_{n_{1,2,3}} \sum_{\omega_{1,2,3}} C^{\mu}_{\alpha\beta\nu}(n_{1,2,3};\omega_{1,2,3}) C^{*}_{\mu\gamma\delta\rho}(n_{1,2,3};\omega_{1,2,3}) \\
&\times \int d^4x\, e^{i(Q-\omega_1 n_1/2+\omega_2 n_2/2-\omega_3 n_3/2)\cdot x} \int d\tau_J d\tau_S \delta(\tau_a^1 - \tau_J - \tau_S) \\
&\times \langle 0|\, \chi^{f\gamma}_{n_1,\omega_1}(x) \delta_{N(\hat{\mathcal{J}}),1} \delta(\tau_J - \hat{\tau}_a^{n_1}) \bar{\chi}^{e\alpha}_{n_1,\omega_1}(0)\, |0\rangle\, \delta\left(E_1 - \frac{\omega_1}{2}\right) \delta^2(\Omega_1 - \mathbf{n}_1) \\
&\times \langle 0|\, \bar{\chi}^{a\delta}_{n_2,-\omega_2}(x) \delta_{N(\hat{\mathcal{J}}),1} \chi^{h\beta}_{n_2,-\omega_2}(0)\, |0\rangle\, \delta\left(E_2 - \frac{\omega_2}{2}\right) \delta^2(\Omega_2 - \mathbf{n}_2) \\
&\times \langle 0|\, (gB^{\perp\rho A}_{n_3,\omega_3})(x) \delta_{N(\hat{\mathcal{J}}),1} (gB^{\perp\nu B}_{n_3,\omega_3}(0)\, |0\rangle\, \delta\left(E_3 - \frac{\omega_3}{2}\right) \delta^2(\Omega_3 - \mathbf{n}_3) \\
&\times \langle 0|\, \overline{Y}^{\dagger ab}_{n_2} Y^{\dagger bc}_{n_3} T^A_{cd} \overline{Y}^{\dagger de}_{n_3} Y^{\dagger ef}_{n_1}(x) \delta_{N(\hat{\mathcal{J}}),0} \delta(\tau_S - \hat{\tau}_a^s) Y^{gh}_{n_1} \overline{Y}^{hi}_{n_3} T^B_{ij} Y^{jk}_{n_3} \overline{Y}^{kl}_{n_2}(0)\, |0\rangle
\end{aligned} \tag{4.29}$$

We have rewritten the cross section to be differential in E_i (the magnitude of $\mathbf{P}_i$) and Ω_i (the direction of $\mathbf{P}_i$). In the sum over label directions, $\mathbf{n}_i$ can be chosen to align with $\mathbf{P}_i$ such that $\tilde{p}_i^{\perp} = 0$. In Eq. (4.29) we have written the label momentum as $\omega_i \equiv \bar{n}_i \cdot \tilde{p}_i$. In Eq. (4.1) we approximate the jet axis by this $\mathbf{n}_i$ and the jet energy by $\bar{n}_i \cdot \tilde{p}_i/2$, so that they do not depend

on soft momenta at all. The operators $\hat{\tau}_a^{n_1}$ and $\hat{\tau}_a^s$ are defined to count only particles inside the measured jet identified by the algorithm.

In the soft matrix element in Eq. (4.29), we have introduced the soft Wilson line $\overline{Y}_n$ in the antifundamental representation to remove the time- and anti-time-ordering operators $T, \bar{T}$ in Eq. (4.24) [24], and related Wilson lines $\mathcal{Y}_n$ in the adjoint representation to those in the fundamental representation by [29]

$$\mathcal{Y}_n^{AB} T^B = Y_n^\dagger T^A Y_n \,. \tag{4.30}$$

Defining the jet functions by the relations

$$\int \frac{d^4k_1}{(2\pi)^4} e^{-ik_1\cdot x} J_{n_1,\omega_1}(\tau_J, n_1\cdot k_1) \left(\frac{\bar{n}\!\!\!/_1}{2}\right)_{\gamma\alpha} \delta^{ef} = \langle 0|\, \chi^{f\gamma}_{n_1,\omega_1}(x) \delta_{N(\hat{\mathcal{J}}),1} \delta(\tau_J - \hat{\tau}_a^{n_1}) \bar{\chi}^{e\alpha}_{n_1,\omega_1}(0)\,|0\rangle \tag{4.31a}$$

$$\int \frac{d^4k_2}{(2\pi)^4} e^{-ik_2\cdot x} J_{n_2,\omega_2}(n_2\cdot k_2) \left(\frac{n\!\!\!/_2}{2}\right)_{\beta\delta} \delta^{ah} = \langle 0|\, \bar{\chi}^{a\delta}_{n_2,\omega_2}(x) \delta_{N(\hat{\mathcal{J}}),1} \chi^{h\beta}_{n_2,\omega_2}(0)\,|0\rangle \tag{4.31b}$$

$$\int \frac{d^4k_3}{(2\pi)^4} e^{-ik_3\cdot x} J_{n_3,\omega_3}(n_3\cdot k_3) g_\perp^{\rho\nu} \delta^{AB} = -\omega_3 \,\langle 0|\, (gB^{\perp\rho A}_{n_3,\omega_3}) \delta_{N(\hat{\mathcal{J}}),1} (gB^{\perp\nu B}_{n_3,\omega_3})\,|0\rangle \,, \tag{4.31c}$$

and the soft function by

$$\begin{aligned} \int \frac{d^4r}{(2\pi)^4} e^{-ir\cdot x} S(\tau_s, r) = \frac{1}{N_C C_F} \,\mathrm{Tr}\, \langle 0|\, \overline{Y}^\dagger_{n_2} \overline{Y}^\dagger_{n_3} T^A Y^\dagger_{n_3} Y^\dagger_{n_1}(x) \delta_{N(\hat{\mathcal{J}}),0} \delta(\tau_S - \hat{\tau}_a^s) \\ \times Y_{n_1} Y_{n_3} T^B Y_{n_3} \overline{Y}_{n_2}(0)\,|0\rangle \end{aligned} \tag{4.32}$$

we can express the cross section Eq. (4.29) as

$$\begin{aligned} \frac{d\sigma}{d\tau_a^1 dE_{1,2,3} d^2\Omega_{1,2,3}} = \frac{L^2 N_C C_F}{6Q^2} \sum_{n_{1,2,3}} \sum_{\omega_{1,2,3}} \int d^4x\, e^{i[Q - (\omega_1 n_1 - \omega_2 n_2 + \omega_3 n_3)/2]\cdot x} \\ \times C^\mu_{\alpha\beta\nu}(n_{1,2,3}; \omega_{1,2,3}) C^*_{\mu\gamma\delta\rho}(n_{1,2,3}, \omega_{1,2,3}) \left(\frac{\bar{n}\!\!\!/_1}{2}\right)_{\gamma\alpha} \left(\frac{n\!\!\!/_2}{2}\right)_{\beta\delta} g_\perp^{\nu\rho} \\ \times \int d\tau_J d\tau_S \delta(\tau_a^1 - \tau_J - \tau_S) \prod_{i=1}^3 \delta\left(E_i - \frac{\omega_i}{2}\right) \delta^2(\Omega_i - \mathbf{n_i}) \\ \times \int \frac{d^4k_1}{(2\pi)^4} e^{-ik_1\cdot x} \int \frac{d^4k_2}{(2\pi)^4} e^{-ik_2\cdot x} \int \frac{d^4k_3}{(2\pi)^4} e^{-ik_3\cdot x} \int \frac{d^4r}{(2\pi)^4} e^{-ir\cdot x} \\ \times J_{n_1,\omega_1}(\tau_J, n_1\cdot k_1) J_{n_2,-\omega_2}(n_2\cdot k_2) J_{n_3,\omega_3}(n_3\cdot k_3) S(\tau_S, r)\,, \end{aligned} \tag{4.33}$$

where now $P_i = E_i(1, \mathbf{n}_i)$. The jet functions depend only on the smallest component of momentum $n_i\cdot k_i$ in each collinear direction. The residual and soft momenta appearing in the exponentials can be reabsorbed into the label momenta by a series of reparameterizations of the label momenta and directions, under which the SCET Lagrangian is invariant [162]. The three-jet operator Eq. (4.21) will receive corrections of order λ^2 (which we can drop) under the reparameterizations we perform below, or can be constructed from the outset to be explicitly reparameterization invariant (RPI) [165].

First, collect the residual and soft momenta together by defining $K = k_1 + k_2 + k_3 + r$. We can decompose x in n_1 light-cone coordinates, so

$$e^{-iK\cdot x} = e^{-i(\bar{n}_1\cdot K\, n_1\cdot x/2 + n_1\cdot K\, \bar{n}_1\cdot x/2 + K_{\perp 1}\cdot x_{\perp 1})}\,. \tag{4.34}$$

Performing a type-A transformation (in the language of [162]) on the label momentum $\tilde{p}_1 = \omega_1 n_1/2$,

$$\omega_1 \to \omega_1 + \bar{n}_1\cdot K\,, \tag{4.35}$$

and a type-IB transformation on the vector n_1 itself,

$$n_1 \to n_1 + \Delta^\perp\,, \quad \Delta^\perp = -\frac{2}{\omega_1}K^\perp\,, \tag{4.36}$$

shifts the label momentum on the jet function 1 by $\omega_1 n_1/2 \to (\omega_1 + \bar{n}_1\cdot K)n_1/2 + K_{\perp 1}$. The summation variables n_1, ω_1 can then be shifted to eliminate $\bar{n}_1\cdot K$ and $K_{\perp 1}$ from the exponentials entirely. We drop all corrections suppressed by λ^2 due to these shifts.

It remains to absorb the $n_1\cdot K$ component of residual and soft momentum, appearing in the exponential factor $e^{-in_1\cdot K\,\bar{n}_1\cdot x/2}$. This cannot be achieved by RPI transformations in the n_1 sector since this momentum is purely residual—there is no label momentum in this direction. However, in a multijet cross section, $\bar{n}_1$ can be written as a linear combination of n_2, n_3, and, say, $n_{\perp 2}$ (unit vector transverse to $n_2, \bar{n}_2$), so that RPI transformations on ω_2, ω_3 and n_2 similar to those above can absorb $n_1\cdot K$ into the label momenta also. Then, the x-dependent residual and soft exponentials all disappear, and we can combine the nine superfluous $\bar{n}_i\cdot k_i$ and $k_{\perp i}$ integrals with the nine discrete sums over label directions and momenta to give continuous integrals over total momenta. Performing these with the remaining energy and direction delta functions in Eq. (4.33) and the x integral with the remaining exponential gives the momentum conservation delta function $\delta^4(Q - E_1 n_1 - E_2 n_2 - E_3 n_3)$.

The resulting cross section Eq. (4.33) takes the form

$$\begin{aligned}\frac{d\sigma}{d\tau_a^1 dE_{1,2,3} d^2\mathbf{n}_{1,2,3}} = \frac{d\sigma^{(0)}}{dE_{1,2,3} d^2\mathbf{n}_{1,2,3}} H(n_{1,2,3}; E_{1,2,3}) \int d\tau_J d\tau_S \delta(\tau_a^1 - \tau_J - \tau_S) \\ \times \int \frac{dn_1\cdot k_1}{2\pi}\int \frac{dn_2\cdot k_2}{2\pi}\int \frac{dn_3\cdot k_3}{2\pi}\int \frac{d^4 r}{(2\pi)^4} \\ \times J_{n_1,2E_1}(\tau_J, n_1\cdot k_1) J_{n_2,2E_2}(n_2\cdot k_2) J_{n_3,2E_3}(n_3\cdot k_3) S(\tau_S, r)\,,\end{aligned} \tag{4.37}$$

where we used that the matching coefficients $C^\mu_{\alpha\beta\nu}(n_i; \tilde{p}_i)$ are such that, by construction, the right-hand side at tree-level is simply the Born cross section (denoted by $\sigma^{(0)}$) for $e^+e^- \to q\bar{q}g$ times $\delta(\tau_a^1)$. The hard function $H = 1 + \mathcal{O}(\alpha_s)$ is determined by calculating the matching coefficients C order-by-order in perturbation theory.

The above may be modified in the obvious ways to describe the antiquark or gluon jet angularities, by moving the appropriate delta function $\delta(\tau_a^i - \tau_a(\text{jet } i))$ into the J_2 or J_3 jet functions. In addition, we may choose from among various jet algorithms. The choice determines what Θ-function restrictions must be inserted into the final state phase space integrations created by cutting the jet and soft diagrams to determine which particles make it into the jet. As long as the algorithm is such that the approximations enumerated above hold, it will not violate factorization of the jet shape cross section. We will discuss factorization and its potential breakdown in the context of particular jet algorithms below.

4.3 Jet Shapes in $e^+e^- \to N$ jets

To generalize the result Eq. (4.37) to an arbitary number N of jets, we simply add more quark and gluon jet fields to the operator matching in Eq. (4.21), and obtain the corresponding number of quark and gluon jet functions in Eq. (4.21), along with a hard coefficient and a soft function for N jet directions. Consider an event with $2N_q$ quark and antiquark jets and N_g gluon jets, where $2N_q + N_g = N$. Furthermore, we can choose to measure the angularity shape for any number of these jets. Achieving a factorization theorem that remains consistent for any of these combinations is a nontrivial task and thus a powerful test of the validity of the effective theory.

For an $N = 2N_q + N_g$ jet event, we generalize the matching of the QCD current in Eq. (4.21) to:

$$\begin{aligned} j^\mu(x) = \sum_{n_1 \cdots n_N} \sum_{\tilde{p}_1 \cdots \tilde{p}_N} & e^{i(\tilde{p}_1 + \cdots + \tilde{p}_N)\cdot x} C^{\mu a_1 \cdots a_{N_q} b_1 \cdots b_{N_q} A_1 \cdots A_{N_g}}_{\alpha_1 \cdots \alpha_{N_q} \beta_1 \cdots \beta_{N_q} \nu_1 \cdots \nu_{N_g}} (n_1, \tilde{p}_1; \cdots; n_N, \tilde{p}_N) \\ & \times \prod_{i=1}^{N_q} \bar{\chi}^{\alpha_i a_i}_{n_i, p_i}(x) \prod_{j=1}^{N_q} \chi^{\beta_j b_j}_{n_j, -\tilde{p}_j}(x) \prod_{k=1}^{N_g} (g B^{\perp \nu_k A_k}_{n_k, -\tilde{p}_k})(x) \,, \end{aligned} \tag{4.38}$$

with implicit sums over Dirac spinor indices α_i, β_j, Lorentz indices ν_k, (anti-)fundamental color indices a_i, b_j, and adjoint color indices A_k. The N jet cross section differential in M jet shapes, with $M < N$, factors in SCET into the form

$$\begin{aligned} \frac{d\sigma(E_1, \mathbf{n_1}; \cdots; E_N, \mathbf{n_N})}{d\tau^1_{a_1} \cdots d\tau^M_{a_M}} &= \sigma^{(0)}(E_1, \mathbf{n}_1; \cdots; E_N, \mathbf{n}_N) H^{a_i b_j A_k}(n_1, E_1; \cdots n_N, E_N) \\ &\times \prod_{l=1}^{M} \int d\tau^l_J d\tau^l_S \delta(\tau^l_a - \tau^l_J - \tau^l_S) \int \frac{dn_1 \cdot k_1}{2\pi} \cdots \int \frac{dn_N \cdot k_N}{2\pi} \\ &\times J^{f_1}_{n_1, 2E_1}(\tau^1_J; n_1 \cdot k_1) \cdots J^{f_M}_{n_M, 2E_M}(\tau^M_J; n_M \cdot k_M) \\ &\times J^{f_{M+1}}_{n_{M+1}, 2E_{M+1}}(n_{M+1} \cdot k_{M+1}) \cdots J^{f_N}_{n_N, 2E_N}(n_N \cdot k_N) \\ &\times \int \frac{d^4 r}{(2\pi)^4} S^{a_i b_j A_k}(\tau^1_S, \ldots, \tau^M_S; r) \,, \end{aligned} \tag{4.39}$$

where $\sigma^{(0)}$ is the Born cross section for e^+e^- to N_q quarks, N_q antiquarks, and N_g gluons; the color indices on the hard and soft functions H and S allow for color mixing; and f_i is the flavor of each jet function (quark, antiquark, or gluon). H itself is determined by calculating the matching coefficients C in Eq. (4.38). The jet functions have the same definitions given in Eq. (4.31), and the soft function is given by the appropriate generalization of Eq. (4.32) with Wilson lines in the directions and color representations corresponding to the choice of fields in Eq. (4.38). We rearrange the order of flavor and color indices in the hard and soft functions to agree with the choices of flavor indices on the jet functions.

4.4 Power Corrections to Factorization in the Presence of Jet Algorithms

Factorization of observables in the presence of jet algorithms can break down in a number of ways, for instance, when power corrections become too large. We will argue in this section

that power corrections for jet angularities induced by all commonly used algorithms can give $\mathcal{O}(1)$ effects unless the jet size R is parametrically larger than λ.[9] In order to use algorithms that have $R \sim \lambda$, we would need to minimize power corrections associated with the assumptions that we made in deriving the factorization formula, Eq. (4.39), regarding the action of jet algorithms on the final state. In general, the size of these power corrections depends both on the algorithm and the observable. Power corrections to the p_T of a jet arising from perturbative emissions (as well as from hadronization and the underlying event in pp collisions) for various jet algorithms were explored in [98]. These power corrections arise for similar reasons as those we discuss below, namely, perturbative emissions changing which partons get combined into the jet. Ref. [98] finds that such power corrections scale like $\ln R$ for small R. This result agrees with our qualitative discussion below, where we argue that power corrections to jet angularities arising from the jet algorithms we use are minimized when R is $\mathcal{O}(1)$.

One assumption that is independent of the choice of algorithm is in setting the jet axis equal to the label direction n. Since this neglects the effects of soft particles, it is valid up to $\mathcal{O}(\lambda^2)$ corrections. It was argued in Refs. [18, 47, 157] for the case of hemisphere jet algorithms that these corrections in turn induce corrections to the angularity τ_a of order $\lambda^{2(2-a)}$, which for $\tau_a \sim \lambda^2$, are subleading for $a < 1$. Essentially the same arguments can be applied to all of the algorithms we consider.

The main difference among jet algorithms is in which soft particles are included in a jet. For observables that scale as $\mathcal{O}(1)$, such as the jet energies and 3-momenta, the contribution of soft momenta can be neglected since they scale as $\mathcal{O}(\lambda^2)$. Clearly then, these observables are not dependent on our choice of jet algorithm and so the assumptions we made about factorization of the algorithm in deriving Eq. (4.39) are trivially satisfied.

However, for observables that scale as $\mathcal{O}(\lambda^2)$ such as angularities, soft contributions become important and so the details of the algorithms we consider become relevant. We now demonstrate that all of the algorithms we consider miscount soft particles in an angular area of $\mathcal{O}(\lambda^2)$ relative to what the soft function can include, which is an area of $\mathcal{O}(R^2)$. This means that any measurement that is sensitive to soft momenta needs jets of size $R \gg \lambda$ for these power corrections to be considered negligible. This miscounting arises due to the fact that factorization requires that collinear particles be combined first, and that the soft function only knows about the parent collinear direction. None of the algorithms that we consider strictly obey this ordering.

In Fig. 4.1, we illustrate the actions of the $\mathrm{k_T}$ and anti-$\mathrm{k_T}$ algorithms in relation to the action of the soft function for the example of one parent particle splitting into two collinear daughter particles separated by an angular distance θ_{ij}. The two dots represent the daughter particles and the "$\times$" denotes the parent particle. Factorization assumes that all soft particles only know about the parent particle, and hence the soft function can only include particles in a circle of radius R around the parent particle.

The $\mathrm{k_T}$ algorithm effectively finds the softest particle and then combines this particle with its nearest neighbor. This process is iterated until all particles within a distance R are combined. Since collinear particles are combined last, all soft particles within two circles of radius R about the

[9] We noted earlier that there may be different λ's for the SCET modes describing different jets. For measured jets, $\lambda^2 \sim \tau_a$, while for unmeasured jets, $\lambda \sim \tan(R/2)$, and for soft gluons outside jets, $\lambda^2 \sim \Lambda/Q$. Here it is mainly important that R be much bigger than the scale associated with τ_a. But if R is too large, the separation parameter $t \propto 1/\tan(R/2)$ becomes too small. We will consider $R \sim 0.7$ to 1 to be safe.

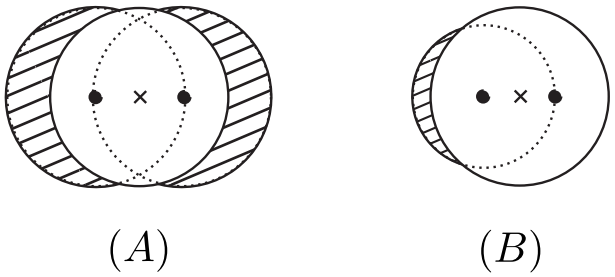

Figure 4.1: Error induced by the (A) k_T and (B) anti-k_T algorithms at NLO. Both the algorithm and the soft function merge the large white circle. The algorithm also merges the cross-hatched area which occupies a region of phase space which is of $\mathcal{O}(\theta_{ij}^2)$ for both algorithms.

daughter particles are included,[10] as shown in Fig. 4.1A. The area that the k_T algorithm includes that the soft function does not is represented by the cross-hatched region, which is an area of $\mathcal{O}(\theta_{ij}^2)$. This must be parametrically smaller than the area included by the soft function for the associated power corrections to be small. We thus require that $R \gg \theta_{ij} \sim \lambda$ in the SCET power counting.

The anti-k_T algorithm at first sight combines particles in a manner that is closer to respecting factorization. It finds the hardest particle first and merges particles at successively larger distance from this particle. For the example of two daughters, it will merge all soft particles with the hardest daughter that are closer than the distance to the softer daughter before merging the two daughters and then merging all soft particles a distance R from the merged daughter (i.e., the parent) particle, as shown in Fig. 4.1B. As the Figure illustrates, the cross-hatched area of the anti-k_T jet tends to be less than that of the k_T jet, but it is still formally of $\mathcal{O}(\theta_{ij}^2)$. Again, we require that $R \gg \lambda$ for this algorithm to be applicable.

Unlike the k_T-type algorithms, cone algorithms such as the SISCone algorithm do not induce errors in which soft particles to include when there are only two collinear daughter particles. However, at higher orders in perturbation theory, stable solutions may exist with overlapping cones when collinear splittings are of the order of the cone radius R. In these cases, the amount of radiation that falls into the overlapping region is used to decide whether the cones are split or merged. If merged, the resulting region has the appearance of Fig. 4.1A. Thus, as for the k_T-type algorithms, we require that R is parametrically larger than the SCET parameter λ for power corrections to all-orders factorization to be small. For the remainder of this chapter, we take R to be $\mathcal{O}(1)$ in the λ power counting and we will mainly be concerned with the resummation of the jet observables such as angularities τ_a in the presence of jet algorithms.[11]

Another requirement for the validity of the factorization theorem is that the factorized jet and soft functions be separately IR safe, which is a stronger condition than the full cross section being IR safe. If the observable [134, 135] or algorithm [85] too strongly weights final states with narrow jets whose invariant masses are the same as the virtuality of soft particles, then the jet

[10] Soft particles in this region can also by removed from this region by merging with other soft particles outside of the region and vice-versa, but this average area suffices for our discussion.

[11] Because small R ($\lesssim 0.3$) jets cannot be well resolved in current experiments, resummation of logarithms of R is not of primary practical importance in the near future.

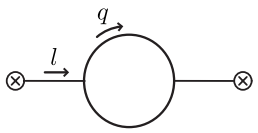

Figure 4.2: A representative diagram for the NLO quark and gluon jet functions. The incoming momentum is $l = \frac{n}{2}\omega + \frac{\bar{n}}{2}l^+$ and particles in the loop carry momentum q ("particle 1") and $l - q$ ("particle 2").

and soft functions for the observable in standard SCET with dimensional regularization become IR divergent. When this occurs it does not necessarily mean that factorization is not possible; but at least not in the standard form derived from the version of SCET we utilized above. It could be, for example, that a scheme to further separate modes by defining the theory with an explicit cutoff [85] or by factorizing modes by rapidity instead of virtuality [163] can restore a version of the factorization theorem. We leave a explicit study of which algorithms and observables give IR safe jet and soft functions in SCET in dimensional regularization for a separate publication. However, we note here that the algorithms and observables (τ_a for $a < 1$) that we consider in this chapter, at least at NLO, do give rise to IR safe jet and soft functions.

In addition to minimizing power corrections to ensure factorizability, in order to resum logarithms of jet algorithm parameters to all orders in perturbation theory, the algorithms have to act at all orders in perturbation theory in a way that mimics what they do at NLO. Otherwise, we cannot use information from a fixed order in perturbation theory to obtain all-orders resummed results. The JADE algorithm is one well-known example in which resummability even of leading logarithms of the jet mass cut y is spoiled by the differences in the jet phase space at different orders in perturbation theory [57]. [12] We do not in this work tackle the full problem of resummability of logarithms of R and other phase space cuts, but instead focus just on resumming logs of the jet shape τ_a when the jets are defined with an algorithm.

5 Jet Functions at $\mathcal{O}(\alpha_s)$ for Jet Shapes

In this section, we calculate the quark and gluon jet functions for jet shapes at next-to-leading order in perturbation theory. The jet functions can be divided into two categories: those for measured jets, which are fixed to have a specific angularity τ_a, and those for unmeasured jets, which are not. We will denote the quark jet function by J^q_ω, the gluon jet function by J^g_ω, where ω is the label momentum, and a jet function $J^{q,g}(\tau_a)$ with an argument of τ_a denotes a measured jet. We will calculate the jet functions for the two classes of jet algorithms, $\mathrm{k_T}$-type and cone-type algorithms.

5.1 Phase Space Cuts

To calculate the jet functions for a particular algorithm, we must impose phase space restrictions in the matrix element. From the jet function definitions, Eq. (4.31), these cuts take two forms. One kind, imposed by the operator $\delta_{N(\hat{\mathcal{J}}),1}$ in Eq. (4.31), is common to every jet function. It is the set of phase space restrictions related to the jet algorithm, and requires exactly one jet to arise from each collinear sector of SCET. The other, imposed by the operator $\delta(\tau_a - \hat{\tau}_a)$, is implemented only on measured jets and restricts the kinematics of the cut final states to produce a fixed value of the jet shape. In this section we describe these phase space cuts in detail.

The typical form of the NLO diagrams in the jet functions is shown in Fig. 4.2. As shown in the figure, the momentum flowing through the graph has label momentum $l^- \equiv \bar{n} \cdot l = \omega$ and residual momentum $l^+ \equiv n \cdot l$, and the loop momentum is q. We will label "particle 1" as the particle in the loop with momentum q and "particle 2" as the particle in the loop with momentum $l - q$. For the quark jet, we take particle 1 as the emitted gluon and particle 2 as the quark.

As usual, the total forward scattering matrix element can be written as a sum over all cuts. Cutting through the loops corresponds to the interference of two real emission diagrams, each with two final state particles, whereas cutting through a lone propagator that is connected to a current corresponds to the interference between a tree-level diagram and a virtual diagram, each with a single final state particle. Thus, the phase space restrictions and measurements we impose act differently depending on where the diagrams are cut. In addition, since we will be working in dimensional regularization (with $d = 4 - 2\epsilon$), which sets scaleless integrals to zero, the only diagrams that contribute are the cuts through the loops. This means that we only need to focus on the form of phase-space restrictions and angularities in the case of final states with two particles.

The regions of phase space for two particles created by cutting through a loop in the jet function diagrams can be divided into three contributions:

1. Both particles are inside the jet.
2. Particle 1 exits the jet with energy $E_1 < \Lambda$.
3. Particle 2 exits the jet with energy $E_2 < \Lambda$.

In contributions (2) and (3), the jet has only one particle, which is the remaining particle with $E > \Lambda$.

It is well known that collinear integrations of jet functions can be allowed to extend over all values of loop momenta so long as a "zero-bin subtraction" is taken from the result to avoid double counting the soft region already accounted for in the soft function [163]. We will demonstrate that contributions (2) and (3) are power suppressed by $\mathcal{O}(\Lambda/\omega)$, which scales as λ^2, after the zero-bin subtraction.

The phase space cuts that enforce both particles to be in the jet depend on the jet algorithm. There are two classes of jet algorithms that we consider, cone-type algorithms and (inclusive) k_T-type algorithms, and all the algorithms in each class yield the same phase space cuts. We label the phase space restrictions as Θ_{cone} and Θ_{k_T}, generically Θ_{alg}. For the cone-type

[12] Another obvious example that will not work, just to illustrate the issue, is using a k_T-type algorithm with R randomly chosen for each recombination. This is clearly such that resummation of logarithms of R cannot be achieved.

algorithms,

$$\Theta_{\text{cone}} \equiv \Theta_{\text{cone}}(q, l^+) = \Theta\left(\tan^2\frac{R}{2} > \frac{q^+}{q^-}\right)\Theta\left(\tan^2\frac{R}{2} > \frac{l^+ - q^+}{\omega - q^-}\right). \tag{4.40}$$

These Θ functions demand that both particles are within R of the label direction. For the k_T-type algorithms, the only restriction is that the relative angle of the particles be less than R:

$$\begin{aligned}\Theta_{k_T} \equiv \Theta_{k_T}(q, l^+) &= \Theta\left(\cos R < \frac{\vec{q}\cdot\vec{l} - q^2}{q\sqrt{l^2 + q^2 - 2\vec{q}\cdot\vec{l}}}\right) \\ &= \Theta\left(\tan^2\frac{R}{2} > \frac{q^+\omega^2}{q^-(\omega - q^-)^2}\right).\end{aligned} \tag{4.41}$$

In the second line we took the collinear scaling of q ($q^+ \ll q^-$). While this is not strictly needed, it makes the calculations significantly simpler.

For the phase space restrictions of zero-bin subtractions, we take the soft limit of the above restrictions. The zero-bin subtractions are the same for all the algorithms we consider. For the case of particle 1, which has momentum q, the zero-bin phase space cuts are given by

$$\Theta^{(0)}_{\text{alg}} = \Theta^{(0)}_{\text{cone}} = \Theta^{(0)}_{k_T} = \Theta\left(\tan^2\frac{R}{2} > \frac{q^+}{q^-}\right). \tag{4.42}$$

The zero bin of particle 2 is given by the replacement $q \to l - q$.

For all the jet algorithms we consider, the zero-bin subtractions of the unmeasured jet functions are scaleless integrals.[13] However, for the measured jet functions, the zero-bin subtractions give nonzero contributions that are needed for the consistency of the effective theory.

In the case of a measured jet, in addition to the phase space restrictions we also demand that the jet contributes to the angularity by an amount τ_a with the use of the delta function $\delta_R = \delta(\tau_a - \hat{\tau}_a)$, which is given in terms of q and l by

$$\delta_R \equiv \delta_R(q, l^+) = \delta\left(\tau_a - \frac{1}{\omega}(\omega - q^-)^{a/2}(l^+ - q^+)^{1-a/2} - \frac{1}{\omega}(q^-)^{a/2}(q^+)^{1-a/2}\right). \tag{4.43}$$

In the zero-bin subtraction of particle 1, the on-shell conditions can be used to write the corresponding zero-bin δ-function as

$$\delta^{(0)}_R = \delta\left(\tau_a - \frac{1}{\omega}(q^-)^{a/2}(q^+)^{1-a/2}\right), \tag{4.44}$$

(and for particle 2 with $q \to l - q$).

5.2 Quark Jet Function

The diagrams corresponding to the quark jet function are shown in Fig. 4.3. The fully inclusive quark jet function is defined as

$$\int d^4x\, e^{il\cdot x}\,\langle 0|\,\chi^{a\alpha}_{n,\omega}(x)\bar{\chi}^{b\beta}_{n,\omega}(0)\,|0\rangle \equiv \delta^{ab}\left(\frac{\bar{n}\!\!\!/}{2}\right)^{\alpha\beta} J^q_\omega(l^+), \tag{4.45}$$

[13] Note that algorithms do exist that give nonzero zero-bin contributions to unmeasured jet functions [85].

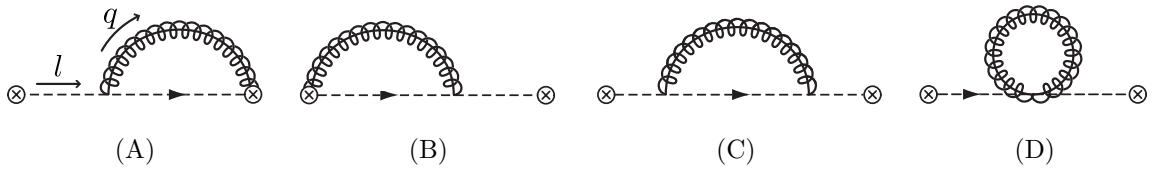

Figure 4.3: Diagrams contributing to the quark jet function. (A) and (B) Wilson line emission diagrams; (C) and (D) QCD-like diagrams. The momentum assignments are the same as in Fig. 4.2.

and has been computed to NLO (see, e.g., [25, 53]) and to NNLO [38]. Below we compute the quark jet function at NLO with phase space cuts for the jet algorithm for both the measured jet, $J^q_\omega(\tau_a)$, and the unmeasured jet, J^q_ω. As discussed above, we will find that the only nonzero contributions come from cuts through the loop when both cut particles are inside the jet.

5.2.1 Measured Quark Jet

The measured quark jet function includes contributions from naive Wilson line graphs (A) and (B) and QCD-like graphs (C) and (D) in Fig. 4.3. The sum of these contributions is

$$\begin{aligned}\tilde{J}^q_\omega(\tau_a) = g^2\mu^{2\epsilon}C_F \int \frac{dl^+}{2\pi}\frac{1}{(l^+)^2}\int \frac{d^dq}{(2\pi)^d}\left(4\frac{l^+}{q^-}+(d-2)\frac{l^+-q^+}{\omega-q^-}\right)2\pi\delta(q^-q^+-q_\perp^2)\\ \times\,\Theta(q^-)\Theta(q^+)2\pi\delta\left(l^+-q^+-\frac{q_\perp^2}{\omega-q^-}\right)\Theta(\omega-q^-)\Theta(l^+-q^+)\,\Theta_{\rm alg}\delta_R\,.\end{aligned} \tag{4.46}$$

The contribution proportional to $d-2$ comes from the QCD-like graphs (C) and (D) in Fig. 4.3. Only the Wilson line graphs have a nonzero zero-bin limit, which comes from taking the scaling limit $q\sim\lambda^2$ of the naive contribution:

$$\begin{aligned}J^{q(0)}_\omega(\tau_a) = 4g^2\mu^{2\epsilon}C_F \int \frac{dl^+}{2\pi}\frac{1}{l^+}\int \frac{d^dq}{(2\pi)^d}\frac{1}{q^-}2\pi\delta(q^-q^+-q_\perp^2)\Theta(q^-)\Theta(q^+)\\ \times\,2\pi\delta\left(l^+-q^+\right)\Theta(l^+-q^+)\,\Theta^{(0)}_{\rm alg}\delta^{(0)}_R\,.\end{aligned} \tag{4.47}$$

All jet algorithms that we use yield the same zero-bin contribution, since the phase space cuts are the same.

To evaluate these integrals, we can analytically extract the coefficient of $\delta(\tau_a)$ by integrating over τ_a and using the fact that remainder is a plus distribution, as defined in Eq. (4.138). We find the naive contribution is

$$\tilde{J}^q_\omega(\tau_a) = \frac{\alpha_s C_F}{2\pi}\frac{1}{\Gamma(1-\epsilon)}\left(\frac{4\pi\mu^2}{\omega^2\tan^2\frac{R}{2}}\right)^\epsilon\left(\frac{1}{\epsilon^2}+\frac{3}{2\epsilon}\right)\delta(\tau_a)+\frac{\alpha_s}{2\pi}\tilde{J}^q_{\rm alg}(\tau_a)\,. \tag{4.48}$$

The only difference between the jet algorithms that we consider resides in the finite distribution $\tilde{J}^q_{\rm alg}(\tau_a)$, which is a complicated function of τ_a that we give in Appendix 4.A. Note that the divergent part of the naive contribution is proportional to $\delta(\tau_a)$. This is due to the fact that the

jet algorithm regulates the distribution for $\tau_a > 0$. The divergent plus distributions come entirely from the zero-bin subtraction, which is given by

$$J_\omega^{q(0)}(\tau_a) = \frac{\alpha_s C_F}{\pi} \frac{1}{\Gamma(1-\epsilon)} \left(\frac{4\pi\mu^2 \tan^{2(1-a)} \frac{R}{2}}{\omega^2} \right)^\epsilon \frac{1}{(1-a)\epsilon} \frac{1}{\tau_a^{1+2\epsilon}} \,. \tag{4.49}$$

Adding the leading-order contribution to all of the NLO graphs and expanding in powers of ϵ, adopting the $\overline{\rm MS}$ scheme, we find the total quark jet function,

$$\begin{aligned} J_\omega^q(\tau_a) = \delta(\tau_a) + \tilde{J}_\omega^q(\tau_a) - J_\omega^{q(0)} = & \left\{ 1 + \frac{\alpha_s C_F}{\pi} \left[\frac{1-\frac{a}{2}}{1-a} \frac{1}{\epsilon^2} + \frac{1-\frac{a}{2}}{1-a} \frac{1}{\epsilon} \ln \frac{\mu^2}{\omega^2} + \frac{3}{4\epsilon} \right] \right\} \delta(\tau_a) \\ & - \frac{\alpha_s C_F}{\pi} \left[\frac{1}{\epsilon} \frac{1}{1-a} \frac{\Theta(\tau_a)}{\tau_a} \right]_+ + \frac{\alpha_s}{2\pi} J_{\rm alg}^q(\tau_a) \,. \end{aligned} \tag{4.50}$$

This agrees with the standard jet function $J(k^+)$ given in [25, 53] by setting $a = 0$ and $k^+ = \omega\tau_a$. We have shown the divergent terms explicitly, and collect the finite pieces in $J_{\rm alg}^q(\tau_a)$, which we give in Eq. (4.149). Note that there is no jet algorithm dependence in the divergent parts of the jet function at this order in perturbation theory.

5.2.2 Gluon Outside Measured Quark Jet

In this section we calculate the contribution to the quark jet function from the region of phase space in which the gluon exits the jet carrying an energy $E_g < \Lambda$. This cut causes the contribution to be power suppressed by Λ/ω, which scales as λ^2. However, we elect to evaluate this case explicitly as it provides a clear example of the zero-bin subtraction giving the proper scaling to the total contribution. We only evaluate this contribution for the cone algorithm; the details of the $\rm k_T$ algorithm calculation are similar. Note that the contribution when the quark is out of the jet is power suppressed at the level of the Lagrangian given in Sec. 4.1, in which soft quarks do not couple to collinear partons at leading order in λ.

For the cone algorithm, the gluon exits the jet when the angle between the jet axis, $\mathbf{n}_1$, and the gluon is greater than R. When the gluon is not in the jet, the cone axis is the quark direction, and so it makes no contribution to the angularity. Therefore, this region of phase space contributes only to the $\delta(\tau_a)$ part of the angularity distribution.

For the naive contributions, requiring the gluon to be outside the jet and have energy less than Λ, we have the integral

$$\begin{aligned} \tilde{J}_\omega^{q,\rm out}(\tau_a) = & g^2 \mu^{2\epsilon} C_F \int \frac{dl^+}{2\pi} \frac{1}{(l^+)^2} \int \frac{d^d q}{(2\pi)^d} \left(4\frac{l^+}{q^-} + (d-2)\frac{l^+ - q^+}{\omega - q^-} \right) 2\pi\delta(q^- q^+ - q_\perp^2) \\ & \times \Theta(q^-)\Theta(q^+) 2\pi\delta\left(l^+ - q^+ - \frac{q_\perp^2}{\omega - q^-} \right) \Theta(\omega - q^-)\Theta(l^+ - q^+) \\ & \times \Theta\left(\frac{q^+}{q^-} - \tan^2\frac{R}{2} \right) \Theta\left(2\Lambda - q^-\right) \delta(\tau_a) \,. \end{aligned} \tag{4.51}$$

Note that the theta function requiring $q^- < 2\Lambda$ is more restrictive than $q^- < \omega$. Evaluating Eq. (4.51) yields a contribution that scales with Λ only below the leading term in $1/\epsilon$:

$$\tilde{J}_\omega^{q,\text{out}}(\tau_a) = -\frac{\alpha_s C_F}{2\pi}\frac{1}{\Gamma(1-\epsilon)}\left(\frac{4\pi\mu^2}{(2\Lambda\tan\frac{R}{2})^2}\right)^\epsilon \delta(\tau_a)\left(\frac{1}{\epsilon^2}+\frac{1}{\epsilon}\left(\frac{4\Lambda}{\omega}-\frac{2\Lambda^2}{\omega^2}\right)+\frac{8\Lambda}{\omega}\right) \tag{4.52}$$

The zero-bin subtraction of Eq. 4.51 is

$$\begin{aligned}\tilde{J}_\omega^{q,\text{out}(0)}(\tau_a) = g^2\mu^{2\epsilon}C_F\int\frac{dl^+}{2\pi}\frac{1}{(l^+)^2}\int\frac{d^dq}{(2\pi)^d}\left(4\frac{l^+}{q^-}+(d-2)\frac{l^+-q^+}{\omega-q^-}\right)2\pi\delta(q^-q^+-q_\perp^2)\\ \times\Theta(q^-)\Theta(q^+)2\pi\delta\left(l^+-q^+\right)\Theta\left(\frac{q^+}{q^-}-\tan^2\frac{R}{2}\right)\Theta\left(2\Lambda-q^-\right)\delta(\tau_a)\,.\end{aligned} \tag{4.53}$$

Evaluating Eq. (4.53), we find the zero bin will exactly remove the leading term in $1/\epsilon$:

$$\tilde{J}_\omega^{q,\text{out}(0)}(\tau_a) = -\frac{\alpha_s C_F}{2\pi}\frac{1}{\Gamma(1-\epsilon)}\left(\frac{4\pi\mu^2}{(2\Lambda\tan\frac{R}{2})^2}\right)^\epsilon \delta(\tau_a)\frac{1}{\epsilon^2} \tag{4.54}$$

Therefore, the difference is power suppressed only after the zero bin is included. Because other contributions when one particle is outside of the jet are similarly power suppressed, we will drop them in our remaining discussion of the jet functions.

5.2.3 Unmeasured Quark Jet

When the angularity of a jet is not measured, the jet function has no τ_a dependence. The naive and zero-bin contributions are the same as Eqs. (4.46) and (4.47) except for the factor of δ_R. The zero-bin contribution is

$$\begin{aligned}J_\omega^{q(0)} = 2g^2\mu^{2\epsilon}C_F n\cdot\bar{n}\int\frac{dl^+}{2\pi}\frac{1}{l^+}\int\frac{d^dq}{(2\pi)^d}\frac{1}{q^-}2\pi\delta(q^-q^+-q_\perp^2)\Theta(q^-)\Theta(q^+)\\ \times 2\pi\delta\left(l^+-q^+\right)\Theta(l^+-q^+)\,\Theta_{\text{alg}}^{(0)}\,.\end{aligned} \tag{4.55}$$

This integral is scaleless and therefore equal to 0 in dimensional regularization. This implies that the NLO part of the quark jet function for an unmeasured jet is just the naive result. We find, making the divergent part explicit,

$$J_\omega^q = 1+\tilde{J}_\omega^q = 1+\frac{\alpha_s C_F}{2\pi}\left\{\frac{1}{\epsilon^2}+\frac{3}{2\epsilon}+\frac{1}{\epsilon}\ln\left(\frac{\mu^2}{\omega^2\tan^2\frac{R}{2}}\right)\right\}+\frac{\alpha_s}{2\pi}J_{\text{alg}}^q\,, \tag{4.56}$$

where the finite part J_{alg}^q is given in Eq. (4.150).[14]

[14]The unmeasured jet function Eq. (4.56) is not simply obtained by integrating the measured jet function Eq. (4.50) over τ_a. This is due to the different relative scaling of R with the SCET expansion parameter λ_i in a measured and unmeasured jet sector, as noted earlier. Namely, $R \sim \lambda_i^0$ in a measured jet sector (where $\lambda \sim \sqrt{\tau_a}$) while $\lambda_k \sim \tan(R/2)$ in an unmeasured jet sector.

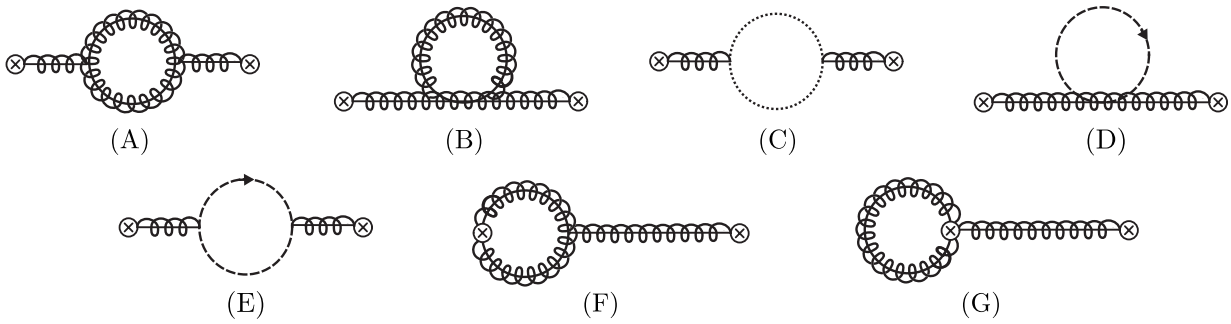

Figure 4.4: Diagrams contributing to the gluon jet function. (A) sunset and (B) tadpole gluon loops; (C) ghost loop; (D) sunset and (E) tadpole collinear quark loops; (F) and (G) Wilson line emission loops. Diagrams (F) and (G) each have mirror diagrams (not shown). The momentum assignments are the same as in Fig. 4.2.

5.3 Gluon Jet Function

The diagrams needed for the gluon jet function at NLO are shown in Fig. 4.4. The fully inclusive jet function, defined as

$$\int d^4x\, e^{il\cdot x}\, \langle 0|\, B^{\mu A}_{\perp,\omega}(x) B^{\nu B}_{\perp,\omega}(0)\, |0\rangle \equiv -\frac{1}{\omega} g_\perp^{\mu\nu} \delta^{AB} J^g_\omega(l^+)\,, \tag{4.57}$$

(with $J^g_\omega(l^+)$ normalized to $2\pi\delta(l^+)$ at tree-level) has been calculated to NLO in Feynman gauge in [31, 15, 126] and was reported to give the same result in both R_ξ and light-cone gauges in [42]. Since our phase space restrictions and the observables act differently on cuts through loops and on cuts through external propagators, it is useful to reproduce these results by explicitly cutting the diagrams.

After some algebra, we find that the sum of all cuts through the loops gives

$$\begin{aligned}\int \frac{dl^+}{2\pi} J^g_\omega(l^+) = \mu^{2\epsilon} \frac{2g^2}{(2\pi)^{d-1}} \int \frac{dl^+}{l^+} \int d^d q\, \delta(q^2)\delta((l-q)^2)\, \Theta(0<q^-<\omega) \\ \times \left[T_R N_f \left(1 - \frac{2}{1-\epsilon} \frac{q^+q^-}{\omega l^+} \right) - C_A \left(2 - \frac{\omega}{q^-} - \frac{\omega}{\omega - q^-} - \frac{q^+q^-}{\omega l^+} \right) \right]. \end{aligned} \tag{4.58}$$

In the absence of phase-space restrictions, this reduces to the standard (inclusive) gluon jet function

$$\frac{J^g_\omega(l^+)}{2\pi\omega} = \frac{\alpha_s}{4\pi} \mu^{2\epsilon} (\omega l^+)^{-1-\epsilon} \left[T_R N_f \left(\frac{4}{3} + \frac{20}{9}\epsilon \right) - C_A \left(\frac{4}{\epsilon} + \frac{11}{3} + \left(\frac{67}{9} - \pi^2 \right) \epsilon \right) \right]. \tag{4.59}$$

The measured and unmeasured jet functions are obtained by inserting $\Theta_{\rm alg}\delta_R$ and $\Theta_{\rm alg}$ into Eq. (4.58), respectively.

We also record the zero bin that needs to be subtracted from Eq. (4.58). To leading-power

it is given by

$$\int \frac{dl^+}{2\pi} J_\omega^{g(0)}(l^+) = \mu^{2\epsilon} C_A \frac{2g^2}{(2\pi)^{d-1}} \int \frac{dl^+}{l^+} \int d^d q \left[\delta(q^2)\delta(l^+ - q^+)\Theta(q^-)\frac{1}{q^-} + \delta((l-q)^2)\delta(q^+)\Theta(\omega - q^-)\frac{1}{\omega - q^-} \right]. \tag{4.60}$$

5.3.1 Measured Gluon Jet

The naive contribution to the measured gluon jet can be written as

$$\tilde{J}_\omega^g(\tau_a) = \frac{\alpha_s}{2\pi}\frac{1}{\Gamma(1-\epsilon)} \left(\frac{4\pi\mu^2}{\omega^2}\right)^\epsilon \frac{1}{1-\frac{a}{2}} \left(\frac{1}{\tau_a}\right)^{1+\frac{2\epsilon}{2-a}} \int_0^1 dx \, (x^{a-1} + (1-x)^{a-1})^{\frac{2\epsilon}{2-a}} \times \left[T_R N_f \left(1 - \frac{2}{1-\epsilon} x(1-x)\right) - C_A \left(2 - \frac{1}{x(1-x)} - x(1-x)\right)\right] \Theta_{\text{alg}}(x)\,, \tag{4.61}$$

where $x \equiv q^-/\omega$. This gives

$$\tilde{J}_\omega^g(\tau_a) = \frac{\alpha_s}{2\pi}\frac{1}{\Gamma(1-\epsilon)} \left(\frac{4\pi\mu^2}{\omega^2 \tan^2\frac{R}{2}}\right)^\epsilon \delta(\tau_a) \left[C_A \left(\frac{1}{\epsilon^2} + \frac{11}{6}\frac{1}{\epsilon}\right) - \frac{2}{3\epsilon} T_R N_f \right] + \frac{\alpha_s}{2\pi} \tilde{J}_{\text{alg}}^g(\tau_a)\,, \tag{4.62}$$

where, as for the quark jet function, the finite distributions $\tilde{J}_{\text{alg}}^g(\tau_a)$ differ among the algorithms we consider. They are given in Appendix 4.A.

The zero-bin result is

$$J_\omega^{g(0)}(\tau_a) = \frac{\alpha_s C_A}{\pi}\frac{1}{\Gamma(1-\epsilon)}\frac{\alpha_s}{2\pi} \left(\frac{4\pi\mu^2 \tan^{2(1-a)}\frac{R}{2}}{\omega^2}\right)^\epsilon \left(\frac{1}{\tau_a}\right)^{1+2\epsilon} \frac{1}{(1-a)\epsilon}\,. \tag{4.63}$$

Subtracting the zero-bin from the naive integral and adding the leading-order contribution, we obtain in $\overline{\text{MS}}$

$$\begin{aligned} J_\omega^g(\tau_a) &= \delta(\tau_a) + \tilde{J}_\omega^g(\tau_a) - J_\omega^{g(0)}(\tau_a) \\ &= \left\{ 1 + \frac{\alpha_s C_A}{\pi} \left[\frac{1-a/2}{1-a} \left(\frac{1}{\epsilon^2} + \frac{1}{\epsilon} \ln\frac{\mu^2}{\omega^2} \right) + \frac{11}{12}\frac{1}{\epsilon} \right] - \frac{\alpha_s}{3\pi} T_R N_f \frac{1}{\epsilon} \right\} \delta(\tau_a) \\ &\quad - \frac{\alpha_s C_A}{\pi}\frac{1}{1-a}\frac{1}{\epsilon} \left(\frac{\Theta(\tau_a)}{\tau_a}\right)_+ + \frac{\alpha_s}{2\pi} J_{\text{alg}}^g(\tau_a)\,. \end{aligned} \tag{4.64}$$

The finite distribution $J_{\text{alg}}^g(\tau_a)$ is given in Eq. (4.149).

5.3.2 Unmeasured Gluon Jet

As for the quark jet function, for unmeasured jets the naive and zero-bin contributions are given by the measured jet contributions without the δ_R constraint. Also, as it was for the quark

jet function, the zero-bin contribution to the unmeasured jet function is a scaleless integral. Thus, the final answer is just the naive result, which is given by

$$J_\omega^g = 1 + \frac{\alpha_s}{2\pi}\left[C_A\left(\frac{1}{\epsilon^2} + \frac{11}{6}\frac{1}{\epsilon} + \frac{1}{\epsilon}\ln\frac{\mu^2}{\omega^2\tan^2\frac{R}{2}}\right) - \frac{2}{3\epsilon}T_R N_f\right] + \frac{\alpha_s}{2\pi}J_{\rm alg}^g\,, \tag{4.65}$$

with the finite part $J_{\rm alg}^g$ given in Eq. (4.157) in the Appendix.

6 Soft Functions at $\mathcal{O}(\alpha_s)$ for Jet Shapes

In this section we compute the soft function for a generic N jet event. In Sec. 6.1, we describe the phase space cuts that we impose on soft particles emitted into the final state. We then give an outline of how we disentangle the various contributions to the N-jet soft function in Sec. 6.2 and proceed to calculate these contributions in the remaining subsections.

6.1 Phase Space Cuts

Soft particles in the final state must satisfy the phase space cuts required by the operator $\delta_{N(\hat{\mathcal{J}}),0}$ in Eq. (4.32), which constrains the soft particles to not create an extra jet. A soft particle allowed in the final state if it is emitted into one of the jets as defined by the jet algorithm, or if it is not in a jet by has energy less than a cutoff Λ. At NLO, only a single soft gluon can be emitted. Therefore, for both cone-type and $\mathrm{k_T}$-type algorithms, the constraint that the soft gluon be in a jet is simply that the angle of the gluon with respect to the jet axis satisfies $\theta_{gJ} < R$. Thus, our requirement on soft gluons is that they obey one of the two following conditions:

$$\begin{aligned} &\text{in jet } i\text{: } \theta_{gJ_i} < R \\ &\text{out of all jets: } E_g < \Lambda \text{ and } \theta_{gJ_i} > R \text{ for all } i\,. \end{aligned} \tag{4.66}$$

These conditions can be written in terms of theta functions on the gluon momentum k. We denote the energy restriction for out-of-jet gluons as

$$\Theta_\Lambda \equiv \Theta(k^0 < \Lambda)\,, \tag{4.67}$$

and we denote the requirement that a gluon be in jet i in terms of the light-cone components $k^\pm$ about the the direction of jet i, n_i, as

$$\Theta_R^i \equiv \Theta\left(\frac{k^+}{k^-} < \tan^2\frac{R}{2}\right)\,. \tag{4.68}$$

For the case when the soft gluon is in a measured jet, we demand that it contributes an amount τ_a to the angularity of a jet with label momentum ω with the use of the delta function

$$\delta_R \equiv \delta\left(\tau_a - \frac{1}{\omega}(k^-)^{a/2}(k^+)^{1-a/2}\right)\,. \tag{4.69}$$

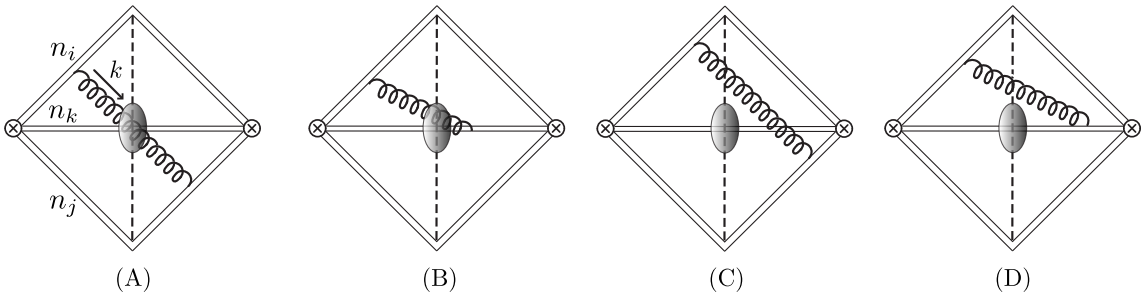

Figure 4.5: Soft function real-emission diagrams. Diagrams (A) and (C) are interference diagrams of Wilson line emission from lines i and j and (B) and (D) are from lines i and k. The shaded region in the center represents the region of phase space corresponding to jet k defined by the jet algorithm, and so the gluons in diagrams (A) and (B) are inside jet k and those in (C) and (D) are not. Each diagram has a corresponding mirror diagram (not shown).

6.2 Calculation of contributions to the N-Jet Soft Function

The topology of the various graphs that we need to compute the soft function is shown in Fig. 4.5. The next-to-leading order part $S_{(1)}$ of the soft function S is the sum of the interference of soft gluon emissions from Wilson lines in directions i and j, S_{ij}, over all lines i and j with $i \neq j$ (since for $i = j$, the diagram is proportional to $n_i^2 = 0$),

$$S_{(1)} = \sum_{i \neq j} S_{ij} \,. \tag{4.70}$$

It is conceptually straightforward to see that S_{ij} is just the sum of the following three classifications of the final state cut gluon:

- The gluon is in a measured jet and thus contributes to the jet angularity.
- The gluon is outside of all the jets and has energy $E_g < \Lambda$.
- The gluon is in an unmeasured jet and has any energy.

However, the second contribution is technically difficult to compute due to the complicated shape of the space with all jets cut out of it, like Swiss cheese. A division of phase space leading to a simpler calculation is the following:

- $S_{ij}^{\text{meas}}(\tau_a^k)$: The gluon is in measured jet k and contributes to the jet's angularity τ_a^k.
- S_{ij}^k: The gluon is in jet k with energy $E_g > \Lambda$ (and does not contribute to τ_a^k).
- $\bar{S}_{ij}^k$: The gluon is in jet k with energy $E_g < \Lambda$ (and does not contribute to τ_a^k).
- S_{ij}^{incl}: The gluon is anywhere with $E_g < \Lambda$ (and does not contribute to any angularity).

In terms of these pieces, the NLO soft function with M measured jets and $N-M$ unmeasured jets is given by

$$\begin{aligned} S_{(1)}(\tau_a^1, \tau_a^2, \ldots, \tau_a^M) = &\sum_{i\neq j} \left[\sum_{k\in\text{meas}} S_{ij}^{\text{meas}}(\tau_a^k) \prod_{l\neq k}^{M} \delta(\tau_a^l) \right] \\ &+ \sum_{i\neq j} \left[\left(S_{ij}^{\text{incl}} - \sum_{k\in\text{meas}} \bar{S}_{ij}^k + \sum_{k\notin\text{meas}} S_{ij}^k \right) \prod_{l}^{M} \delta(\tau_a^l) \right] . \end{aligned} \tag{4.71}$$

From the definitions above, it is easy to see that the term in large parentheses on the second line is equivalent to the sum of the last two contributions on the original list above, i.e., the contributions from a gluon not in any jet with $E_g < \Lambda$ and from a gluon in an unmeasured jet with any energy.

We can simplify this expression by noting that the contribution from a gluon in jet k with no energy restriction involves a scaleless integral over the energy that vanishes in dimensional regularization and thus

$$S_{ij}^k + \bar{S}_{ij}^k = 0 \,. \tag{4.72}$$

Using this relation, the soft function simplifies to

$$S_{(1)}(\tau_a^1, \ldots, \tau_a^M) = S_{(1)}^{\text{unmeas}} \prod_{l}^{M} \delta(\tau_a^l) + \sum_{k\in\text{meas}} S_{(1)}^{\text{meas}}(\tau_a^k) \prod_{l\neq k}^{M} \delta(\tau_a^l) \,, \tag{4.73}$$

where the first term in Eq. (4.73) is a universal contribution that is needed for every N-jet observable, defined as

$$S_{(1)}^{\text{unmeas}} \equiv \sum_{i\neq j} \left(S_{ij}^{\text{incl}} + \sum_{k=1}^{N} S_{ij}^k \right) . \tag{4.74}$$

The second term, defined as,

$$S_{(1)}^{\text{meas}}(\tau_a^k) \equiv \sum_{i\neq j} S_{ij}^{\text{meas}}(\tau_a^k) \,, \tag{4.75}$$

depends on our choice of angularities as the observable.

We now proceed to set up the one-loop expressions for the contributions in Eq. (4.73). The integrals involved are highly nontrivial and so in this section we simply quote the result of each integral, referring the reader to Appendix 4.B for details. Most of these integrals are most easily written in terms of the variable t_{ij}, defined in Eq. (4.5) as $t_{ij} \equiv \tan\frac{\psi_{ij}}{2} / \tan\frac{R}{2}$, where ψ_{ij} is the angle between jet directions i and j. (That is, $n_i \cdot n_j = 1 - \cos\psi_{ij}$.) In Table 4.2, we summarize the divergent parts of the soft function.

The Feynman rules for the emission of a soft gluon from fundamental- and adjoint-representation Wilson lines (corresponding to quark and gluon jets, respectively) have the same kinematic structure. The difference is entirely encoded in the color charge of the Wilson lines which, using the color space formalism of [69, 70], we denote as $\mathbf{T}_i$ for emission from Wilson line i. Thus, we can consider the N-jet soft function without specifying the color representation of the final-state jets.

6.2.1 Inclusive Contribution: S_{ij}^{incl}

The contribution to the soft function from a gluon going in any direction with energy $E_g < \Lambda$ is given by the integral

$$S_{ij}^{\text{incl}} = -g^2\mu^{2\epsilon}\,\mathbf{T}_i\cdot\mathbf{T}_j\int\frac{d^dk}{(2\pi)^d}\frac{n_i\cdot n_j}{(n_i\cdot k)(n_j\cdot k)}2\pi\delta(k^2)\Theta(k^0)\,\Theta_\Lambda\,. \tag{4.76}$$

We evaulate this integral in Sec. 4.B.1 of the Appendix and find

$$S_{ij}^{\text{incl}} = -\frac{\alpha_s}{2\pi}\frac{\mathbf{T}_i\cdot\mathbf{T}_j}{\Gamma(1-\epsilon)}\left(\frac{4\pi\mu^2}{4\Lambda^2}\right)^\epsilon\left(\frac{1}{\epsilon^2}-\frac{1}{\epsilon}\ln\frac{n_i\cdot n_j}{2}-\frac{\pi^2}{6}-\text{Li}_2\left(1-\frac{2}{n_i\cdot n_j}\right)\right)\,. \tag{4.77}$$

Note that this calculation is related to the inclusive, timelike soft function that has applications elsewhere (see, e.g., [147, 43, 40]), generalized for non back-to-back jets:

$$\frac{dS_{ij}^{\text{incl}}}{d\Lambda} = -g^2\mu^{2\epsilon}\,\mathbf{T}_i\cdot\mathbf{T}_j\int\frac{d^dk}{(2\pi)^d}\frac{n_i\cdot n_j}{(n_i\cdot k)(n_j\cdot k)}2\pi\delta(k^2)\Theta(k^0)\delta(k^0-\Lambda)\,. \tag{4.78}$$

6.2.2 Soft gluon inside jet k with $E_g > \Lambda$: S_{ij}^k

Using Eq. (4.72), the contribution S_{ij}^k from a gluon emitted into jet k from lines i and j is given by the integral

$$S_{ij}^k = g^2\mu^{2\epsilon}\,\mathbf{T}_i\cdot\mathbf{T}_j\int\frac{d^dk}{(2\pi)^d}\frac{n_i\cdot n_j}{(n_i\cdot k)(n_j\cdot k)}2\pi\delta(k^2)\Theta(k^0)\,\Theta_R^k\Theta_\Lambda\,. \tag{4.79}$$

Much like for the S_{ij}^{meas} contribution, if $k = i, j$, there is an additional divergence (arising from $n_k\cdot k\to 0$) relative to the case $k\neq i,j$, and so we evaluate these two cases separately below.

6.2.2.1 Case 1: $k = i$ or j The integrals for this case are performed in Sec. 4.B.2 of the Appendix, with the result that S_{ij}^j is

$$\begin{aligned}S_{ij}^j = S_{ij}^i = \frac{\alpha_s\mathbf{T}_i\cdot\mathbf{T}_j}{4\pi}\Bigg[&\frac{1}{\epsilon^2}\frac{1}{\Gamma(1-\epsilon)}\left(\frac{4\pi\mu^2}{4\Lambda^2}\right)^\epsilon\left(\frac{t_{ij}^2}{t_{ij}^2-1}\tan^2\frac{R}{2}\right)^{-\epsilon}+\text{Li}_2\left(\frac{-1}{t_{ij}^2-1}\right)\\&+2\,\text{Li}_2\left(\frac{-1}{\cos^2\frac{\psi_{ij}}{2}(t_{ij}^2-1)}\right)\Bigg]\,.\end{aligned} \tag{4.80}$$

6.2.2.2 Case 2: $k\neq i,j$ These contributions are at most $1/\epsilon$ divergent since the matrix element does not have the $n_k\cdot k\to 0$ singularity. We show in Appendix 4.B.3.2 that the result takes the form

$$S_{ij}^k\big|_{k\neq i,j} = -\frac{\alpha_s}{4\pi}\mathbf{T}_i\cdot\mathbf{T}_j\left[\frac{1}{\epsilon}\ln\left(\frac{t_{ik}^2t_{jk}^2-2t_{ik}t_{jk}\cos\beta_{ij}+1}{(t_{ik}^2-1)(t_{jk}^2-1)}\right)+F(t_{ik},t_{jk},\beta_{ij})\right]\,, \tag{4.81}$$

where β_{ij} is the angle between the i-k and j-k planes and the finite function F is given in Eq. (4.191) and is $\mathcal{O}(1/t^2)$.

6.2.3 Soft gluon inside measured jet k: $S_{ij}^{\rm meas}(\tau_a^k)$

The contribution of a gluon emitted into jet 1 (the measured jet) from lines i and j is given by the integral

$$S_{ij}^{\rm meas}(\tau_a^k) = -g^2\mu^{2\epsilon}\,\mathbf{T}_i\cdot\mathbf{T}_j\int\frac{d^dk}{(2\pi)^d}\frac{n_i\cdot n_j}{(n_i\cdot k)(n_j\cdot k)}2\pi\delta(k^2)\Theta(k^0)\,\Theta_R^k\delta_R\,. \tag{4.82}$$

The singularity structure of this integral depends on whether or not $k = i$ or j. Thus, we evaluate the case $k = i$ or j and the case $k \neq i, j$ separately below.

6.2.3.1 Case 1: $k = i$ or j We consider first $S_{ij}^{\rm meas}(\tau_a^i)$. Using the results of Sec. 4.B.2 of the Appendix, we obtain the result in terms of t_{ij},

$$\begin{aligned}S_{ij}^{\rm meas}(\tau_a^i) &= S_{ji}^{\rm meas}(\tau_a^i)\\ &= -\frac{\alpha_s}{2\pi}\mathbf{T}_i\cdot\mathbf{T}_j\left[\frac{1}{\epsilon}\frac{1}{1-a}\left(\frac{1}{\tau_a^i}\right)^{1+2\epsilon}\frac{1}{\Gamma(1-\epsilon)}\left(\frac{4\pi\mu^2}{\omega^2}\right)^{\epsilon}\left(\frac{t_{ij}^2}{t_{ij}^2-1}\tan^2\frac{R}{2}\right)^{\epsilon(1-a)}\right.\\ &\qquad\left.+\,\frac{1+a}{2}\delta(\tau_a^i)\,\mathrm{Li}_2\left(\frac{-1}{t_{ij}^2-1}\right)\right].\end{aligned} \tag{4.83}$$

6.2.3.2 Case 2: $k \neq i, j$ The remaining contributions to the observed jet angularity are $S_{ij}^{\rm meas}$ for $k \neq i, j$. Using the results from Sec. 4.B.3.3 in the Appendix, this contribution is

$$\begin{aligned}S_{ij}^{\rm meas}(\tau_a^k)\big|_{i,j\neq k} = -\frac{\alpha_s}{2\pi}\mathbf{T}_i\cdot\mathbf{T}_j\Bigg[&\left(\frac{1}{\tau_a^k}\right)^{1+2\epsilon}\ln\left(\frac{t_{ik}^2t_{jk}^2-2t_{ik}t_{jk}\cos\beta_{ij}+1}{(t_{ik}^2-1)(t_{jk}^2-1)}\right)\\ &+\,\delta(\tau_a^k)\,G(t_{ik},t_{jk},\beta_{ij})\Bigg],\end{aligned} \tag{4.84}$$

where G is $\mathcal{O}(1/t^2)$ and is given in Eq. (4.194) and, again, β_{ij} is the angle between the i-k and j-k planes.

6.3 Total N-Jet Soft Function in the large-t Limit

In this section, we add together the necessary ingredients calculated above to obtain the N-jet soft function from Eq. (4.73). The results for the divergent pieces are summarized in Table 4.2 . In Sec. 7 we use Table 4.2 to show that the consistency of factorization is explicitly violated by terms of order $1/t^2$, and so in this section we give the full soft function (including the finite terms) to $\mathcal{O}(1/t^2)$.

Using color-conservation ($\sum_i \mathbf{T}_i = 0$), we find that the observable-independent part,

contribution	divergent terms
S_{ij}^{incl}	$-\frac{1}{\epsilon}\frac{\alpha_s}{2\pi}\mathbf{T}_i\cdot\mathbf{T}_j\left(\frac{1}{\epsilon}-\ln\frac{n_i\cdot n_j}{2}+\ln\frac{\mu^2}{4\Lambda^2}\right)$
S_{ij}^{i}	$\frac{1}{\epsilon}\frac{\alpha_s}{4\pi}\mathbf{T}_i\cdot\mathbf{T}_j\left(\frac{1}{\epsilon}-\ln\frac{t_{ij}^2\tan^2(R/2)}{t_{ij}^2-1}+\ln\frac{\mu^2}{4\Lambda^2}\right)$
S_{ij}^{k}	$-\frac{1}{\epsilon}\frac{\alpha_s}{4\pi}\mathbf{T}_i\cdot\mathbf{T}_j\ln\frac{t_{ik}^2t_{jk}^2-2t_{ik}t_{jk}\cos\beta_{ij}+1}{(t_{ik}^2-1)(t_{jk}^2-1)}$
$S_{(1)}^{\text{unmeas}}$	$\frac{1}{\epsilon}\frac{\alpha_s}{2\pi}\Big[\sum_{i=1}^N\mathbf{T}_i^2\ln\tan^2(R/2)+\sum_{i\neq j}\mathbf{T}_i\cdot\mathbf{T}_j\ln(n_i\cdot n_j/2)\Big]+\mathcal{O}(1/t^2)$
$S_{ij}^{\text{meas}}(\tau_a^i)$	$\frac{1}{\epsilon}\frac{\alpha_s}{4\pi}\mathbf{T}_i\cdot\mathbf{T}_j\Big[\Big(\frac{1}{1-a}\big(\frac{1}{\epsilon}+\ln\frac{\mu^2}{\omega_i^2}\big)+\ln\frac{t_{ij}^2\tan^2(R/2)}{t_{ij}^2-1}\Big)\delta(\tau_a^i)-\frac{2}{1-a}\Big(\frac{1}{\tau_a^i}\Big)_+\Big]$
$S_{ij}^{\text{meas}}(\tau_a^k)$	$\frac{1}{\epsilon}\frac{\alpha_s}{4\pi}\mathbf{T}_i\cdot\mathbf{T}_j\ln\frac{t_{ik}^2t_{jk}^2-2t_{ik}t_{jk}\cos\beta_{ij}+1}{(t_{ik}^2-1)(t_{jk}^2-1)}\delta(\tau_a^k)$
$S_{(1)}^{\text{meas}}(\tau_a^i)$	$-\frac{1}{\epsilon}\frac{\alpha_s}{2\pi}\mathbf{T}_i^2\Big[\Big(\frac{1}{1-a}\big(\frac{1}{\epsilon}+\ln\frac{\mu^2}{\omega_i^2}\big)+\ln\tan^2(R/2)\Big)\delta(\tau_a^i)-\frac{2}{1-a}\Big(\frac{1}{\tau_a^i}\Big)_+\Big]+\mathcal{O}(1/t^2)$

Table 4.2: Summary of the divergent parts of the soft function at NLO. The first block contains the the observable-independent contributions: soft gluons emitted by jets i and j in any direction with energy $E_g<\Lambda$ in row 1; soft gluons entering jet k with $E_g>\Lambda$ (with $k=i$ or j in the second row and $k\neq i,j$ in the third). In the last row of the first block, we summed over i and j and took the large-t limit to get the total $S_{(1)}^{\text{unmeas}}$. Similarly, in the second block we give the contributions to the angularities τ_a^k (with $k=i$ or j in the first row and $k\neq i,j$ in the second) and summed over i and j and took the large-t limit to get $S_{(1)}^{\text{meas}}$ in the third row.

$S_{(1)}^{\text{unmeas}}$, defined in Eq. (4.74), is given for large t by

$$\begin{aligned}S_{(1)}^{\text{unmeas}}=\frac{\alpha_s}{2\pi}\sum_i\mathbf{T}_i^2\Bigg[&\frac{1}{\epsilon}\ln\left(\tan^2\frac{R}{2}\right)+\ln\left(\frac{\mu^2}{4\Lambda^2\tan\frac{R}{2}}\right)\ln\left(\tan^2\frac{R}{2}\right)-\frac{\pi^2}{6}\Bigg]\\&+\frac{\alpha_s}{2\pi}\sum_{i\neq j}\mathbf{T}_i\cdot\mathbf{T}_j\Bigg[\frac{1}{\epsilon}\ln\frac{n_i\cdot n_j}{2}+\ln\left(\frac{\mu^2}{4\Lambda^2}\right)\ln\left(\frac{n_i\cdot n_j}{2}\right)\\&\qquad+\mathrm{Li}_2\left(1-\frac{2}{n_i\cdot n_j}\right)\Bigg]+\mathcal{O}(1/t^2)\,.\end{aligned}\tag{4.85}$$

In addition to $\tan(R/2)$ which, according the the discussion in Sec. 4.4, we take to be $\mathcal{O}(1)$, the finite parts from this contribution are sensitive to the scale μ_S^Λ, where

$$\mu_S^\Lambda\equiv 2\Lambda\tan^{1/2}\frac{R}{2}\sim 2\Lambda\,.\tag{4.86}$$

The remaining part of the soft function that is dependent on angularities as our choice of jet observable is the sum over $S_{(1)}^{\text{meas}}(\tau_a^i)$ (defined in Eq. (4.75)) for each jet i, where $S_{(1)}^{\text{meas}}(\tau_a^i)$ is

given by

$$S_{(1)}^{\text{meas}}(\tau_a^i) = -\frac{\alpha_s}{2\pi}\mathbf{T}_i^2\frac{1}{1-a}\left\{\left[\frac{1}{\epsilon^2}+\frac{1}{\epsilon}\ln\left(\frac{\mu^2}{\omega_i^2}\tan^{2(1-a)}\frac{R}{2}\right)-\frac{\pi^2}{12}\right.\right.$$
$$\left.+\frac{1}{2}\ln^2\left(\frac{\mu^2}{\omega^2}\tan^{2(1-a)}\frac{R}{2}\right)\right]\delta(\tau_a^i) \qquad (4.87)$$
$$\left.-2\left[\left(\frac{1}{\epsilon}+\ln\left(\frac{\mu^2\tan^{2(1-a)}\frac{R}{2}}{(\omega\tau_a^i)^2}\right)\right)\frac{\Theta(\tau_a^i)}{\tau_a^i}\right]_+\right\}+\mathcal{O}(1/t^2)\,.$$

The finite part of this contribution is sensitive to the scale μ_S^i, where

$$\mu_S^i \equiv \frac{\omega_i\tau_a^i}{\tan^{1-a}\frac{R}{2}}\,, \qquad (4.88)$$

which, in principle, differs for each jet i and from the scale μ_Λ in the unmeasured part of the soft function Eq. (4.85). After discussing resummation of large logarithms through RG evolution, we will describe in Sec. 7.4 a framework to "refactorize" the soft function into pieces depending on multiple separated soft scales. This framework will enable us to resum logarithms of all of these potentially disparate scales.

7 Resummation and Consistency Relations at NLL

The factorized cross section Eq. (4.39) is written in terms of hard, jet, and soft functions evaluated at a factorization scale μ. Since the physical cross section is independent of μ, the anomalous dimensions of these functions are closely related. We derive and verify this relation in Sec. 7.3. In Sec. 7.1 and Sec. 7.2, we work out the form of the renormalization-group equations (RGEs) satisfied by the hard, jet, and soft functions, and obtain their solutions so that we can express each function at the scale μ in terms of its value at a scale μ_0 where logarithms in it are minimized. In Sec. 7.4, we present a framework to refactorize the soft function and give the total resummed distribution in Sec. 7.5.

7.1 General Form of Renormalization Group Equations and Solutions

We will build solutions for the hard, jet, and soft functions from two forms of RGEs. The first form is for a function which does not depend on the observable τ_a and is multiplicatively renormalized,

$$F^{\text{bare}} = Z_F(\mu)F(\mu)\,, \qquad (4.89)$$

and satisfies the RGE,

$$\mu\frac{d}{d\mu}F(\mu) = \gamma_F(\mu)F(\mu)\,, \qquad (4.90)$$

where the anomalous dimension γ_F is found from the Z-factor by the relation

$$\gamma_F(\mu) = -\frac{1}{Z_F(\mu)}\mu\frac{d}{d\mu}Z_F(\mu)\,, \qquad (4.91)$$

and takes the general form,

$$\gamma_F(\mu) = \Gamma_F[\alpha] \ln \frac{\mu^2}{\omega^2} + \gamma_F[\alpha] \,. \tag{4.92}$$

We call $\Gamma_F[\alpha]$ the "cusp part" of the anomalous dimension and $\gamma_F[\alpha]$ the "non-cusp part". They have the perturbative expansions

$$\Gamma_F[\alpha_s] = \left(\frac{\alpha_s}{4\pi}\right) \Gamma_F^0 + \left(\frac{\alpha_s}{4\pi}\right)^2 \Gamma_F^1 + \cdots \tag{4.93}$$

and

$$\gamma_F[\alpha_s] = \left(\frac{\alpha_s}{4\pi}\right) \gamma_F^0 + \left(\frac{\alpha_s}{4\pi}\right)^2 \gamma_F^1 + \cdots \,. \tag{4.94}$$

The RGE Eq. (4.90) has the solution

$$F(\mu) = U_F(\mu, \mu_0) F(\mu_0) \,, \tag{4.95}$$

where the evolution kernel U_F is given by

$$U_F(\mu, \mu_0) = e^{K_F(\mu,\mu_0)} \left(\frac{\mu_0}{\omega}\right)^{\omega_F(\mu,\mu_0)} \,, \tag{4.96}$$

where K_F and ω_F will be defined below in Eq. (4.103).

The second form of RGE is for a function dependent on the jet shape τ_a is renormalized through a convolution,

$$F^{\rm bare}(\tau_a) = \int d\tau_a' Z_F(\tau_a - \tau_a'; \mu) F(\tau_a', \mu) \,, \tag{4.97}$$

and satisfying the RGE

$$\mu \frac{d}{d\mu} F(\tau_a; \mu) = \int d\tau_a' \, \gamma_F(\tau_a - \tau_a'; \mu) F(\tau_a'; \mu) \,, \tag{4.98}$$

with an anomalous dimension calculated from

$$\gamma_F(\tau_a; \mu) = -\int d\tau' \, Z_F^{-1}(\tau_a - \tau_a'; \mu) \, \mu \frac{d}{d\mu} Z_F(\tau_a'; \mu) \,, \tag{4.99}$$

and taking the general form

$$\gamma_F(\tau_a; \mu) = -\Gamma_F[\alpha_s] \left(\frac{2}{j_F} \left[\frac{\Theta(\tau_a)}{\tau_a} \right]_+ - \ln \frac{\mu^2}{\omega^2} \, \delta(\tau_a) \right) + \gamma_F[\alpha_s] \delta(\tau_a) \,. \tag{4.100}$$

The solution of an RGE of the form Eq. (4.98) has the solution [147, 39, 10, 166, 125]

$$F(\tau_a; \mu) = \int d\tau' \, U_F(\tau_a - \tau_a'; \mu, \mu_0) F(\tau_a'; \mu_0) \,, \tag{4.101}$$

where the evolution kernel U_F is given to all orders in α_s by the expression

$$U_F(\tau_a; \mu, \mu_0) = \frac{e^{K_F + \gamma_E \omega_F}}{\Gamma(-\omega_F)} \left(\frac{\mu_0}{\omega}\right)^{j_F \omega_F} \left[\frac{\Theta(\tau_a)}{(\tau_a)^{1+\omega_F}} \right]_+ \,, \tag{4.102}$$

where γ_E is the Euler constant.

In Eqs. (4.96) and (4.102), the exponents ω_F and K_F are given in terms of the cusp and non-cusp parts of the anomalous dimensions by the expressions

$$\omega_F(\mu,\mu_0) \equiv \frac{2}{j_F}\int_{\alpha_s(\mu_0)}^{\alpha_s(\mu)}\frac{d\alpha}{\beta[\alpha]}\Gamma_F[\alpha]\,, \tag{4.103a}$$

$$K_F(\mu,\mu_0) \equiv \int_{\alpha_s(\mu_0)}^{\alpha_s(\mu)}\frac{d\alpha}{\beta[\alpha]}\gamma_F[\alpha] + 2\int_{\alpha_s(\mu_0)}^{\alpha_s(\mu)}\frac{d\alpha}{\beta[\alpha]}\Gamma_F[\alpha]\int_{\alpha_s(\mu_0)}^{\alpha}\frac{d\alpha'}{\beta[\alpha']}\,. \tag{4.103b}$$

In the case of Eq. (4.96) or if $\Gamma_F[\alpha]$ happens to be zero, we define j_F to be 1. To achieve NLL accuracy in the evolution kernels U_F, we need the cusp part of the anomalous dimension to two loops and the non-cusp part to one loop, in which case the parameters ω_F, K_F in Eq. (4.103) are given explicitly by

$$\omega_F(\mu,\mu_0) = -\frac{\Gamma_F^0}{j_F\,\beta_0}\left[\ln r + \left(\frac{\Gamma_{\rm cusp}^1}{\Gamma_{\rm cusp}^0} - \frac{\beta_1}{\beta_0}\right)\frac{\alpha_s(\mu_0)}{4\pi}(r-1)\right]\,, \tag{4.104a}$$

$$\begin{aligned} K_F(\mu,\mu_0) = -\frac{\gamma_F^0}{2\beta_0}\ln r - \frac{2\pi\Gamma_F^0}{(\beta_0)^2}\Bigg[&\frac{r-1-r\ln r}{\alpha_s(\mu)} \\ &+ \left(\frac{\Gamma_{\rm cusp}^1}{\Gamma_{\rm cusp}^0} - \frac{\beta_1}{\beta_0}\right)\frac{1-r+\ln r}{4\pi} + \frac{\beta_1}{8\pi\beta_0}\ln^2 r\Bigg]\,. \end{aligned} \tag{4.104b}$$

Here $r = \frac{\alpha_s(\mu)}{\alpha_s(\mu_0)}$, and β_0, β_1 are the one-loop and two-loop coefficients of the beta function,

$$\beta[\alpha_s] = \mu\frac{d\alpha_s}{d\mu} = -2\alpha_s\left[\beta_0\left(\frac{\alpha_s}{4\pi}\right) + \beta_1\left(\frac{\alpha_s}{4\pi}\right)^2 + \cdots\right]\,, \tag{4.105}$$

where (with $T_R = 1/2$)

$$\beta_0 = \frac{11C_A}{3} - \frac{2N_f}{3} \qquad \text{and} \qquad \beta_1 = \frac{34C_A^2}{3} - \frac{10C_AN_f}{3} - 2C_FN_f\,. \tag{4.106}$$

The two-loop running coupling $\alpha_s(\mu)$ at any scale is given by

$$\frac{1}{\alpha_s(\mu)} = \frac{1}{\alpha_s(M_Z)} + \frac{\beta_0}{2\pi}\ln\left(\frac{\mu}{M_Z}\right) + \frac{\beta_1}{4\pi\beta_0}\ln\left[1 + \frac{\beta_0}{2\pi}\alpha_s(M_Z)\ln\left(\frac{\mu}{M_Z}\right)\right]\,. \tag{4.107}$$

In Eq. (4.104), we have used the fact that, for the hard, jet, and soft functions for which we will solve, the cusp part of the anomalous dimension $\Gamma_F[\alpha_s]$ is proportional to *the* cusp anomalous dimension $\Gamma_{\rm cusp}[\alpha_s]$, where

$$\Gamma_{\rm cusp}[\alpha_s] = \left(\frac{\alpha_s}{4\pi}\right)\Gamma_{\rm cusp}^0 + \left(\frac{\alpha_s}{4\pi}\right)^2\Gamma_{\rm cusp}^1 + \cdots\,. \tag{4.108}$$

The ratio of the one-loop and two-loop coefficients of $\Gamma_{\rm cusp}$ is [148]

$$\frac{\Gamma_{\rm cusp}^1}{\Gamma_{\rm cusp}^0} = \left(\frac{67}{9} - \frac{\pi^2}{3}\right)C_A - \frac{10N_f}{9}\,. \tag{4.109}$$

$\Gamma_{\rm cusp}^1$ and β_1 are needed in the expressions of ω_F and K_F for complete NLL resummation since we formally take $\alpha_s^2\ln\tau_a \sim \mathcal{O}(\alpha_s)$.

7.2 RG Evolution of Hard, Jet, and Soft Functions

7.2.1 Hard Function

The hard function is related to the matching coefficient C_N of the N-jet operator in Eq. (4.38). If there are multiple operators with different color structures, C_N is a vector of coefficients. The hard function is then a matrix $H_{ab} = C_b^\dagger C_a$. The hard function is contracted in the cross section Eq. (4.39) with a matrix of soft functions.

The anomalous dimensions of the matching coefficients C_a have been calculated in the literature (for example, Table III of Ref. [87]). For an operator with N legs with color charges $\mathbf{T}_i^2$, the anomalous dimension is

$$\gamma_{C_N}(\alpha_s) = -\sum_{i=i}^{N}\left[\mathbf{T}_i^2\Gamma(\alpha_s)\ln\frac{\mu}{\omega_i} + \frac{1}{2}\gamma_i(\alpha_s)\right] - \frac{1}{2}\Gamma(\alpha_s)\sum_{i\neq j}\mathbf{T}_i\cdot\mathbf{T}_j\ln\left(\frac{-n_i\cdot n_j - i0^+}{2}\right), \quad (4.110)$$

where $\mathbf{T}_i$ is a matrix of color charges in the space of operators, and γ_i is given for quarks and gluons by

$$\gamma_q = \frac{3\alpha_s C_F}{2\pi}, \quad \gamma_g = \frac{\alpha_s}{\pi}\frac{11C_A - 2N_F}{6}. \quad (4.111)$$

The coefficient $\Gamma(\alpha_s)$ is the *cusp anomalous dimension* and is given to one-loop order by $\Gamma(\alpha_s) = \alpha_s/\pi$. The anomalous dimension of the hard function itself is given by $\gamma_H = \gamma_{C_N}^\dagger + \gamma_{C_N}$, and takes the form of Eq. (4.92), with cusp and non-cusp parts $\Gamma_H[\alpha_s]$ and $\gamma_H[\alpha_s]$ given to one loop in Table 4.3, with the result

$$\gamma_H(\alpha_s) = -\Gamma(\alpha_s)\mathbf{T}^2\ln\frac{\mu^2}{\bar{\omega}_H^2} - \sum_{i=1}^{N}\gamma_i(\alpha_s) - \Gamma(\alpha_s)\sum_{i\neq j}\mathbf{T}_i\cdot\mathbf{T}_j\ln\frac{n_i\cdot n_j}{2}, \quad (4.112)$$

where $\mathbf{T}^2 = \sum_{i=1}^N \mathbf{T}_i^2$ is the sum of all the Casimirs, and the effective hard scale $\bar{\omega}_H$ appearing as the scale ω in the logarithm in Eq. (4.92) is given by the color-weighted average of the jet energies,

$$\bar{\omega}_H = \prod_{i=1}^{N}\omega_i^{\mathbf{T}_i^2/\mathbf{T}^2} \quad (4.113)$$

7.2.2 Jet Functions

There are two forms of jet functions, those for measured and those for unmeasured jets. Unmeasured jet functions $J_\omega^{q,g}(\mu)$ satisfy multiplicative RGEs, with anomalous dimensions given by the infinite parts of Eqs. (4.56) and (4.65),

$$\gamma_{J_i} = \Gamma(\alpha_s)\mathbf{T}_i^2\ln\frac{\mu^2}{\omega_i^2\tan^2\frac{R}{2}} + \gamma_i, \quad (4.114)$$

which falls into the general form Eq. (4.92), with cusp and non-cusp parts of the anomalous dimension given in Table 4.3, and the scale ω in Eq. (4.92) being $\omega_i\tan\frac{R}{2}$. The part γ_i is given by Eq. (4.111).

	$\Gamma_F[\alpha_s]$	$\gamma_F[\alpha_s]$	j_F	ω
γ_H	$-\Gamma\sum_i \mathbf{T}_i^2$	$-\sum_i \gamma_i - \Gamma\sum_{i\neq j}\mathbf{T}_i\cdot\mathbf{T}_j \ln\frac{n_i\cdot n_j}{2}$	1	$\bar{\omega}_H$
$\gamma_{J_i}(\tau_a^i)$	$\Gamma\mathbf{T}_i^2\frac{2-a}{1-a}$	γ_i	$2-a$	ω_i
$\gamma_S^{\text{meas}}(\tau_a^i)$	$-\Gamma\mathbf{T}_i^2\frac{1}{1-a}$	0	1	$\omega_i\tan^{-1+a}\frac{R}{2}$
γ_{J_i}	$\Gamma\mathbf{T}_i^2$	γ_i	1	$\omega_i\tan\frac{R}{2}$
γ_S^{unmeas}	0	$\Gamma\sum_i \mathbf{T}_i^2 \ln\tan^2\frac{R}{2} + \Gamma\sum_{i\neq j}\mathbf{T}_i\cdot\mathbf{T}_j\ln\frac{n_i\cdot n_j}{2}$	1	—
$\mathcal{O}(1/t^2)$	0	$\Gamma\sum_{i\neq j}\mathbf{T}_i\cdot\mathbf{T}_j\Big[\delta_{i\notin\text{meas}}\,2\ln\frac{t_{ij}^2}{t_{ij}^2-1}$ $+\Gamma\sum_{\substack{k\neq i,j\\ k\notin\text{meas}}}\ln\Big(\frac{t_{ik}^2t_{jk}^2-2t_{ik}t_{jk}\cos\beta_{ij}+1}{(t_{ik}^2-1)(t_{jk}^2-1)}\Big)\Big]$	1	—

Table 4.3: Anomalous dimensions for the jet and soft functions. We give the cusp and non-cusp parts of the anomalous dimensions, $\Gamma_F[\alpha_s]$ and $\gamma_F[\alpha_s]$. Γ is the cusp anomalous dimension itself, equal to α_s/π at one loop. γ_i is given for quark and gluon jets in Eq. (4.111). The third column gives the value of j_F appearing in Eq. (4.100) or Eq. (4.103). The last column gives the values of ω appearing in the logarithm $\ln\mu^2/\omega^2$ multiplying the cusp part of the anomalous dimension in Eqs. (4.92) and (4.100). The scale $\bar{\omega}_H$ is the color-weighted averages of all jet energies defined in Eq. (4.113). All rows except for the last are given in the large-t limit and in the last row we give the remaining terms that are present for arbitrary t. This last row explictly violates consistency at $\mathcal{O}(1/t^2)$. The first group of rows are needed for measured jets and the second group for unmeasured jets. In the large-t limit, for any number of measured and unmeasured jets, the consistency relation Eq. (4.121) is satisfied.

Measured jet functions satisfy RGEs of the form Eq. (4.98), with anomalous dimensions given by the infinite parts of Eqs. (4.50) and (4.64),

$$\gamma_{J_i}(\tau_a^i) = \mathbf{T}_i^2\left[\Gamma(\alpha_s)\frac{2-a}{1-a}\ln\frac{\mu^2}{\omega_i^2}+\gamma_i\right]\delta(\tau_a^i) - 2\Gamma(\alpha_s)\mathbf{T}_i^2\frac{1}{1-a}\left[\frac{\Theta(\tau_a^i)}{\tau_a^i}\right]_+, \tag{4.115}$$

which takes the form Eq. (4.100) with cusp and non-cusp parts of the anomalous dimension split up as in Table 4.3, and the scale ω in Eq. (4.100) being ω_i.

7.2.3 Soft Function

The total N-jet soft function is given by Eq. (4.85) for unmeasured jets added to the sum over measured jets of Eq. (4.87). This soft function depends on the M jet shapes $\tau_a^1,\ldots,\tau_a^M$, and satisfies the RGE

$$\mu\frac{d}{d\mu}S(\tau_1,\ldots,\tau_M;\mu) = \int d\tau_1'\cdots d\tau_M'\,\gamma_S(\tau_1-\tau_1',\ldots,\tau_M-\tau_M';\mu)S(\tau_1',\ldots,\tau_M';\mu)\,. \tag{4.116}$$

From the infinite parts of the soft function given in Table 4.2, we find the anomalous dimension $\gamma_S(\tau_1, \ldots, \tau_M; \mu)$ decomposed into a sum of terms,

$$\gamma_S(\tau_1, \ldots, \tau_M; \mu) = \gamma_S^{\text{unmeas}}(\mu)\delta(\tau_1)\cdots\delta(\tau_M) + \sum_{k=1}^{M} \gamma_S^{\text{meas}}(\tau_k; \mu) \prod_{j\neq k} \delta(\tau_j)\,, \tag{4.117}$$

where the pieces $\gamma_S^{\text{unmeas}}(\mu)$ and $\gamma_S^{\text{meas}}(\tau_k; \mu)$ are given in terms of their cusp and non-cusp parts in Table 4.3, with the result

$$\gamma_S^{\text{unmeas}}(\mu) = \Gamma(\alpha_s)\mathbf{T}_i^2 \ln \tan^2 \frac{R}{2} + \Gamma(\alpha_s) \sum_{i\neq j} \mathbf{T}_i \cdot \mathbf{T}_j \ln \frac{n_i \cdot n_j}{2}\,, \tag{4.118}$$

which takes the form of Eq. (4.92) with no cusp part, and

$$\gamma_S^{\text{meas}}(\tau_k; \mu) = -\Gamma(\alpha_s)\mathbf{T}_i^2 \frac{1}{1-a} \left\{ \ln \left(\frac{\mu^2 \tan^{2(1-a)} \frac{R}{2}}{\omega_k^2} \right) \delta(\tau_k) - 2 \left[\frac{\Theta(\tau_k)}{\tau_k} \right]_+ \right\}, \tag{4.119}$$

which takes the form of Eq. (4.100) with no non-cusp part, and the scale ω in Eq. (4.100) being $\omega_k / \tan^{1-a} \frac{R}{2}$.

The solution of the RGE Eq. (4.116) is given by

$$S(\tau_1, \ldots, \tau_M; \mu) = \int d\tau_1' \cdots d\tau_M'\, S(\tau_1', \ldots, \tau_M'; \mu_0) U_S^{\text{unmeas}}(\mu, \mu_0) \prod_{k=1}^{M} U_S^k(\tau_k - \tau_k'; \mu, \mu_0)\,, \tag{4.120}$$

where U_S^{unmeas} is given by the form of Eq. (4.96) and $U_S^k(\tau_a^k)$ by the form of Eq. (4.102).

The solution Eq. (4.120) is appropriate if all the scales appearing in the soft function are similar, and thus all large logarithms in the finite part can be minimized at a single scale μ_0. As we noted in Sec. 6.3, however, the potentially disparate scales $\omega_i \tau_a^i$, set by the jet shapes of the measured jets, and Λ, set by the cutoff on particles outside jets, appear together in the soft function, and logarithms of ratios of these scales may be large. In this case, the soft function should be "refactorized" into pieces depending only on one of these scales at a time. We describe a framework for doing so below in Sec. 7.4.

But first, we verify the consistency of the anomalous dimensions for the hard, jet, and soft functions to the order we have calculated them.

7.3 Consistency Relation among Anomalous Dimensions

We summarize the anomalous dimensions of the hard, jet, and soft functions in Table 4.3. We separate contributions to the jet and soft anomalous dimensions that arise from measured jets, from unmeasured jets, and those that are universally present. In all rows except the last row, we take the large-t limit and give the additional terms that arise (from the soft function) for arbitrary t.

Consistency of the effective theory requires that the anomalous dimensions satisfy

$$0 = \Big(\gamma_H(\mu) + \gamma_S^{\text{unmeas}}(\mu) + \sum_{i\notin \text{meas}} \gamma_{J_i}(\mu) \Big) \delta(\tau_a^i) + \sum_{i\in\text{meas}} \Big(\gamma_{J_i}(\tau_a^i; \mu)) + \gamma_S^{\text{meas}}(\tau_a^i; \mu) \Big)\,. \tag{4.121}$$

From the results tabulated in Table 4.3, up to corrections of $\mathcal{O}(1/t^2)$, we see that, remarkably, this relation is indeed satisfied! This is highly nontrivial, as jet and soft anomalous dimensions depend on the jet radius R and the jet shape τ_a, while the hard function does not; in addition, the hard and soft functions know the directions n_i of all N jets, while the jet functions do not. These dependencies cancel precisely between the R-dependent pieces of unmeasured jet contributions to the jet and soft functions, between τ_a-dependent pieces of the measured jet contributions, and between $n_i \cdot n_j$-dependent pieces of the hard and soft functions. The sum of all jet and soft anomalous dimensions then precisely matches the hard anomalous dimensions, satisfying Eq. (4.121).

Making the satisfaction of consistency even more nontrivial, individual contributions to the infinite part of the soft function, and therefore its anomalous dimension, given by Table 4.2 depend on the energy cut parameter Λ as well. However, these terms cancel in the sum over the contributions S_{ij}^{incl} and S_{ij}^{i} in the first two rows of Table 4.2. The double poles of the form $\frac{1}{\epsilon}\ln\Lambda$ arise from regions of phase space where a soft gluon can become both collinear to a jet direction (giving a $1/\epsilon$) and soft (giving a $\ln\Lambda$). These regions exist in the integral over all directions giving S_{ij}^{incl} but are subtracted back out in the contributions S_{ij}^{i}. In the surviving "Swiss cheese" region the regions giving these double poles are cut out.

The $\mathcal{O}(1/t^2)$ terms that violate consistency arise whenever there are unmeasured jets. While this limit is not required for the contribution of measured jets to the anomalous dimension to satisfy the consistency condition Eq. (4.121), the finite parts of measured jet contributions to the soft function contain large logarithms of ω/Λ that can not be minimized with a scale choice but are suppressed by $\mathcal{O}(1/t^2)$ (cf. Eq. (4.195) of Appendix 4.B). This is the manifestation of the fact that jets need to be well-separated, as explained in Sec. 4. For the remainder of the chapter, we work strictly in the large-t limit.

7.4 Refactorization of the Soft Function

Our results for the soft function in Sec. 6.3 make clear that in general there are multiple scales that appear in the soft function: the $\mu_S^1, \ldots, \mu_S^M$ associated with the M measured jets and the scale μ_S^Λ associated with the out-of-jet cutoff Λ. When these scales are all comparable, we can RG evolve the soft function from the single scale μ_S. However, when any of them differ considerably from the others, we need to "refactorize" the soft function into multiple contributions, each of which is sensitive to a single energy scale. For illustration, take the scales μ_S^i to be such that $\mu_S^1 \gg \mu_S^2 \gg \cdots \gg \mu_S^M$ as in Fig. 4.6. We also take $\mu_S^{l-1} \ll \mu_S^\Lambda \ll \mu_S^l$ for our discussion, but the result is independent of whether μ_S^Λ lies in the range $\mu_S^1 < \mu_S^\Lambda < \mu_S^M$ or not.

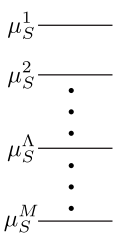

Figure 4.6: Soft scales.

We can express the soft function appearing in Eq. (4.39) as

$$S(\tau_a^1, \tau_a^2, \ldots, \tau_a^M; \mu) = \langle 0 | \mathcal{O}_S^\dagger \Theta(\Lambda - \hat{\Lambda}) \prod_{i=1}^{M} \delta(\tau_a^i - \hat{\tau}_a^i) \mathcal{O}_S | 0 \rangle \,, \tag{4.122}$$

where the operator τ_a^i returns the contribution to τ_a of final-state soft particles entering jet i, and $\hat{\Lambda}$ returns the energy of final-state soft particles outside of all N jets. We have kept the dependence on the scales μ_S^i and on Λ implicit on the left-hand side.

There are N Wilson lines appearing in the operator $\mathcal{O}_S$,

$$\mathcal{O}_S = Y_1 \ldots Y_M Y_{M+1} \ldots Y_N \,, \tag{4.123}$$

corresponding to the M measured jets and $N-M$ unmeasured jets. The scales associated with soft gluons entering the M measured jets whose shapes are measured to be $\tau_1, \ldots, \tau_M$ are $\mu_S^1, \ldots, \mu_S^M$, given by Eq. (4.88). The scale associated with soft gluons outside of measured jets is μ_S^Λ given by Eq. (4.86). We have illustrated the ladder of these scales in Fig. 4.6. Each of these soft scales can be associated with different soft fields A_s^i whose momenta scale as $\lambda_i^2 \omega_i$ where λ_i is associated with the typical transverse momentum $\lambda_i \omega_i$ of the collinear modes for the ith jet. For measured jets, λ_i is determined by τ_a^i, while for unmeasured jets $\lambda_i \sim \tan(R/2)$. For soft gluons outside jets, however, the soft momentum is set by the cutoff scale Λ, which is why μ_S^Λ appears in the ladder of Fig. 4.6.

At a scale μ larger than all μ_S^i and μ_S^Λ, the soft function is calculated as we presented in Sec. 6. In particular, we take the quantities τ_a^i and Λ to be nonzero and finite. At a scale μ below μ_S^1, we integrate out soft gluons of virtuality μ_S^1 and match onto a theory with soft gluons of virtuality μ_S^2. The scale μ_S^1 associated with τ_a^1 is taken to infinity, and phase space integrals for soft gluons entering the measured jet 1 become zero (see, e.g., Eq. (4.175)). Therefore, the matching coefficient from the theory above μ_S^1 to the theory below is just the measured jet 1 contribution $S^{\text{meas}}(\tau_a^1)$ to the soft function given by Eq. (4.87). The same occurs when matching from the theory above each scale μ_S^i for soft gluons entering measured jet i to the scale below μ_S^i, giving a matching coefficient $S^{\text{meas}}(\tau_a^i)$.

When going through the scale μ_S^Λ, in the theory above this scale, the calculation of unmeasured contributions to the soft function gives the result Eq. (4.85), by treating Λ as a nonzero, finite cutoff. In the theory below μ_S^Λ, we take Λ to infinity, making all phase space integrals originally cutoff by Λ to be scaleless and thus zero. So the matching coefficient between the theory above and below μ_S^Λ is just S^{unmeas}.

After performing the above matchings all the way down to the lowest soft scale Fig. 4.6, we find that the original soft function $S(\tau_a^1, \ldots, \tau_a^M; \mu)$ can be expressed to all orders as

$$S(\tau_a^1, \ldots, \tau_a^M; \mu) = S^{\text{unmeas}}(\mu) \prod_{i=1}^{M} S^{\text{meas}}(\tau_a^i; \mu) \, \langle 0 | \, \mathcal{O}_S^\dagger \mathcal{O}_S \, | 0 \rangle \,, \tag{4.124}$$

where to next-to-leading order S^{meas} and S^{unmeas} are given by

$$S^{\text{unmeas}}(\mu) = 1 + S_{(1)}^{\text{unmeas}}(\mu) \tag{4.125}$$

$$S^{\text{meas}}(\tau_a^i; \mu) = \delta(\tau_a^i) + S_{(1)}^{\text{meas}}(\tau_a^i; \mu) \,, \tag{4.126}$$

where $S^{\rm unmeas}_{(1)}$ is given by Eq. (4.85) and $S^{\rm meas}_{(1)}$ is given by Eq. (4.87). Note that no operators restricting the jet shape or the phase space appear in the final matrix element of soft fields living at the lowest scale on the ladder in Fig. 4.6. If all the scales on the ladder are at a perturbative scale, we can now just use $\langle \mathcal{O}_S^\dagger \mathcal{O}_S \rangle = 1$ to eliminate the final matrix element. If any scale is nonperturbative, we should have stopped the matching procedure before that scale, and defined the surviving soft matrix element still containing additional delta function operators as a nonperturbative shape function.

Since the factors $S^{\rm unmeas}(\mu)$ and $S^{\rm meas}(\tau_a^i, \mu)$ are now matching coefficients between two theories above and below the respective scales μ_S^Λ and μ_S^i, we can run each of the individual factors separately from their natural scale, instead of from a single soft scale μ_0 as in Eq. (4.120). The result for the RG-evolved soft function is then Eq. (4.124) where each factor at NLO is given by the solution of its RGE,

$$S^{\rm unmeas}(\mu) = U_S^{\rm unmeas}(\mu, \mu_\Lambda) S^{\rm unmeas}(\mu_\Lambda) \tag{4.127a}$$

$$S^{\rm meas}(\tau_a^i, \mu) = \int d\tau' U_S^i(\tau_a^i - \tau'; \mu, \mu_S^i) S^{\rm meas}(\tau', \mu_S^i)\,. \tag{4.127b}$$

These solutions allow us now to resum logarithms of all of the scales appearing in the ladder in Fig. 4.6 when these scales are widely disparate. However, the result we obtained in Eq. (4.116) when we took all scales to be of the same order and had a single soft scale has the form Eq. (4.127) at NLL accuracy. We will use equation Eq. (4.127) in all cases to interpolate between these two extremes.

7.5 Total Resummed Distribution

Collecting together the above results for the running of hard, jet, and soft functions in the factorized cross section Eq. (4.39), we obtain the RG-improved N-jet cross section differential in M jet shapes,

$$\begin{aligned}
\frac{1}{\sigma^{(0)}} \frac{d\sigma_N}{d\tau_{a_1}^1 \cdots d\tau_{a_M}^M} &= H(\mu_H) \left(\frac{\mu_H}{\bar\omega_H}\right)^{\omega_H(\mu,\mu_H)} \prod_{k=M+1}^N J_{\omega_k}^k(\mu_J^k) \left(\frac{\mu_J^k}{\omega_k \tan\frac{R}{2}}\right)^{\omega_J^k(\mu,\mu_J^k)} S^{\rm unmeas}(\mu_\Lambda) \\
&\quad \times \prod_{i=1}^M \Bigg\{ \left[1 + f_J^i(\tau_a^i, \mu_J^i) + f_S^i(\tau_a^i, \mu_S^i)\right] \left(\frac{\mu_S^i \tan^{1-a}\frac{R}{2}}{\omega_i}\right)^{\omega_S^i(\mu,\mu_S^i)} \\
&\quad \times \left(\frac{\mu_J^i}{\omega_i}\right)^{(2-a)\omega_J^i(\mu,\mu_J^i)} \frac{1}{\Gamma[-\omega_J^i(\mu,\mu_J^i) - \omega_S^i(\mu,\mu_S^i)]} \frac{1}{(\tau_a^i)^{1+\omega_J^i(\mu,\mu_J^i)+\omega_S^i(\mu,\mu_S^i)}} \Bigg\}_+ \\
&\quad \times \exp\left[\mathcal{K}(\mu; \mu_H, \mu_J^{1,\ldots,N}, \mu_S^{1,\ldots,M}, \mu_S^\Lambda) + \gamma_E \Omega(\mu; \mu_J^{1,\ldots,M}, \mu_S^{1,\ldots,M})\right],
\end{aligned} \tag{4.128}$$

where $\bar\omega_H$ is the color-weighted average of jet energies,

$$\bar\omega_H = \prod_{i=1}^N \omega_i^{\mathbf{T}_i^2/\mathbf{T}^2}\,, \tag{4.129}$$

the evolution parameters $\omega_F(\mu,\mu_F)$ and $K_F(\mu,\mu_F)$ are defined in Eq. (4.103), and we have defined the collective parameters,

$$\begin{aligned}\mathcal{K}(\mu;\mu_H,\mu_J^{1,\ldots,N},\mu_S^{1,\ldots,M},\mu_S^\Lambda) &= K_H(\mu,\mu_H)+\sum_{i=1}^N K_J^i(\mu,\mu_J^i)+\sum_{j=1}^M K_S^j(\mu,\mu_S^j)\\ &\quad + K_S^{\rm unmeas}(\mu,\mu_S^\Lambda)\end{aligned} \tag{4.130a}$$

$$\Omega(\mu;\mu_J^{1,\ldots,M},\mu_S^{1,\ldots,M}) = \sum_{i=1}^M \Omega_i(\mu;\mu_J^i,\mu_S^i) \equiv \sum_{i=1}^M [\omega_J^i(\mu,\mu_J^i)+\omega_S^i(\mu,\mu_S^i)]\,. \tag{4.130b}$$

The functions $f_{J,S}^i$ are generated by the finite pieces of the measured jet and soft functions,

$$\begin{aligned}f_J^i(\tau_a^i;\mu_J^i) = \frac{\alpha_s(\mu_J^i)\mathbf{T}_i^2}{\pi}\Bigg\{&\frac{2-a}{1-a}\ln^2\frac{\mu_J^i}{\omega_i(\tau_a^i)^{\frac{1}{2-a}}}+\left[c_i+\frac{2}{1-a}H(-1-\Omega_i)\right]\ln\frac{\mu_J^i}{\omega_i(\tau_a^i)^{\frac{1}{2-a}}}\\ &+(2-a)\ln^2\tan\frac{R}{2}-c_i\ln\tan\frac{R}{2}\Bigg\}+\frac{\alpha_s(\mu_J^i)}{2\pi}d_J(\tau_a^i)\end{aligned} \tag{4.131a}$$

$$f_S^i(\tau_a^i;\mu_S^i) = -\frac{\alpha_s(\mu_S^i)\mathbf{T}_i^2}{\pi}\frac{1}{1-a}\left\{\ln^2\frac{\mu_S^i\tan^{1-a}\frac{R}{2}}{\omega_i\tau_a^i}+2H(-1-\Omega_i)\ln\frac{\mu_S^i\tan^{1-a}\frac{R}{2}}{\omega_i\tau_a^i}+d_S(\tau_a^i)\right\}, \tag{4.131b}$$

where $c_i = 3/2$ for quark jets and $\beta_0/2C_A$ for gluon jets. $H(-1-\Omega_i)$ is the harmonic number function, with Ω_i given by Eq. (4.130b). The functions $d_{J,S}$ are additional contributions from the finite parts of jet and soft functions that do not contain any logarithms. They are given in Eq. (4.199) in the Appendix. Since we will use these finite parts only to tell us what scales to choose in order to minimize the large logarithms, and not actually include them in the final result at NLL accuracy, we do not need the exact form of the distributions $d_{J,S}(\tau_a)$. Similarly, the terms containing large logarithms in the unmeasured jet functions and unmeasured contribution to the soft function are

$$J_\omega^i(\mu_J) = 1+\left[\Gamma(\alpha_s(\mu_J))\mathbf{T}_i^2\ln^2\frac{\mu_J}{\omega\tan\frac{R}{2}}+\gamma_k[\alpha_s(\mu_J)]\ln\frac{\mu_J}{\omega\tan\frac{R}{2}}+d_J^i\right] \tag{4.132a}$$

$$\begin{aligned}S^{\rm unmeas}(\mu_\Lambda) = 1&+\Gamma(\alpha_s(\mu_\Lambda))\sum_i\mathbf{T}_i^2\left[\ln\left(\frac{\mu_\Lambda}{2\Lambda\tan^{1/2}\frac{R}{2}}\right)\ln\tan^2\frac{R}{2}-\frac{\pi^2}{8}\right]\\ &+\Gamma(\alpha_s(\mu_\Lambda))\sum_{i\neq j}\mathbf{T}_i\cdot\mathbf{T}_j\left[\ln\frac{\mu}{2\Lambda}\ln\frac{n_i\cdot n_j}{2}+\mathrm{Li}_2\left(1-\frac{2}{n_i\cdot n_j}\right)\right],\end{aligned} \tag{4.132b}$$

where d_J^i is the part of the unmeasured jet function containing no large logarithms (given in Eqs. (4.151) and (4.158) in the Appendix).

The finite parts of the measured and unmeasured jet and soft functions given in Eqs. (4.131) and (4.132) show that to minimize large logarithms in the NLO finite parts in the resummed distribution Eq. (4.128), we should choose initial scales for the running to be

$$\mu_H = \bar{\omega}_H \tag{4.133a}$$

$$\mu_J^i = \omega_i (\tau_a^i)^{\frac{1}{2-a}} \ , \quad \mu_J^k = \omega_k \tan\frac{R}{2} \tag{4.133b}$$

$$\mu_S^i = \frac{\omega_i \tau_a^i}{\tan^{1-a}\frac{R}{2}} \ , \quad \mu_\Lambda = 2\Lambda \tan^{1/2}\frac{R}{2} \, . \tag{4.133c}$$

These choices eliminate all large logarithms in the NLO hard, jet, and soft functions. They still leave logs of $\tan\frac{R}{2}$ and $n_i \cdot n_j$ in the unmeasured part of the soft function, and logs of $\tan\frac{R}{2}$ in the measured jet function, but we already take R numerically of $\mathcal{O}(1)$ [15] to minimize power corrections from our implementation of the jet algorithm, and $n_i \cdot n_j \approx 1$ since the jet separation parameter t_{ij} is large compared to 1. All logs of R, Λ, and τ_a^i are eliminated in the unmeasured jet function and measured part of the soft function.

8 Plots of Distributions and Comparisons to Monte Carlo

Having resummed the jet shape distributions in τ_a to NLL accuracy, in this section we plot the distributions for various values of a and R, compare to Monte Carlo simulated events, and perform scale variation on the resummed distribution. We use the process $e^+e^- \to 3$ jets to study our predictions of jet shapes, where the jets arise from partons in the "Mercedes-Benz" configuration, with each parton having equal energy. In these configurations, the partons lie in a plane and are equally separated with a pairwise angle of $2\pi/3$. This allows us to study event shape distributions of well-separated jets where t is reasonably large. We choose three values of R to study, $R = 1.0$, 0.7, and 0.4. With these values of R, the $1/t^2$ suppression factor for corrections to the large-t limit are 0.10, 0.044, and 0.014 respectively. We will measure the angularity of only one of the three jets; the other two jets will be unmeasured.

In general, the $\mathbf{T}_i \cdot \mathbf{T}_j$ color correlations in the soft and hard functions lead to operator mixing in color space under RG evolution. This implies that the RG kernels U_S and U_H are matrices in color space and must be studied on a process-by-process basis (see, e.g., [87, 144, 142, 105, 174, 175]). For the case of $N = 2, 3$ jets there is only one color-singlet operator and hence no mixing. This can be seen, for example, by noting that all color correlations reduce to the Casimir invariants (C_F and C_A) in this case (cf. Appendix 4.D). We have restricted the example process we use in this work to $N = 3$ jets, avoiding the additional complication of color-correlations that comes with a larger number of jets.

The NLL resummed distribution for one quark or gluon jet shape in a three-jet final state,

[15] We still consider $\tan(R/2)$ to be of order λ_k in the collinear sectors describing unmeasured jets, as implied by Eq. (4.133). This means λ_k is effectively much larger than the parameter λ_i in a measured jet sector.

choosing jet 1 to be the measured jet, is

$$\begin{aligned}\frac{1}{\sigma^{(0)}}\frac{d\sigma_3}{d\tau_a^1} &= \left(\frac{\mu_H}{\bar{\omega}_H}\right)^{\omega_H(\mu,\mu_H)} \left(\frac{\mu_J^1}{\omega_1}\right)^{(2-a)\omega_J^1(\mu,\mu_J^1)} \left(\frac{\mu_J^2}{\omega_2\tan\frac{R}{2}}\right)^{\omega_J^2(\mu,\mu_J^2)} \left(\frac{\mu_J^3}{\omega_3\tan\frac{R}{2}}\right)^{\omega_J^2(\mu,\mu_J^2)} \\ &\times \left(\frac{\mu_S^1\tan^{1-a}\frac{R}{2}}{\omega_1}\right)^{\omega_S^1(\mu,\mu_S^1)} \exp\left[\mathcal{K}(\mu;\mu_H,\mu_J^1,\mu_J^2,\mu_J^3,\mu_S^1,\mu_S^\Lambda)+\gamma_E\Omega(\mu;\mu_J^1,\mu_S^1)\right] \\ &\times \frac{1}{\Gamma[-\Omega(\mu;\mu_J^1,\mu_S^1)]}\frac{1}{(\tau_a^1)^{1+\Omega(\mu;\mu_J^1,\mu_S^1)}}\,,\end{aligned} \tag{4.134}$$

where the various evolution parameters $\omega_{J,S}^i$, Ω, $\mathcal{K}$ are all defined in Eqs. (4.103) and (4.130). The best scale choices Eq. (4.133) for this case are

$$\mu_H = \left(\omega_1^{\mathbf{T}_1^2}\omega_2^{\mathbf{T}_2^2}\omega_3^{\mathbf{T}_3^2}\right)^{\frac{1}{2C_F+C_A}} \tag{4.135a}$$

$$\mu_J^1 = \omega_1(\tau_a^1)^{\frac{1}{2-a}}\ ,\ \mu_J^{2,3} = \omega_{2,3}\tan\frac{R}{2} \tag{4.135b}$$

$$\mu_S^1 = \frac{\omega_1\tau_a^1}{\tan^{1-a}\frac{R}{2}}\ ,\ \mu_\Lambda = 2\Lambda\tan^{1/2}\frac{R}{2}\,. \tag{4.135c}$$

In Eq. (4.134) we have used tree-level initial conditions for the hard, jet, and soft functions at these scales. Eq. (4.134) evolves these functions to the arbitrary scale μ at NLL accuracy.

With these choices, we plot Eq. (4.134) in Fig. 4.7 for several values of a and R for a quark or gluon jet shape in a three-jet final state in e^+e^- annihilation at center-of-mass energy $Q = 500$ GeV. The jets are chosen to be in a Mercedes-Benz configuration, where all jets have equal energies of 150 GeV. We choose the jet energy cutoff Λ to be 15 GeV. We choose the factorization scale to be $\mu = \mu_H$.

We compare the results of a jet algorithm implemented on Monte Carlo simulated events with our NLL resummed predictions for a variety of a and R values in Fig. 4.8. Because the resummed NLL distribution we choose to study applies to an exclusive process, three-jet events in the Mercedes-Benz configuration, we implement cuts on the simulated events to obtain a sample that matches onto this configuration. We use MadGraph/MadEvent v.4.4.21 [6] to generate parton-level $e^+e^- \to q\bar{q}g$ events at a center-of-mass energy $Q = 500$ GeV, with cuts imposed to obtain partons in the Mercedes-Benz configuration. We shower and hadronize the events with Pythia v.6.414 [177] using p_T-ordered parton showers. The process of hadronization will induce a shift in the angularity distribution, which we do not model in our resummed distribution. Therefore, we produce two samples: one sample with only QCD final-state showering, no initial-state radiation, and no hadronization, and another sample with complete showering, initial-state radiation, and hadronization. The anti-k_T jet algorithm is run on the final state particles from Pythia, and we use FastJet [64] to implement the jet algorithm. The anti-k_T algorithm is particularly well suited for this comparison, as very few particles at an angle $\theta > R$ to the jet axis are included in the jet. With anti-k_T, the phase space cut on an individual particle matches well with the phase space cuts in the next-to-leading order calculation.

To select a sample of events to compare to our NLL resummed distributions, we make cuts on the final state jets, requiring each of the three hard, well-separated partons from MadGraph to

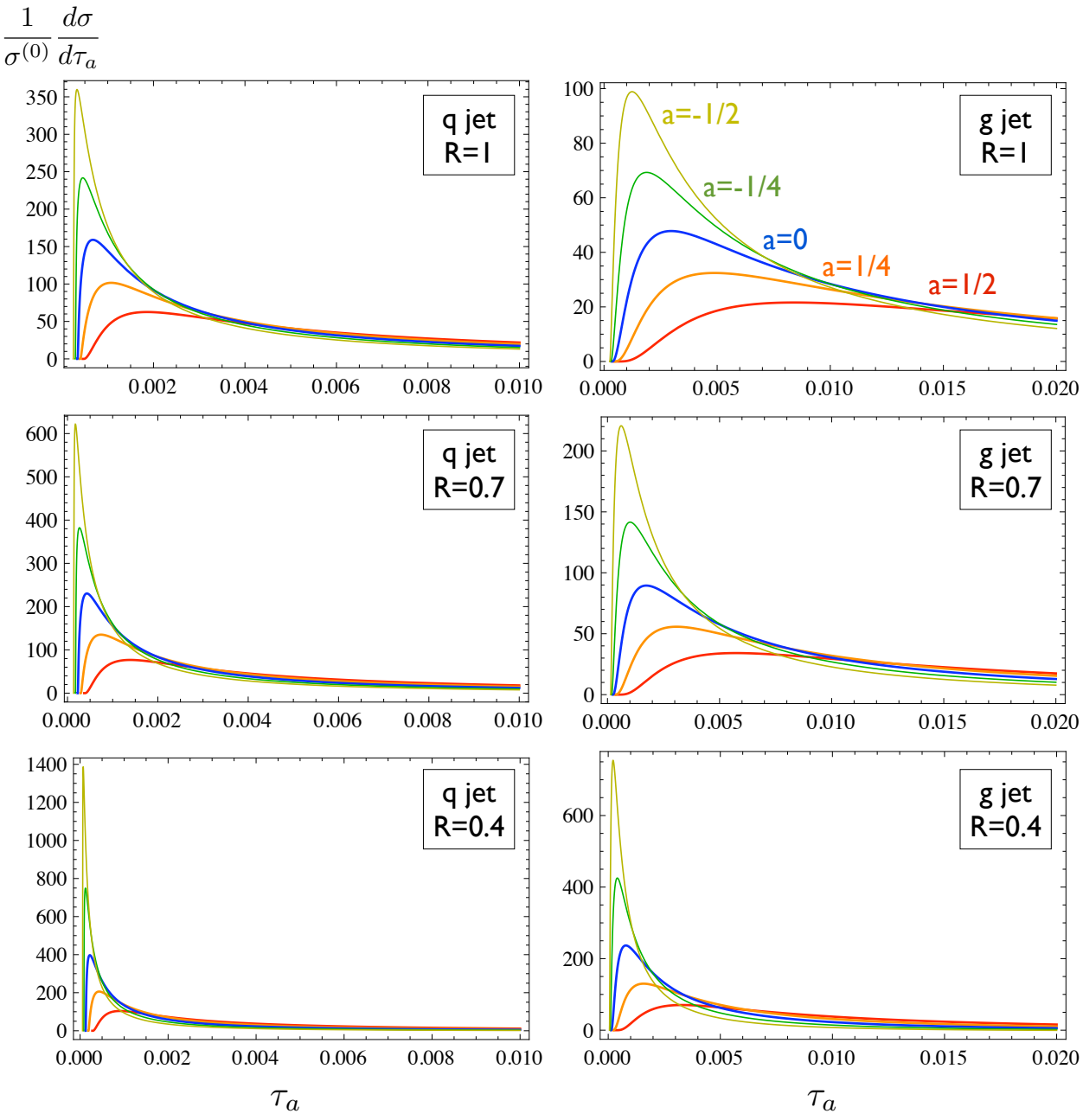

Figure 4.7: Quark and gluon jet shapes for several values of a and R. The NLL resummed distribution in Eq. (4.134) is plotted for $a = -\frac{1}{2}, -\frac{1}{4}, 0, \frac{1}{4}, \frac{1}{2}$ for quark and gluon jets with $R = 1, 0.7, 0.4$. The plots are for jets produced in e^+e^- annihilation at center-of-mass energy $Q = 500$ GeV, with three jets produced in a Mercedes-Benz configuration with equal energies $E_J = 150$ GeV, and minimum threshold $\Lambda = 15$ GeV to produce a jet.

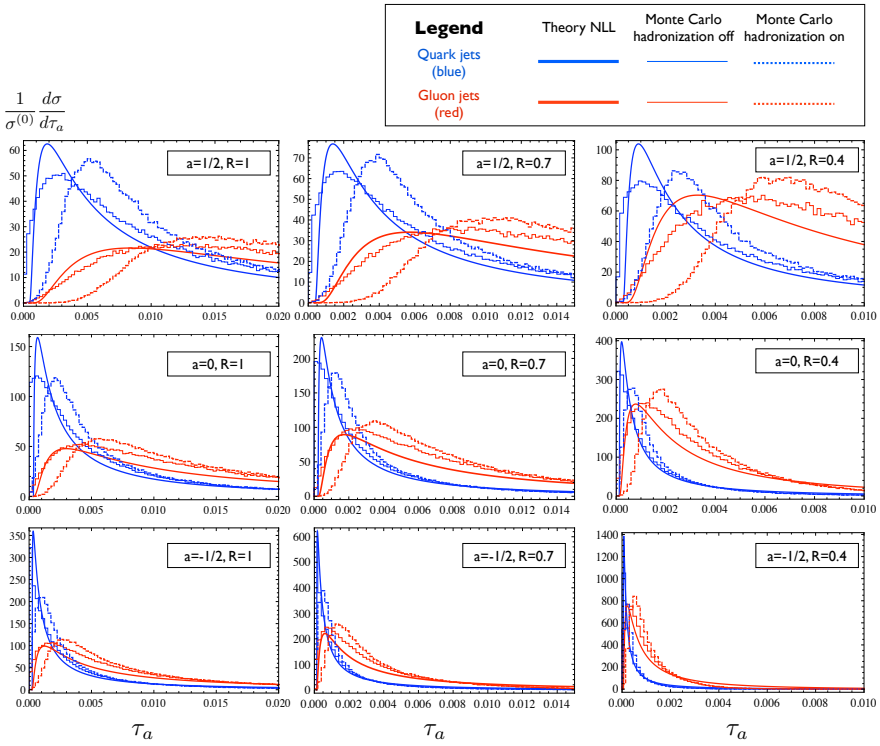

Figure 4.8: Quark vs. gluon jet shapes with comparison to Monte Carlo. Solid, straight curves represent the NLL resummed jet shape distribution in Eq. (4.134), and jagged curves are histograms from the Monte Carlo, normalized as described in the text. The solid histogram has no hadronization, while the dashed histogram includes the effects of hadronization. The distributions are plotted for $a = -\frac{1}{2}, 0, \frac{1}{2}$ with quark (blue) and gluon (red) jets compared on the same plot, for jets of size $R = 1.0, 0.7, 0.4$. Gluon jet shape distributions peak at larger values of τ_a than quark jets, indicative of their broader shape. The plots are for jets produced in e^+e^- annihilation at center-of-mass energy $Q = 500$ GeV, with three jets produced in a Mercedes-Benz configuration with equal energies $E_J = 150$ GeV, angular separation $\psi = 2\pi/3$ between all pairs of jets, and minimum threshold $\Lambda = 15$ GeV to produce a jet.

be associated with a jet. This involves a cut on the jet direction and momentum:

$$\frac{\mathbf{p}_{\text{parton}} \cdot \mathbf{p}_{\text{jet}}}{|\mathbf{p}_{\text{parton}}|\,|\mathbf{p}_{\text{jet}}|} > 0.9 \quad \text{and} \quad \frac{||\mathbf{p}_{\text{parton}}| - |\mathbf{p}_{\text{jet}}||}{|\mathbf{p}_{\text{parton}}|} < 0.15\,. \tag{4.136}$$

We analyze events passing these cuts, and tag each associated jet as coming from a quark or a gluon based on which parton it matches onto. The angularity value for each jet is computed from the constituent particles of the jet, using the matching parton direction as the jet axis. The jet direction only differs from the parton direction by a power correction (see Sec. 4.2). In Fig. 4.8, we isolate some of the quark and gluon jet shapes in Fig. 4.7 and compare to Monte Carlo events.

The relative normalization between Monte Carlo events and the NLL resummed angularity distribution is important. Both our calculation and the Monte Carlo simulation are most accurate in the region that includes the peak of the distribution and the larger-τ side of the peak, but

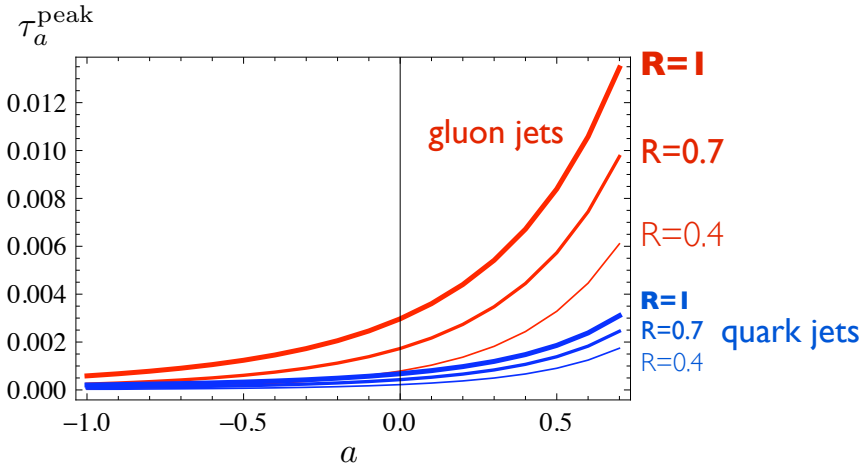

Figure 4.9: Location of peak of jet shape distribution as a function of a for quark and gluon jets. We plot the value of τ_a at the peak of the jet shape distribution for a between -1.0 and 0.8 for quark vs. gluon jets, using $R = 1, 0.7, 0.4$.

both are inaccurate as $\tau \to 0$ and in the tail region. Therefore, each will differ in the relative normalization between the peak region and the tail region. An accurate prediction of the tail region requires matching onto a calculation at fixed-order in α_s in full QCD as in [73, 41, 134]. In Fig. 4.8, we choose to normalize the area of the Monte Carlo distribution to the total area of the NLL resummed theory distribution. We find the area under the theory curves for gluon jets to be 1 within small numerical errors, and for quark jets, 0.5 for $R = 0.4$, 0.65 for $R = 0.7$, and 0.8 for $R = 1$. This suppression in the normalization is due to the fact that quark jet shape distributions are peaked closer to $\tau_a = 0$, where α_s evaluated at the measured jet and soft scales $\mu^1_{J,S}(\tau_a)$ grows large, causing the evolution kernels to suppress the distribution. Gluon jet shapes, being peaked at larger τ_a, are not as prone to this suppression. This should be cured by convolving the perturbative distribution with a nonperturbative shape function that moves the peak of the distribution to larger τ_a, as also suggested by the Monte Carlo predictions with hadronization turned on.

Nevertheless, the shapes of the theory and Monte Carlo distributions are very similar in the peak region. Across the values of a and R that we sample, the dependence of the shape and the location of the peak value agrees very well between the theory distributions and the Monte Carlo distributions without hadronization for both quark and gluon jets.

In Fig. 4.9 we plot the location of the peak of the jet shape distributions as a function of a for three values of R, displaying the different variation of the peak of quark and gluon jet shape distributions. The peak value increases with increasing R and a, as wide angle radiation is included (increasing R) and less suppressed (increasing a). Although the difference in the peak value between the quark and gluon jet angularity distributions is large, the width of each distribution creates substantial overlap in angularity values between quark and gluon jets. Distinguishing between quark and gluon jets using jet angularities is a complex task which we will explore in [115]; for now, we note only that the NLL resummed distributions indicate that discrimination between quark and gluon jets using jet angularities is possible.

As a rough estimate of the theoretical uncertainty in our NLL resummed predictions for

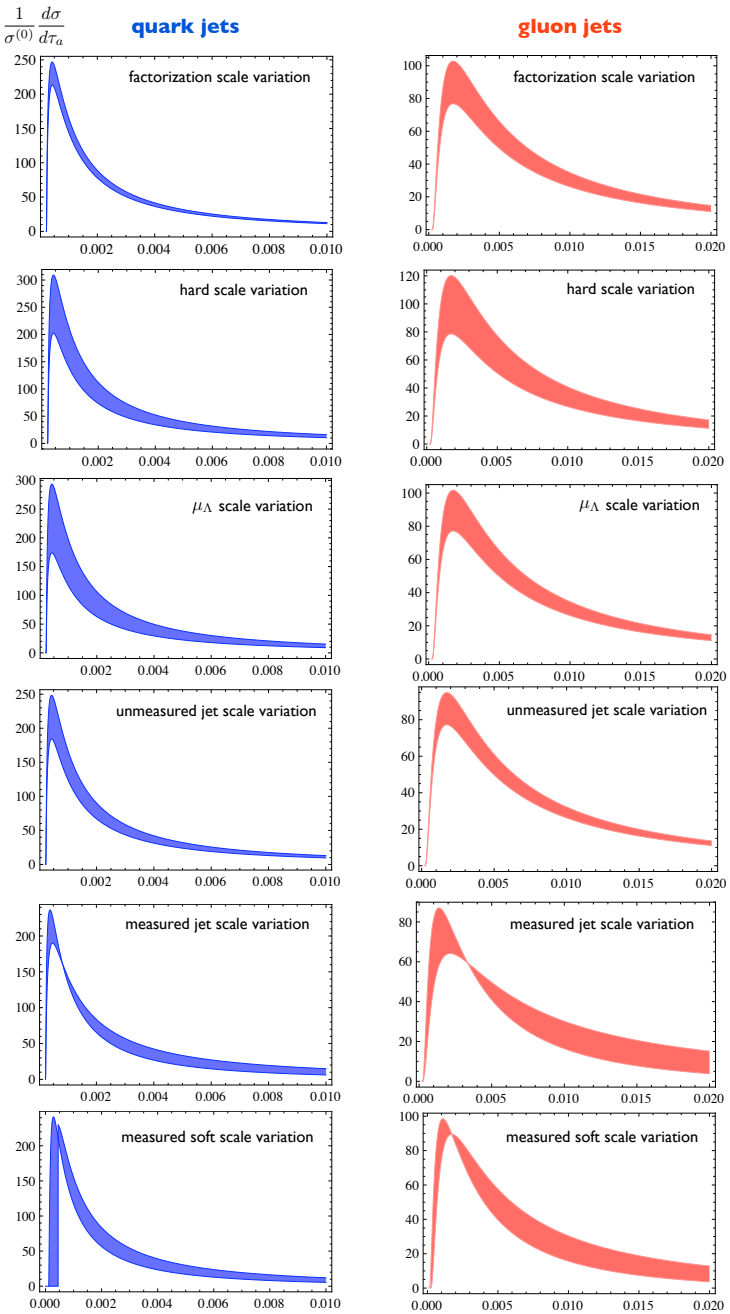

Figure 4.10: Scale variation of quark and gluon jet shapes. For $\tau_a = 0$ and $R = 0.7$, we display the variation of the NLL resummed jet shape distributions with the hard scale μ_H, the jet cutoff scale μ_Λ, the unmeasured jet scales $\mu_J^{2,3}$, the measured jet scale $\mu_J^1(\tau_a)$, and the measured soft scale $\mu_S(\tau_a)$. In each case we vary the scale between 1/2 and 2 times the natural choices in Eq. (4.133), except for the measured soft scale, which we varied between 1 and 2 times the choice in Eq. (4.133). We keep the factorization scale fixed at the default hard scale given by Eq. (4.135), $\mu = \omega_i$.

these jet shape distributions, we show in Fig. 4.10 the variation of the $a = 0$ quark and gluon τ_a jet shape distributions for jets of radius $R = 0.7$ with changes in the various scales that appear in the resummed cross section Eq. (4.134). These are the initial scales at which the hard, jet, and soft functions are evaluated to minimize logarithms in the NLO fixed-order part, from which the evolution kernels run them to the common factorization scale μ. In the top row of Fig. 4.10, we vary the factorization scale μ between $\bar{\omega}_H/2$ and $2\bar{\omega}_H$. In the next four rows, we vary the hard scale μ_H, the soft jet energy cutoff scale μ_Λ, the unmeasured jet scales $\mu_J^{2,3}$, and the measured jet scale $\mu_J^1(\tau_a^1)$ between half and twice the natural values given in Eq. (4.135). In the last row, we vary the measured soft scale $\mu_S^1(\tau_a^1)$ between one and two times the value in Eq. (4.135). This is because too low a value of $\mu_S^1(\tau_a^1)$ as $\tau_a \to 0$ brings it into the nonperturbative region where $\alpha_s(\mu_S^1)$ blows up, so that the perturbative estimate of uncertainty is not very meaningful. We note that, while the uncertainty in the vertical scale of the distributions is considerable in some cases, the location of the peak and the shape as a function of τ_a along the horizontal axis is remarkably stable.

9 Conclusions

In this work, we have factorized an N-jet exclusive cross section differential in $M \leq N$ jet observables and resummed logarithms of the jet observable τ_a to NLL accuracy. We demonstrated that the anomalous dimensions of the hard, jet, and soft functions in the factorization theorem satisfy the nontrivial consistency condition Eq. (4.121) to NLO in α_s, for any number of quark and gluon jets, any number of jets whose shapes are measured, and any size R of the jets, as long as the jets are well-separated, meaning $t \gg 1$. This condition ensures the validity of an effective theory with N collinear directions that are assumed to be distinct. We identified and estimated important power corrections to the factorized form of the cross section. We also illustrated that zero-bin subtractions give nonzero contributions to the anomalous dimensions crucial for consistency.

Armed with consistent factorization and the fixed-order jet and soft functions, we resummed large logarithms in the jet shape distribution by running each individual function from the scale where logs in it are minimized to the common factorization scale μ. We thereby resummed logs of the jet shape τ_a to NLL accuracy, and logs of the scale Λ/E_J of soft radiation outside of jets (up to possible missing non-global logs), but not all logs of the angular cut R, which we took to be order 1. This is the first such calculation of a resummed jet shape distribution in an exclusive multijet cross section.

We constructed a framework to deal with all the scales that appear in the multijet soft function which depends on the values τ_a^i of all M jet shapes and the phase space cuts Λ, R. By refactorizing the full soft function into individual pieces depending on one of these scales at a time, we were able to sum logs of ratios of these scales.

We demonstrated the utility and accuracy of our results by comparing our NLL resummed prediction for quark and gluon jet shapes in $e^+e^- \to 3$ jets to the output of Monte Carlo event generators, MadGraph/MadEvent and Pythia. Our predictions agreed with the Monte Carlo output without hadronization very well. The change in shape and location of the peak value of τ_a as functions of a and R match particularly well between the theory and Monte Carlo.

Our results provide a basis for future studies of other jet observables at both e^+e^- and hadron colliders, requiring recalculation of those parts of our jet and soft functions actually depending on the choice of observable. Studying jets at hadron colliders requires the construction

of observables appropriate for that environment and the switching of two of our outgoing jets to incoming beams, which can be described by beam functions in SCET [183].

Precision calculations of jet shapes will allow improved discrimination of jets of different origins. We are applying the results of our predictions of light quark and gluon jet shapes to distinguish quark and gluon jets with greater efficiency than achieved before, and will present the results in [115]. Extensions to the shapes of heavy jets and calculations of other types of jet shapes such as the $\Psi(r/R)$ shape introduced in [117, 118, 1] can also be performed.

4.A Jet Function Calculations

4.A.1 Finite Pieces of the Quark Jet Function

4.A.1.0.1 Measured Quark Jet Function The finite pieces the jet functions, which depend on the jet algorithm, share common features. For cone-type algorithms, the finite piece of the naive part of the quark jet function, $\tilde{J}^q_{\rm alg}(\tau_a)$, is given by

$$\tilde{J}^q_{\rm cone}(\tau_a) = C_F \left(\frac{7}{2} + 3\ln 2 - \frac{\pi^2}{3}\right)\delta(\tau_a) + \frac{C_F}{1-\frac{a}{2}}\left[\mathcal{I}^q_{\rm cone}\frac{\Theta(\tau_a)\Theta(\tau_a^{\rm max}-\tau_a)}{\tau_a}\right]_+ \tag{4.137}$$

where in this Appendix, plus distributions are defined by [183]

$$[\Theta(x)g(x)]_+ = \lim_{\epsilon\to 0}\frac{d}{dx}[\Theta(x-\epsilon)G(x)], \qquad \text{with} \qquad G(x) = \int_1^x dx' g(x')\,, \tag{4.138}$$

defined so as to satisfy the boundary condition $\int_0^1 dx[\Theta(x)g(x)]_+ = 0$. The quantity $\mathcal{I}^q_{\rm cone}$ depends implicitly on τ_a and R and is given by

$$\mathcal{I}^q_{\rm cone} = \int_{x_{\rm cone}}^{1-x_{\rm cone}} dx\,\frac{2(1-x)+x^2}{x} = 2\log\frac{1-x_{\rm cone}}{x_{\rm cone}} - \frac{3}{2} + 3x_{\rm cone}\,. \tag{4.139}$$

The parameter $x_{\rm cone} = x_{\rm cone}(\tau_a)$ is the lower limit on the $x = q^-/\omega$ scaled gluon momentum integral imposed by the cone restriction. It is given by the solution of the equation

$$f_{\rm cone}(x_{\rm cone}) = \frac{\tau_a}{\tan^{2-a}\frac{R}{2}}\,, \tag{4.140}$$

where $f_{\rm cone}(x)$ is defined as

$$f_{\rm cone}(x) \equiv x^{2-a}[x^{-1+a} + (1-x)^{-1+a}] \tag{4.141}$$

in the range $0 < x < 1/2$, which is plotted in Fig. 4.11A. The upper limit $\tau_a^{\rm max}$ is given by the maximum value over x of Eq. (4.140). Similarly, for k_T-type algorithms, $\tilde{J}^q_{k_T}(\tau_a)$ is given by

$$\tilde{J}^q_{k_T}(\tau_a) = C_F\left(\frac{13}{2} - 2\frac{\pi^2}{3}\right)\delta(\tau_a) + \frac{C_F}{1-\frac{a}{2}}\left[\mathcal{I}^q_{k_T}\,\frac{\Theta(\tau_a)\Theta(\tau_a^{\rm max}-\tau_a)}{\tau_a}\right]_+ . \tag{4.142}$$

$\mathcal{I}^q_{k_T}$ is given by

$$\mathcal{I}^q_{k_T} = \int_{\mathcal{R}} dx\,\frac{2(1-x)+x^2}{x} \tag{4.143}$$

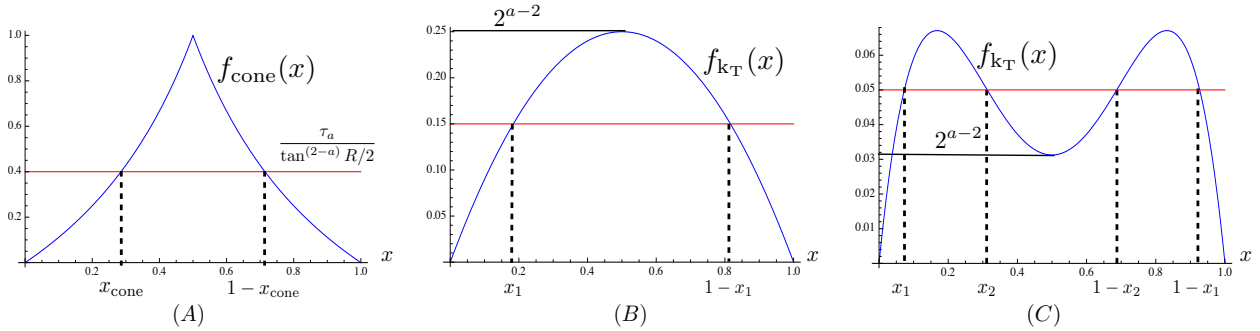

Figure 4.11: Regions of integration for the (A) cone and $\mathrm{k_T}$-type algorithms for (B) $a > -1$ and (C) $a < -1$. The allowed region of x is when the (blue) functions $f_{\rm cone,\,k_T}(x)$ lie above the (red) lines of constant $\tau_a/\tan^{(2-a)} R/2$. When $a < -1$ for the $\mathrm{k_T}$ algorithm, there are two regions of integration when $\tau_a > 2^{a-2}\tan^{(2-a)} R/2$.

where $\mathcal{R}$ is the region in x where the constraint

$$f_{\rm k_T}(x) \equiv x^{2-a}(1-x)^{2-a}[x^{-1+a} + (1-x)^{-1+a}] \geq \frac{\tau_a}{\tan^{2-a}\frac{R}{2}} \tag{4.144}$$

is satisfied. We plot this region in Fig. 4.11B and C for the cases $a > -1$ and $a < -1$, repsectively. The upper limit $\tau_a^{\rm max}$ is given by the maximum value over x of the right-hand side of Eq. (4.144). In general, the constraint Eq. (4.144) is symmetric about $x = \frac{1}{2}$, and so the region $\mathcal{R}$ is symmetric about the same point. In general, if $a > -1$ or $\tau_a < 2^{a-2}\tan^{(2-a)}\frac{R}{2}$, then $\mathcal{R}$ is a single range in x. Otherwise, $\mathcal{R}$ is two disjoint ranges in x. Since $\tau_a \geq 2^{a-2}\tan^{(2-a)}\frac{R}{2}$ can only occur for $a < -1$, we can write $\mathcal{I}^q_{\rm k_T}$ as

$$\mathcal{I}^q_{\rm k_T} = \int_{x_1}^{1-x_1} dx\, \frac{2(1-x)+x^2}{x} - \Theta\left(\tau_a > 2^{a-2}\tan^{(2-a)}\frac{R}{2}\right)\int_{x_2}^{1-x_2} dx\, \frac{2(1-x)+x^2}{x} \tag{4.145}$$

Note that $\mathcal{I}^q_{\rm cone}$ and $\mathcal{I}^q_{\rm k_T}$ involve the same integrand, but for each algorithm the integral is over different ranges. In addition, both $x_{\rm cone}$ and x_1 approach the same limiting value for small τ_a,

$$x \xrightarrow{\tau_a \to 0} \frac{\tau_a}{\tan^{(2-a)}\frac{R}{2}}\,. \tag{4.146}$$

Thus, we can extract the small τ_a behavior of both distributions by writing

$$\left[\frac{1}{\tau_a}\ln\left(\frac{1-x}{x}\right)\right]_{\dot{+}} = \left[\frac{1}{\tau_a}\ln\left(\frac{\tau_a}{\tan^{(2-a)}\frac{R}{2}}\frac{1-x}{x}\right)\right]_{\dot{+}} - \left[\frac{1}{\tau_a}\ln\left(\frac{\tau_a}{\tan^{(2-a)}\frac{R}{2}}\right)\right]_{+}, \tag{4.147}$$

where $x = x_{\rm cone}$ or x_1 for the cone and $\mathrm{k_T}$ algorithms, respectively. Defining

$$r_q(x) = 3x + 2\ln\frac{1-x}{x}\,, \tag{4.148}$$

using Eq. (4.147), and including the zero-bin subtraction in Eq. (4.49), we find that the finite distributions of the full measured quark jet functions are

$$J^q_{\rm cone}(\tau_a) = C_F\left[\frac{3}{2}\ln\frac{\mu^2}{\omega^2\tan^2\frac{R}{2}} + \frac{1-\frac{a}{2}}{1-a}\ln^2\frac{\mu^2}{\omega^2} + \left(1-\frac{a}{2}\right)\ln^2\tan^2\frac{R}{2} + \frac{7}{2} + 3\ln 2\right. \tag{4.149a}$$
$$\left. - \frac{\pi^2}{6}\left(2+\frac{1-\frac{a}{2}}{1-a}\right)\right]\delta(\tau_a) - C_F\left\{\left[\frac{4}{1-a}\ln\frac{\mu}{\omega\tau_a^{1/(2-a)}} + \frac{3}{2-a}\right]\frac{\Theta(\tau_a)}{\tau_a}\right\}_+$$
$$+ \frac{C_F}{1-\frac{a}{2}}\left\{\frac{\Theta(\tau_a)\Theta(\tau_a^{\rm max}-\tau_a)}{\tau_a}\left[r_q(x_{\rm cone}) + 2\ln\left(\frac{\tau_a}{\tan^{(2-a)}\frac{R}{2}}\right)\right]\right\}_{\dot{+}}$$

and

$$J^q_{\rm k_T}(\tau_a) = C_F\left[\frac{3}{2}\ln\frac{\mu^2}{\omega^2\tan^2\frac{R}{2}} + \frac{1-\frac{a}{2}}{1-a}\ln^2\frac{\mu^2}{\omega^2} + \left(1-\frac{a}{2}\right)\ln^2\tan^2\frac{R}{2} + \frac{13}{2}\right. \tag{4.149b}$$
$$\left. - \frac{\pi^2}{6}\left(4+\frac{1-\frac{a}{2}}{1-a}\right)\right]\delta(\tau_a) - C_F\left\{\left[\frac{4}{1-a}\ln\frac{\mu}{\omega\tau_a^{1/(2-a)}} + \frac{3}{2-a}\right]\frac{\Theta(\tau_a)}{\tau_a}\right\}_+$$
$$+ \frac{C_F}{1-\frac{a}{2}}\left\{\frac{\Theta(\tau_a)\Theta(\tau_a^{\rm max}-\tau_a)}{\tau_a}\left[r_q(x_1) + 2\ln\left(\frac{\tau_a}{\tan^{(2-a)}\frac{R}{2}}\right)\right.\right.$$
$$\left.\left. - \Theta\left(\tau_a^{\frac{1}{2-a}} > 2\tan\frac{R}{2}\right) r_q(x_2)\right]\right\}_{\dot{+}}.$$

4.A.1.0.2 Unmeasured Quark Jet Function The finite pieces for the unmeasured quark jet function are

$$J^q_{\rm alg} = \frac{3C_F}{2}\ln\left(\frac{\mu^2}{\omega^2\tan^2\frac{R}{2}}\right) + \frac{C_F}{2}\ln^2\left(\frac{\mu^2}{\omega^2\tan^2\frac{R}{2}}\right) + d_J^{q,\,\rm alg}, \tag{4.150}$$

where the constant term $d_J^{q,\,\rm alg}$ is given by

$$d_J^{q,\,\rm cone} = C_F\left(\frac{7}{2} + 3\ln 2 - \frac{5\pi^2}{12}\right) \tag{4.151a}$$

and

$$d_J^{q,\,\rm k_T} = C_F\left(\frac{13}{2} - \frac{3\pi^2}{4}\right), \tag{4.151b}$$

for the cone and $\rm k_T$ algorithms, respectively.

4.A.2 Finite Pieces of the Gluon Jet Function

4.A.2.0.3 Measured Gluon Jet Function The finite distributions of the naive gluon jet function are given by

$$\tilde{J}^g_{\rm cone}(\tau_a) = \delta(\tau_a)\left[C_A\left(\frac{137}{36}+\frac{11}{3}\ln 2-\frac{\pi^2}{3}\right)-T_R N_f\left(\frac{23}{18}+\frac{4}{3}\ln 2\right)\right] + \frac{1}{1-\frac{a}{2}}\left[\mathcal{I}^g_{\rm cone}\frac{\Theta(\tau_a)\Theta(\tau_a^{\rm max}-\tau_a)}{\tau_a}\right]_{\dot{+}}, \tag{4.152}$$

and

$$\tilde{J}^g_{\rm k_T}(\tau_a) = \delta(\tau_a)\left[C_A\left(\frac{67}{9}-\frac{2\pi^2}{3}\right)-T_R N_f\left(\frac{23}{9}\right)\right]+\frac{1}{1-\frac{a}{2}}\left[\mathcal{I}^g_{\rm k_T}\frac{\Theta(\tau_a)\Theta(\tau_a^{\rm max}-\tau_a)}{\tau_a}\right]_{\dot{+}}, \tag{4.153}$$

where the integrals $\mathcal{I}^g_{\rm alg}$ are given by

$$\mathcal{I}^g_{\rm alg} = \int dx\left[C_A\left(\frac{1}{x(1-x)}+x(1-x)-2\right)+T_R N_f\left(1-2x(1-x)\right)\right], \tag{4.154}$$

with the cone and $\rm k_T$ regions of integration the same as for the quark jet functions. The value $\tau_a^{\rm max}$ is the same as in the measured quark jet function, for the respective jet algorithm.

Going through similar steps as for the quark jet function, defining

$$r_g(x) = 2C_A\ln\left(\frac{1-x}{x}\right)+C_A\,x\left(\frac{2}{3}x^2-x+4\right)-T_R N_f\,x\left(\frac{4}{3}x^2-2x+2\right), \tag{4.155}$$

and using Eq. (4.147) to make all logarithmic dependence on τ_a explicit, we find for the cone and $\rm k_T$-type jet function finite distributions

$$\begin{aligned} J^g_{\rm cone}(\tau_a) = \delta(\tau_a)\Bigg[&\frac{\beta_0}{2}\ln\frac{\mu^2}{\omega^2\tan^2\frac{R}{2}}+C_A\frac{1-\frac{a}{2}}{1-a}\ln^2\frac{\mu^2}{\omega^2}+C_A\left(1-\frac{a}{2}\right)\ln^2\tan^2\frac{R}{2} \\ &+C_A\left(\frac{137}{36}+\frac{11}{3}\ln 2-\frac{\pi^2}{6}\left(2+\frac{1-\frac{a}{2}}{1-a}\right)\right)-T_R N_f\left(\frac{23}{18}+\frac{4}{3}\ln 2\right)\Bigg] \\ &-\left\{\left[\frac{4C_A}{1-a}\ln\frac{\mu}{\omega\tau_a^{1/(2-a)}}+\frac{\beta_0}{2-a}\right]\frac{\Theta(\tau_a)}{\tau_a}\right\}_+ \\ &+\frac{1}{1-\frac{a}{2}}\left\{\frac{\Theta(\tau_a)\Theta(\tau_a^{\rm max}-\tau_a)}{\tau_a}\left[r_g(x_{\rm cone})+2C_A\ln\left(\frac{\tau_a}{\tan^{(2-a)}\frac{R}{2}}\right)\right]\right\}_{\dot{+}}, \end{aligned} \tag{4.156a}$$

and

$$J^g_{\mathrm{k_T}}(\tau_a) = \delta(\tau_a)\Bigg[\frac{\beta_0}{2}\ln\frac{\mu^2}{\omega^2\tan^2\frac{R}{2}} + C_A\frac{1-\frac{a}{2}}{1-a}\ln^2\frac{\mu^2}{\omega^2} + C_A\left(1-\frac{a}{2}\right)\ln^2\tan^2\frac{R}{2} \\ + C_A\left(\frac{67}{9} - \frac{\pi^2}{6}\left(4 + \frac{1-\frac{a}{2}}{1-a}\right)\right) - T_R N_f\left(\frac{23}{9}\right)\Bigg] \\ - \left\{\left[\frac{4C_A}{1-a}\ln\frac{\mu}{\omega\tau_a^{1/(2-a)}} + \frac{\beta_0}{2-a}\right]\frac{\Theta(\tau_a)}{\tau_a}\right\}_+ \\ + \frac{1}{1-\frac{a}{2}}\left\{\frac{\Theta(\tau_a)\Theta(\tau_a^{\max}-\tau_a)}{\tau_a}\left[r_g(x_1) + 2C_A\ln\left(\frac{\tau_a}{\tan^{(2-a)}\frac{R}{2}}\right)\right.\right. \\ \left.\left. - \Theta\left(\tau_a^{\frac{1}{2-a}} > 2\tan\frac{R}{2}\right) r_g(x_2)\right]\right\}_+ , \tag{4.156b}$$

where x_{cone} and $x_{1,\,2}$ are given in Eqs. (4.139) and (4.144).

4.A.2.0.4 Unmeasured Gluon Jet Function For the unmeasured gluon jet functions, the finite pieces are given by

$$J^g_{\mathrm{alg}} = \frac{C_A}{2}\ln^2\frac{\mu^2}{\omega^2\tan^2\frac{R}{2}} + \frac{\beta_0}{2}\ln\frac{\mu^2}{\omega^2\tan^2\frac{R}{2}} + d_J^{g,\,\mathrm{alg}} \tag{4.157}$$

where the constant part $d_J^{g,\,\mathrm{alg}}$ for the cone and $\mathrm{k_T}$ algorithms is given by

$$d_J^{g,\,\mathrm{cone}} = C_A\left(\frac{137}{36} + \frac{11}{3}\ln 2 - \frac{5\pi^2}{12}\right) - T_R N_f\left(\frac{23}{18} + \frac{4}{3}\ln 2\right) \tag{4.158a}$$

and

$$d_J^{g,\,\mathrm{k_T}} = C_A\left(\frac{67}{9} - \frac{3\pi^2}{4}\right) - T_R N_f\left(\frac{23}{9}\right), \tag{4.158b}$$

respectively.

4.B Soft function calculations

4.B.1 S_{ij}^{incl}

To evaluate the expression Eq. (4.76), we first define

$$S_{ij}^{\mathrm{incl}} \equiv \frac{1}{\epsilon}\frac{\alpha_s}{2\pi}\left(\frac{4\pi\mu^2}{4\Lambda^2}\right)^{\epsilon}\mathbf{T}_i\cdot\mathbf{T}_j\,\mathcal{I}^{\mathrm{incl}}(n_i\cdot n_j)\,. \tag{4.159}$$

We need $\mathcal{I}^{\rm incl}$ to $\mathcal{O}(\epsilon)$. Working in a coordinate system with $\vec{n}_i$ aligned along the z-axis and $\vec{n}_j$ in the xz-plane and defining $n \equiv 1 - n_i \cdot n_j = n_j^z$, we have

$$\begin{aligned}\mathcal{I}^{\rm incl}(n_i \cdot n_j) &= \frac{n_i \cdot n_j \, 4^\epsilon \, \Gamma(1-\epsilon)}{2\sqrt{\pi}\Gamma(\frac{1}{2}-\epsilon)} \int_0^\pi d\theta \sin^{1-2\epsilon}\theta \frac{1}{1-\cos\theta} \frac{1}{1 - n_j^x \sin\theta\cos\phi - n_j^z \cos\theta} \\ &= \frac{4^\epsilon}{2}\Gamma(1-\epsilon) \int_{-1}^{+1} du\,(1-u)^{-1-\epsilon}(1+u)^{-\epsilon} \frac{1-n}{1-un} \, {}_2\tilde{F}_1\left(\frac{1}{2}, 1; 1-\epsilon; z\right) \end{aligned} \tag{4.160}$$

where $z = \frac{(1-n^2)(1-u^2)}{(1-un)^2}$. The integration over $u = \cos\theta$ has singularities at the points $u = 1$ and $u = n$ which correspond to $z = 1$ and $z = 0$, respectively. To isolate these singularities, we split the integration over u into the ranges $(-1, \delta)$ and $(\delta, 1)$ where $n < \delta < 1$,

$$\mathcal{I}^{\rm incl}(n_i \cdot n_j) = \mathcal{I}_1^{\rm incl}(n_i \cdot n_j) + \mathcal{I}_2^{\rm incl}(n_i \cdot n_j)\,, \tag{4.161}$$

where

$$\begin{aligned}\mathcal{I}_1^{\rm incl}(n_i \cdot n_j) &\equiv \frac{4^\epsilon}{2}\Gamma(1-\epsilon) \int_{-1}^{\delta} du\,(1-u)^{-1-\epsilon}(1+u)^{-\epsilon} \frac{1-n}{1-un} \, {}_2\tilde{F}_1\left(\frac{1}{2}, 1; 1-\epsilon; z\right) \\ \mathcal{I}_2^{\rm incl}(n_i \cdot n_j) &\equiv \frac{4^\epsilon}{2}\Gamma(1-\epsilon) \int_{\delta}^{1} du\,(1-u)^{-1-\epsilon}(1+u)^{-\epsilon} \frac{1-n}{1-un} \, {}_2\tilde{F}_1\left(\frac{1}{2}, 1; 1-\epsilon; z\right). \end{aligned} \tag{4.162}$$

Over the range of integration of u in $\mathcal{I}_1^{\rm incl}$, $z \in [0, 1)$ for $\delta < 1$. For $\mathcal{I}_2^{\rm incl}$, $z \in (0, 1]$.

Furthermore, the singularity at $u = n$ in $\mathcal{I}_1^{\rm incl}$ is made more explicit through the use of the identity

$$\begin{aligned}{}_2\tilde{F}_1\left(\frac{1}{2}, 1; 1-\epsilon; z\right) &= f_a(z) + f_b(z) \\ f_a(z) &= \frac{\sqrt{\pi}}{\cos(\epsilon\pi)} \left(\frac{1-nu}{|u-n|}\right)^{1+2\epsilon} {}_2\tilde{F}_1\left(\frac{1}{2}-\epsilon, -\epsilon; \frac{1}{2}-\epsilon; 1-z\right) \\ f_b(z) &= \frac{\pi}{\cos(\epsilon\pi)} \frac{\epsilon}{\Gamma(1/2-\epsilon)\Gamma(1-\epsilon)} {}_2\tilde{F}_1\left(\frac{1}{2}, 1; \frac{3}{2}-\epsilon; 1-z\right). \end{aligned} \tag{4.163}$$

$f_a(z)$ gives an $\mathcal{O}(1/\epsilon)$ contribution and we proceed by using the following trick that we exploit multiple times throughout the Appendix.

To integrate a product of functions $f(x,\epsilon)g(x,\epsilon)$ where f is singular at the point x_0, we write the integation as

$$\int dx\, f(x,\epsilon)g(x,\epsilon) = \int dx\, f(x,\epsilon)g(x_0,\epsilon) + \int dx\, f(x,\epsilon)\Big(g(x,\epsilon) - g(x_0,\epsilon)\Big)\,. \tag{4.164}$$

The first integral has relatively simple x dependence since $g(x_0,\epsilon)$ does not depend on x. The term in parenthesis in the second integral vanishes at least as fast as x for regular functions g and so the entire integrand can be expanded in ϵ.

We can now evaluate $f_a(z)$ by adding and subtracting the non-singular part of the integrand (which is the hypergeometric function) evaluated at $u = n$ as in Eq. (4.164), whereas $f_b(z)$

is $\mathcal{O}(\epsilon)$ and so we can simply expand about $\epsilon = 0$. Adding these contributions, we find that

$$\mathcal{I}_1^{\text{incl}}(n_i \cdot n_j) = \frac{4^\epsilon}{2}\Bigg[\frac{\sqrt{\pi}\,\Gamma(1-\epsilon)\left(1-n^2\right)^\epsilon}{\cos(\pi\epsilon)\Gamma\left(\frac{1}{2}-\epsilon\right)}\int_{-1}^{\delta}\frac{du}{|u-n|^{1+2\epsilon}} - \int_{-1}^{\delta} du\frac{\text{sgn}(n-u)}{1-u}\left(1-\epsilon\ln\left(\frac{4(n-u)^2}{1-n^2}\right)\right) + \epsilon\int_{-1}^{\delta}\frac{du}{1-u}\frac{2}{|u-n|}\tanh^{-1}\left(\frac{|u-n|}{1-nu}\right)\Bigg]. \tag{4.165}$$

For $\mathcal{I}_2^{\text{incl}}$, the part of the integrand that is not singular at $u = 1$ is everything that multiplies $(1-u)^{-1-\epsilon}$, and so we add and subtract this part as in Eq. (4.164). This gives

$$\mathcal{I}_2^{\text{incl}}(n_i \cdot n_j) = \frac{4^\epsilon}{2}\Bigg[-\frac{1}{\epsilon}2^{-\epsilon}(1-\delta)^{-\epsilon} + \int_\delta^1 \frac{du}{u-n}\left(1+\frac{1-n}{1-u}\log\left(\frac{(n-1)^2(u+1)}{4(n-u)^2}\right) - \log(1-u) + \frac{u-n}{1-u}\log(2)\right)\Bigg]. \tag{4.166}$$

The integrals in Eqs. (4.165) and (4.166) give rise to many terms. However, we find that, after some lengthy algebra, the dependence on δ cancels in the sum as it must and that the result can be simplified to

$$\mathcal{I}^{\text{incl}}(n_i \cdot n_j) = -\frac{1}{\epsilon} + \ln\left(\frac{n_i \cdot n_j}{2}\right) + \epsilon\left(\frac{\pi^2}{6} + \text{Li}_2\left(1 - \frac{2}{n_i \cdot n_j}\right)\right). \tag{4.167}$$

4.B.2 S_{ij}^i and $S_{ij}^{\text{meas}}(\tau_a^i)$

4.B.2.1 Common Integrals

In evaluating the soft contributions S_{ij}^i and $S_{ij}^{\text{meas}}(\tau_a^i)$, we find an integral of the following form:

$$I(\alpha, \beta, t) = 2t^2\int_0^1 \frac{du}{u}u^{2\alpha\epsilon}f(u;\beta,t)\,, \tag{4.168}$$

where $t > 1$ and

$$f(u;\beta,t) = \frac{(\tan^{-2}\frac{R}{2} + u^2)^{2\beta\epsilon}}{(u+t)^2}\,{}_2F_1\left(1, \frac{1}{2}-\epsilon; 1-2\epsilon; \frac{4tu}{(u+t)^2}\right). \tag{4.169}$$

To evaluate this integral, we add and subtract the part of the integrand that is not singular at $u = 0$, namely $f(u;\beta,t)$, as in Eq. (4.164). This allows us to write

$$I(\alpha,\beta,t) = 2\tan^{-4\beta\epsilon}\frac{R}{2}\int_0^1 du\Bigg\{u^{-1+2\alpha\epsilon} + \frac{1}{t^2-u^2}\left[u + 2\epsilon\left(\alpha u\ln u + \frac{t^2}{u}\ln\frac{t^2}{t^2-u^2} + \frac{\beta t^2}{u}\ln\left(1+\tan^2\frac{R}{2}u^2\right)\right)\right]\Bigg\}, \tag{4.170}$$

where we used that

$$f(0;\beta,t) = \frac{1}{t^2}\tan^{-4\beta\epsilon}\frac{R}{2}\,, \tag{4.171}$$

and that the expansion of the hypergeometric about $\epsilon = 0$ for $t > u$ is

$${}_2F_1\left(1,\frac{1}{2}-\epsilon;1-2\epsilon;\frac{4tu}{(u+t)^2}\right) = \frac{t+u}{t-u}\left(1+2\epsilon\ln\frac{t^2}{t^2-u^2}+\mathcal{O}(\epsilon^2)\right). \tag{4.172}$$

Evaluating the integals, we obtain

$$\begin{aligned} I(\alpha,\beta,t) = \frac{\tan^{-4\beta\epsilon}\frac{R}{2}}{\alpha\epsilon}\left(\frac{t^2}{t^2-1}\right)^{\alpha\epsilon} &+ \epsilon\big(\alpha+2\beta-2\big)\,\mathrm{Li}_2\left(\frac{-1}{t^2-1}\right) \\ &- 2\beta\epsilon\,\mathrm{Li}_2\left(-\frac{1+t^2\tan^2\frac{R}{2}}{t^2-1}\right)+\mathcal{O}(\epsilon^2)\,. \end{aligned} \tag{4.173}$$

4.B.2.2 $S_{ij}^{\rm meas}(\tau_a^i)$

To evaluate Eq. (4.82) for the case that $k = i$, we use light cone coordinates in the frame of jet i, $k^+ = n_i\cdot k$ and $k^- = \bar{n}_i\cdot k$. In terms of these variables, the on-shell condition can be used to give

$$n_j\cdot k = k^+\cos^2\frac{\psi_{ij}}{2} + k^-\sin^2\frac{\psi_{ij}}{2} - \sqrt{k^+k^-}\sin\psi_{ij}\cos\phi, \tag{4.174}$$

with $\cos\psi_{ij} = 1 - n_i\cdot n_j$, and ϕ the angle in $k_\perp$-space (the azimuthal angle about $\vec{n}_i$). We can do the $k_\perp$ and k^+ integrals using the on-shell and τ_a delta functions respectively. The resulting $S_{ij}^{\rm meas}(\tau_a^i)$ has non-trivial integrals over k^- and ϕ:

$$\begin{aligned} S_{ij}^{\rm meas}(\tau_a^i) = -\frac{\alpha_s}{4\pi}\left(\frac{4\pi\mu^2}{\omega^2}\right)^{\epsilon}(n_i\cdot n_j)(\mathbf{T}_i\cdot\mathbf{T}_j)\frac{1}{\sqrt{\pi}\,\Gamma(\frac{1}{2}-\epsilon)}\frac{2\omega}{2-a}\frac{1}{(\tau_a^i)^{2\epsilon}}\int_0^\pi d\phi\sin^{-2\epsilon}\phi \\ \times\int_0^\infty\frac{dk^-}{(k^-)^2}\left(\frac{\omega\tau_a^i}{k^-}\right)^{-1}\Theta\left(\tan^2\frac{R}{2}-\left(\frac{\omega\tau_a^i}{k^-}\right)^{\frac{2}{2-a}}\right)\left(\frac{\omega\tau_a^i}{k^-}\right)^{2\epsilon\frac{1-a}{2-a}} \\ \times\left[\left(\frac{\omega\tau_a^i}{k^-}\right)^{\frac{2}{2-a}}\cos^2\frac{\psi_{ij}}{2}+\sin^2\frac{\psi_{ij}}{2}-\left(\frac{\omega\tau_a^i}{k^-}\right)^{\frac{1}{2-a}}\sin\psi_{1j}\cos\phi\right]^{-1}. \end{aligned} \tag{4.175}$$

Making the change of variables $u = \cot\frac{R}{2}\sqrt{k^+/k^-} = \cot\frac{R}{2}\left(\frac{\omega\tau_a^i}{k^-}\right)^{\frac{1}{2-a}}$, we find that $S_{ij}^{\rm meas}(\tau_a^i)$ can be written as

$$S_{ij}^{\rm meas}(\tau_a^i) = -\frac{\alpha_s}{2\pi}\mathbf{T}_i\cdot\mathbf{T}_j\,\frac{1}{\Gamma(1-\epsilon)}\left(\frac{4\pi\mu^2}{\omega^2}\tan^{2(1-a)}\frac{R}{2}\right)^{\epsilon}\left(\frac{1}{\tau_a^i}\right)^{1+2\epsilon} I(1-a,0,t_{ij})\,, \tag{4.176}$$

where $I(\alpha,\beta,t)$ is defined in Eq. (4.168). Using Eq. (4.173) we find the result given in Eq. (4.83).

4.B.2.3 S_{ij}^i

The Θ-functions in Eq. (4.79) are easiest to deal with if we shift to variables where each Θ-function is in a different variable. The simplest choices are just the arguments of the Θ functions Θ_Λ and Θ_R^i, k^0 and $u = \cot\frac{R}{2}\sqrt{k^+/k^-}$, respectively, where $k^\pm$ are defined with respect to direction n_i. This gives a form similar to the integral in $S_{ij}^{\rm meas}(\tau_a^i)$,

$$S_{ij}^j = -\frac{1}{\epsilon}\frac{\alpha_s}{4\pi}\mathbf{T}_i\cdot\mathbf{T}_j\,\frac{1}{\Gamma(1-\epsilon)}\left(\frac{4\pi\mu^2}{4\Lambda^2}\tan^2\frac{R}{2}\right)^\epsilon I(-1,1,t_{ij})\,. \tag{4.177}$$

where $I(\alpha,\beta,t)$ is defined in Eq. (4.168) and evaluates to Eq. (4.173). This gives Eq. (4.80).

4.B.3 $S_{ij}^{\rm meas}(\tau_a^k)$ and S_{ij}^k for $k \neq i,j$

We again use light cone coordinates centered on jet k. The integrations involved in $S_{ij}^{\rm meas}(\tau_a^k)$ and S_{ij}^k only give rise to a $1/\epsilon$ pole as explained in the text, but integrating the eikonal factor $1/(n_i\cdot k)(n_j\cdot k)$ is more complicated than for the other cases since there is a third direction, n_k, involved.

For unmeasured jets when there are $n \geq 3$ total final state jets, S_{ij}^k is needed. However, as we explain in the text, measured jets violate consistency at $\mathcal{O}(1/t^2)$ even for $n = 2$ (non back-to-back) jets and the contribution of S_{ij}^k does not ameliorate this fact when $n \geq 3$. To show this, we need to evaluate the divergent contribution of S_{ij}^k. In addition, we give the form of the finite pieces which are $\mathcal{O}(1/t^2)$.

For each measured jet when there are $n \geq 3$, the sum $S_{ij}^{\rm meas}(\tau_a^k) + S_{ij}^k\delta(\tau_a^k)$ is needed. However, in this case the $1/\epsilon$ pole cancels in this sum and we are left with only a single, finite integral to evaluate. This is clear from the expressions for $S_{ij}^{\rm meas}(\tau_a^k)$ and S_{ij}^k which we derive in Sec. 4.B.3.2 and Sec. 4.B.3.3, respectively. We evaluate the sum explicitly in Sec. 4.B.3.4.

4.B.3.1 Common Integrals

We find the following integral arising in both $S_{ij}^{\rm meas}(\tau_a^k)$ and S_{ij}^k:

$$\begin{aligned} I(u;t_a,t_b,\beta) &\equiv -\frac{2\epsilon}{\pi}\int_0^\pi d\theta_1\,\sin^{-2\epsilon}\theta_1\int_0^\pi d\theta_2\,\sin^{-1-2\epsilon}\theta_2\,\frac{t_a^2+t_b^2-2t_at_b\cos\beta}{u^2+t_a^2-2ut_a\cos\theta_1} \\ &\quad\times\frac{1}{u^2+t_b^2-2ut_b(\cos\beta\cos\theta_1+\sin\beta\sin\theta_1\cos\theta_2)} \\ &= I^{(0)}(u;t_a,t_b,\beta)+\epsilon I^{(1)}(u;t_a,t_b,\beta)+\mathcal{O}(\epsilon^2)\,, \end{aligned} \tag{4.178}$$

where the $\mathcal{O}(\epsilon^0)$ and $\mathcal{O}(\epsilon^1)$ parts of I are

$$I^{(0)}(u;t_a,t_b,\beta) = \frac{2}{\pi}\int_0^\pi \mathrm{d}\theta\frac{A}{A^2-B^2}\frac{t_a^2+t_b^2-2t_at_b\cos\beta}{u^2+t_a^2-2ut_a\cos\theta} \tag{4.179}$$

$$I^{(1)}(u;t_a,t_b,\beta) = -\frac{2}{\pi}\int_0^\pi \mathrm{d}\theta\left[\frac{2\ln(\sin\theta)A}{A^2-B^2}+\frac{B}{A^2-B^2}\log\frac{A-B}{A+B}\right]\frac{t_a^2+t_b^2-2t_at_b\cos\beta}{u^2+t_a^2-2ut_a\cos\theta}\,,$$

where we defined

$$\begin{aligned} A &= u^2 + t_b^2 - 2ut_b \cos\beta \cos\theta \\ B &= 2ut_b \sin\beta \sin\theta \,. \end{aligned} \tag{4.180}$$

We can evaluate $I^{(0)}$ straightforwardly. For the range of our interest, $t_{a,b} > 1$ and $0 < u < 1$, it gives

$$I^{(0)}(u; t_a, t_b, \beta) = \frac{2(t_a^2 + t_b^2 - 2t_a t_b \cos\beta)(t_a^2 t_b^2 - u^4)}{(t_a^2 - u^2)(t_b^2 - u^2)(t_a^2 t_b^2 - 2t_a t_b u^2 \cos\beta + u^4)} \,. \tag{4.181}$$

In addition, we will need the following integrals over $I^{(0)}(u)$:

$$f_1(t_a, t_b, \beta) \equiv \int_0^1 du\, u\, I^{(0)}(u; t_a, t_b, \beta) = \ln\left(\frac{t_a^2 t_b^2 - 2t_a t_b \cos\beta + 1}{(t_a^2 - 1)(t_b^2 - 1)}\right), \tag{4.182}$$

and

$$\begin{aligned} f_2(t_a, t_b, \beta, r) &\equiv \int_0^1 du\, u\, I^{(0)}(u; t_a, t_b, \beta) \ln(r + u^2) \\ &= -\Bigg\{ g(t_a, r) + g(t_b, r) + 2\ln(r+1)\ln(t_a t_b) \\ &\quad + 2\,\mathrm{Re}\left[\mathrm{Li}_2\left(\frac{t_a t_b - e^{i\beta}}{r e^{i\beta} + t_a t_b}\right) - \mathrm{Li}_2\left(\frac{t_a t_b}{r e^{i\beta} + t_a t_b}\right) \right. \\ &\qquad \left. + \ln\left(\frac{t_a t_b}{t_a t_b - e^{i\beta}}\right) \ln\left(r + t_a t_b e^{-i\beta}\right) \right] \Bigg\}, \end{aligned} \tag{4.183}$$

where

$$g(t, r) \equiv \mathrm{Li}_2\left(\frac{t^2}{t^2 + r}\right) - \mathrm{Li}_2\left(\frac{t^2 - 1}{t^2 + r}\right) + \ln(t^2 - 1)\ln(r + t^2) - \ln(t^2)\ln\left((r+1)(r+t^2)\right). \tag{4.184}$$

For $r = 0$, this simplifies to

$$f_2(t_a, t_b, \beta, 0) = -\,\mathrm{Li}_2\left(\frac{1}{t_a^2}\right) - \mathrm{Li}_2\left(\frac{1}{t_b^2}\right) + 2\,\mathrm{Re}\left[\mathrm{Li}_2\left(\frac{e^{i\beta}}{t_a t_b}\right)\right]. \tag{4.185}$$

Notice that both f_1 and f_2 are $\mathcal{O}(1/t^2)$.

The $\mathcal{O}(\epsilon^1)$ piece, $I^{(1)}$, is less trivial. However, the only property of $I^{(1)}$ that we need is that

$$f_3(t_a, t_b, \beta) \equiv \int_0^1 du\, u I^{(1)}(u; t_a, t_b, \beta) = \mathcal{O}(1/t^2)\,, \tag{4.186}$$

which can be seen by taking the large-t limit of $I^{(1)}$ in Eq. (4.179). The integral is finite an suppressed by $1/t^2$.

4.B.3.2 S_{ij}^k

To compute S_{ij}^k, we choose a coordinate system such the $\vec{n}_k$ is in the z-direction and $\vec{n}_i$ lies in the xz-plane. In terms of the light-cone coordinates about n_k and the variable $u = \cot\frac{R}{2}\sqrt{k^+/k^-}$, we have

$$\begin{aligned} n_i \cdot k &= k^+ \cos^2\frac{\psi_{ik}}{2} + k^- \sin^2\frac{\psi_{ik}}{2} - \sqrt{k^+k^-}\sin\psi_{ik}\cos\theta_1 \\ &= k^- \cos^2\frac{\psi_{ik}}{2}\tan^2\frac{R}{2}\Big[u^2 + t_{ik}^2 - 2ut_{ik}\cos\theta_1\Big] \\ n_j \cdot k &= k^+ \cos^2\frac{\psi_{jk}}{2} + k^- \sin^2\frac{\psi_{jk}}{2} - \sqrt{k^+k^-}(n_j^x\cos\theta_1 + n_j^y\sin\theta_1\cos\theta_2) \\ &= k^- \cos^2\frac{\psi_{jk}}{2}\tan^2\frac{R}{2}\Big[u^2 + t_{jk}^2 - 2ut_{jk}\big(\cos\beta_{ij}\cos\theta_1 + \sin\beta_{ij}\sin\theta_1\cos\theta_2\big)\Big]\,, \end{aligned} \tag{4.187}$$

where β_{ij} is defined as the angle between the ik- and jk-planes. Using the relation

$$\frac{n_i \cdot n_j}{\cos^2\frac{\psi_{ik}}{2}\cos^2\frac{\psi_{jk}}{2}\tan^2\frac{R}{2}} = 2(t_{ik}^2 + t_{jk}^2 - 2t_{ik}t_{jk}\cos\beta_{ij})\,, \tag{4.188}$$

we find that S_{ij}^k can be written as

$$S_{ij}^k = -\frac{1}{\epsilon}\frac{\alpha_s}{4\pi}\mathbf{T}_i\cdot\mathbf{T}_j\frac{1}{\Gamma(1-\epsilon)}\left(\frac{4\pi\mu^2}{4\Lambda^2}\right)^\epsilon\tan^{2\epsilon}\frac{R}{2}\int_0^1 du\,u^{1-2\epsilon}\Big(\tan^{-2}\frac{R}{2} + u^2\Big)^{2\epsilon} I(u;t_{ik},t_{jk},\beta_{ij})\,, \tag{4.189}$$

where $I(u,t_a,t_b,\beta_{ij})$ is defined in Eq. (4.178). Expanding in ϵ, we find

$$S_{ij}^k = -\frac{\alpha_s}{4\pi}\mathbf{T}_i\cdot\mathbf{T}_j\left[\frac{1}{\epsilon}f_1(t_{ik},t_{jk},\beta_{ij}) + F(t_{ik},t_{jk},\beta_{ij})\right], \tag{4.190}$$

where the finite part is given by

$$\begin{aligned} F(t_a,t_b,\beta) \equiv \Bigg[& f_1(t_a,t_b,\beta)\ln\left(\frac{\mu^2}{4\Lambda^2}\tan^2\frac{R}{2}\right) - f_2(t_a,t_b,\beta,0) \\ &+ 2f_2\Big(t_a,t_b,\beta,\tan^{-2}\frac{R}{2}\Big) + f_3(t_a,t_b,\beta)\Bigg]\,, \end{aligned} \tag{4.191}$$

and f_1, f_2, and f_3 are given in Eqs. (4.182), (4.183), and (4.186), respectively.

4.B.3.3 $S_{ij}^{\rm meas}(\tau_a^k)$

Using the same coordinate system as for S_{ij}^k, we find that $S_{ij}^{\rm meas}(\tau_a^k)$ can be written as

$$\begin{aligned} S_{ij}^{\rm meas}(\tau_a^k) = -\frac{\alpha_s}{2\pi}\mathbf{T}_i\cdot\mathbf{T}_j\frac{1}{\Gamma(1-\epsilon)}&\left(\frac{4\pi\mu^2}{\omega^2}\tan^{2(1-a)}\frac{R}{2}\right)^\epsilon\left(\frac{1}{\tau_a^k}\right)^{1+2\epsilon} \\ &\times\int_0^1 du\,u^{1+2\epsilon(1-a)}I(u;t_{12},t_{ik},\beta_{ij})\,. \end{aligned} \tag{4.192}$$

Expanding in ϵ gives

$$S_{ij}^{\text{meas}}(\tau_a^k) = -\frac{\alpha_s}{2\pi}\mathbf{T}_i\cdot\mathbf{T}_j\left[\left(\frac{1}{\tau_a^k}\right)^{1+2\epsilon} f_1(t_{ik},t_{jk},\beta_{ij}) + \delta(\tau_a^k)\, G(t_{ik},t_{jk},\beta_{ij})\right], \tag{4.193}$$

where

$$G(t_a,t_b,\beta) \equiv -\frac{1}{2}\left[f_1(t_a,t_b,\beta)\ln\left(\frac{\mu^2}{\omega^2}\tan^{2(1-a)}\frac{R}{2}\right) + (1-a)f_2(t_a,t_b,\beta,0) + f_3(t_a,t_b,\beta)\right], \tag{4.194}$$

and f_1, f_2, and f_3 are given in Eqs. (4.182), (4.183), and (4.186), respectively.

4.B.3.4 $S_{ij}^k + S_{ij}^{\text{meas}}(\tau_a^k)$

The sum of Eqs. (4.190) and (4.193) is finite. We find

$$\begin{aligned} S_{ij}^{\text{meas}}(\tau_a^k) + S_{ij}^k\delta(\tau_a^k) = \frac{\alpha_s}{4\pi}\mathbf{T}_i\cdot\mathbf{T}_j\Bigg[&\delta(\tau_a^k)\Bigg(f_1(t_{ik},t_{jk},\beta_{ij})\ln\left(\frac{4\Lambda^2}{\omega^2}\tan^{-2a}\frac{R}{2}\right) \\ &+ (2-a)f_2(t_{ik},t_{jk},\beta_{ij},0) - 2f_2\Big(t_{12},t_{ik},\beta_{ij},\tan^{-2}\frac{R}{2}\Big)\Bigg) \\ &- 2\left(\frac{1}{\tau_a^k}\right)_+ f_1(t_{ik},t_{jk},\beta_{ij})\Bigg]. \end{aligned} \tag{4.195}$$

where f_1 and f_2 are given in Eqs. (4.182) and (4.183), respectively.

4.C Convolutions and Finite Terms in the Resummed Distribution

In evaluating the final resummed distribution Eq. (4.128), each measured jet function must be convolved against a corresponding soft function piece S^{meas}. These convolutions take the form.

$$\int d\tau_J d\tau_S d\tau_J'\, d\tau_S'\, J(\tau_J',\mu_J) S^{\text{meas}}(\tau_S',\mu_S)\left[\frac{\Theta(\tau_J-\tau_J')}{(\tau_J-\tau_J')^{1+\omega_J^i}}\right]_+\left[\frac{\Theta(\tau_S-\tau_S')}{(\tau_S-\tau_S')^{1+\omega_S^i}}\right]_+ \delta(\tau-\tau_J-\tau_S)\,. \tag{4.196}$$

For the class of functions of the form $x^{-1-\omega}$ with $\omega\neq 0$ and $\omega<1$, we define the plus distribution by

$$\begin{aligned} \left[\frac{\Theta(x)}{x^{1+\omega}}\right]_+ &\equiv \lim_{\beta\to 0}\left[\frac{\Theta(x-\beta)}{x^{1+\omega}} - \frac{\beta^{-\omega}}{\omega}\delta(x-\beta)\right] \\ &= -\frac{\delta(x)}{\omega} + \sum_{n=0}^{\infty}(-\omega)^n\left[\frac{\Theta(x)\ln^n x}{x}\right]_+, \end{aligned} \tag{4.197}$$

where the plus functions on the second line are given by Eq. (4.138),

$$\left[\frac{\Theta(x)\ln^n(x)}{x}\right]_+ \equiv \lim_{\beta\to 0}\left[\frac{\Theta(x-\beta)\ln^n(x)}{x}+\frac{\ln^{n+1}\beta}{n+1}\delta(x-\beta)\right]. \tag{4.198}$$

Using the techniques of, for example, Appendix B of Ref. [134], we find that the final result can be written in the form Eqs. (4.128) and (4.131) with the functions $d_J(\tau_a^i)$ given by

$$\begin{aligned} d_J^{q,\mathrm{cone}}(\tau_a^i) = C_F\Bigg[&\frac{3}{2-a}H(-1-\Omega_i)+\frac{7}{2}+3\ln 2-\frac{\pi^2}{6}\left(2+\frac{1-\frac{a}{2}}{1-a}\right)\\ &+\frac{4}{(1-a)(2-a)}\left(\frac{\pi^2}{12}+H(-1-\Omega_i)^2-\frac{1}{2}\psi^{(1)}(-\Omega_i)\right)\\ &+\frac{1}{1-\frac{a}{2}}\int d\tau_J d\tau_J'\Bigg\{\left[\frac{1}{\tau_J'}\left(r_q(x_{\mathrm{cone}})+2\ln\left(\frac{\tau_J'}{\tan^{(2-a)}\frac{R}{2}}\right)\right)\right]_{\dot{+}}\\ &\times\left[\frac{\Theta(\tau_J-\tau_J')}{(\tau_J-\tau_J')^{1+\omega_J^i}}\right]_+\left[\frac{\Theta(\tau_S-\tau_S')}{(\tau_a^i-\tau_J)^{1+\omega_S^i}}\right]_+\Bigg\}\Bigg] \end{aligned} \tag{4.199a}$$

and

$$\begin{aligned} d_J^{q,\mathrm{kT}}(\tau_a^i) = C_F\Bigg[&\frac{3}{2-a}H(-1-\Omega_i)+\frac{13}{2}-\frac{\pi^2}{6}\left(4+\frac{1-\frac{a}{2}}{1-a}\right)\\ &+\frac{4}{(1-a)(2-a)}\left(\frac{\pi^2}{12}+H(-1-\Omega_i)^2-\frac{1}{2}\psi^{(1)}(-\Omega_i)\right)\\ &+\frac{1}{1-\frac{a}{2}}\int d\tau_J d\tau_J'\Bigg\{\left[\frac{1}{\tau_J'}\left(r_q(x_1)+2\ln\left(\frac{\tau_J'}{\tan^{(2-a)}\frac{R}{2}}\right)-\Theta\left(\tau_a^{\frac{1}{2-a}}>\frac{1}{2}\tan\frac{R}{2}\right)r_q(x_2)\right)\right]_{\dot{+}}\\ &\times\left[\frac{\Theta(\tau_J-\tau_J')}{(\tau_J-\tau_J')^{1+\omega_J^i}}\right]_+\left[\frac{\Theta(\tau_S-\tau_S')}{(\tau_a^i-\tau_J)^{1+\omega_S^i}}\right]_+\Bigg\}\Bigg], \end{aligned} \tag{4.199b}$$

for quarks and by

$$\begin{aligned} d_J^{g,\mathrm{cone}}(\tau_a^i) = &\frac{\beta_0}{2-a}H(-1-\Omega_i)+\frac{4C_A}{(1-a)(2-a)}\left(\frac{\pi^2}{12}+H(-1-\Omega_i)^2-\frac{1}{2}\psi^{(1)}(-\Omega_i)\right)\\ &+C_A\left(\frac{137}{36}+\frac{11}{3}\ln 2-\frac{\pi^2}{6}\left(2+\frac{1-\frac{a}{2}}{1-a}\right)\right)-T_R N_f\left(\frac{23}{18}+\frac{4}{3}\ln 2\right)\\ &+\frac{1}{1-\frac{a}{2}}\int d\tau_J d\tau_J'\Bigg\{\left[\frac{1}{\tau_J'}\left(r_q(x_1)+2\ln\left(\frac{\tau_J'}{\tan^{(2-a)}\frac{R}{2}}\right)\right)\right]_{\dot{+}}\\ &\times\left[\frac{\Theta(\tau_J-\tau_J')}{(\tau_J-\tau_J')^{1+\omega_J^i}}\right]_+\left[\frac{\Theta(\tau_S-\tau_S')}{(\tau_a^i-\tau_J)^{1+\omega_S^i}}\right]_+\Bigg\} \end{aligned} \tag{4.199c}$$

and

$$d_J^{g,\mathrm{k_T}}(\tau_a^i) = \frac{\beta_0}{2-a} H(-1-\Omega_i) + \frac{4C_A}{(1-a)(2-a)} \left(\frac{\pi^2}{12} + H(-1-\Omega_i)^2 - \frac{1}{2}\psi^{(1)}(-\Omega_i) \right) + C_A \left(\frac{67}{9} - \frac{\pi^2}{6} \left(4 + \frac{1-\frac{a}{2}}{1-a} \right) \right) - T_R N_f \left(\frac{23}{9} \right) + \frac{1}{1-\frac{a}{2}} \int d\tau_J d\tau_J' \left\{ \left[\frac{1}{\tau_J'} \left(r_q(x_1) + 2\ln \left(\frac{\tau_J'}{\tan^{(2-a)} \frac{R}{2}} \right) - \Theta \left(\tau_a^{\frac{1}{2-a}} > \frac{1}{2} \tan \frac{R}{2} \right) r_g(x_2) \right) \right]_+ \times \left[\frac{\Theta(\tau_J - \tau_J')}{(\tau_J - \tau_J')^{1+\omega_J^i}} \right]_+ \left[\frac{\Theta(\tau_S - \tau_S')}{(\tau_a^i - \tau_J)^{1+\omega_S^i}} \right]_+ \right\} \tag{4.199d}$$

for gluons, where in all cases x_{cone}, $x_{1,2}$ (defined in Eqs. (4.139) and (4.144)) are evaluated at $\tau = \tau_J'$ and $r_{q,g}$ are defined in Eqs. (4.148) and (4.155). For the soft function, $d_S(\tau_a^i)$ is given by

$$d_S(\tau_a^i) = \frac{\pi^2}{8} + H(-1-\Omega_i)^2 - \psi^{(1)}(-\Omega_i)\,. \tag{4.199e}$$

4.D Color Algebra for $n = 2, 3$ Jets

For the two and three jet cases, there are no color correlations since all color generator inner products $\mathbf{T}_i \cdot \mathbf{T}_j$ can be expressed in terms of the Casimir invariants C_A and C_F. For $n = 2$, there is a quark jet with charge $\mathbf{T}_q$ and an anti-quark jet with charge $\mathbf{T}_{\bar{q}}$ that each square to C_F. There is only one inner-product in this case and using color conservation ($\sum_i \mathbf{T}_i = 0$), we have that

$$\mathbf{T}_q \cdot \mathbf{T}_{\bar{q}} = -\mathbf{T}_q^2 = -\mathbf{T}_{\bar{q}}^2 = -C_F\,. \tag{4.200}$$

For $n = 3$ jets color conservation gives that, for example,

$$\begin{aligned} \mathbf{T}_1 \cdot \mathbf{T}_2 &= \frac{1}{2}\left[(\mathbf{T}_1 + \mathbf{T}_2)^2 - \mathbf{T}_1^2 - \mathbf{T}_2^2 \right] \\ &= \frac{1}{2}\left[\mathbf{T}_3^2 - \mathbf{T}_1^2 - \mathbf{T}_2^2 \right]\,. \end{aligned} \tag{4.201}$$

Referring to the quark, anti-quark, and gluon generators as $\mathbf{T}_q$, $\mathbf{T}_{\bar{q}}$, and $\mathbf{T}_g$, respectively, using $\mathbf{T}_q^2 = \mathbf{T}_{\bar{q}}^2 = C_F$ and $\mathbf{T}_g^2 = C_A$ in Eq. (4.201) gives

$$\begin{aligned} \mathbf{T}_q \cdot \mathbf{T}_{\bar{q}} &= \frac{C_A}{2} - C_F \\ \mathbf{T}_q \cdot \mathbf{T}_g &= \mathbf{T}_{\bar{q}} \cdot \mathbf{T}_g = -\frac{C_A}{2}\,. \end{aligned} \tag{4.202}$$

Chapter 5

Factorization of Boosted Multijet Processes for Threshold Resummation[1]

1 Introduction

Factorization of cross-sections is the basis of every theoretical prediction at hadron colliders. In its simplest form, factorization states the measured hadronic cross-section σ can be obtained by convolving a perturbatively calculable cross-section $\hat{\sigma}$ with nonperturbative parton distribution functions (PDFs) [94, 90],

$$\sigma = f \otimes f \otimes \hat{\sigma}\,. \tag{5.1}$$

The PDFs are universal, and can therefore be extracted from one process and used to make predictions in another. Moreover, $\hat{\sigma}$ will in general depend on a hard scale Q (for example, the partonic center-of-mass energy $\sqrt{\hat{s}}$), while the PDFs depend on the scale at which they are measured, say $\Lambda_{\rm QCD}$. The evolution of the PDFs between these two scales resums logarithms of $Q/\Lambda_{\rm QCD}$. This basic paradigm illustrates the two main uses of factorization: separation of universal, non-perturbative contributions to a cross-section from perturbatively calculable contributions, and resummation of logarithms of ratios of scales to which each contribution is sensitive.

When $\hat{\sigma}$ depends only on a single scale, Eq. (5.1) is the end of the story. The situation is more involved when $\hat{\sigma}$ itself depends on multiple, widely disparate scales. For example, in many collider physics processes involving jets, $\hat{\sigma}$ can depend on mass scales associated with the jets such as M_J, hard scales like $\sqrt{\hat{s}}$, and seesaw scales like $M_J^2/\sqrt{\hat{s}}$. In such cases large logarithms of ratios of these scales can spoil the convergence of the fixed order perturbative expansion of $\hat{\sigma}$. One must further factorize $\hat{\sigma}$ in order to resum these large logarithms and, perhaps, to separate out any other non-perturbative physics that is not captured in the PDFs [92, 93, 145, 144].

In this chapter we will focus on so-called threshold logarithms. When a process approaches its kinematical threshold, there is limited phase space available for radiation. This gives rise to an incomplete cancellation between real and virtual diagrams, resulting in large logarithmic terms. This is common in situations where the invariant mass of the final state is near the maximum

[1] This chapter was originally cowritten with Christian W. Bauer and Nicholas Daniel Dunn [17].

available energy, which limits the amount of energy that can go into excess radiation. Examples of this type of resummation can be found for Drell-Yan, deep-inelastic scattering (DIS), B meson decay, and top production [5, 180, 179, 71, 72, 95, 52, 122, 151, 155, 2, 50, 144, 158, 19, 160, 39, 83]. It has been suggested [7, 78] that a similar effect occurs at hadron colliders away from hadronic endpoint due to the steepness of parton luminosities and this effect was explored more quantitatively in [40]. In this chapter, we will concentrate on hadronic threshold and assume that the invariant mass of the final state is near the maximum allowed by the collider; however, we plan on exploring resummation away from the hadronic endpoint in future work [16]. For this reason we will derive a factorization theorem that can be applied away from hadronic threshold without loss of information.

An extremely useful tool to prove factorization is effective field theory. In the case of jet physics, Soft-Collinear Effective Theory (SCET) [19, 21, 33, 29] is the relevant effective field theory that can be used to derive factorization in many hard scattering processes [20]. The SCET Lagrangian is constructed by integrating out all modes of QCD except for soft modes and collinear modes with respect to some fixed number of directions n_i. Matching QCD onto SCET gives rise to a hard function that contains the physics of the hard scales in the problem, and matrix elements of the remaining soft and collinear fields give rise to soft and jet functions, respectively.

The first applications of SCET involved cases with particularly simple jet definitions, such as in Drell-Yan [137, 40] where there are no jets, hemisphere jets in event shapes [26, 24, 156, 157, 124, 172, 125, 18, 41, 135, 134], or completely inclusive jets as in $B \to X_s\gamma$ [19], DIS [160, 39, 83] and prompt photon production [42]. Factorization of jets defined with more generic algorithms was considered in [23] and two-jet rates defined with jet algorithms were computed using SCET in [24, 187, 85]. A study of various different jet algorithms and the dependence on the jet parameters in the framework of SCET was discussed in [85]. More recently, a NLL analysis of jet shapes in multijet events using modern jet algorithms in e^+e^- collisions was performed in [114, 116].

The goal of this chapter is to derive a factorization formula for an arbitrary number of jets in the presence of any number of non-strongly interacting particles in the threshold limit. We allow for a nonzero total rapidity and calculate the ingredients of this formula to allow resummation of threshold logarithms at NLL accuracy. This is conceptually distinct from the case of a single final state jet, which can be measured indirectly by simply demanding that a non-strongly interacting particle is produced with nonzero p_{T}. When there is more than one final state jet, jet algorithms must be used to identify jets, and so the technology of incorporating jet algorithms into a factorization formula, developed in [23] and applied to e^+e^- collisions in [116, 114], must be employed. The consistency of this factorization (that is, the fact that the cross-section is independent of the factorization scale μ) is only demonstrated here in the true hadronic endpoint. However, we plan on investigating the consistency of this factorization away from hadronic endpoint using the steepness of parton luminosities in [16].

Factorization formulas for the case of a single, inclusive jet have soft functions that depend on the null component of the total soft momentum in the direction of the jet. When there are no jets (e.g., Drell-Yan), the soft function depends on the timelike component of the total soft momentum. In extending threshold resummation to more than one jet using jet algorithms, we find a soft function that depends on the timelike component of the total soft momentum outside of the jets and on the null component of the soft momentum within each of the jets. Thus, our result reduces to the previously considered cases of zero and one inclusive jet when our jet algorithm either includes none or all of the final state soft momentum, respectively.

The organization of this chapter is as follows. In Sec. 2, we define precisely what we mean by threshold production of N jets and discuss the corresponding kinematics. In Sec. 3, we briefly discuss different classes of jet algorithms used at hadron colliders. We then derive our factorization theorem in Sec. 4, beginning for notational simplicity with the case of a single (quark or gluon) final state jet, then extending these results to the case of N jets. We derive the anomalous dimensions for the objects that appear in our N jet factorization formula in Sec. 5 and use these in Sec. 6 to show that our factorization theorem is formally consistent, at least in the hadronic endpoint region. Finally, we present our conclusions in Sec. 7.

2 Kinematics of Threshold Resummation

To explain our approach to threshold resummation, how it includes both the cases of Drell-Yan and direct gauge boson production as limiting cases, and how it is extendable to arbitrary N-jet production, we first discuss the kinematics. By demanding that the final state contains N jets each with fixed transverse momentum $p_{\rm T}$ and pseudo-rapidity η, together with some number of non-strongly interacting particles with total 4-momentum q, we are requiring that there is a minimum partonic center-of-mass energy

$$\hat{s}_{\rm min} = \Big(q + \sum_i^N p_J^i\Big)^2 , \tag{5.2}$$

where p_J^i is the momentum of the ith jet. This momentum is defined in terms of the $p_J^{\rm T}$ and η_J of the jet as

$$p_J \equiv (p_J^{\rm T} \cosh\eta_J, \mathbf{p}_J^{\rm T}, p_J^{\rm T} \sinh\eta_J) . \tag{5.3}$$

Of course, the actual partonic center-of-mass energy $\hat{s}$ typically exceeds this minimum value, and in general can be as large as the available machine center-of-mass energy s. Therefore the dimensionless variable z, defined as

$$z \equiv \frac{\hat{s}_{\rm min}}{\hat{s}} , \tag{5.4}$$

can range from

$$\tau \le z \le 1 , \qquad \text{with} \qquad \tau \equiv \frac{\hat{s}_{\rm min}}{s} . \tag{5.5}$$

Going to hadronic threshold ($\tau \to 1$) forces $z \to 1$, such that the only emissions kinematically allowed are collinear radiation off the hard partons that form jets, as well as soft radiation. Radiation collinear to one of the jets with momentum scaling as $E_{\rm cm}(1, \lambda^2, \lambda)$ (in the light-cone coordinates of the jet) and soft radiation scaling as $E_{\rm cm}(\lambda^2, \lambda^2, \lambda^2)$, each contribute an equal amount to $\hat{s}$, where $\lambda \sim \sqrt{1-z}$ is a small, dimensionless parameter. In this limit of restricted radiation, partonic momentum conservation can be written as

$$p_I = q + k_s + \sum_i^N p_c^i , \tag{5.6}$$

where p_I is the total initial-state (partonic) momentum, k_s is the total soft momentum and p_c^i is the momentum carried by collinear fields in the direction of jet i. The total momentum can be separated into two components: the first is the minimum momentum needed to create N jets of

fixed $p_{\rm T}$ and η together with the non-strongly interacting particles of total momentum q, while the second brings the invariant mass of the final state above its minimum value $\hat{s}_{\rm min}$. To do this, we note that an arbitrary four-vector p can be written as the sum of a massless four-vector which characterizes the transverse momentum and pseudorapidity of p and a purely timelike four-vector with a magnitude equal to the +-component of p in light-cone coordinates about $n = (1, \mathbf{p}/|\mathbf{p}|)$, (i.e., $p^+ \equiv p^0 - |\mathbf{p}|$) which characterizes the off-shellness of p. That is, for any four-vector p, we can write

$$p^\mu = p_J^\mu + p^+ v^\mu \,, \tag{5.7}$$

where $v^\mu = (1, \mathbf{0})$ and p_J is given in Eq. (5.3) with $p_J^{\rm T}$ and η_J the transverse momentum and pseudorapidity of p, respectively. We want to apply this relation to the total 4-momentum in each of the jets. To do this, we note that the jet algorithm will group some of the soft momentum k_s into parts that belong to jet i, k_i, and a part that is not included in any of the jets, $k_{\rm out}$,

$$k_s = \sum_i^N k_i + k_{\rm out} \,. \tag{5.8}$$

Using this together with the relation Eq. (5.7) and the fact that

$$(p_c^i + k_i)^+ \equiv p_c^{i,0} + k_i^0 - \left|\mathbf{p}_c^i + \mathbf{k}_i\right| = p_c^{i+} + k_i^+ + \mathcal{O}(\lambda^4) \,, \tag{5.9}$$

where on the right hand side, k_i^+ is plus with respect to p_J and p_c^{i+} is plus with respect to p_c, we can write momentum conservation Eq. (5.6) at leading order in λ as

$$p_I^\mu = q^\mu + k_{\rm out}^\mu + \sum_i^N p_J^\mu + v^\mu \Big[\sum_i^N (p_i^+ + k_i^+) \Big] \,. \tag{5.10}$$

Here, we have also used that out-of-jet collinear radiation is power suppressed [116].

Given these definitions, we can write

$$\begin{aligned} 1 - z &= \frac{2}{\hat{s}} p_I \cdot \left(k_{\rm out} + v \Big[\sum_i^N (p_i^+ + k_i^+) \Big] \right) + \mathcal{O}(\lambda^4) \\ &= \frac{2}{\hat{s}} \Big(p_I \cdot k_{\rm out} + p_I^0 \sum_i^N (p_i^+ + k_i^+) \Big) + \mathcal{O}(\lambda^4) \,, \end{aligned} \tag{5.11}$$

where $\hat{s} = p_I^2$. We see that since p_I is timelike, $1 - z$ depends on the timelike component of the soft momentum outside of the jets and on the null component of the momentum within the jets.

So far we have discussed the kinematics in the hadronic endpoint defined as $\tau \to 1$, which is the main focus of this chapter. However, z can be forced close to one not only in this hadronic endpoint, but also in the limit of steeply falling parton luminosities. In this case, final states with small values of $\hat{s}$ are preferred, giving again $z \to 1$. Our analysis is independent of the precise mechanism which guarantees that $1 - z$ can be regarded as a small quantity, and can therefore be used away from the true hadronic endpoint.

We are now in a position to discuss how our parameterization of $1 - z$ reduces to the standard variable in the case of Drell-Yan and cases when there is one inclusive jet, such as $B \to$

$X_s\gamma$, DIS, and direct gauge boson production. As we will see in Sec. 4, Eq. (5.11) implies the soft function in general depends on the timelike component of $k_{\rm out}$ and on the null components (with respect to the corresponding jet directions) of the soft momenta in each of the jets k_i. In Drell-Yan, there are no jets in the final state and so the entire soft momentum k_s is just $k_{\rm out}$. This is why the soft function in Drell-Yan depends only on the timelike component of the total soft momentum. For a single inclusive jet (i.e., defined with a jet algorithm that includes all of the hadronic momentum), all the soft momentum is included in the jet, such that $k_s = k_1$. This explains why the soft function in this latter type of process only depends on the null component of the total soft momentum. In Ref. [144], on the other hand, threshold resummation for dijet production was considered and it was found that the soft function only depended on the timelike component of momentum outside of the jets. This apparent discrepancy is due to the fact that the limit of small jet size $R \to 0$ was taken and the contribution of in-jet soft particles vanishes in this limit.[2] From the discussion above, the soft function will have dependence on the null component of in-jet momentum for jets of finite size.

3 Jet Algorithms at Hadron Colliders

Perturbative calculations require a precise definition of the phase space boundaries imposed by the jet algorithms. There are two general types of jet algorithms, cone algorithms and cluster algorithms. Cone algorithms decide on which particles belong to a given jet based on cones of fixed size R, while cluster algorithms group particles together into jets based on a relative measure of their distance. These jet algorithms act on the entire set of particles in the final state to decide how many jets are contained in a given event and which particles belong to which jet. Almost all jet algorithms depend on a jet-size R, and a distance $\Delta\mathcal{R}_{ij}$ that measures the distance between two particles in $\eta - \phi$ space

$$\Delta\mathcal{R}_{ij} = \sqrt{(\Delta\eta_{ij})^2 + (\Delta\phi_{ij})^2}\,. \tag{5.12}$$

As already discussed in the previous section, the relevant degrees of freedom in jet production close to $z = 1$ are collinear and soft particles. To perform perturbative calculations in this region we therefore need a restriction on these degrees of freedom to decide whether they belong to a given jet or not. Collinear particles in a given direction all belong to the same jet. This is in contrast with soft particles, which can either belong to a jet or not. Note that the treatment of jet algorithms in SCET is only correct to leading order in the power counting parameter λ. Therefore, we assume that all jets have energy much in excess of their mass, and that all jets are widely separated.

Standard cone algorithms, such as SISCone and Snowmass, are quite simple. The restrictions they impose on each particle to belong to a given jet are independent of other particles in the event, and only depend on the angular distance from the jet direction. The restriction for both

[2] Note that double counting is avoided in [144] by removing collinear modes from the soft function ("eikonal subtractions") whereas in SCET double counting is avoided by removing soft modes from the jet functions ("zero-bin subtractions" [163]). In SCET there is no freedom to choose how to avoid double-counting since it is only when soft modes in the collinear sector are removed that we find soft and jet functions which are separately IR finite [134, 135] and thus the limit $R \to 0$ does not lead to a vanishing contribution from in-jet soft momentum.

soft and collinear particles to be in a jet j with direction n is therefore

$$\hat{\Theta}^R_{\text{soft},j} = \hat{\Theta}^R_{\text{coll},j} = \prod_i \Theta(\Delta\mathcal{R}_{i,n} < R)\,. \tag{5.13}$$

For the purposes of this chapter, we only need results at relative order α_s, and therefore only have to consider one extra particle in the final state. The restrictions therefore simplify, and for the extra particle i we can write

$$\hat{\Theta}^R_{\text{soft},j} = \hat{\Theta}^R_{\text{coll},j} = \Theta(\Delta\mathcal{R}_{i,n} < R)\,. \tag{5.14}$$

Cluster algorithms iterate a process of calculating a distance measure d_{ij} for all pairs of particles and removing the one with the minimum distance. The precise definition of d_{ij} depends on the choice of algorithm.[3] This makes the action of the jet algorithm considerably more complicated. As explained above, all collinear particles in a given direction have to end up in the same jet, which allows us to write a generic restriction for the action of a cluster algorithm on a set of collinear particles in a given direction as

$$\hat{\Theta}^R_{\text{coll},j} = \prod_{k=0}^{N-1} \Theta(\Delta\mathcal{R}^{N-k}_{\text{min}} < R)\,. \tag{5.15}$$

Here N denotes the total number of collinear particles in the direction of the jet n_j. $\Delta\mathcal{R}^{N-k}_{\text{min}}$ denotes the $\Delta\mathcal{R}_{ij}$ between the pair of collinear particles in the set of $N-k$ remaining particles with the smallest d_{ij}. For soft particles, such a generic formula is not possible (at least analytically), since different soft particles can end up in different jets, and the restriction on a given particle depends on all other soft particles in the event. At relative order α_s, however, the restrictions Θ^R_i for cluster algorithms simplify and are given by

$$\hat{\Theta}^R_{\text{soft},j} = \Theta(\Delta\mathcal{R}_{i,n} < R) \tag{5.16}$$

for soft particles and by

$$\hat{\Theta}^R_{\text{coll},j} = \Theta(\Delta\mathcal{R}_{k,l} < R) \tag{5.17}$$

for collinear particles, where k and l label the new particles after the collinear splitting. For more information about jet algorithms in SCET see [116].

4 N-Jet Factorization Theorem

In this section, we present the factorization theorem for the cross-section to produce N jets, defined with respect to a jet algorithm, differential in the 3-momentum (p_{T} and pseudo-rapidity η) of each jet and of the non-strongly interacting particles. To keep the notation simple, we begin in Sec. 4.1 by discussing the case of a single jet produced via the channel $qg \to q$. We then discuss the differences between this derivation and the one needed for the channel $q\bar{q} \to g$. It will be clear from these derivations that, aside from the promotion of the hard and soft functions to matrices

[3] An example for such a distance measure is $d_{ij} = \min\{p_{\text{T}_i}, p_{\text{T}_j}\}\Delta\mathcal{R}_{ij}$ for the k_{T} algorithm.

which arise from mixing of operators in color space, there is nothing conceptually or technically new for arbitrary N jet production in our approach. This allows us to generalize our results to the N jet factorization formula in Sec. 4.2.

In writing down a factorization theorem, we first assume that we can match QCD onto operators in SCET containing $N+2$ distinct collinear fields. This is valid when a (direct or indirect) measurement constrains the final state to be N-jet like. In our case this is ensured by the fact that we take the variable $1-z$ to be small, together with the assumption that the jets are well separated from each other and from the beams (with the latter requirement ensuring that the probability of initial state collinear radiation to produce a jet is power suppressed relative to the probability of the jet arising from the hard interaction). Our derivation is agnostic as to the cause of $1-z \ll 1$, and in [16] we explore in greater detail in what regimes the steepness of parton luminosities allow the factorization theorem we derive here to be applied away from the hadronic endpoint. We will assume in this section that the reader has some familiarity with SCET. For details, we refer the reader to the original SCET literature [19, 21, 33, 29].

4.1 Case of a Single Jet

4.1.1 $q\bar{q} \to g$

Working to leading order in the electroweak coupling constant, we first write the full theory matrix element mediating the partonic interaction as

$$\langle qX|O|P_1P_2\rangle = \sum_i M_i^{\alpha\beta\mu} T_{ab}^A \,\langle X|\bar{\psi}_a^\alpha \psi_b^\beta A_\mu^A|P_1P_2\rangle\,. \tag{5.18}$$

Here, $|q\rangle$ represents the non-strongly interacting final state of total momentum q, $|P_1\rangle$ and $|P_2\rangle$ are the incoming hadrons with the corresponding momentum, and $|X\rangle$ represents the hadronic final state. This equation defines the $M_i^{\alpha\beta\mu}$. Note that we have used the fact that there is only one color singlet in the decomposition of $3\otimes\bar{3}\otimes 8$.

In terms of M_i, the matching of QCD onto the fields of SCET takes the form

$$\begin{aligned} M_i^{\alpha\beta\mu}\mathcal{Q}^{\alpha\beta\mu}(x) &\equiv M_i^{\alpha\beta\mu}\big[\bar{\psi}_a^\alpha \psi_b^\beta A_\mu^A\big](x) \\ &= \sum_j M_j^{\alpha\beta\mu} \sum_{\{\tilde{p}\}} C_{ij}(\{\tilde{p}\}) e^{i(\tilde{p}_1+\tilde{p}_2-\tilde{p}_3)\cdot x}\big[(\bar{\chi}_{-\tilde{p}_1})_a^\alpha (\chi_{\tilde{p}_2})_b^\beta (B_{-\tilde{p}_3})_\mu^A\big](x)\,. \end{aligned} \tag{5.19}$$

At tree level, we have

$$C_{ij}(\{\tilde{p}\}) = \delta_{ij}\,. \tag{5.20}$$

The matching condition in momentum space takes the form

$$\begin{aligned} M_i^{\alpha\beta\mu}\mathcal{Q}^{\alpha\beta\mu}(k) &\equiv M_i^{\alpha\beta\mu}\int \mathrm{d}^4x\, e^{-ik\cdot x}\mathcal{Q}^{\alpha\beta\mu}(x) \\ &= \sum_j M_j^{\alpha\beta\mu}\bigg(\prod_{i=1}^3 \int \!\!\!\!\!\!\int \mathrm{d}^4p_i\bigg) C_{ij}(\{\tilde{p}\})\big[\bar{\chi}_b^\beta(-p_1)\,\chi_a^\alpha(p_2)\,B_\mu^A(-p_3)\big] \\ &\quad\times (2\pi)^4\delta^4(p_1+p_2-p_3-k)\,, \end{aligned} \tag{5.21}$$

where we turned the sums over labels and integrals over residual momenta into integrals over the full $\mathrm{d}^4 p_i$ and used the shorthand notation

$$\int \!\!\!\!\!\!- \mathrm{d}^4 p \equiv \int \frac{\mathrm{d}^4 p}{(2\pi)^4} \,. \tag{5.22}$$

Using this matching condition, we can write the cross-section differential in the jet pseudo-rapidity η_J and transverse momentum p_J^{T} as

$$\begin{aligned}
\frac{\mathrm{d}\sigma}{\mathrm{d}^2 p_J^{\mathrm{T}} \mathrm{d}\eta_J \mathrm{d}\Phi_q} &= \frac{1}{2E_{\mathrm{cm}}^2} \sum_X^{\text{rest.}} |\langle qX|O|P_1P_2\rangle|^2_{\text{spin avg.}} \delta(\eta_J - \eta(X)) \delta^2(\mathbf{p}_J^{\mathrm{T}} - \mathbf{p}^{\mathrm{T}}(X)) \\
&\quad \times (2\pi)^4 \delta^4(P_1 + P_2 - q - p_X) \\
&= \frac{1}{2E_{\mathrm{cm}}^2} \sum_X^{\text{rest.}} \sum_{\text{spin}} \sum_{i,j,i',j'} M_j^{\alpha\beta\mu} \overline{M}_{j'}^{\bar\beta\bar\alpha\bar\mu} \frac{T_{ab}^A T_{\bar b\bar a}^{\bar A}}{4C_A^2} \Big(\prod_{k=1}^3 \int \!\!\!\!\!\!- \mathrm{d}^4 p_k \!\!\!\!\!\!- \int \mathrm{d}^4 p_k' \Big) C_{ij}(\{\tilde p_k\}) C^*_{i'j'}(\{\tilde p_k'\}) \\
&\quad \times \langle P_1P_2|\bar\chi_b^{\bar\beta}(p_2')\, \chi_{\bar a}^{\bar\alpha}(-p_1') B_{\bar\mu}^{\dagger\bar A}(-p_3')|X\rangle\langle X|\bar\chi_a^{\alpha}(-p_1)\, \chi_b^{\beta}(p_2) B_\mu^A(-p_3)|P_1P_2\rangle \\
&\quad \times \delta(\eta_J - \eta(X)) \delta^2(\mathbf{p}_J^{\perp} - \mathbf{p}^{\perp}(X))\, (2\pi)^4 \delta^4(p_1 + p_2 - p_3 - q) \,.
\end{aligned} \tag{5.23}$$

Here we defined $\mathrm{d}\Phi_q$ as the phase space measure of the m non-strongly interacting final-state particles,

$$\mathrm{d}\Phi_q \equiv \prod_k^m \frac{\mathrm{d}^3 q_k}{2E_k} \,. \tag{5.24}$$

The restriction on the sum over final states X ("rest.") is that they include exactly one jet as defined by the jet algorithm and the delta functions that fix $\eta(X)$ and $\mathbf{p}^{\mathrm{T}}(X)$ act on the part of X identified to be the jet, which we assume to be sufficiently separated from the beams such that contributions from collinear initial state radiation are power suppressed. We also define $\overline{M} \equiv \gamma^0 M^\dagger \gamma^0$. To arrive at this equation, we used the hadronic momentum conserving delta function in the first line to shift the operator $O^\dagger$ to the point x, applied the matching condition Eq. (5.21), and then integrated over x which resulted in the partonic momentum conserving delta function on the last line.

We can simplify Eq. (5.23) using the following observations. First, we can use the BPS field redefinition [29] to decouple soft and collinear modes to $\mathcal{O}(\lambda^2)$,

$$\chi_n(x) \to Y_n(x) \chi_n(x) \tag{5.25a}$$

$$\bar\chi_n(x) \to \bar\chi_n(x) Y_n^\dagger(x) \tag{5.25b}$$

$$B_n(x) \to \mathcal{Y}_n(x) B_n(x) = Y_n^\dagger(x) B_n(x) Y_n(x) \,, \tag{5.25c}$$

where Y_n is a soft Wilson line, for which we adopt the conventions[4]

$$Y_n^{\text{in}}(x) = P \exp\left[\mathrm{i} g_s \int_{-\infty}^0 \mathrm{d}s\, n \cdot A_s(x + sn) \right] , \tag{5.26a}$$

[4]For a discussion of the various conventions for in- and outgoing Wilson lines and how they are related see for example Ref. [9]. There is also a nice discussion of how soft Wilson lines arise in the path integral formulation of SCET in Appendix C of Ref. [40].

for an incoming particle (where P denotes path ordering) and

$$Y_n^{\text{out}\,\dagger}(x) = P\exp\left[\mathrm{i}g_s\int_0^\infty \mathrm{d}s\, n\cdot A_s(x+s\,n)\right], \tag{5.26b}$$

for an outgoing particle. In momentum space, the field redefinition in Eq. (5.25) induces the shift $p_c \to p_c + k_s$ where k_s is the total soft momentum carried by the Wilson lines.

Second, we can implement the restriction on the final state X that there is one jet at the operator level to all orders by using the jet algorithm operator $\hat{\Theta}_i^R$, defined in Sec. 3. This allows us to complete the sum over X and factorize the collinear and soft matrix elements from one another.

The final state collinear matrix element can be written as

$$\big\langle 0\big|B_\mu^{\dagger A}(-p_3')\,\hat{\Theta}^R_{\text{coll},3}\delta(\eta_J-\hat{\eta})\delta^2(\mathbf{p}_J^{\mathrm{T}}-\hat{\mathbf{p}}^{\mathrm{T}})\,B_\nu^B(-p_3)\big|0\big\rangle = -E_J(2\pi)^4\delta^4(p_3'-p_3)\delta^{AB}g_{\mu\nu}^{\perp 3}J_\omega^g(p_3)\,, \tag{5.27}$$

which defines the gluon jet function $J_w^g(p)$. Integrating Eq. (5.27) over the full p_3 and p_3', which contain integrals over residual momentum and sums over the labels ω and n_3 of the $B_\perp$ field, fixes the labels to be $n_3 = (1, \mathbf{p}_J^{\mathrm{T}}/\left|\mathbf{p}_J^{\mathrm{T}}\right|\cosh\eta_J, \tanh\eta_J)$ and $\omega = 2p_J^{\mathrm{T}}\cosh\eta_J$. The label "3" on $\hat{\Theta}_R^3$ and on $g_{\mu\nu}^{\perp 3}$ indicates these are defined with respect to the direction n_3 of the jet. Note that this jet function depends on the choice of the jet algorithm.

For an algorithm that is inclusive over collinear initial state radiation, the initial state collinear matrix elements give rise to PDFs from the relations [20, 23]

$$\begin{aligned}
\int \mathrm{d}^4p\,\mathrm{d}^4p'\langle P|\bar{\chi}_{a'}^{\alpha'}(p')\chi_a^\alpha(p)|P\rangle_{\text{spin avg.}} &= E_{\text{cm}}\delta_{aa'}\Big(\frac{\bar{n}\!\!\!/}{2}\Big)^{\alpha\alpha'}\int_0^1 \mathrm{d}x f_q(x)\\
\int \mathrm{d}^4p\,\mathrm{d}^4p'\langle P|\chi_{a'}^{\alpha'}(-p')\bar{\chi}_a^{\alpha}(-p)|P\rangle_{\text{spin avg.}} &= E_{\text{cm}}\delta_{aa'}\Big(\frac{n\!\!\!/}{2}\Big)^{\alpha'\alpha}\int_0^1 \mathrm{d}x f_{\bar{q}}(x)\,,
\end{aligned} \tag{5.28}$$

with $p_{1,2}$ set to $x_{1,2}E_{\text{cm}}\frac{n_{1,2}}{2} = \frac{1}{2}\omega_{1,2}\,n_{1,2}$ (where $n_1 \equiv n$ and $n_2 \equiv \bar{n}$) and $p_{1,2}' = p_{1,2}$.

The color structure in the matrix elements Eqs. (5.27) and (5.28) leads to a trace over the color structure of the Wilson lines in the soft function. We can write the soft function in terms of the variables of interest k_{out} and k_3 (the out-of-jet and in-jet momenta) as

$$\begin{aligned}
\int \mathrm{d}^4k_s S(k_s,\{n_i\}) &= \frac{1}{C_AC_F}\int \mathrm{d}^4k_s \big\langle 0\big|\overline{\mathbf{T}}\Big[Y_{n_2}^\dagger Y_{n_3}^\dagger T^A Y_{n_3}Y_{n_1}\Big]\delta^4(k_s^\mu - i\partial^\mu)\mathbf{T}\Big[Y_{n_1}^\dagger Y_{n_3}^\dagger T^A Y_{n_3}Y_{n_2}\Big]\big|0\big\rangle\\
&= \int \mathrm{d}^4k_{\text{out}}\,\mathrm{d}^4k_3\, S(k_{\text{out}},k_3,\{n_i\})\,,
\end{aligned} \tag{5.29}$$

where $\{n_i\} = \{n_q, n_{\bar{q}}, n_g\}$ and $\mathbf{T}$ ($\overline{\mathbf{T}}$) denotes (anti-) time-ordering. $S(k_{\text{out}},k_3,\{n_i\})$ is then defined as

$$\begin{aligned}
S(k_{\text{out}},k_3,\{n_i\}) \equiv \frac{1}{C_AC_F}\big\langle 0\big|\overline{\mathbf{T}}\Big[Y_{n_2}^\dagger Y_{n_3}^\dagger T^A Y_{n_3}Y_{n_1}\Big]\delta^4(k_3-\hat{k}_3)\\
\times\delta^4(k_{\text{out}}-\hat{k}_{\text{out}})\mathbf{T}\Big[Y_{n_1}^\dagger Y_{n_3}^\dagger T^A Y_{n_3}Y_{n_2}\Big]\big|0\big\rangle\,,
\end{aligned} \tag{5.30}$$

and it is understood that the replacement $k_s \to k_{\rm out} + k_3$ should be made wherever k_s appears. The operators $\hat{k}_{\rm out}$ and $\hat{k}_3$ are defined as

$$\begin{aligned}\hat{k}_3^\mu &\equiv \hat{\Theta}^R_{\rm soft,3} i\partial^\mu \\ \hat{k}_{\rm out}^\mu &\equiv \Big(1 - \hat{\Theta}^R_{\rm soft,3}\Big) i\partial^\mu \,. \end{aligned} \tag{5.31}$$

Finally, using that the spin- and color-averaged square of the Born matrix element M_B, $\big|\overline{M_B}\big|^2$, can be written in terms of M_i as

$$\begin{aligned}\big|\overline{M_B}\big|^2 \equiv \frac{1}{4C_A^2} \sum_{\rm spin,color} |M_B|^2 &= -\frac{{\rm Tr}[T^A T^A]}{4C_A^2} \sum_{i,i'} M_i^{\alpha\beta\mu} \overline{M}_{i'}^{\bar\alpha\bar\beta\bar\mu} (\not{p}_1)^{\alpha\bar\alpha} (\not{p}_2)^{\bar\beta\beta} g^{\perp 3}_{\mu\bar\mu} \\ &= -\frac{C_F}{4C_A} \hat{s} \sum_{i,i'} M_i^{\alpha\beta\mu} \overline{M}_{i'}^{\bar\alpha\bar\beta\bar\mu} \Big(\frac{\not{n}_1}{2}\Big)^{\alpha\bar\alpha} \Big(\frac{\not{n}_2}{2}\Big)^{\bar\beta\beta} g^{\perp 3}_{\mu\bar\mu} \,, \end{aligned} \tag{5.32}$$

we see that the Dirac structure of the matrix elements in Eqs. (5.27) and (5.28) naturally gives rise to the Born cross-section.

To simplify the notation, we define a hard function H which includes all perturbative corrections contained in the matching coefficients C_{ij} as

$$H(\{n_i, \omega_i\}) \equiv -\frac{\frac{C_F}{4C_A}\hat{s} \sum_{i,i',j,j'} C_{ij}(\{\tilde{p}_k\}) C^*_{i'j'}(\{\tilde{p}_k\}) M_j^{\alpha\beta\mu} \overline{M}_{j'}^{\bar\beta\bar\alpha\bar\mu} \Big(\frac{\not{n}_1}{2}\Big)^{\alpha\bar\alpha} \Big(\frac{\not{n}_2}{2}\Big)^{\bar\beta\beta} g^{\perp 3}_{\mu\bar\mu}}{|\overline{M_B}|^2} \,, \tag{5.33}$$

where ω_i are the labels on the three collinear fields. H by definition is 1 to leading order in α_s. Putting this together we arrive at the expression

$$\begin{aligned}\frac{{\rm d}\sigma}{{\rm d}^2 p_J^{\rm T}\, {\rm d}\tanh\eta_J\, {\rm d}\Phi_q} = \frac{E_J}{2E_{\rm cm}^2} \int \frac{{\rm d}x_1}{x_1} \frac{{\rm d}x_2}{x_2} |\overline{M_B}|^2 \int \not{\rm d}^4 p_3 \int {\rm d}^4 k_\emptyset \int {\rm d}^4 k_3 \\ \times H(\{n_i, \omega_i\}) f_q(x_1) f_{\bar q}(x_2) J^g_\omega(p_3) S_{q\bar q \to g}(k_\emptyset, k_3, \{n_i\}) \\ \times (2\pi)^4 \delta^4\Big(x_1 E_{\rm cm} \frac{n}{2} + x_2 E_{\rm cm} \frac{\bar n}{2} - q - k_\emptyset - p_3 - k_3\Big) \,. \end{aligned} \tag{5.34}$$

The final step is to simplify the momentum-conserving delta function. We use Eqs. (5.7) and (5.10) to write it, up to power corrections in λ, as

$$\begin{aligned}&\delta^4\Big(x_1 E_{\rm cm} \frac{n}{2} + x_2 E_{\rm cm} \frac{\bar n}{2} - q - k_{\rm out} - p_3 - k_3\Big) \\ &\quad = \frac{2}{E_{\rm cm}^2 \tau} \delta\Big(1 - z - \frac{1}{Q^2}\Big[2p_I \cdot k_{\rm out} + 2p_I^0 (p_c^+ + k_3^+)\Big]\Big) \\ &\qquad \times \delta^2(\mathbf{p}_J^{\rm T} + \mathbf{q}_J^{\rm T})\, \delta\bigg(Y - \tanh^{-1}\Big(\frac{p_J^{\rm T} \sinh\eta_J + q_z}{p_J^{\rm T}\cosh\eta_J + q_0}\Big)\bigg) \,, \end{aligned} \tag{5.35}$$

To arrive at Eq. (5.35) we made the change of variables

$$\begin{aligned} x_1 &= \sqrt{\frac{\tau}{z}} e^Y \\ x_2 &= \sqrt{\frac{\tau}{z}} e^{-Y} \,. \end{aligned} \tag{5.36}$$

In switching from $x_{1,2}$ to z and the total rapidity Y, we will also need that

$$\int \frac{\mathrm{d}x_1}{x_1}\frac{\mathrm{d}x_2}{x_2} = \int_\tau^1 \frac{\mathrm{d}z}{z}\int_{-\frac{1}{2}\ln\frac{z}{\tau}}^{\frac{1}{2}\ln\frac{z}{\tau}} \mathrm{d}Y\,. \tag{5.37}$$

Now, since there is no dependence on the soft momenta other than on the components $p_I\cdot k_{\mathrm{out}}$ and k_3^+, and the only unconstrained component of p_3 is the plus-component, p_3^+, we can integrate over the other variables to obtain our final expression

$$\begin{aligned}\frac{\mathrm{d}\sigma}{\mathrm{d}^2p_J^{\mathrm{T}}\,\mathrm{d}\tanh\eta_J\,\mathrm{d}\Phi_q} &= \frac{\pi}{E_{\mathrm{cm}}^4\tau}\int_\tau^1\frac{\mathrm{d}z}{z}\int_{-\frac{1}{2}\ln\frac{z}{\tau}}^{\frac{1}{2}\ln\frac{z}{\tau}}\mathrm{d}Y\,|\overline{M_B}|^2 H_{q\bar q\to gX}(\{n_i,\omega_i\})f_q(x_1)f_{\bar q}(x_2)\\ &\quad\times\int\mathrm{d}p_3^+\,J_\omega^g(p_3^+)\int\mathrm{d}k_\emptyset^0\int\mathrm{d}k_3^+\,S_{q\bar q\to g}(k_\emptyset^0,k_3^+)\delta^2(\vec p_J^{\,\mathrm{T}}+\vec q^{\,\mathrm{T}})\\ &\quad\times\delta\biggl(Y-\tanh^{-1}\biggl(\frac{p_J^{\mathrm{T}}\sinh\eta_J+q_z}{p_J^{\mathrm{T}}\cosh\eta_J+q_0}\biggr)\biggr)\\ &\quad\times\delta\left[1-z-\frac{2}{\sqrt{\hat s}}\left(\frac{\sqrt{\tau}E_{\mathrm{cm}}}{\sqrt{\hat s}}\cosh Y\bigl(p_c^+ + k_{\mathrm{in}}^+\bigr)+k_\emptyset^0\right)\right]\,.\end{aligned} \tag{5.38}$$

The soft function in Eq. (5.38) is defined as

$$\begin{aligned}S_{q\bar q\to g}(k_{\mathrm{out}}^0,k_3^+,\{n_i\}) &\equiv \frac{1}{C_AC_F}\langle 0|\overline{\mathbf{T}}\Bigl[Y_{n_2}^\dagger Y_{n_3}^\dagger T^A Y_{n_3}Y_{n_1}\Bigr]\delta(k_3^+-\hat k_3^+)\delta\Bigl(k_{\mathrm{out}}^0-\frac{p_I\cdot\hat k_{\mathrm{out}}}{|p_I|}\Bigr)\\ &\qquad\times\mathbf{T}\Bigl[Y_{n_1}^\dagger Y_{n_3}^\dagger T^A Y_{n_3}Y_{n_2}\Bigr]|0\rangle\\ &= \delta(k_{\mathrm{out}}^0)\delta(k_3^+)+\mathcal{O}(\alpha_s)\,.\end{aligned} \tag{5.39}$$

Note that, despite our notation, $k_{\mathrm{out}}^0\equiv p_I\cdot k_{\mathrm{out}}/|p_I|$ in general has a nonzero spatial component. This function is most easily computed in the partonic center-of-mass frame where k_{out}^0 is in fact purely timelike. The jet function in Eq. (5.38) is defined as

$$J_\omega^g(p^+)g_\perp^{\mu\nu}\delta^{AB}\equiv-\frac{\omega}{2\pi}\int\mathrm{d}^4x\,e^{ip\cdot x}\,\langle 0|\,B_{\perp,\omega}^{\mu,A}(x)\hat\Theta_{\mathrm{coll},3}^R B_{\perp,\omega}^{\nu,B}(0)\,|0\rangle=\delta(p^+)g_\perp^{\mu\nu}\delta^{AB}+\mathcal{O}(\alpha_s)\,, \tag{5.40}$$

where, again, the label ω is set to $\omega=2E_J=2p_{\mathrm{T}}^J\cosh\eta_J$.

4.1.2 $qg\to q$

The majority of the above discussion goes through in much the same way for the channel $qg\to q$. The main differences are that the matrix element of final state fields gives rise to a quark jet function, defined by

$$\int\!\!\not{\mathrm{d}}^4p_3'\,\langle 0|\chi_{\alpha'}^{c'}(p_3')\,\hat\Theta_{\mathrm{coll},3}^R\delta(\eta_J-\hat\eta)\delta^2(\mathbf{p}_J^{\mathrm{T}}-\hat{\mathbf{p}}^{\mathrm{T}})\bar\chi_\alpha^c(p_3)|0\rangle=\delta^{c'c}\Bigl(\frac{\not p_3}{2}\Bigr)_{\alpha'\alpha}J_\omega^q(p_3)\,, \tag{5.41}$$

which, after integrating over all but the p^+ component, becomes

$$J_\omega^q(p^+)\delta^{ab}\equiv\frac{1}{2\pi}\int\mathrm{d}^4x\,e^{ip\cdot x}\,\langle 0|\,\frac{\bar{\not n}}{2}\chi_{n,\omega}^a(x)\hat\Theta_{\mathrm{coll},3}^R\bar\chi_{n,\omega}^b(0)\,|0\rangle=\delta(p^+)\delta^{ab}+\mathcal{O}(\alpha_s)\,. \tag{5.42}$$

For the initial state gluon, we obtain the gluon PDF via the relation

$$\int \not{d}^4p\, \not{d}^4p' \langle P|B_\nu^{\dagger A}(p')B_\mu^B(p)|P\rangle = \frac{g_{\mu\nu}^\perp}{D-2}\delta_{AB}\int_0^1 \frac{\mathrm{d}x}{x} f_g(x)\,. \tag{5.43}$$

Finally, the soft function is defined as in Eq. (5.29) but with the appropriate modification in the definition of the Wilson lines for incoming and outgoing fields given in Eq. (5.26). The final result after these differences are taken into account is of the form Eq. (5.38) but with the substitutions $f_{\bar{q}} \to f_g$, $J^g \to J^q$, and $S_{q\bar{q}\to g} \to S_{qg\to q}$.

4.2 Extension to N Jets

The above results clearly generalize. The only nontrivial complication is due to mixing in color space. To avoid cumbersome notation, we will explain what generalizes and state the result rather than write down the N-jet derivation. Explicitly, for every quark, anti-quark and gluon in the final (initial) state, the all-orders jet function (PDF) has precisely the Dirac and color structure to contract with the non-QCD matrix element $M_i^{\alpha\beta\ldots\mu\ldots}$ to give the Born matrix element at tree level. The PDFs and jet functions have the same definitions as in the single jet case. However, due to the fact that operators with different color structures in general mix, the hard and soft functions in these formulas should be interpreted as matrices in color space.

Since the main difference in the generalization to N jets is in the soft function, we will discuss it in more detail. It takes the general form

$$S(k^0_{\rm out}, \{n_i, k_i^+\}) \equiv \frac{1}{\mathcal{N}} \langle 0|\, O_S^\dagger\, \delta\Big(k^0_{\rm out} - \frac{p_I\cdot \hat{k}_{\rm out}}{|p_I|}\Big) \prod_i^N \delta(k_i^+ - \hat{k}_i^+)\, O_S\, |0\rangle\ , \tag{5.44}$$

where $\mathcal{N}$ is a normalization factor such that the soft function is unity (times delta functions in its arguments) at tree level and the operator O_S is the product of Wilson lines that arise from the BPS field redefinitions Eq. (5.25), appropriately traced. As for the one jet case, the arguments k_i in the soft function run over all final state jets and the n_i include all directions, both initial and final. The operators $\hat{k}_{\rm out}$ and $\hat{k}_i$ that appear in Eq. (5.44) are defined as

$$\begin{aligned} \hat{k}_i^\mu &\equiv \hat{\Theta}^R_{{\rm soft},i}\, i\partial^\mu \\ \hat{k}^\mu_{\rm out} &\equiv \Big(1 - \sum_i^N \hat{\Theta}^R_{{\rm soft},i}\Big) i\partial^\mu\,. \end{aligned} \tag{5.45}$$

The result of going through the same steps as for the single jet case leads to the N-jet factorization

formula,

$$\begin{aligned}\frac{\mathrm{d}\sigma}{\prod_i^N \mathrm{d}^2 p_{J_i}^{\mathrm{T}} \mathrm{d}\tanh\eta_{J_i}\mathrm{d}\Phi_q} &= \frac{1}{E_{\mathrm{cm}}^4\tau}\int_\tau^1 \frac{\mathrm{d}z}{z}\int_{-\frac{1}{2}\ln\frac{z}{\tau}}^{\frac{1}{2}\ln\frac{z}{\tau}} \mathrm{d}Y\,|\overline{M_B}|^2 H(\{n_i,\omega_i\}) f_1(x_1) f_2(x_2) \\ &\times \prod_i^N \int \frac{\mathrm{d}p_i^+}{2\cdot(2\pi)^3} J_i(p_i^+) \prod_i^N \int \mathrm{d}k_i^+ \int \mathrm{d}k_\emptyset^0 S(k_\emptyset^0, \{n_i, k_i^+\}) \\ &\times (2\pi)^4\,\delta\left[1 - z - \frac{2}{\sqrt{\hat{s}}}\left(\frac{\sqrt{\tau}E_{\mathrm{cm}}}{\sqrt{\hat{s}}}\cosh Y \sum_i^N \left(p_i^+ + k_i^+\right) + k_\emptyset^0\right)\right] \\ &\times \delta\left(Y - \tanh^{-1}\left(\frac{\sum_i^N p_{J_i}^\perp \sinh\eta_{J_i} + q_z}{\sum_i^N p_{J_i}^\perp \cosh\eta_{J_i} + q_0}\right)\right) \delta^2\Big(\sum_i^N \vec{p}_{J_i}^{\,\mathrm{T}} + \vec{q}^{\,\mathrm{T}}\Big)\,. \end{aligned} \tag{5.46}$$

5 Anomalous dimensions

Now that we have shown that a generic N-jet cross-section factorizes in the limit of $1 - z \ll 1$, we are left to calculate each ingredient of the factorization theorem. In this chapter we focus on the consistency of the factorization theorem to $\mathcal{O}(\alpha_s)$, and we therefore need the one-loop anomalous dimensions for the hard, jet and soft functions. Note that the results presented here are enough to resum threshold logarithms at NLL[5].

5.1 Hard, Jet and Parton Distribution Functions

Both the Born-level matrix element and the hard function, which can be found by calculating the the virtual corrections to the Born-level matrix element in the $\overline{\mathrm{MS}}$ scheme, are process dependent, so they can not be calculated generically. However, the hard anomalous dimension, defined as

$$\frac{\mathrm{d}H(\{n_i,\omega_i\};\mu)}{\mathrm{d}\ln\mu} \equiv \gamma_H\left(\{n_i,\omega_i\};\mu\right) H\left(\{n_i,\omega_i\};\mu\right)\,, \tag{5.47}$$

only depends on the directions n_i, label momenta ω_i, and color charges $\mathbf{T}_i$ of the collinear particles and is given by [87]

$$\gamma_H(\{n_i,\omega_i\};\mu) = \sum_{i\in\{\mathrm{partons}\}} \left(-\Gamma_{\mathrm{cusp}}\,\mathbf{T}_i^2 \ln\frac{\mu^2}{\omega_i^2} - \gamma_i\right) - 2\,\Gamma_{\mathrm{cusp}} \sum_{\langle i,j\rangle} \mathbf{T}_i\cdot\mathbf{T}_j \ln\frac{n_i\cdot n_j}{2}\,. \tag{5.48}$$

The cusp anomalous dimension at two loops is given by

$$\Gamma_{\mathrm{cusp}} = \frac{\alpha_s}{\pi} + \frac{\alpha_s^2}{4\pi^2}\left[C_A\left(\frac{67}{9} - \frac{\pi^2}{3}\right) - \frac{20}{9}C_F T_F n_f\right]\,. \tag{5.49}$$

The γ_i to one-loop are given by

$$\gamma_q = \frac{3\alpha_s}{2\pi}C_F \qquad \text{and} \qquad \gamma_g = \frac{\alpha_s}{2\pi}\beta_0\,, \tag{5.50}$$

[5]There are several different ways to define precisely what is meant by NLL. In this chapter, we will use the convention of [40].

for quarks and gluons respectively, where β_0 is defined as

$$\beta_0 = \frac{11 C_A}{3} - \frac{2 N_f}{3} \,. \tag{5.51}$$

The sum on $\langle i, j \rangle$ is a sum over all distinct pairs of partons i and j for $i \neq j$.

The quark and gluon jet functions have been calculated previously, e.g.[25, 53, 15], and were first calculated with a jet algorithm in [116]. Their anomalous dimensions, defined by

$$\frac{\mathrm{d} J_i(p_i^+;\mu)}{\mathrm{d}\ln\mu} = \int_0^{p_i^+} \mathrm{d}p'^+_i \gamma_{J_i}(p_i^+ - p'^+_i;\mu) J_i(p'^+_i;\mu) \,, \tag{5.52}$$

are given by

$$\gamma_{J_i}(p_i^+;\mu) = \left(2\,\Gamma_{\mathrm{cusp}}\,\mathbf{T}_i^2 \ln\frac{\mu}{\omega_i} + \gamma_i\right)\delta(p_i^+) - 2\,\Gamma_{\mathrm{cusp}}\,\mathbf{T}_i^2\,\frac{1}{\mu}\left(\frac{\mu}{p_i^+}\right)_+ \,. \tag{5.53}$$

The expressions for Γ_{cusp} and γ_i are the same as for the hard function. Note that the algorithm in [116] used a polar angle for the measure and not Eq. (5.12). However, since the anomalous dimension in that case did not depend on the algorithm parameter R, the result must be independent of which measure is chosen since the precise definition of the jet boundaries is not associated with any singularities. It does however affect the finite parts of the jet function, which become important starting at NNLL accuracy.

It it well known that the parton distribution functions are not perturbatively calculable; in practice, they can be expressed as universal matrix elements, which are then extracted from experiment. However, the evolution of the PDFs with μ can be computed,

$$\frac{\mathrm{d} f_i(x_i;\mu)}{\mathrm{d}\ln\mu} = \frac{\alpha_s}{\pi}\int_{x_i}^1 \frac{\mathrm{d}z}{z} P_{ij}(z) f_j\left(\frac{x_i}{z};\mu\right) \,, \tag{5.54}$$

where the repeated index j is summed over and P_{ij} are the Altarelli-Parisi splitting functions. Near hadronic threshold, the splitting functions simplify and can be written as

$$\frac{\alpha_s}{\pi} P_{ij}(x) = \left[2\,\Gamma_{\mathrm{cusp}}\,\mathbf{T}_i^2\,\frac{1}{(1-x)_+} + \gamma_i\,\delta(1-x)\right]\delta_{ij} \,. \tag{5.55}$$

5.2 Soft Function

In general, the soft function depends on the null component of the soft momentum inside each jet as well as the timelike component k^0_{out}. At order α_s, the soft function can be written as a sum of functions that depend only on one momentum variable, with trivial dependence on the others and is given by

$$S(k^0_{\mathrm{out}}, \{n_i, k_i^+\}) = S_{\mathrm{out}}(k^0_{\mathrm{out}}) \prod_{i\in\{\mathrm{jets}\}} \delta(k_i^+) + \delta(k^0_{\mathrm{out}}) \sum_{i\in\{\mathrm{jets}\}} S_{\mathrm{in}}(k_i^+) \prod_{\substack{j\in\{\mathrm{jets}\}\\ j\neq i}} \delta(k_j^+) \,, \tag{5.56}$$

where the sum over $i \in \{\mathrm{jets}\}$ is over all i corresponding to outgoing jets and does not include the incoming partons (and we remind the reader that the dependence here on k_i is only over final state

jets but the n_i run over all initial and final partons). The time-like component of the soft function, $S_{\rm out}$, receives contributions from soft gluons that are not inside any of the outgoing jets. We can find this by calculating the contribution of soft gluons going anywhere and then subtracting the contribution from gluons that enter one of the jets. This can be written in the hadronic center-of-mass frame as

$$S_{\rm out}(k^0_{\rm out}) = -\sum_{\langle i,j\rangle} \mathbf{T}_i\cdot\mathbf{T}_j\, 2g^2\mu^{2\epsilon}\int \frac{\mathrm{d}^d k}{(2\pi)^d}\frac{n_i\cdot n_j}{(n_i\cdot k)(n_j\cdot k)} \times 2\pi\delta(k^2)\delta\Big(\frac{p_I\cdot k}{|p_I|} - k^0_{\rm out}\Big)\Big[1-\sum_{k\in\{\rm jets\}}\hat\Theta^R_{{\rm soft},k}\Big]\,, \tag{5.57}$$

where $\hat\Theta^R_k$ is the restriction that the gluon is in jet k, defined by a jet algorithm of size R as in Sec. 3. This is most easily calculated in the partonic center-of-mass frame. Denoting the directions and energies of the collinear partons in this frame as $\tilde n_i$ and $\tilde\omega_i$ respectively, we have that

$$S_{\rm out}(k^0_{\rm out}) = -\sum_{\langle i,j\rangle} \mathbf{T}_i\cdot\mathbf{T}_j\, 2g^2\mu^{2\epsilon}\int \frac{\mathrm{d}^d k}{(2\pi)^d}\frac{\tilde n_i\cdot\tilde n_j}{(\tilde n_i\cdot k)(\tilde n_j\cdot k)}2\pi\delta(k^2)\delta(k^0-k^0_{\rm out})\Big[1-\sum_{k\in\{\rm jets\}}\hat\Theta^R_{{\rm soft},k}\Big]\,, \tag{5.58}$$

where we have used the fact that, for an $\eta-\phi$ algorithm, the jet algorithm restrictions are frame invariant.

The null components of the soft function, $S_{\rm in}(k_i^+)$, are defined in the hadronic center-of-mass frame as

$$S_{\rm in}(k_k^+) = -\sum_{\langle i,j\rangle} \mathbf{T}_i\cdot\mathbf{T}_j\, 2g^2\mu^{2\epsilon}\int \frac{\mathrm{d}^d k}{(2\pi)^d}\frac{n_i\cdot n_j}{(n_i\cdot k)(n_j\cdot k)}2\pi\delta(k^2)\delta(n_k\cdot k - k_k^+)\hat\Theta^R_{{\rm soft},k}\,. \tag{5.59}$$

In the partonic center-of-mass frame, this can be written as

$$S_{\rm in}(k_k^+) = -\sum_{\langle i,j\rangle} \mathbf{T}_i\cdot\mathbf{T}_j\, 2g^2\mu^{2\epsilon}\int \frac{\mathrm{d}^d k}{(2\pi)^d}\frac{\tilde n_i\cdot\tilde n_j}{(\tilde n_i\cdot k)(\tilde n_j\cdot k)}2\pi\delta(k^2)\frac{\omega_k}{\tilde\omega_k}\delta\left(k^+ - \frac{\omega_k}{\tilde\omega_k}k_k^+\right)\hat\Theta^R_{{\rm soft},k}\,. \tag{5.60}$$

The calculation of $S_{\rm in}$ and $S_{\rm out}$ in the partonic center-of-mass frame can be related to the calculation of the soft function in [116]. While [116] uses a polar angle measure, we will show that, even though $S_{\rm in}$ and $S_{\rm out}$ separately depend on the parameter R, the anomalous dimension is R-independent. This implies that all algorithms with the same singularity structure as the polar angle algorithm used in [116] have the same anomalous dimension for this observable. Specifically, the anomalous dimension calculated in the partonic center-of-mass frame should be the same for both a polar angle measure and an $\eta-\phi$ measure. Since the $\eta-\phi$ measure is boost invariant, the R-indepence of the anomalous dimension must be true in all frames[6]. The relations of $S_{\rm in}$ and $S_{\rm out}$ to the soft function in [116] are given by

[6]We have verified this explicitly for small R by making the replacement $R\to R/\cosh\eta$, which relates the polar angle and $\eta-\phi$ measures in the small R limit.

$$S_{\rm out}(k^0_{\rm out}) = 2\sum_{\langle i,j\rangle}\frac{\rm d}{{\rm d}\Lambda}\left[S^{\rm incl}_{ij} + \sum_{k\in\{\rm jets\}} S^k_{ij}\right]_{\Lambda=k^0_{\rm out}}, \tag{5.61}$$

and

$$S_{\rm in}(k^+_k) = 2\sum_{\langle i,j\rangle}\frac{1}{\tilde\omega_k}S^{\rm meas}_{ij}(\tau^k_0)\,. \tag{5.62}$$

where $S^{\rm incl}_{ij}$, S^k_{ij} and $S^{\rm meas}_{ij}$ are defined and computed in [116]. In calculating $S^{\rm meas}_{ij}$, we use the definitions $\tau^k_0 = k^+_k/\tilde\omega_k$ and $\delta_R = \delta\left(\tau^k_0 - k^+/\omega_k\right)$, where τ_a and δ_R are originally defined in [116].

The anomalous dimension of this soft function is defined as

$$\begin{aligned}\frac{{\rm d}S(k^0_{\rm out},\{n_i,k^+_i\};\mu)}{{\rm d}\ln\mu} = &\prod_{i\in\{\rm jets\}}\int_0^{k^+_i}{\rm d}k'^+_i\int_0^{k^0_{\rm out}}{\rm d}k'^0_{\rm out}\,\gamma_S(k^0_{\rm out}-k'^0_{\rm out},\{n_i,k^+_i-k'^+_i\};\mu)\\ &\times S(k'^0_{\rm out},\{n_i,k'^+_i\};\mu)\,.\end{aligned} \tag{5.63}$$

Using the results of [116], together with Eqs. (5.61) and (5.62), the result for the anomalous dimension can be written as

$$\gamma_S(k^0_{\rm out},\{n_i,k^+_i\};\mu) = \sum_{i\in\{\rm jets\}}\gamma_{S_i}(k^+_i;\mu)\prod_{\substack{j\in\{\rm jets\}\\ j\neq i}}\delta(k^+_j)\,\delta(k^0_{\rm out}) + \gamma_{S_{\rm out}}(k^0_{\rm out};\mu)\prod_{i\in\{\rm jets\}}\delta(k^+_i)\,. \tag{5.64}$$

with

$$\gamma_{S_i}(k^+_i;\mu) = 2\,\Gamma_{\rm cusp}\mathbf{T}^2_i\,\frac{\omega_i}{\mu\,\tilde\omega_i}\left(\frac{\mu\,\tilde\omega_i}{k^+_i\omega_i}\right)_+ \tag{5.65}$$

$$\gamma_{S_{\rm out}}(k^0_{\rm out};\mu) = \Gamma_{\rm cusp}\sum_{\langle i,j\rangle}\mathbf{T}_i\cdot\mathbf{T}_j\left(2\ln\frac{\tilde n_i\cdot\tilde n_j}{2}\right)\delta(k^0_{\rm out}) - 4\,\Gamma_{\rm cusp}\,(\mathbf{T}^2_1+\mathbf{T}^2_2)\frac{1}{\mu}\left(\frac{\mu}{2k^0_{\rm out}}\right)_+. \tag{5.66}$$

6 Consistency of Factorization to $\mathcal{O}(\alpha_s)$

Consistency is a nontrivial check of our factorization theorem. The factorized cross-section should be independent of the factorization scale μ in the threshold limit and thus renormalization group invariant. Starting from the generic N-jet cross-section, Eq. (5.46), ignoring multiplicative factors that do not affect the derivative, and using the shorthand notation

$$\frac{{\rm d}\sigma}{{\rm d}\ln\mu} \equiv \frac{\rm d}{{\rm d}\ln\mu}\frac{{\rm d}\sigma}{\prod_i {\rm d}^2p^{\rm T}_{J_i}{\rm d}\eta_{J_i}{\rm d}\Phi_q}\,, \tag{5.67}$$

we have that

$$\begin{aligned}\frac{\mathrm{d}\sigma}{\mathrm{d}\ln\mu} \propto \int_\tau^1 \frac{\mathrm{d}z}{z} \int_{-\frac{1}{2}\ln\frac{z}{\tau}}^{\frac{1}{2}\ln\frac{z}{\tau}} \mathrm{d}Y H(\{n_i,\omega_i\};\mu) f_1(x_1;\mu) f_2(x_2;\mu) \\ \times \prod_{i\in\{\text{jets}\}} \int \mathrm{d}p_i^+ J_i(p_i^+;\mu) \prod_{i\in\{\text{jets}\}} \int \mathrm{d}k_i^+ \int \mathrm{d}k_{\text{out}}^0 S(k_{\text{out}}^0,\{n_i,k_i^+\};\mu) \\ \times \left(\frac{\mathrm{d}\ln H(\{n_i,\omega_i\};\mu)}{\mathrm{d}\ln\mu} + \frac{\mathrm{d}\ln f_1(x_1;\mu)}{\mathrm{d}\ln\mu} + \frac{\mathrm{d}\ln f_2(x_2;\mu)}{\mathrm{d}\ln\mu} \right. \\ \left. + \sum_{i\in\{\text{jets}\}} \frac{\mathrm{d}\ln J_i(p_i^+;\mu)}{\mathrm{d}\ln\mu} + \frac{\mathrm{d}\ln S(k_{\text{out}}^0,\{n_i,k_i^+\};\mu)}{\mathrm{d}\ln\mu} \right) \\ \times \delta\left[1 - z - \frac{2}{\sqrt{\hat{s}}} \left(\frac{\sqrt{\tau} E_{\text{cm}} \cosh Y}{\sqrt{\hat{s}}} \sum_{i\in\{\text{jets}\}} (p_i^+ + k_i^+) + k_{\text{out}}^0 \right) \right] . \end{aligned} \tag{5.68}$$

There are several simplifications we can make to check the independence of μ. First, μ only enters perturbative expressions, and whether or not the cross section depends on μ is independent of non-perturbative physics. This allows us to use the perturbative definition of the parton distribution functions. Second, given that the μ dependence of each of the factorization ingredients starts at order α_s, we can use the tree level expressions for the hard, jet and soft functions, as well as for the PDFs,

$$f_i(x;\mu) = \delta(1-x) \tag{5.69}$$

$$H(\{n_i,\omega_i\};\mu) = 1 \tag{5.70}$$

$$J_i(p_i^+;\mu) = \delta(p_i^+) \tag{5.71}$$

$$S(k_{\text{out}}^0,\{n_i,k_i^+\};\mu) = \delta(k_{\text{out}}^0) \prod_{i\in\{\text{jets}\}} \delta(k_i^+) . \tag{5.72}$$

Using this and working to lowest order in α_s, we can simplify Eq. (5.68) to get

$$\begin{aligned}\frac{\mathrm{d}\sigma}{\mathrm{d}\ln\mu} \propto \frac{\alpha_s}{\pi} P_{11}(\tau) + \frac{\alpha_s}{\pi} P_{22}(\tau) + \frac{\hat{s}}{2E_{\text{cm}}\sqrt{\tau}} \sum_{i\in\{\text{jets}\}} \gamma_{J_i}\left(\frac{\hat{s}}{2E_{\text{cm}}\sqrt{\tau}}(1-\tau);\mu \right) \\ + \frac{\hat{s}}{2E_{\text{cm}}\sqrt{\tau}} \sum_{i\in\{\text{jets}\}} \gamma_{S_i}\left(\frac{\hat{s}}{2E_{\text{cm}}\sqrt{\tau}}(1-\tau);\mu \right) + \gamma_H(\mu)\,\delta(1-\tau) \\ + \frac{\sqrt{\hat{s}}}{2} \gamma_{S_{\text{out}}}\left(\frac{\sqrt{\hat{s}}}{2}(1-\tau);\mu \right) . \end{aligned} \tag{5.73}$$

After plugging in Eqs. (5.48), (5.53), and (5.64), rescaling the plus functions using the identity

$$\left(\frac{1}{ax}\right)_+ = \frac{\ln a}{a}\delta(x) + \frac{1}{a}\left(\frac{1}{x}\right)_+ , \tag{5.74}$$

and combining the various terms, we find

$$\frac{\mathrm{d}\sigma}{\mathrm{d}\ln\mu} \propto \Gamma_{\mathrm{cusp}} \left[\sum_{i\neq j} \mathbf{T}_i\cdot\mathbf{T}_j \left(2\ln\frac{\tilde{n}_i\cdot\tilde{n}_j}{n_i\cdot n_j} \right) + \mathbf{T}_1^2 \ln\frac{\omega_1^2}{\hat{s}} + \mathbf{T}_2^2 \ln\frac{\omega_2^2}{\hat{s}} + \sum_{i\in\{\mathrm{jets}\}} \mathbf{T}_i^2 \left(2\ln\frac{\omega_i}{\tilde{\omega}_i} \right) \right] . \quad (5.75)$$

After making the simplification

$$\sum_{i\neq j} \mathbf{T}_i\cdot\mathbf{T}_j \left(2\ln\frac{\tilde{n}_i\cdot\tilde{n}_j}{n_i\cdot n_j} \right) = \sum_{\substack{i,j \\ i\neq j}} \mathbf{T}_i\cdot\mathbf{T}_j \left(\ln\frac{\omega_i}{\tilde{\omega}_i} + \ln\frac{\omega_j}{\tilde{\omega}_j} \right) = \sum_{i\in\{\mathrm{partons}\}} \mathbf{T}_i^2 \left(-2\ln\frac{\omega_i}{\tilde{\omega}_i} \right) , \quad (5.76)$$

where we have used that $\tilde{p}_i\cdot\tilde{p}_j = p_i\cdot p_j$ and $\sum_i \mathbf{T}_i = 0$, Eq. (5.75) gives

$$\frac{\mathrm{d}\sigma}{\mathrm{d}\ln\mu} = 0 . \quad (5.77)$$

This result confirms that our factorization theorem is consistent at hadronic threshold and justifies using the renormalization group to resum logarithms of $1-\tau$.

7 Conclusions and Outlook

We have derived a factorization theorem for the production of N jets, together with any number of non-strongly interacting particles, such as electroweak gauge bosons. This factorization theorem allows us to write the physical cross-section in terms of a convolution of parton distribution functions, a hard function, jet functions for each observed jet and a soft function describing among other things the color recombination between the initial and final state partons. Both the jet and the soft functions depend on the precise form of the jet algorithm chosen.

The main new ingredient in this factorization theorem is a soft function that depends on a time-like component of the soft momentum outside of the observed jets, and the light-like component of the soft momentum in a given jet. This function is directly related to the soft function first proposed and calculated for the case of jet production in e^+e^- collisions in [116, 114]. This soft function allows us to interpolate between the soft function arising for final states without observed jets (which depends only on a time-like component of the soft momentum) and the soft function for completely inclusive jet production (which depends only on the light-like component of the soft momentum).

We have derived the UV divergent parts of all ingredients of the factorization theorem to $\mathcal{O}(\alpha_s)$. These were then used to show that the combination of all ingredients of the factorization theorem is independent of the arbitrary factorization scale μ, and therefore the derived results satisfy the nontrivial requirement of consistency. While consistency was shown in this work only in the true hadronic endpoint, we have kept the kinematics general enough (in particular allowing for a nonzero overall boost) to allow for a generalization of our results to the case where the steepness of the parton luminosities force events to be close to the partonic threshold. This result, which is by far more interesting phenomenologically, will be the subject of future work [16].

Our results can be used to explicitly resum threshold logarithms to NLL accuracy (in the log-counting convention of [40]) for any process in hadron collisions with any number of jets and

non-strongly interacting particles in the final state. The technology of going from the anomalous dimensions we present here to explicit resummed distributions is well known. Beyond one jet, in addition to the standard resummation methods, we need the matrices $\mathbf{T}_i \cdot \mathbf{T}_j$, but these have been computed for many processes (see, e.g., [87, 144, 142, 105, 174, 175]), including all $2 \to 2$ and $2 \to 3$ partonic channels. The only other ingredient needed to obtain a NLL distribution is the Born matrix element.

In addition, if our results are extended to include two-loop results of the anomalous dimensions together with the full algorithm-dependent one-loop finite parts, NNLL results can be obtained for all processes for which the virtual NLO corrections are known. Together with recent advances in calculations of NLO cross-sections (e.g., W^+W^-j [65, 103] and $Wjjj$ [46]), this would have a significant impact on the precision frontier of predictions at the LHC.

Bibliography

[1] F. Abe et al. A measurement of jet shapes in $p\bar{p}$ collisions at $\sqrt{s} = 1.8$ TeV. *Phys. Rev. Lett.*, 70:713–717, 1993.

[2] R. Akhoury and I. Z. Rothstein. The Extraction of V_{ub} from Inclusive B Decays and the Resummation of End Point Logs. *Phys. Rev.*, D54:2349–2362, 1996.

[3] Leandro G. Almeida et al. Substructure of high-p_t jets at the LHC. *Phys. Rev.*, D79:074017, 2009.

[4] Leandro G. Almeida, Seung J. Lee, Gilad Perez, Ilmo Sung, and Joseph Virzi. Top jets at the LHC. *Phys. Rev.*, D79:074012, 2009.

[5] Guido Altarelli, N. Cabibbo, G. Corbo, L. Maiani, and G. Martinelli. Leptonic Decay of Heavy Flavors: A Theoretical Update. *Nucl. Phys.*, B208:365–380, 1982.

[6] Johan Alwall, Pavel Demin, Simon de Visscher, Rikkert Frederix, Michel Herquet, Fabio Maltoni, Tilman Plehn, David L. Rainwater, and Tim Stelzer. MadGraph/MadEvent v4: The new web generation. *JHEP*, 09:028, 2007.

[7] David Appell, George Sterman, and Paul B. Mackenzie. Soft Gluons and the Normalization of the Drell-Yan Cross-Section. *Nucl. Phys.*, B309:259, 1988.

[8] R. B. Appleby and G. P. Salam. Theory and phenomenology of non-global logarithms. 2003.

[9] Christian M. Arnesen, Joydip Kundu, and Iain W. Stewart. Constraint equations for heavy-to-light currents in SCET. *Phys. Rev.*, D72:114002, 2005.

[10] Christopher Balzereit, Thomas Mannel, and Wolfgang Kilian. Evolution of the light-cone distribution function for a heavy quark. *Phys. Rev.*, D58:114029, 1998.

[11] A. Banfi, G. Marchesini, and G. Smye. Away-from-jet energy flow. *JHEP*, 08:006, 2002.

[12] Andrea Banfi, Gavin P. Salam, and Giulia Zanderighi. Resummed event shapes at hadron — hadron colliders. *JHEP*, 08:062, 2004.

[13] Andrea Banfi, Gavin P. Salam, and Giulia Zanderighi. Principles of general final-state resummation and automated implementation. *JHEP*, 03:073, 2005.

[14] Christian W. Bauer, Oscar Cata, and Grigory Ovanesyan. On different ways to quantize Soft-Collinear Effective Theory. 2008.

[15] Christian W. Bauer, Cheng-Wei Chiang, Sean Fleming, Adam K. Leibovich, and Ian Low. Resumming the color-octet contribution to radiative Upsilon decay. *Phys. Rev.*, D64:114014, 2001.

[16] Christian W. Bauer, Nicholas Daniel Dunn, and Andrew Hornig. work in progress.

[17] Christian W. Bauer, Nicholas Daniel Dunn, and Andrew Hornig. Factorization of Boosted Multijet Processes for Threshold Resummation. 2010.

[18] Christian W. Bauer, Sean Fleming, Christopher Lee, and George Sterman. Factorization of e^+e^- event shape distributions with hadronic final states in Soft Collinear Effective Theory. *Phys. Rev.*, D78:034027, 2008.

[19] Christian W. Bauer, Sean Fleming, and Michael E. Luke. Summing Sudakov logarithms in $B \to X_s\gamma$ in effective field theory. *Phys. Rev.*, D63:014006, 2000.

[20] Christian W. Bauer, Sean Fleming, Dan Pirjol, Ira Z. Rothstein, and Iain W. Stewart. Hard scattering factorization from effective field theory. *Phys. Rev.*, D66:014017, 2002.

[21] Christian W. Bauer, Sean Fleming, Dan Pirjol, and Iain W. Stewart. An effective field theory for collinear and soft gluons: Heavy to light decays. *Phys. Rev.*, D63:114020, 2001.

[22] Christian W. Bauer, Andrew Hornig, and Frank J. Tackmann. work in progress.

[23] Christian W. Bauer, Andrew Hornig, and Frank J. Tackmann. Factorization for generic jet production. *Phys. Rev.*, D79:114013, 2009.

[24] Christian W. Bauer, Christopher Lee, Aneesh V. Manohar, and Mark B. Wise. Enhanced nonperturbative effects in Z decays to hadrons. *Phys. Rev.*, D70:034014, 2004.

[25] Christian W. Bauer and Aneesh V. Manohar. Shape function effects in $B \to X_s\gamma$ and $B \to X_u l\bar{\nu}$ decays. *Phys. Rev.*, D70:034024, 2004.

[26] Christian W. Bauer, Aneesh V. Manohar, and Mark B. Wise. Enhanced nonperturbative effects in jet distributions. *Phys. Rev. Lett.*, 91:122001, 2003.

[27] Christian W. Bauer, Dan Pirjol, and Iain W. Stewart. A proof of factorization for $b \to d\pi$. *Phys. Rev. Lett.*, 87:201806, 2001.

[28] Christian W. Bauer, Dan Pirjol, and Iain W. Stewart. Power counting in the Soft-Collinear Effective Theory. *Phys. Rev.*, D66:054005, 2002.

[29] Christian W. Bauer, Dan Pirjol, and Iain W. Stewart. Soft-collinear factorization in effective field theory. *Phys. Rev.*, D65:054022, 2002.

[30] Christian W. Bauer, Dan Pirjol, and Iain W. Stewart. On power suppressed operators and gauge invariance in SCET. *Phys. Rev.*, D68:034021, 2003.

[31] Christian W. Bauer and Matthew D. Schwartz. Improving jet distributions with effective field theory. *Phys. Rev. Lett.*, 97:142001, 2006.

[32] Christian W. Bauer and Matthew D. Schwartz. Event generation from effective field theory. *Phys. Rev.*, D76:074004, 2007.

[33] Christian W. Bauer and Iain W. Stewart. Invariant operators in collinear effective theory. *Phys. Lett.*, B516:134–142, 2001.

[34] Christian W. Bauer, Frank J. Tackmann, and Jesse Thaler. Geneva (i): A new framework for event generation. *JHEP*, 12:010, 2008.

[35] Christian W. Bauer, Frank J. Tackmann, and Jesse Thaler. Geneva (ii): A phase space generator from a reweighted parton shower. *JHEP*, 12:011, 2008.

[36] Thomas Becher and Matthias Neubert. Threshold resummation in momentum space from effective field theory. *Phys. Rev. Lett.*, 97:082001, 2006.

[37] Thomas Becher and Matthias Neubert. Toward a NNLO calculation of the $\bar{B} \to X_s\gamma$ decay rate with a cut on photon energy. I: Two-loop result for the soft function. *Phys. Lett.*, B633:739–747, 2006.

[38] Thomas Becher and Matthias Neubert. Toward a NNLO calculation of the $\bar{B} \to X_s\gamma$ decay rate with a cut on photon energy. II: Two-loop result for the jet function. *Phys. Lett.*, B637:251–259, 2006.

[39] Thomas Becher, Matthias Neubert, and Ben D. Pecjak. Factorization and momentum-space resummation in deep-inelastic scattering. *JHEP*, 01:076, 2007.

[40] Thomas Becher, Matthias Neubert, and Gang Xu. Dynamical threshold enhancement and resummation in Drell-Yan production. *JHEP*, 07:030, 2008.

[41] Thomas Becher and Matthew D. Schwartz. A precise determination of α_s from LEP thrust data using effective field theory. *JHEP*, 07:034, 2008.

[42] Thomas Becher and Matthew D. Schwartz. Direct photon production with effective field theory. *JHEP*, 02:040, 2010.

[43] Andrei V. Belitsky. Two-loop renormalization of Wilson loop for Drell-Yan production. *Phys. Lett.*, B442:307–314, 1998.

[44] Andrei V. Belitsky, G. P. Korchemsky, and G. Sterman. Energy flow in QCD and event shape functions. *Phys. Lett.*, B515:297–307, 2001.

[45] M. Beneke and Vladimir M. Braun. Renormalons and power corrections. 2000.

[46] C. F. Berger et al. Next-to-Leading Order QCD Predictions for W+3-Jet Distributions at Hadron Colliders. *Phys. Rev.*, D80:074036, 2009.

[47] Carola F. Berger, Tibor Kucs, and George Sterman. Event shape / energy flow correlations. *Phys. Rev.*, D68:014012, 2003.

[48] Carola F. Berger and Lorenzo Magnea. Scaling of power corrections for angularities from dressed gluon exponentiation. *Phys. Rev.*, D70:094010, 2004.

[49] Carola F. Berger and George Sterman. Scaling rule for nonperturbative radiation in a class of event shapes. *JHEP*, 09:058, 2003.

[50] Edmond L. Berger and Harry Contopanagos. Perturbative gluon resummation of the top quark production cross-section. *Phys. Lett.*, B361:115–120, 1995.

[51] Siegfried Bethke. Experimental tests of asymptotic freedom. *Prog. Part. Nucl. Phys.*, 58:351–386, 2007.

[52] Ikaros I. Y. Bigi, Mikhail A. Shifman, N. G. Uraltsev, and A. I. Vainshtein. On the motion of heavy quarks inside hadrons: Universal distributions and inclusive decays. *Int. J. Mod. Phys.*, A9:2467–2504, 1994.

[53] S. W. Bosch, B. O. Lange, M. Neubert, and Gil Paz. Factorization and shape-function effects in inclusive B-meson decays. *Nucl. Phys.*, B699:335–386, 2004.

[54] G. Bozzi, S. Catani, D. de Florian, and M. Grazzini. The q_T spectrum of the Higgs boson at the LHC in QCD perturbation theory. *Phys. Lett.*, B564:65–72, 2003.

[55] S. Brandt, C. Peyrou, R. Sosnowski, and A. Wroblewski. The principal axis of jets. An attempt to analyze high- energy collisions as two-body processes. *Phys. Lett.*, 12:57–61, 1964.

[56] Gustaaf Brooijmans. High p^T hadronic top quark identification. Part I: Jet mass and Ysplitter. ATL-PHYS-CONF-2008-008.

[57] N. Brown and W. James Stirling. Jet cross sections at leading double logarithm in e^+e^- annihilation. *Phys. Lett.*, B252:657–662, 1990.

[58] Andrzej J. Buras. Weak Hamiltonian, CP violation and rare decays. 1998.

[59] S. J. Burby and E. W. Nigel Glover. Resumming the light hemisphere mass and narrow jet broadening distributions in e^+e^- annihilation. *JHEP*, 04:029, 2001.

[60] J. M. Butterworth, B. E. Cox, and Jeffrey R. Forshaw. WW scattering at the CERN LHC. *Phys. Rev.*, D65:096014, 2002.

[61] J. M. Butterworth, John R. Ellis, and A. R. Raklev. Reconstructing sparticle mass spectra using hadronic decays. *JHEP*, 05:033, 2007.

[62] Jonathan M. Butterworth, Adam R. Davison, Mathieu Rubin, and Gavin P. Salam. Jet substructure as a new Higgs search channel at the LHC. *Phys. Rev. Lett.*, 100:242001, 2008.

[63] Jonathan M. Butterworth, John R. Ellis, Are R. Raklev, and Gavin P. Salam. Discovering baryon-number violating neutralino decays at the LHC. *Phys. Rev. Lett.*, 103:241803, 2009.

[64] Matteo Cacciari and Gavin P. Salam. Dispelling the N^3 myth for the k_T jet-finder. *Phys. Lett.*, B641:57–61, 2006.

[65] John M. Campbell, R. Keith Ellis, and David L. Rainwater. Next-to-leading order QCD predictions for W + 2jet and Z + 2jet production at the CERN LHC. *Phys. Rev.*, D68:094021, 2003.

[66] S. Catani, Yuri L. Dokshitzer, M. Olsson, G. Turnock, and B. R. Webber. New clustering algorithm for multi - jet cross-sections in e+ e- annihilation. *Phys. Lett. B*, 269:432–438, 1991.

[67] S. Catani, Yuri L. Dokshitzer, M. H. Seymour, and B. R. Webber. Longitudinally invariant k(t) clustering algorithms for hadron hadron collisions. *Nucl. Phys. B*, 406:187–224, 1993.

[68] S. Catani, Yuri L. Dokshitzer, and B. R. Webber. The k-perpendicular clustering algorithm for jets in deep inelastic scattering and hadron collisions. *Phys. Lett. B*, 285:291–299, 1992.

[69] S. Catani and M. H. Seymour. The dipole formalism for the calculation of QCD jet cross sections at next-to-leading order. *Phys. Lett.*, B378:287–301, 1996.

[70] S. Catani and M. H. Seymour. A general algorithm for calculating jet cross sections in NLO QCD. *Nucl. Phys.*, B485:291–419, 1997.

[71] S. Catani and L. Trentadue. Resummation of the QCD Perturbative Series for Hard Processes. *Nucl. Phys.*, B327:323, 1989.

[72] S. Catani and L. Trentadue. Comment on QCD exponentiation at large x. *Nucl. Phys.*, B353:183–186, 1991.

[73] S. Catani, L. Trentadue, G. Turnock, and B. R. Webber. Resummation of large logarithms in e^+e^- event shape distributions. *Nucl. Phys.*, B407:3–42, 1993.

[74] S. Catani, G. Turnock, and B. R. Webber. Heavy jet mass distribution in e^+e^- annihilation. *Phys. Lett.*, B272:368–372, 1991.

[75] S. Catani, G. Turnock, and B. R. Webber. Jet broadening measures in e^+e^- annihilation. *Phys. Lett.*, B295:269–276, 1992.

[76] S. Catani, G. Turnock, B. R. Webber, and L. Trentadue. Thrust distribution in e^+e^- annihilation. *Phys. Lett.*, B263:491–497, 1991.

[77] S. Catani and B. R. Webber. Resummed C-parameter distribution in e^+e^- annihilation. *Phys. Lett.*, B427:377–384, 1998.

[78] Stefano Catani, Michelangelo L. Mangano, and Paolo Nason. Sudakov resummation for prompt photon production in hadron collisions. *JHEP*, 07:024, 1998.

[79] Stefano Catani, Michelangelo L. Mangano, Paolo Nason, and Luca Trentadue. The resummation of soft gluon in hadronic collisions. *Nucl. Phys.*, B478:273–310, 1996.

[80] T. Chandramohan and L. Clavelli. Consequences of second-order QCD for jet structure in e^+e^-annihilation. *Nucl. Phys.*, B184:365, 1981.

[81] Junegone Chay and Chul Kim. Collinear effective theory at subleading order and its application to heavy-light currents. *Phys. Rev.*, D65:114016, 2002.

[82] Junegone Chay and Chul Kim. Deep inelastic scattering near the endpoint in soft-collinear effective theory. *Phys. Rev. D*, 75:016003, 2007.

[83] Pan-ying Chen, Ahmad Idilbi, and Xiang-dong Ji. Qcd factorization for deep-inelastic scattering at large bjorken x(b) approx. 1-o(lambda(qcd)/q). *Nucl. Phys. B*, 763:183–197, 2007.

[84] P. S. Cherzor and N. A. Sveshnikov. Jet observables and energy-momentum tensor. 1997.

[85] William Man-Yin Cheung, Michael Luke, and Saba Zuberi. Phase Space and Jet Definitions in SCET. *Phys. Rev.*, D80:114021, 2009.

[86] Jui-yu Chiu, Andreas Fuhrer, Andre H. Hoang, Randall Kelley, and Aneesh V. Manohar. Soft-collinear factorization and zero-bin subtractions. *Phys. Rev.*, D79:053007, 2009.

[87] Jui-yu Chiu, Andreas Fuhrer, Randall Kelley, and Aneesh V. Manohar. Factorization Structure of Gauge Theory Amplitudes and Application to Hard Scattering Processes at the LHC. *Phys. Rev.*, D80:094013, 2009.

[88] L. Clavelli. Jet invariant mass in quantum chromodynamics. *Phys. Lett.*, B85:111, 1979.

[89] L. Clavelli and D. Wyler. Kinematical bounds on jet variables and the heavy jet mass distribution. *Phys. Lett.*, B103:383, 1981.

[90] John C. Collins and Davison E. Soper. Back-to-back jets in qcd. *Nucl. Phys. B*, 193:381, 1981.

[91] John C. Collins and Davison E. Soper. Parton distribution and decay functions. *Nucl. Phys. B*, 194:445, 1982.

[92] John C. Collins and Davison E. Soper. The theorems of perturbative qcd. *Ann. Rev. Nucl. Part. Sci.*, 37:383–409, 1987.

[93] John C. Collins, Davison E. Soper, and George Sterman. Factorization of hard processes in QCD. *Adv. Ser. Direct. High Energy Phys.*, 5:1–91, 1988.

[94] John C. Collins and George Sterman. Soft partons in QCD. *Nucl. Phys.*, B185:172, 1981.

[95] H. Contopanagos and G. Sterman. Normalization of the Drell-Yan cross-section in QCD. *Nucl. Phys.*, B400:211–224, 1993.

[96] Harry Contopanagos, Eric Laenen, and George Sterman. Sudakov factorization and resummation. *Nucl. Phys.*, B484:303–330, 1997.

[97] M. Dasgupta and G. P. Salam. Resummation of non-global QCD observables. *Phys. Lett.*, B512:323–330, 2001.

[98] Mrinal Dasgupta, Lorenzo Magnea, and Gavin P. Salam. Non-perturbative QCD effects in jets at hadron colliders. *JHEP*, 02:055, 2008.

[99] Mrinal Dasgupta and Gavin P. Salam. Event shapes in e^+e^- annihilation and deep inelastic scattering. *J. Phys.*, G30:R143, 2004.

[100] Daniel de Florian and Massimiliano Grazzini. The back-to-back region in e^+e^- energy energy correlation. *Nucl. Phys.*, B704:387–403, 2005.

[101] A. De Rujula, John R. Ellis, E. G. Floratos, and M. K. Gaillard. QCD predictions for hadronic final states in e^+e^- annihilation. *Nucl. Phys.*, B138:387, 1978.

[102] G. Dissertori et al. First determination of the strong coupling constant using NNLO predictions for hadronic event shapes in e^+e^- annihilations. *JHEP*, 02:040, 2008.

[103] S. Dittmaier, S. Kallweit, and P. Uwer. NLO QCD corrections to WW+jet production at hadron colliders. *Phys. Rev. Lett.*, 100:062003, 2008.

[104] Yu. L. Dokshitzer and G. Marchesini. On large angle multiple gluon radiation. *JHEP*, 03:040, 2003.

[105] Yu. L. Dokshitzer and G. Marchesini. Hadron collisions and the fifth form factor. *Phys. Lett.*, B631:118–125, 2005.

[106] Yuri L. Dokshitzer, A. Lucenti, G. Marchesini, and G. P. Salam. On the QCD analysis of jet broadening. *JHEP*, 01:011, 1998.

[107] Yuri L. Dokshitzer, G. Marchesini, and G. P. Salam. Revisiting non-perturbative effects in the jet broadenings. *Eur. Phys. J. direct*, C1:3, 1999.

[108] Yuri L. Dokshitzer, G. Marchesini, and B. R. Webber. Dispersive approach to power-behaved contributions in QCD hard processes. *Nucl. Phys.*, B469:93–142, 1996.

[109] Yuri L. Dokshitzer and B. R. Webber. Calculation of power corrections to hadronic event shapes. *Phys. Lett.*, B352:451–455, 1995.

[110] Yuri L. Dokshitzer and B. R. Webber. Power corrections to event shape distributions. *Phys. Lett.*, B404:321–327, 1997.

[111] R. Keith Ellis, D. A. Ross, and A. E. Terrano. The perturbative calculation of jet structure in e^+e^- annihilation. *Nucl. Phys.*, B178:421, 1981.

[112] S. D. Ellis, J. Huston, K. Hatakeyama, P. Loch, and M. Tonnesmann. Jets in hadron-hadron collisions. *Prog. Part. Nucl. Phys.*, 60:484–551, 2008.

[113] S. D. Ellis, J. Huston, and M. Tonnesmann. On building better cone jet algorithms. 2001.

[114] Stephen D. Ellis, Andrew Hornig, Christopher Lee, Christopher K. Vermilion, and Jonathan R. Walsh. Consistent factorization of jet observables in exclusive multijet cross-sections. 2009.

[115] Stephen D. Ellis, Andrew Hornig, Christopher Lee, Christopher K. Vermilion, and Jonathan R. Walsh. *in preparation*, 2010.

[116] Stephen D. Ellis, Andrew Hornig, Christopher Lee, Christopher K. Vermilion, and Jonathan R. Walsh. Jet Shapes and Jet Algorithms in SCET. 2010.

[117] Stephen D. Ellis, Zoltan Kunszt, and Davison E. Soper. Jets in hadron colliders at order α_s^3. *Conf. Proc.*, C910725V1:417–418, 1991.

[118] Stephen D. Ellis, Zoltan Kunszt, and Davison E. Soper. Jets at hadron colliders at order α_s^3: A look inside. *Phys. Rev. Lett.*, 69:3615–3618, 1992.

[119] Stephen D. Ellis and Davison E. Soper. Successive combination jet algorithm for hadron collisions. *Phys. Rev.*, D48:3160–3166, 1993.

[120] Stephen D. Ellis, Christopher K. Vermilion, and Jonathan R. Walsh. Recombination algorithms and jet substructure: Pruning as a tool for heavy particle searches. 2009.

[121] Stephen D. Ellis, Christopher K. Vermilion, and Jonathan R. Walsh. Techniques for improved heavy particle searches with jet substructure. *Phys. Rev.*, D80:051501, 2009.

[122] Adam F. Falk, Elizabeth Ellen Jenkins, Aneesh V. Manohar, and Mark B. Wise. QCD Corrections and the Endpoint of the Lepton Spectrum in Semileptonic B Decays. *Phys. Rev.*, D49:4553–4559, 1994.

[123] Edward Farhi. A QCD test for jets. *Phys. Rev. Lett.*, 39:1587–1588, 1977.

[124] Sean Fleming, Andre H. Hoang, Sonny Mantry, and Iain W. Stewart. Jets from massive unstable particles: Top-mass determination. *Phys. Rev.*, D77:074010, 2008.

[125] Sean Fleming, Andre H. Hoang, Sonny Mantry, and Iain W. Stewart. Top jets in the peak region: Factorization analysis with NLL resummation. *Phys. Rev.*, D77:114003, 2008.

[126] Sean Fleming, Adam K. Leibovich, and Thomas Mehen. Resumming the color octet contribution to $e^+e^- \to J/\psi + X$. *Phys. Rev.*, D68:094011, 2003.

[127] Yang Gao, Chong Sheng Li, and Jian Jun Liu. Transverse momentum resummation for higgs production in soft-collinear effective theory. *Phys. Rev. D*, 72:114020, 2005.

[128] Einan Gardi. Dressed gluon exponentiation. *Nucl. Phys.*, B622:365–392, 2002.

[129] A. G. Grozin and G. P. Korchemsky. Renormalized sum rules for structure functions of heavy mesons decays. *Phys. Rev.*, D53:1378–1390, 1996.

[130] Andre H. Hoang and Stefan Kluth. Hemisphere soft function at $\mathcal{O}(\alpha_s^2)$ for dijet production in e^+e^- annihilation. 2008.

[131] Andre H. Hoang and Aneesh V. Manohar. Charm quark mass from inclusive semileptonic B decays. *Phys. Lett.*, B633:526–532, 2006.

[132] Andre H. Hoang and Iain W. Stewart. Designing gapped soft functions for jet production. *Phys. Lett.*, B660:483–493, 2008.

[133] Diego M. Hofman and Juan Maldacena. Conformal collider physics: Energy and charge correlations. *JHEP*, 05:012, 2008.

[134] Andrew Hornig, Christopher Lee, and Grigory Ovanesyan. Effective predictions of event shapes: Factorized, resummed, and gapped angularity distributions. *JHEP*, 05:122, 2009.

[135] Andrew Hornig, Christopher Lee, and Grigory Ovanesyan. Infrared safety in factorized hard scattering cross-sections. *Phys. Lett.*, B:doi:10.1016/j.physletb.2009.05.039, 2009.

[136] John E. Huth et al. Toward a standardization of jet definitions. 1990. Presented at Summer Study on High Energy Physics, Research Directions for the Decade, Snowmass, CO, Jun 25 - Jul 13, 1990.

[137] Ahmad Idilbi and Xiang-dong Ji. Threshold resummation for drell-yan process in soft-collinear effective theory. *Phys. Rev. D*, 72:054016, 2005.

[138] Ahmad Idilbi, Xiang-dong Ji, and Feng Yuan. Transverse momentum distribution through soft-gluon resummation in effective field theory. *Phys. Lett. B*, 625:253–263, 2005.

[139] Ahmad Idilbi and Thomas Mehen. Demonstration of the equivalence of soft and zero-bin subtractions. *Phys. Rev.*, D76:094015, 2007.

[140] Ahmad Idilbi and Thomas Mehen. On the equivalence of soft and zero-bin subtractions. *Phys. Rev.*, D75:114017, 2007.

[141] Ambar Jain, Ignazio Scimemi, and Iain W. Stewart. Two-loop jet function and jet mass for top quarks. *Phys. Rev.*, D77:094008, 2008.

[142] Nikolaos Kidonakis, Gianluca Oderda, and George Sterman. Evolution of color exchange in QCD hard scattering. *Nucl. Phys.*, B531:365–402, 1998.

[143] Nikolaos Kidonakis, Gianluca Oderda, and George Sterman. NLL resummation for dijet production. 1998.

[144] Nikolaos Kidonakis, Gianluca Oderda, and George Sterman. Threshold resummation for dijet cross sections. *Nucl. Phys.*, B525:299–332, 1998.

[145] Nikolaos Kidonakis and George Sterman. Resummation for QCD hard scattering. *Nucl. Phys.*, B505:321–348, 1997.

[146] G. P. Korchemsky. Shape functions and power corrections to the event shapes. 1998.

[147] G. P. Korchemsky and G. Marchesini. Resummation of large infrared corrections using Wilson loops. *Phys. Lett.*, B313:433–440, 1993.

[148] G. P. Korchemsky and A. V. Radyushkin. Renormalization of the Wilson loops beyond the leading order. *Nucl. Phys.*, B283:342–364, 1987.

[149] G. P. Korchemsky and S. Tafat. On power corrections to the event shape distributions in QCD. *JHEP*, 10:010, 2000.

[150] Gregory P. Korchemsky, Gianluca Oderda, and George Sterman. Power corrections and nonlocal operators. 1997.

[151] Gregory P. Korchemsky and George Sterman. Infrared factorization in inclusive B meson decays. *Phys. Lett.*, B340:96–108, 1994.

[152] Gregory P. Korchemsky and George Sterman. Power corrections to event shapes and factorization. *Nucl. Phys.*, B555:335–351, 1999.

[153] Graham D. Kribs, Adam Martin, Tuhin S. Roy, and Michael Spannowsky. Discovering the Higgs boson in new physics events using jet substructure. 2009.

[154] David Krohn, Jesse Thaler, and Lian-Tao Wang. Jet Trimming. *JHEP*, 02:084, 2010.

[155] Eric Laenen, J. Smith, and W. L. van Neerven. Top quark production cross-section. *Phys. Lett.*, B321:254–258, 1994.

[156] Christopher Lee and George Sterman. Universality of nonperturbative effects in event shapes. 2006.

[157] Christopher Lee and George Sterman. Momentum flow correlations from event shapes: Factorized soft gluons and Soft-Collinear Effective Theory. *Phys. Rev.*, D75:014022, 2007.

[158] Adam K. Leibovich and I. Z. Rothstein. The resummed rate for B –¿ X/s gamma. *Phys. Rev.*, D61:074006, 2000.

[159] Zoltan Ligeti, Iain W. Stewart, and Frank J. Tackmann. Treating the b quark distribution function with reliable uncertainties. *Phys. Rev.*, D78:114014, 2008.

[160] Aneesh V. Manohar. Deep inelastic scattering as $x \to 1$ using Soft-Collinear Effective Theory. *Phys. Rev.*, D68:114019, 2003.

[161] Aneesh V. Manohar. Infrared scales and factorization in qcd. *Phys. Lett. B*, 633:729–733, 2006.

[162] Aneesh V. Manohar, Thomas Mehen, Dan Pirjol, and Iain W. Stewart. Reparameterization invariance for collinear operators. *Phys. Lett.*, B539:59–66, 2002.

[163] Aneesh V. Manohar and Iain W. Stewart. The zero-bin and mode factorization in quantum field theory. *Phys. Rev.*, D76:074002, 2007.

[164] Aneesh V. Manohar and Mark B. Wise. Power suppressed corrections to hadronic event shapes. *Phys. Lett.*, B344:407–412, 1995.

[165] Claudio Marcantonini and Iain W. Stewart. Reparameterization invariant collinear operators. *Phys. Rev.*, D79:065028, 2009.

[166] Matthias Neubert. Advanced predictions for moments of the $\bar{B} \to X_s\gamma$ photon spectrum. *Phys. Rev.*, D72:074025, 2005.

[167] F. R. Ore, Jr. and George Sterman. An operator approach to weighted cross-sections. *Nucl. Phys.*, B165:93, 1980.

[168] Dan Pirjol and Iain W. Stewart. A complete basis for power suppressed collinear-ultrasoft operators. *Phys. Rev.*, D67:094005, 2003.

[169] Tilman Plehn, Gavin P. Salam, and Michael Spannowsky. Fat Jets for a Light Higgs. *Phys. Rev. Lett.*, 104:111801, 2010.

[170] Gavin P. Salam. Towards jetography. 2009.

[171] Gavin P. Salam and Gregory Soyez. A practical Seedless Infrared-Safe Cone jet algorithm. *JHEP*, 05:086, 2007.

[172] Matthew D. Schwartz. Resummation and NLO matching of event shapes with effective field theory. *Phys. Rev.*, D77:014026, 2008.

[173] Michael H. Seymour. Searches for new particles using cone and cluster jet algorithms: A comparative study. *Z. Phys.*, C62:127–138, 1994.

[174] Malin Sjodahl. Color evolution of $2 \to 3$ processes. *JHEP*, 12:083, 2008.

[175] Malin Sjodahl. Color structure for soft gluon resummation — a general recipe. *JHEP*, 09:087, 2009.

[176] T. Sjöstrand and P. Z. Skands. Multiple interactions and the structure of beam remnants. *JHEP*, 03:053, 2004.

[177] Torbjörn Sjöstrand, Stephen Mrenna, and Peter Skands. Pythia 6.4 physics and manual. *JHEP*, 05:026, 2006.

[178] Torbjörn Sjöstrand and Maria van Zijl. A multiple interaction model for the event structure in hadron collisions. *Phys. Rev. D*, 36:2019, 1987.

[179] George Sterman. Soft Gluon Corrections to Short Distance Hadronic Cross-Sections. *Phys. Lett.*, B179:281, 1986.

[180] George Sterman. Summation of Large Corrections to Short Distance Hadronic Cross-Sections. *Nucl. Phys.*, B281:310, 1987.

[181] George Sterman. Partons, factorization and resummation. 1995.

[182] George Sterman and Steven Weinberg. Jets from quantum chromodynamics. *Phys. Rev. Lett.*, 39:1436, 1977.

[183] Iain W. Stewart, Frank J. Tackmann, and Wouter J. Waalewijn. Factorization at the LHC: From PDFs to initial state jets. 2009.

[184] N. A. Sveshnikov and F. V. Tkachov. Jets and quantum field theory. *Phys. Lett.*, B382:403–408, 1996.

[185] Fyodor V. Tkachov. Measuring the number of hadronic jets. *Phys. Rev. Lett.*, 73:2405–2408, 1994.

[186] Fyodor V. Tkachov. Measuring multijet structure of hadronic energy flow or what is a jet? *Int. J. Mod. Phys. A*, 12:5411–5529, 1997.

[187] Michael Trott. Jets in effective theory: Summing phase space logs. *Phys. Rev.*, D75:054011, 2007.